Genomic and Transcriptomic Approaches to Pathways affected in DiGeorge Syndrome

Kelly Lammerts van Bueren

Thesis submitted in fulfilment of the degree of Doctor of Philosophy

University of London

Institute of Child Health (University College London)

December 2007

ProQuest LLC
789 East Eisenhower Parkway
P.O. Box 1346
Ann Arbor, MI 48106-1346

DECLARATION

I, Kelly Lammerts van Bueren confirm that the work presented in this thesis, unless otherwise stated, is my own and has not been submitted for a degree at any other university.

ACKNOWLEDGEMENTS

I would first like to thank my supervisor, Pete Scambler for giving me the opportunity to come to London to work on this project. He has been a fantastic mentor and I would like to thank him for all his guidance and support and for sharing with me his vast knowledge. I am in awe of his brain.

I would also like to say a big thank you to all members of MMU, both past and present, who were so welcoming from the beginning and have made my time here so memorable. They have provided much help, laughter, and encouragement. In particular, thank you to the "Tbx" group, especially Paris, Scary, Sarah and Chela who helped me so much throughout my PhD and put up with all of my questions.

I really cannot overstate how grateful I am to Paris and Scary for proofreading my thesis and for all their support, particularly over the last few months. Thank you so much for all the coffees at Carluccio's.

I wish to thank all my friends both here and in Australia for their encouragement and for keeping me sane. Thank you especially to Amy and Hayden.

Finally, I couldn't have done this without the support of my mum, dad and sister, Ami. I am forever grateful for the late night talks with Ami, who has given me so much encouragement over the last 4 years. My mum and dad have given me endless love and support, they have always believed in me and wanted the best for me. It is to them that I dedicate this thesis.

ABSTRACT

This thesis describes the identification and characterisation of genes important in development of the pharyngeal apparatus and heart, the major structures affected in DiGeorge syndrome (DGS). DGS is characterised by craniofacial, cardiovascular, thymus and parathyroid defects. It is most commonly caused by heterozygous deletion of a 3Mb region of chromosome 22q11 encompassing at least 30 genes. Haploinsufficiency of the *TBX1* transcription factor is considered to be the major underlying cause of this syndrome. Animal models of DiGeorge syndrome have demonstrated the importance of *Tbx1* in pharyngeal and heart development and therefore, identifying the downstream targets of *Tbx1* is of vital importance in understanding the development of these systems.

This project was aimed at identifying cell autonomous effects of *Tbx1* by isolating *Tbx1-lacZ* expressing cells and comparing the gene expression profiles of *Tbx1* null and heterozygous cells by microarray analysis. Validation of the downregulated gene, *Hes1* has been further investigated by the characterisation of pharyngeal and heart defects in mice carrying null alleles of this potential *Tbx1* target. In addition, BAC recombineering was also conducted to generate a transgenic mouse carrying a GFP-labelled, reversible, mutant *Tbx1* allele. This modified *Tbx1* allele should provide the basis for further enrichment of *Tbx1* targets by allowing isolation of *Tbx1*-expressing cells from transgenic mice and subsequent restoration of *Tbx1* function by cre-mediated recombination. Furthermore, in order to identify other pathways important in heart development, DGS patients with atypical chromosome rearrangements were analysed. This approach led to the identification of a potentially disrupted gene, *HIC2*, whose function was analysed using gene trap mouse models and which was shown to play a role in heart development.

Overall these experiments have led to the elucidation of novel genes and genetic pathways affected in DGS and have contributed to a better understanding of the mechanisms controlling morphogenesis of the pharyngeal apparatus and heart.

TABLE OF CONTENTS

LIST OF FIGURES

LIST OF TABLES

ABBREVIATIONS

22q11DS	22q11 deletion syndrome
aa	amino acid
ASD	atrial septal defect
AVC	atrioventricular canal
β-gal	β-galactosidase
BAC	bacterial artificial chromosome
BCIP	5-bromo-4-chloro-3-indolyl-phosphate
BLAST	basic local alignment search tool
bp	base pair
BSA	bovine serum albumin
cDNA	complementary DNA
CES	cat eye syndrome
cM	centiMorgan
CMFDG	5-chloromethylfluorescein di-β-D-galactopyranoside
CNC	cardiac neural crest
CTAFS	Conotruncal anomaly face syndrome
DAB	3,3-diaminobenzidine tetrahydrochloride
DAPI	4',6-diamidino-2-phenylindole
der	derivative
DGS	DiGeorge syndrome
DIG	digoxygenin
DMEM	dulbecco's modified eagle medium
DMSO	dimethyl sulfoxide
DNA	deoxyribonucleic acid
dNTP	deoxynucleotide triphosphates
dsDNA	double-stranded DNA
E	embryonic stage (mouse)
EBV	epstein barr virus
EDTA	ethylene diamine tetra-acetic acid
EMT	epithelial to mesenchymal transition

EST	expressed sequence tags
FA	formaldehyde
FACS	fluorescent activated cell sorting
FCS	fetal calf serum
FGF	fibroblast growth factor
FHF	first heart field
FIGE	field inversion gel electrophoresis
FISH	fluorescent *in situ* hybridisation
FRT	flipase recognition target
GFP	green fluorescent protein
GO	gene ontology
GT	gene trap
HEPES	4-(2-hydroxyethyl)-1-piperazineethanesulfonic acid
IAA-B	interrupted aortic arch type B
IRES	internal ribosomal entry site
kb	kilobase
l	litre
LB	luria bertani
LCR	low copy repeat
loxP	locus of crossover in P1
LV	left ventricle
m	milli
M	molar
µ	micro
Mb	mega base
MRI	magnetic resonance imaging
mRNA	messenger RNA
n	nano
NBT	4-nitro-blue-tetrazoliumchloride
NC	neural crest
Neo	neomycin
NTMT	NaCl, Tris-HCl, $MgCl_2$, Tween-20 buffer
OCT	optimal cutting temperature compound

OFT	outflow tract
ORF	open reading frame
PAA	pharyngeal arch artery
PBS	phosphate buffered saline
PBTX	phosphate buffered saline + triton-X-100
PCR	polymerase chain reaction
PFA	paraformaldehyde
PSM	presomitic mesoderm
PTA	persistent truncus arteriosus
qRT-PCR	quantitative real time PCR
RA	retinoic acid
RAA	right-sided aortic arch
RNA	ribonucleic acid
RT-PCR	reverse transcriptase PCR
RV	right ventricle
SA	splice acceptor
SDS	sodium dodecyl sulphate
SHF	second heart field
SHH	sonic hedgehog
SNP	single nucleotide polymorphism
TAE	tris-acetate-EDTA
TBE	T-box DNA binding element
TBTX	tris-buffered saline + triton-X-100
TDR	typically deleted region
TESPA	3-aminopropyltriethoxysilane
Tm	melting temperature
UTR	untranslated region
UV	ultra violet
VCFS	Velocardiofacial syndrome
VSD	ventricular septal defect
WISH	whole mount *in situ* hybridisation
wt	wild type
x-gal	5-bromo-4-chloro-3-indoyl-β-d-galactopyranoside

CHAPTER 1. INTRODUCTION

1.1 DIGEORGE SYNDROME

DiGeorge syndrome (DGS) is most frequently caused by a 3Mb heterozygous deletion of chromosome 22q11, and represents the most common microdeletion in humans, occurring at a frequency of approximately 1 in 4000 births (Scambler, 2000). DGS, Velocardiofacial syndrome (VCFS) and Conotruncal Anomaly Face Syndrome (CTAFS) represent different clinical manifestations of the same genetic deletion and together are referred to as the 22q11 Deletion syndromes (22q11DS) (Scambler, 2000). DGS is one of the most clinically variable syndromes and over 180 symptoms have been associated with the deletion (Robin and Shprintzen, 2005). However, the major features of DGS can be attributed to aberrant development of the pharyngeal apparatus which results in craniofacial anomalies, thymus and parathyroid gland hypo/aplasia and cardiovascular defects which mainly affect the outflow tract (OFT) and derivatives of the pharyngeal arch arteries (PAA). Patients also exhibit other physical malformations including renal and skeletal defects and often display behavioural problems ranging from cognitive deficits and learning difficulties to pyschiatric disorders such as schizophrenia (Scambler, 2000). Most patients with DGS (~ 90%) have the common 3Mb, 22q11 deletion encompassing approximately 30 genes. Another 8% have a smaller, 1.5Mb nested deletion and some DGS patients have rare, atypical deletions of chromosome 22q11 (Carlson et al., 1997; Morrow et al., 1995). However, the size of the deletion does not correlate with the penetrance or severity of the disease. DGS may be a contiguous gene syndrome in which more than one gene contributes to the phenotype.

1.2 THE PHARYNGEAL APPARATUS

Many of the structures affected in DGS derive from the pharyngeal apparatus, an important, transient structure in vertebrates functioning in feeding and respiration and also in the formation of the heart, thyroid, parathyroid and thymus (Graham, 2003). The pharyngeal apparatus is apparent as a series of paired bulges in vertebrate embryos. These bulges form on the lateral surface of the head in a cranial to caudal manner and are separated externally by ectodermal clefts and internally by endodermal pouches (Figure 1.1). In amniotes, 5 pharyngeal arches form, numbered 1, 2, 3, 4 and 6, separated by 4 pouches. Each pharygeal arch is composed of a number of embryonic cell types; the outer ectoderm, inner endoderm and, within each arch, a group of neural crest (NC) cells that surround the mesoderm. In addition, each pharyngeal arch surrounds an aortic arch artery (Figure 1.1). The complex interactions between these different cell types are carefully co-ordinated for development to occur normally and each cell type contributes to a different tissue of the pharynx. The ectoderm forms the epidermis and sensory neurons of the pharynx, the endoderm forms the internal epithelial lining and endocrine glands (parathyroid, thyroid and thymus) while the mesoderm gives rise to the endothelial cells and musculature of the arch arteries. The NC forms the connective and skeletal tissues of the arches (Graham, 2003).

While the pharyngeal arches may appear to be organised in the same manner, each arch forms distinct derivatives. The most anterior arch, pharyngeal arch one develops into the jaw. Pharyngeal arch two develops into the hyoid apparatus. The more posterior arches form the pharynx in birds and mammals (Graham, 2003). The distinct identity of each arch is evident molecularly by the spatially restricted expression of genes within the arches (Muller et al., 1996; Wall and Hogan, 1995). For example, *Hoxa2* is only expressed in the pharyngeal arches up to arch 2 whereas *Hoxa3* has a rostral boundary at the level of pharyngeal arch three. In addition, each pharyngeal arch is polarised; *Bmp7* is normally expressed only in the rostral half of each pouch whereas *Fgf8* is expressed in the caudal region (Wall and Hogan, 1995).

Figure 1.1 . The pharyngeal apparatus
(**A**) Lateral view of a mouse embryo. (**B**) Frontal view of the pharyngeal apparatus. The pharyngeal apparatus is a transient structure in vertebrates which arises as a series of paired bulges on the lateral surface of the head (**A**) separated by pharyngeal pouches internally (arrows) and pharyngeal arches externally. The outer ectoderm (green) gives rise to the epidermis and sensory neurons of the pharynx and the endoderm (blue) forms the epithelial lining of the pharynx and endocrine glands. The neural crest (red) forms skeletal and connective tissue and the mesoderm (yellow) gives rise to the endothelial cells and musculature of the arch arteries. In addition each arch has a unique identity and forms distinct head structures. Abbreviations: A, anterior, P, posterior (Lindsay, 2001).

1.2.1 The role of the neural crest

Until recently the NC cell population was considered to play the most important role in patterning the pharyngeal arches. The NC is a multipotential cell population which forms at the border between the neural plate and surface ectoderm (Basch and Bronner-Fraser, 2006). It delaminates from the dorsal neural tube, migrates throughout the body and differentiates into multiple cells types (Graham, 2003). NC can be divided into 2 subpopulations; the cranial neural crest and the trunk neural crest. The cranial NC originate from the mid-diencephalon to somite 5, segregating into three distinct streams. These are the trigeminal, hyoid and post-otic streams each of which gives rise to discrete structures (Graham et al., 2004). The trigeminal neural crest arises from the midbrain and rhombomeres one and two and forms part of the trigeminal ganglion and skeletal elements of the lower and upper jaw (Lumsden et al., 1991; Schilling and Kimmel, 1994). The hyoid stream arises from rhombomere four and gives rise to the hyoid skeleton, part of the second pharyngeal arch and the proximal facial ganglion neurons (Lumsden et al., 1991; Schilling and Kimmel, 1994). Finally, the post-otic stream or cardiac neural crest (CNC) arises from rhombomeres six, seven and eight in the hindbrain (to the level of somite three) and migrates through pharyngeal arches three, four and six to form proximal and jugular ganglia neurons and skeletal elements of the caudal arches. These cell also contribute to the aorticopulmonary septum, the pharyngeal-derived endocrine glands and the tunica media of the persisting arch arteries (Bockman and Kirby, 1984; Kirby et al., 1983; Le Lievre and Le Douarin, 1975; Lumsden et al., 1991; Schilling and Kimmel, 1994).

Due to their segregation and contribution to the structure of the pharyngeal arches, NC cells were thought to play a major role in pharyngeal morphogenesis. This theory was originally supported by experiments in which neural crest from the first arch was grafted in place of second arch neural crest and resulted in derivatives of a distinctly pharyngeal arch one phenotype ie. skeletal elements of the jaw (Noden, 1983). However, subsequent studies showed that when the neural tube was ablated before neural crest could form, the pharyngeal arches still developed normally and had identity as evidenced by the expression of regionally-restricted pharyngeal arch markers *Bmp7*, *Fgf8*, *Pax1* and *Shh* (Gavalas et al., 2001; Veitch et al., 1999). Thus it became apparent that the neural crest was not the sole source of patterning signals and other pharyngeal arch tissues may play a more important role in patterning and segmentation.

The neural crest may not be as important for patterning the pharyngeal apparatus as once thought. However, it does not act entirely passively in this process. Through the restricted expression of transcription factors, regionalised neural crest is able to modulate its response to the endoderm. For example, *Hox* genes, as well as being regionally restricted in the pharyngeal endoderm, are also regionally restricted within the pharyngeal neural crest streams. The first arch does not express any Hox genes, *Hoxa2* is normally restricted to the neural crest within pharyngeal arch two and *Hoxa3*, *Hoxb3* and *Hoxd3* are expressed only within arch three (Hunt et al., 1991). However, when *Hoxa2* is ectopically expressed within arch one, normal jaw development is repressed and pharyngeal arch two skeletal elements form instead (Grammatopoulos et al., 2000; Pasqualetti et al., 2000). In addition, the ability of neural crest to form distinct skeletal structures in response to pharyngeal endoderm cues is species-specific. Grafting experiments between duck and quail demonstrate that when neural crest from pharyngeal arch one is transferred to another species, the resulting neural crest derivatives are always donor-specific in shape (Tucker and Lumsden, 2004).

1.2.2 The role of the endoderm in patterning the pharyngeal apparatus

The endoderm displays regionalised *Hox* gene expression and is required for formation of epibranchial placodes within the adjacent head mesenchyme (Begbie et al., 1999; Manley and Capecchi, 1995). In fact, a segmented pharyngeal endoderm appears to have evolved prior to neural crest since it is present in all chordates (Mahadevan et al., 2004). In amphioxus, an organism which represents the last common invertebrate ancestor of the vertebrates, pharyngeal pouches display regionalised gene expression (Holland and Holland 1996). Subsequent reports have now shown that neural crest depends on signals from the endoderm for identity, survival and differentiation which is carried out in part by *Fgf* signalling (Couly et al., 2002; Crump et al., 2004; David et al., 2002; Nissen et al., 2003; Ruhin et al., 2003; Trumpp et al., 1999; Walshe and Mason, 2003). Transplantation experiments in chick and zebrafish show that pharyngeal endoderm is sufficient and necessary for correct formation and orientation of neural crest derived skeletal elements (Couly et al., 2002; David et al., 2002; Ruhin et al., 2003). In the zebrafish mutant, *vgo*, the pharyngeal arches are not segmented properly. The endodermal pouches fail to form, while neural crest migration is initially normal. This defect is rescued by implantation of wild type pharyngeal endoderm, implying that the endoderm may function in patterning the arches (Piotrowski and Nusslein-Volhard, 2000). This finding was not surprising considering that previous experiments had indicated the potential importance of the endoderm in patterning.

Anterior-posterior patterning of the pharyngeal endoderm requires pathways involving retinoic acid (RA), particularly for formation of the caudal arches and pouches. RA levels are controlled by RA-synthesizing enzymes which include retinaldeyhyde dehydrogenases (Raldh1-4) and RA-metabolising enzymes (Cytochrome P450 enzymes, Cyp26a1, b1 and c1). The effects of RA are mediated through RA receptors (RARα, β and γ) and retinoid X receptors (RXRα, β and γ) which bind as heterodimers to RA-response elements in target genes (Mark et al., 2004). Alterations in RA homeostasis by disrupting RA-synthesizing enzymes such as *Raldh2* in the pharyngeal mesoderm (Kopinke et al., 2006; Niederreither et al., 2003; Vermot et al., 2003) or the vitamin A forming enzyme, *bcox* in zebrafish (Lampert et al., 2003) lead to aplasia of the arches caudal to pharyngeal arch 2 and the same defects are seen when RA-receptor function is disrupted (Dupe et al., 1999; Wendling et al., 2000). The endoderm is primarily affected, exhibiting downregulation of specific markers such as *Hoxa1*,

Hoxb1, and *Pax9* which are required for endodermal patterning (Wendling et al., 2000). A similar phenotype occurs in the presence of excess RA when the Cyp26 RA-metabolising enzymes are disrupted (Roberts et al., 2006).

In conclusion, the patterning of the pharyngeal apparatus is now considered to be due to a consensual process that involves interactions between all cell types of the pharyngeal apparatus and the genes involved in the aetiology of DGS are likely to play a part in this process.

1.3 HEART DEVELOPMENT

Congenital heart defects presented by DGS patients often involve abnormalities of the OFT or great vessels of the heart. Defects in OFT septation and alignment result in heart malformations including common arterial trunk and tetralogy of Fallot, a complex heart defect consisting of an overriding aorta, pulmonary stenosis, ventricular septal defect and right ventricular hypertrophy. Great vessel defects in DGS patients mainly involve derivatives of the fourth PAA and thus, the most common anomalies are aberrant origin of the right subclavian artery and interrupted aortic arch type B (Figure 1.3) (Robin and Shprintzen, 2005; Sullivan, 2004).

1.3.1 An overview of heart development

The heart forms from a set of mesodermal cells which emerge from the primitive streak during gastrulation (Garcia-Martinez and Schoenwolf, 1993; Tam et al., 1997). These cells migrate in an anterior-lateral direction to a position under the head folds where they form a crescent shape in which the apex lies toward the anterior end and the lateral arms extend caudally which in mice occurs at ≈ E7.75 (Figure 1.2A). At approximately E8.0, cells within the cardiac crescent move ventrally and fuse to form a primitive heart tube composed of endothelial cells surrounded by a layer of myocardial cells (Figure 1.2B). The heart first begins to beat at this timepoint and blood flows from the caudal, inflow regions in an anterior direction and out through the arterial OFT (Buckingham et al., 2005). The heart grows through myocardial proliferation and the addition of cells to the arterial and venous poles. It undergoes looping in which the heart tube swings to the right and the inflow regions move dorsally and anteriorly, to a position adjacent to the OFT (Buckingham et al., 2005) (Figure 1.2C). During looping, the chambers of the

heart form by ballooning out from the heart tube at discrete positions. From the end of looping, the heart undergoes extensive remodelling in which myocardial trabeculae develop within the lumen of the ventricles and the outer layer of the ventricles thickens to form the compact layer (Figure 1.2D) (Christoffels et al., 2000). Myocardial cells within the left and right ventricles contribute to formation of an interventricular septum (Franco et al., 2006). Endocardial cushions develop within the atrioventricular canal (AVC), forming precursors of the mitral and tricuspid valves. Endocardial cushions also form within the OFT as precursors of the aortic and pulmonary valves and aorticopulmonary (AP) septum which separates the aorta from the pulmonary artery (Markwald et al., 1977; Markwald et al., 1975; Nakajima et al., 2000). Further remodelling of the heart results in the correct alignment of the septa, and valves to form the mammalian four chambered heart (Dunwoodie, 2007).

Figure 1.2 An overview of heart development
The top picture is a ventral view of the heart and the bottom picture represents transverse (**A, B**) and frontal (**C, D**) sections of the heart. (**A**) Mesodermal precursors of the heart emerge from the primitive streak and form in a crescent shape at a position just under the head folds. (**B**). These precursor cells move ventrally and fuse to form a primitve heart tube. (**C**) Between E8.5 and E10.5, the heart tube elongates and undergoes rightward looping. The chambers of the heart begin to balloon out from the heart tube. (**D**) During heart remodelling, myocardial trabeculae form within the ventricles, endocardial cushions from within the OFT and AVC as precursors to cardiac valves and septa and an interatrial and interventricular septum develops. Abbreviations: avc, atrioventricular canal; avs, atrioventricular septum; ca common atrium; cc, cardiac crescent; co, coelum; dm, dorsal mesocardium; dp, dorsal pericardium; e, endocardium; ec, endocardial cushion; fe, foregut endoderm; fg, foregut; hm, head mesoderm; ias, interatrial septum; ivs, interventricular septum; la, left atrium; lv, left ventricle; m, myocardium; ne, neural epithelium; oft, outflow tract; ra, right atrium; rv, right ventricle; som, somatic mesoderm; spm, splanchnic mesoderm; tr, trabeculae. (Stennard and Harvey, 2005)

During the looping and remodelling of the heart, the pharyngeal arch arteries play a role in formation of the great vessels. The arch arteries form sequentially and are initially a series of bilateral vessels which pass through each pharyngeal arch and connect the heart tube to the dorsal aortae via the aortic sac (Figure 1.3A). Throughout development, the arteries of pharyngeal arches one and two regress to form capillary beds. The more caudal arch arteries, three, four and six remodel to form part of the common carotid arteries, aortic arch, right subclavian artery and ductus arteriosus (Kirby and Waldo, 1995) (Figure 1.3B).

Figure 1.3 Formation of the great vessels of the heart
(**A**) At E10.5, PAAs 3 (green), 4 (red and purple) and 6 (blue) form as three pairs of symmetrical vessels connecting the heart to the dorsal aorta. NC cells which delaminate from the neural tube also contribute to the formation of the arch arteries. (**B**) The origins of great vessels of the mature heart which arise from the aortic arch arteries. Orange vessels represent the seventh intersegmental arteries and their derivatives.
Abbreviations: AoA, aortic arch; DA, ductus arteriosus; L, left; LCC, left common carotid; LSCA, left subclavian artery; NC, neural crest; NT, neural tube; PA, pulmonary artery; PAA, pharyngeal arch artery; R, right; RCC, right common carotid; RSCA, right subclavian artery. (Modified from (Yamagishi and Srivastava, 2003)).

1.3.2 The heart fields

It has recently become apparent that the heart forms from two sources of myocardial cells. Early studies in chick and mouse show that cells are progressively added to the arterial and venous poles of the heart during development (de la Cruz et al., 1977; Stalsberg and DeHaan, 1969; Viragh and Challice, 1973). However, the origin of these cells has only recently been discovered. The cardiac crescent which was originally thought to give rise to the entire heart, is now considered to mainly represent cells of the first heart field (FHF) which forms the primitive heart tube and mainly gives rise to the left ventricle, parts of the atria and some of the right ventricle (Meilhac et al., 2004; Zaffran et al., 2004). The second heart field (SHF) consists of mesodermal cells which initially lie dorsal and medial to the cardiac crescent and then later dorsal to the heart tube, and contributes the majority of cells to the OFT, right ventricle (RV) and also to parts of the atria (Figure 1.4) (Cai et al., 2003a; Kelly et al., 2001; Meilhac et al., 2004; Mjaatvedt et al., 2001; Verzi et al., 2005; Waldo et al., 2001; Zaffran et al., 2004).

Figure 1.4 Heart fields in the mouse embryo
At E7.5, the first heart field (FHF) (red) is positioned just under the head folds within the cardiac crescent. The second heart field (SHF) (green) is positioned more dorsal and medial to the cardiac crescent. At E8.0, the FHF contributes cells to the primitive heart tube and the SHF is contained within pharyngeal and splanchnic mesoderm. SHF precursors contribute cells to the arterial and venous poles of the elongating heart tube from E8.5 to E10.5. Myocardial cells derived from the FHF give rise to the left ventricle, the atria and part of the right ventricle. The SHF mainly gives rise to the outflow tract, right ventricle and parts of the atria. Abbreviations: PA, primitive atria; PhA, pharyngeal arches; LA, left atrium; LV, left ventricle; OFT, outflow tract; RA, right atrium; RV, right ventricle. (Buckingham et al., 2005)

The identification of the two heart fields was established initially through tissue ablation and cell lineage analysis in chick which revealed that the pharyngeal mesoderm forms a second source of myocardial cells which contribute to the OFT (Mjaatvedt et al., 2001; Waldo et al., 2001). Recent studies have also indicated that these cells contribute to smooth muscle at the arterial pole of the heart and to the right ventricle (Rana et al., 2007; Waldo et al., 2005b). In the mouse, the random integration of a *lacZ* reporter transgene upstream of the *Fgf10* locus showed that cells initially medial to the cardiac crescent and later contained within the pharyngeal mesoderm and splanchnic mesoderm contribute to the OFT and RV of the heart (Kelly et al., 2001; Kitamoto et al., 2005). DiI labelling studies confirmed these results and also showed that the primitive heart tube mainly exhibits left ventricular identity (Zaffran et al., 2004). In addition, Cai et al (2003) showed that *Isl1* marks a more extensive SHF domain which also contributes cells to the venous pole of the heart (Cai et al., 2003a).

The existence of two heart fields was further supported by retrospective clonal analysis which was used to investigate the contribution of precursor cells to different regions of the heart through analysis of clonal descendents from single cells (Meilhac et al., 2004). This study revealed that two lineages contribute to the heart, probably arising from a common progenitor pool of approximately 140 myocardial founder cells which segregates just prior to formation of the cardiac crescent. The first lineage contributes cells to both ventricles, atria and the AVC, whereas the second lineage contributes cells to the OFT, RV, both atria and the AVC (Meilhac et al., 2004) corresponding to *Isl1*-expressing SHF precursors (Cai et al., 2003a). Thus, the first and second lineages can be distinguished by their contribution to the left ventricle and OFT, respectively (Meilhac et al., 2004).

These studies demonstrated that the two heart fields make distinct regionalised contributions to the heart. While there is some controversy over how extensively the SHF contributes to the heart, it is clear that the SHF is molecularly distinct and recent studies have begun to elucidate the transcriptional pathways underlying SHF development.

Isl1 has been proposed to be central to regulation of SHF development. *Isl1*$^{-/-}$ mutants exhibit severe heart defects in which the heart tube fails to undergo looping and consists only of a primitive left ventricle and atrium, consistent with its important role in

proliferation and survival of SHF precursors (Cai et al., 2003a). Gene knockouts, cell lineage tracing, expression analyses and *in vitro* promoter analyses have identified transcription factors (*Mef2c*, *Nkx2.5*, *Foxh1*, *Foxc1*, *Foxc2*, *Gata4*, *Smyd1*, *Hand2*, *Tbx1*, *Pitx2c*) and signalling molecules (*Shh*, *Fgf8*, *Fgf10*, *Bmp4*, *Bmp7*) which function in SHF development (Abu-Issa et al., 2002; Ai et al., 2006; Cai et al., 2003a; Dodou et al., 2004; Frank et al., 2002; Gottlieb et al., 2002; Ilagan et al., 2006; Jerome and Papaioannou, 2001; Kelly et al., 2001; Kume et al., 2001; Lin et al., 2006; Lin et al., 1997; Lindsay et al., 2001; Merscher et al., 2001; Park et al., 2006; Seo and Kume, 2006; Srivastava et al., 1997; Verzi et al., 2005; von Both et al., 2004; Washington Smoak et al., 2005). These studies have also led to a putative transcriptional network governing SHF development in which combinatorial signalling and reinforcing regulatory feedback loops may play an important role (Figure 1.5) (Black, 2007; Xu and Baldini, 2007).

Figure 1.5 A putative transcriptional network governing SHF development
Isl1 plays a key role in SHF development and functions together with other transcription factors to regulate development of SHF derivatives, in particular the outflow tract and right ventricle of the heart. (Modified from (Xu and Baldini, 2007))

1.3.3 The cardiac neural crest

In addition to the heart fields, the cardiac neural crest (CNC) also contributes substantially to development of the heart, specifically in OFT and pharyngeal arch artery development. The CNC refers to the neural crest which originates from the level of the otic placode to somite three (Figure 1.6) (Kirby and Waldo, 1995). CNC cells from this region migrate through pharyngeal arches three, four and six and contribute to the smooth muscle of the arch arteries and the connective tissue of the thymus, parathyroid and thyroid glands (Figure 1.6) (Bockman and Kirby, 1984; Le Lievre and Le Douarin, 1975). CNC is also important in aorticopulmonary septation (Kirby et al., 1983). Quail-chick chimera experiments and cell lineage analyses in mice have demonstrated that CNC cells migrate into the endocardial cushions of the OFT and together with the aortic sac form the aorticopulmonary septation complex (Epstein et al., 2000; Gitler et al., 2003; Jiang et al., 2000; Li et al., 2000; Phillips et al., 1987). This complex participates in septation of the aorta and pulmonary artery through remodelling of the aortic sac and OFT and fusion of the endocardial cushions (Hutson and Kirby, 2007; Waldo et al., 1998).

Figure 1.6 Cardiac neural crest
Cardiac neural crest (CNC) migrates from the neural tube at the level of the otic vesicle to somite 3, through pharyngeal arch arteries 3, 4 and 6 to the aorticopulmonary septum. The CNC contributes to the smooth muscle of the arch arteries and participates in septation of the aorta and pulmonary trunk. Abbreviations: Ao, aorta, P, pulmonary trunk; oto, otocyst; S, somite. (Hutson and Kirby, 2007).

Ablation of the neural crest leads to a phenocopy of DGS with pharyngeal arch artery defects (Bockman et al., 1989; Bockman et al., 1987; Waldo et al., 1996), hypoplastic or aplastic thymus and parathyroid glands (Bockman and Kirby, 1984) and failure of the OFT to undergo septation resulting in persistent truncus arteriosus (PTA) (Nishibatake et al., 1987). Furthermore, NC ablation also affects addition of SHF-derived myocardium to the OFT causing abnormal cardiac looping and OFT alignment defects (Waldo et al., 2005a; Waldo et al., 2005b; Yelbuz et al., 2002). In these embryos, SHF cells over-proliferate and fail to migrate and differentiate into OFT myocardium. This defect was shown to be due to increased levels of *Fgf8* within the pharynx and could be rescued by treating embryos with an Fgf8 antibody (Hutson et al., 2006). However, downregulating *Fgf8* expression in sham-operated embryos also causes SHF defects indicating that precise levels of *Fgf8* are required for normal OFT development (Hutson et al., 2006).

Genes which play important roles in CNC function have generally been identified through analysis of mouse models. Some of the genes which have been implicated in CNC migration, proliferation, survival and patterning include members of the Tgfß superfamily (*Bmpr1a*, *Alk2*, *Bmpr2*, *Msx2*) (Delot et al., 2003; Kaartinen et al., 2004; Kwang et al., 2002; Stottmann et al., 2004), genes involved in Wnt signalling (*Dvl2*, *Wnt1*, *Wnt3a*, Wnt5a, APC) (Hamblet et al., 2002; Hasegawa et al., 2002; Ikeya et al., 1997; Saint-Jeannet et al., 1997; Schleiffarth et al., 2007), Semaphorin signalling (*Sema3c*, *PlexinA2*, *Npn1*, *PlexinD1*) (Feiner et al., 2001; Gitler et al., 2004; Gu et al., 2003; Kawasaki et al., 1999) Vegf signalling (VEGF165, Hif1-alpha) (Compernolle et al., 2003; Stalmans et al., 2003) and Fgf signalling (*Fgf8*) (Abu-Issa et al., 2002; Frank et al., 2002; Macatee et al., 2003). These studies have demonstrated that CNC interactions with adjacent tissues such as the ectoderm, endoderm, SHF and myocardium play an important role in normal CNC development.

1.4 MECHANISM OF DELETION

Chromosome 22q11 is highly susceptible to rearrangements and is associated with several disorders including DGS, cat eye syndrome (CES) and der(22) syndrome (Shaikh et al., 2001). CES patients have a supernumary, bisatellited chromosome 22pter-q11 resulting from an inverted duplication of chromosome 22 (Mears et al., 1994; Mears et al., 1995; Schinzel et al., 1981). Der(22) syndrome is associated with partial trisomy of chromosome 11 and 22 which can occur in offspring from carriers of the non-robertsonian, constitutional translocation t(11;22)(q23;q11) (Fraccaro et al., 1980; Zackai and Emanuel, 1980). However, the most common chromosome 22 disorder is DGS in which the majority of patients (approx 90%) share a common 3Mb deletion of chromosome 22q11, termed the typically deleted region (TDR) (Figure 1.7). A smaller proportion of DGS patients (approx 8%) have a nested 1.5Mb deletion within the TDR (Carlson et al., 1997; Morrow et al., 1995). Some patients with DGS have other rare, variant deletions of chromosome 22q11 (Amati et al., 1999; Carlson et al., 1997; Levy et al., 1995; McQuade et al., 1999; Rauch et al., 1999; Saitta et al., 1999; Weksberg et al., 2006). The instability of chromosome 22 has been attributed to the presence of multiple, highly homologous low copy repeat (LCR) sequences which span the chromosome and act as substrates for aberrant recombination events (Edelmann et al., 1999a; Edelmann et al., 1999b; Saitta et al., 2004; Shaikh et al., 2000) (Figure 1.7, 1.8).

Figure 1.7 Chromosome 22q11 LCRs and deletions associated with DGS
Eight LCRs, LCR-A to H are contained within 22q11, which mediate aberrant recombination events resulting in deletions, duplications and translocations. Most patients with DGS have a 3Mb deletion which occurs between LCR-A and D. Some patients have a smaller, 1.5Mb deletion which occurs between LCR-A and B. Unique markers and genes located within chromosome 22q11 are indicated in black. Abbreviations: Cen, centromere; Tel, telomere (Modified from (Shaikh et al., 2007)).

LCRs consist of repeated modules which share high levels of sequence identity (97-98%) (Figure 1.8) (Edelmann et al., 1999a; Shaikh et al., 2000). There are at least eight LCRs located on chromosome 22q11, (LCR-A to LCR-H) with LCR-A being most centromeric (Edelmann et al., 1999a; Shaikh et al., 2000) (Figure 1.7). LCR-A and LCR-D, the largest and most complex of the LCRs, mediate the common 3Mb deletion and are also the sites of CES breakpoints (Edelmann et al., 1999b; McTaggart et al., 1998; Shaikh et al., 2000). The distal breakpoint of the 1.5Mb DGS deletion and the t(11;22) translocation occurs within LCR-B (Figure1.7) (Funke et al., 1999). In addition, the more distal LCRs, E to H, have been associated with DGS patients containing atypical chromosome 22 deletions (Rauch et al., 1999; Saitta et al., 1999; Shaikh et al., 2007). Rearrangements between LCRs on chromosome 22 have been proposed to occur due to aberrant inter and intrachromosomal homologous recombination events (Saitta et al., 2004; Shaikh et al., 2001). In comparison, the t(11;22) translocation is mediated by non-homologous recombination between A/T rich palindromes on chromosome 22q11 and 11q23 (Edelmann et al., 2001a; Kurahashi and Emanuel, 2001; Kurahashi et al., 2000). Other de novo translocations involving chromosome 22 also often occur within the 22q11 LCRs (Spiteri et al., 2003) demonstrating that LCRs are responsible for mediating many aberrant recombination events involving chromosome 22.

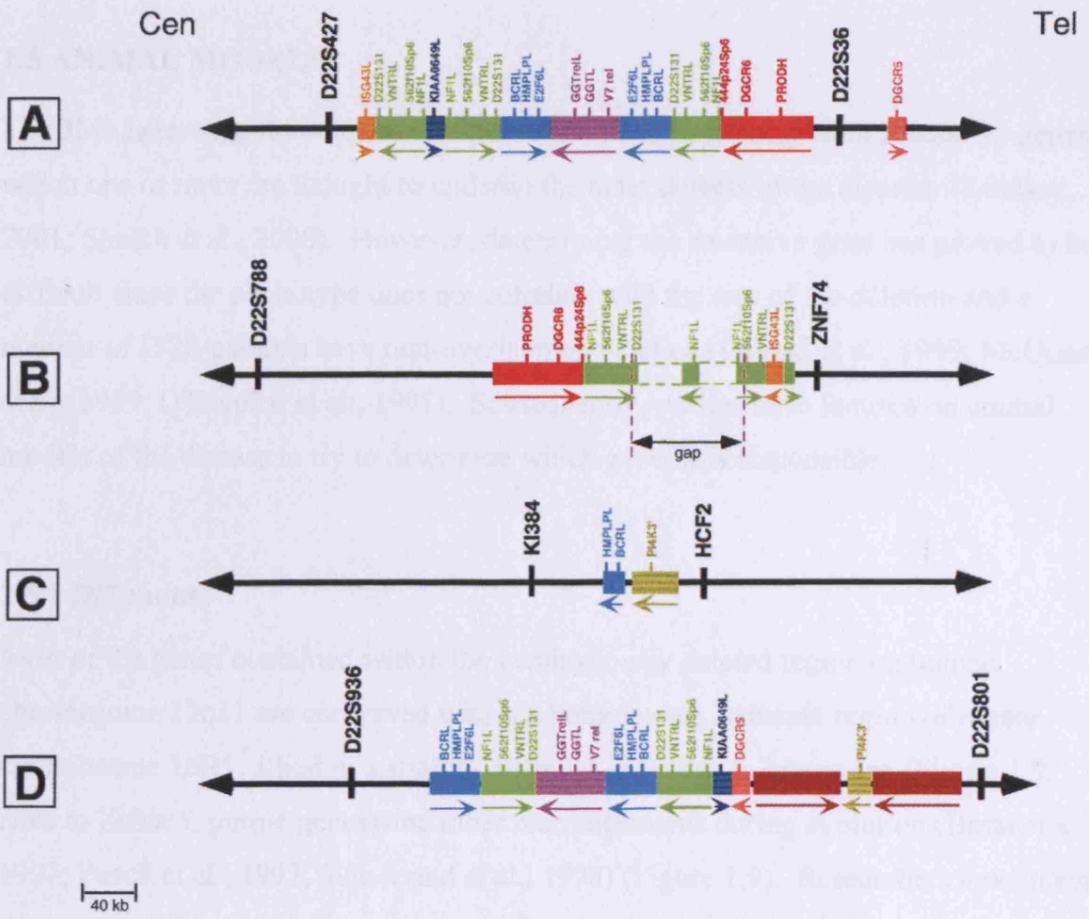

Figure 1.8 LCR organisation
The arrangement of repeated modules within LCR-A to D. Each repeated module is represented by a different colour and the arrows represent the orientation of the module with respect to other copies within the same LCR or on a different LCR. Unique markers are represented in black at the ends of each LCR. (Modified from (Shaikh et al., 2000)).

1.5 ANIMAL MODELS

The 3Mb heterozygous deletion of chromosome 22q11 encompasses at least 30 genes of which one or more are thought to underlie the main defects of the disorder (Lindsay, 2001; Shaikh et al., 2000). However, determining the causative gene has proved to be difficult since the phenotype does not correlate with the size of the deletion and a number of DGS patients have non-overlapping deletions (Amati et al., 1999; McQuade et al., 1999; O'Donnell et al., 1997). Subsequently, studies have focused on animal models of the disease to try to determine which gene(s) is responsible.

1.5.1 *Df1* mouse

Most of the genes contained within the hemizygously deleted region on human chromosome 22q11 are conserved within a homologous, syntenic region of mouse chromosome 16B1, albeit in a slightly different order due to inversions (Figure 1.9, *Hira* to *Zdhhc8*, purple genes) and other rearrangements during evolution (Botta et al., 1997; Puech et al., 1997; Sutherland et al., 1998) (Figure 1.9). Researchers have taken advantage of this conservation by examining the phenotypic consequences of engineered deletions of chromosome 16.

Figure 1.9 Human chromosome 22q11 and the syntenic region of mouse chromosome 16
The 3Mb typical deletion (large grey box) on human chromosome 22q11 contains approximately 30 genes of which most are conserved in a syntenic region of mouse chromosome 16 although in a different order (as shown by the different coloured genes where each colour represent a block of contiguous genes). The smaller, 1.5Mb 22q11 deletion (small grey box) is also shown as well as the *Df1* deletion which models DGS in mice. Other engineered deletions of mouse chromosome 16 are shown in purple and green. The orange boxes represent LCRs on 22q11. (Modified from (Paylor and Lindsay, 2006)).

Df1/+ mice represent the first mouse model of DGS and were generated through Cre-loxP-mediated deletion of at least 22 genes (including *Tbx1*) within chromosome 16 (Lindsay et al., 1999) (Figure 1.9). All *Df1/+* heterozygotes exhibit fourth pharyngeal arch artery hypo/aplasia at E10.5 (Figure 1.10D) (Lindsay and Baldini, 2001; Lindsay et al., 1999; Taddei et al., 2001). Depending on the genetic background, a proportion of mutants recover from this defect during development (Lindsay and Baldini, 2001; Taddei et al., 2001). At E18.5, *Df1/+* heterozygotes exhibit great vessel defects such as interrupted aortic arch type B (IAA-B) and aberrant right subclavian artery, consistent with the earlier pharyngeal arch artery abnormalities (Figure 1.10D). Some *Df1/+* mutants also exhibit tetralogy of Fallot-like defects including overriding aorta, pulmonary stenosis and VSD (Lindsay et al., 1999). In addition, *Df1/+* mice exhibit a neurobehavioural phenotype similar to DGS patients (Paylor et al., 2001). On certain backgrounds, *Df1/+* mice have thymic and parathyroid hypoplasia (Taddei et al., 2001). Thus, these mutants represent a good model for DGS.

The *Df1/+* phenotype was rescued with the corresponding duplication, *Dp1* indicating that the defects were due to haploinsufficiency of one or more of the genes within the deletion and not due to long-range effects on other genes (Lindsay et al., 1999). Additional, overlapping deletions of this syntenic region also helped to narrow down the causative region of cardiovascular defects (Figure 1.9) (Kimber et al., 1999; Lindsay et al., 2001; Puech et al., 2000). Four candidate genes, *Gnb1l*, *Tbx1*, *Gp1bβ* and *Cdcrel1* were contained within the critical region. Genetic complementation studies using a 140Kb P1-derived artificial chromosome (PAC) containing these four genes rescued the *Df1/+* cardiovascular defects confirming that one of these genes was responsible for the phenotype (Lindsay et al., 2001). *Gp1bβ* and *Cdcrel1* were not implicated in DGS because *Gp1bβ* mutations have been associated with Bernard Soulier syndrome, a recessive bleeding disorder with no other cardiovascular defects (Ludlow et al., 1996; Moran et al., 2000) and *Cdcrel1*$^{-/-}$ mice exhibit no phenotype (Lindsay et al., 2001). Of the two genes that were left, only *Tbx1* was strongly expressed within developmental structures affected in DGS, namely the pharyngeal arches, head mesenchyme and otic vesicle (Chapman et al., 1996).

1.5.2 *Tbx1* mouse

Three groups concurrently identified *Tbx1* as a critical, haploinsufficient gene in DGS, generating knockout mouse mutants which displayed many defects reminiscent of the disease in humans (Jerome and Papaioannou, 2001; Lindsay et al., 2001; Merscher et al., 2001). Heterozygous *Tbx1* mutants were found to be phenotypically identical to *Df1*/+ mice, displaying the same cardiovascular defects (Figure 1.10D). Similarly, *Df1*/+;*Tbx1*$^{+/-}$ compound heterozygotes were identical to *Tbx1*$^{-/-}$ homozygotes which exhibit more severe abnormalities in pharyngeal development (Figure 1.10D). At E10.5, *Tbx1*$^{-/-}$ embryos have a hypoplastic second pharyngeal arch and the caudal arches fail to segment resulting in absent third, fourth and sixth pharyngeal arches and arch arteries (Figure 1.10C). *Tbx1*$^{-/-}$ mutants also have a hypoplastic outflow tract and small otic vesicle at this stage (Jerome and Papaioannou, 2001; Lindsay et al., 2001; Vitelli et al., 2002a). These defects reflect areas of *Tbx1* expression during pharyngeal development (Figure 1.10A, A', B).

Tbx1 is first expressed at E7.5 within SHF mesoderm dorsal to the cardiac crescent and head mesenchyme (Chapman et al., 1996; Huynh et al., 2007). From E8.0, *Tbx1* is detected within the pharyngeal endoderm, mesoderm, ectoderm and head mesenchyme (Zhang et al., 2005) (Figure 1.10A, A') and is expressed in the otic placode from E8.5 (Raft et al., 2004). Pharyngeal mesoderm, endoderm, head mesenchyme and otic vesicle expression are strong at E9.5 (Figure 1.10B) and persist until E12.5 (Chapman et al., 1996; Lindsay et al., 2001; Raft et al., 2004).

Later in development, *Tbx1*$^{-/-}$ mice mainly exhibit defects in structures which derive from the pharyngeal region. At E18.5, mutants present with craniofacial abnormalities including bone and muscle malformations and cleft palate which occur due to aberrant development of the first and second pharyngeal arches (Jerome and Papaioannou, 2001; Kelly et al., 2004). In addition, *Tbx1*$^{-/-}$ mutants exhibit great vessel anomalies and failure of OFT septation and alignment resulting in persistent truncus arteriosus with an accompanying VSD (Figure 1.10D). Thymic, parathyroid and thyroid hypo/aplasia are also apparent in *Tbx1*$^{-/-}$ mice as well as outer, middle and inner ear defects (Jerome and Papaioannou, 2001; Liao et al., 2004; Lindsay et al., 2001; Vitelli et al., 2002a; Vitelli et al., 2003).

Figure 1.10 *Tbx1* expression and mouse mutant phenoty

Tbx1-lacZ knockin embryos. Expression of *Tbx1* at E8.5 in a whole embryo (**A**) and a transverse section (**A'**) within the pharyngeal endoderm, mesoderm and ectoderm. (**B**) Expression of *Tbx1* at E9.5 within the head mesenchyme, otic vesicle, pharyngeal and splanchnic mesoderm and pharyngeal endoderm, (**C**) $Tbx1^{-/-}$ embryos at E9.5 have a hypoplastic second pharyngeal arch and the caudal arches do not form. (**D**) Heart defects in *Tbx1* mutant mice. **a.** At E10.5, in $Tbx1^{+/-}$ and *Df1*/+ embryos, the 4th PAA is hypoplastic or fails to form. In $Tbx1^{-/-}$ embryos, the caudal pharyngeal arches, pouches and arch arteries fail to develop and the heart connects directly to the dorsal aorta via the aortic sac. **b.** In E18.5 *Df1*/+ and $Tbx1^{+/-}$ embryos, defects in 4th PAA development lead to aberrant right subclavian artery and interrupted aortic arch (asterisk). In $Tbx1^{-/-}$ embryos, failure of development of the pharyngeal apparatus leads to great vessel anomalies and defects in OFT alignment and septation resulting in persistent truncus arteriosus, in which there is only one outflow vessel from the heart. AO, aorta; AS, aortic sac; DA, dorsal aorta; hm, head mesenchyme; LCC, left common carotid; LPA, left pulmonary artery; LSA, left subclavian artery; ov, otic vesicle; p, pharynx; pe; pharyngeal endoderm; pm, pharyngeal mesoderm; PT, pulmonary trunk; RCC, right common carotid; RSA, right subclavian artery; se, surface ectoderm; TA, truncus arteriosus. (Jerome and Papaioannou, 2001; Lindsay, 2001; Zhang et al., 2005)

The phenotype of *Tbx1*$^{-/-}$ mice closely resembles defects which occur due to NC ablation (Bockman et al., 1989; Bockman et al., 1987; Waldo et al., 1996). NC migration through the pharyngeal arches is defective in *Tbx1*$^{-/-}$ mutants. However, *Tbx1* is not expressed in NC cells or their derivatives. Thus, NC abnormalities are considered to occur secondary to loss of patterning or directional cues from other pharyngeal tissues (Chapman et al., 1996; Vitelli et al., 2002a).

The critical role of *TBX1* in the aetiology of DGS is supported by the identification of frameshift and missense mutations within *TBX1* in DGS patients who do not have the 22q11 deletion (Paylor et al., 2006; Stoller and Epstein, 2005; Yagi et al., 2003; Zweier et al., 2007). Frameshift mutations disrupt a TBX1 nuclear localisation signal and a C-terminal transactivation domain (Paylor et al., 2006; Stoller and Epstein, 2005). There is conflicting data associated with missense mutations occurring in the T-box domain or just downstream. These mutations have been reported as gain of function (GOF) mutations according to some reporter assays (Zweier et al., 2007) and loss of function mutations according to other reporter assays (P. Ataliotis, pers. comm.). Considering that overexpression of *Tbx1* in the mouse causes DGS-like defects similar to loss of function mutants, it is possible that GOF mutations in human *TBX1* also result in a DGS-like phenotype (Liao et al., 2004; Merscher et al., 2001).

1.6 T-BOX GENES AND DEVELOPMENT

Tbx1 is a member of the evolutionarily conserved T-box family of transcription factors, whose members are defined by a common T-box DNA binding domain (Naiche et al., 2005). The first T-box gene identified, *T* or *Brachyury* was named after its short tail mouse mutant phenotype (Herrmann et al., 1990). Since then, at least 18 T-box genes have been found in vertebrates and these have been divided into 5 subfamilies based on phylogenetic analyses (Figure 1.11A) (Papaioannou, 2001). T-box genes are involved in multiple developmental processes including gastrulation, craniofacial, heart and limb morphogenesis. Mutations in several T-box genes have been linked to human disorders (Naiche et al., 2005). Most of the disorders associated with T-box genes occur in the heterozygous state such as Ulnar-Mammary syndrome (*TBX3*), Small Patella syndrome (*TBX4*), Holt Oram syndrome (*TBX5*) and congenital heart defects caused by *TBX20* mutations (Bamshad et al., 1999; Bamshad et al., 1997; Basson et al., 1997; Bongers et al., 2004; Kirk et al., 2007; Li et al., 1997). Similarly, mouse studies have shown that several T-box genes such as *Tbx3*, *Tbx5* and *Tbx20* are haploinsufficient demonstrating that development of many organs are sensitive to altered T-box gene dosage (Bruneau et al., 2001; Davenport et al., 2003; Jerome-Majewska et al., 2005; Stennard et al., 2005).

All T-box proteins share a conserved, 180 amino acid, sequence-specific T-box DNA binding domain. However, all other domains are highly divergent reflecting their different functional roles in development (Figure 1.11B) (Naiche et al., 2005). Studies on the original T-box gene, *Brachyury* identified a palindromic T-box DNA binding element (TBE) consisting of two 5'-AGGTGTGAAA-3' T-half sites which Brachyury binds as a homodimer (Kispert and Herrmann, 1993). Subsequent studies have shown that many T-box factors can bind to the T-half site (Bruneau et al., 2001; Lamolet et al., 2001; Papapetrou et al., 1997; Paxton et al., 2002; Sinha et al., 2000; Stennard et al., 2003). However, T-box proteins form different quaternary structures (Coll et al., 2002; Muller and Herrmann, 1997; Zweier et al., 2007)and have different affinities for the number, orientation and specific sequence of these T-half sites which may help to confer functional specificity (Conlon et al., 2001; Ghosh et al., 2001; Lingbeek et al., 2002; Sinha et al., 2000). *In vitro* studies show that Tbx1 preferentially binds to a palindromic pair of T-half sites (Sinha et al., 2000; Zweier et al., 2007) although Tbx1 also appears to be able to activate potential *in vivo* targets through a single, putative T-half site (Nowotschin et al., 2006; Xu et al., 2004).

T-box transcription factors function as activators, repressors or both depending on the developmental context (Plageman and Yutzey, 2005). For instance, Tbx1 and Tbx5 are transcriptional activators (Ataliotis et al., 2005; Bruneau et al., 2001; Hiroi et al., 2001; Plageman and Yutzey, 2004; Stoller and Epstein, 2005; Xu et al., 2004; Zaragoza et al., 2004; Zweier et al., 2007) whereas Tbx15 and Tbx18 are transcriptional repressors (Farin et al., 2007). Tbx2, Tbx3 and Tbx20 contain both activation and repression domains (Carlson et al., 2001; He et al., 1999; Paxton et al., 2002; Plageman and Yutzey, 2004; Stennard et al., 2003).

Tbx1, Tbx2, Tbx3, Tbx5, Tbx18 and *Tbx20* are expressed in distinct but overlapping domains within cardiac progenitors and the heart and are involved in many aspects of vertebrate heart development including expansion of heart precursors, cardiac chamber formation and patterning, and conduction system, valve and septum formation (Hoogaars et al., 2007; Plageman and Yutzey, 2005). T-box proteins interact with each other and with other transcription factors such as Nkx2.5, Gata4 and Isl1 to co-ordinately regulate target genes (Brown et al., 2005; Farin et al., 2007; Garg et al., 2003; Hoogaars et al., 2007; Krause et al., 2004; Nowotschin et al., 2006; Stennard et al., 2003; Takeuchi et al., 2005). For example, during cardiac chamber formation, Tbx2 appears to compete with Tbx5 for interaction with Nkx2.5 to regulate target gene expression. Tbx5 interacts with Nkx2.5 to synergistically activate the target gene, *Nppa* whereas in non-chamber myocardium, Tbx2 interacts with Nkx2.5 to repress *Nppa* (Bruneau et al., 2001; Christoffels et al., 2004; Habets et al., 2002; Hiroi et al., 2001; Takeuchi et al., 2003). Thus, during heart development, the regulation of transcriptional targets by T-box genes is precisely controlled through their individual affinity for particular DNA sequences, their spatial and temporal expression and their interactions with other transcription factors.

Figure 1.11 T-box transcription factor family and structure
(**A**) Phylogenetic tree of T-box genes subdivided into 5 families based on sequence analysis (Naiche et al 05). (**B**) Protein structure of members of the Tbx1 subfamily. The T-box DNA binding domain is highly conserved within member domains (R). Tbx20 can function as an activator or repressor. The red boxes represent nuclear localisation signals identified within Tbx1 and Tbx18. (Modified from (Plageman and Yutzey, 2005)).

1.7 *TBX1* AND ITS ROLE IN DEVELOPMENT

1.7.1 Specific requirements for *Tbx1* in development

Conventional mouse knockouts have demonstrated that *Tbx1* plays a critical role in the pathogenesis of structures affected in DGS. The time, tissue and dose-specific requirements for *Tbx1* throughout development have recently been elucidated through conditional ablation studies and the analysis of a series of alleles expressing various levels of *Tbx1* (Figure 1.12, Tables 1.1 and 1.2). These experiments have revealed that knocking out *Tbx1* at E7.5 recapitulates the germline deletion phenotype. *Tbx1* exhibits precise time-dependent roles in the development of each pharyngeal-derived structure and can be required at multiple stages throughout development of the same structure such as the thymus (Figure 1.12) (Xu et al., 2005). In addition, tissue-specific deletion studies in which *Tbx1* has been ablated from the pharyngeal epithelia (ectoderm and endoderm) (Zhang et al., 2005), pharyngeal endoderm (Arnold et al., 2006b) and pharyngeal mesoderm (Zhang et al., 2006) have emphasised the requirement for *Tbx1* in multiple tissues for normal pharyngeal development (Table 1.1). *Tbx1* expression within the mesoderm and endoderm is necessary for pharyngeal segmentation, NC migration, OFT, thymus and ear development (Arnold et al., 2006b; Zhang et al., 2006). Secondary palate morphogenesis solely relies on *Tbx1* expression in the pharyngeal epithelia. Also, it appears that *Tbx1* within the pharyngeal ectoderm is required for normal fourth PAA development (Arnold et al., 2006b; Zhang et al., 2005). Reactivation of *Tbx1* within the mesoderm of hypomorphic $Tbx1^{Neo2/-}$ embryos was also carried out through Cre-mediated excision of the floxed *Neo2* cassette contained within the *Tbx1* allele. Mesodermal reactivation of *Tbx1* rescues OFT alignment and septation defects, hypoplasia of the second pharyngeal arch and outer ear and third and sixth arch arteries anomalies demonstrating a cell-autonomous requirement for *Tbx1* in development of these structures (Zhang et al., 2006).

These studies have begun to characterise the tissue-specific roles for *Tbx1* in development. However, there has been no standardised approach to conducting these experiments. Different groups have carried out these tissue-specific deletion studies and thus, pharyngeal-derived defects have been investigated to different degrees. Strain-dependent tissue expression of the *Foxg1-Cre* driver has also made it difficult to be fully confident of the results (Arnold et al., 2006b; Zhang et al., 2005). Zhang *et al* (2005) showed that *Foxg1-Cre* drove expression in the mesoderm, endoderm and

ectoderm whereas Arnold *et al* (2006) described *Foxg1-Cre* expression only within the endoderm in a different mouse strain. In addition, reactivation studies have not been conducted within the endoderm or ectoderm. Therefore, the precise roles which *Tbx1* plays within each tissue during development have yet to be clearly defined.

Tbx1 function is extremely dose-sensitive, as both under and overexpression of *Tbx1* causes a DGS-like phenotype in mice (Funke et al., 2001; Hu et al., 2004; Jerome and Papaioannou, 2001; Liao et al., 2004; Lindsay et al., 2001; Merscher et al., 2001; Xu et al., 2004). Through analysis of nine different genotypes representing progressively lower levels of *Tbx1* mRNA, Zhang and Baldini (2007) demonstrated that different pharyngeal structures exhibit different sensitivities to altered *Tbx1* dosage (Table 1.2). Specifically, the penetrance and severity of thymic and PAA defects generally increase with decreasing *Tbx1* levels and the phenotype varies over a broad range of *Tbx1* doses. These structures are also the most dosage sensitive, with defects occurring even when *Tbx1* is expressed at 70% of wild type levels. In contrast, cleft palate is only present in $Tbx1^{-/-}$ mutants (Zhang and Baldini, 2007).

Figure 1.12 Time requirements for *Tbx1* during development
Each pharyngeal structure or process analysed requires *Tbx1* at specific time intervals for normal development. The arrow indicates that the endpoint for *Tbx1*'s role in secondary palate development is unknown. (Modified from (Xu et al., 2005)).

Table 1.1 Tissue-specific requirements for *Tbx1* in development

	Tissue-specific deletion of *Tbx1*	
	Endoderm and otic vesicle (*Foxg1-Cre*)	**Mesoderm** (*Mesp1-Cre*)
Pharyngeal segmentation and arch artery development	✖	✖*
OFT septation and alignment	✖	✖*
Thymus	✖	✖
Thyroid	✖	nd
Parathyroid	✖	nd
Secondary palate	✖	✔
Ear - outer	✖	✖*
Ear - middle	✖	nd
Ear - inner	✖	✖
Craniofacial bones	✖	nd
Craniofacial muscles	✖	✖
Neural crest migration	nd	✖
Fourth arch artery[#]	✔	✔

(Arnold et al., 2006b; Dastjerdi et al., 2007; Xu et al., 2007a; Xu et al., 2007b; Zhang et al., 2006)
Abbreviations: OFT, outflow tract; ✖ represents defects in a particular structure or process; ✔ represents no defects; nd, not determined
*Mesodermal reactivation of *Tbx1* in a $Tbx1^{Neo2/-}$ background partially or fully rescues defects in these structures (Zhang et al., 2006).
[#]Epithelial-specific (endoderm and ectoderm) deletion of *Tbx1* causes fourth arch artery defects (Zhang et al., 2005).

Table 1.2 *Tbx1* dose-dependent phenotypes

Tbx1 genotype (% of wild type *Tbx1* expression)	Phenotype					
	Lethality	**Aortic arch**	**Thymus**	**OFT alignment and septation**	**Cleft palate**	**Pharyngeal arch development**
Neo2/+ (70%)	low	✖ (11%)	m. hypo (29%)	✔	✔	✔
Neo/+ (53%)	low	✖	m. hypo	✔	✔	✔
+/- (50%)	low	✖ (38%)	m. hypo (41%)	Alignment defects	✔	✔
Neo2/Neo2 (34%)	100%	✖ (100%) Most bilateral	s. hypo	✖	✔	Hypo 4th PA
Neo2/Neo (18.5%)	100%	✖	aplasia	Variable. Alignment & septation defects	✔	
Neo2/- (15%)	100%	✖	aplasia	Incomplete and complete PTA	✔	No caudal arches but hypo 4th pouch and 6th PAA present
Neo/Neo (4%)	100%	✖	aplasia	PTA	✔	No caudal arches, pouches or PAAs
-/- (0%)	100%	✖	aplasia	PTA	✖	No caudal arches, pouches or PAAs

(Lindsay et al., 1999; Xu et al., 2004; Zhang and Baldini, 2007)

Abbreviations: Neo, A PGKneo cassette inserted into *Tbx1* intron 5; Neo2, A floxed PGKneo cassette inserted into *Tbx1* intron 5; ✖ represents defects in a structure, ✔ means no defects present, m. hypo, mild hypoplasia; s. hypo, severe hypoplasia; hypo 4th PA, hypoplastic 4th pharyngeal arch; PAA, pharyngeal arch artery; PTA, persistent truncus arteriosus.

1.7.2 *Tbx1* and pharyngeal segmentation

The pharyngeal apparatus develops in a cranial to caudal manner by the sequential addition of pharyngeal arches between E8 and E10.5 within the mouse. However, the molecular pathways required for this process are not well characterised. *Tbx1* is expressed in an anterior-posterior and medial-lateral gradient within the pharyngeal endoderm so that it appears strongest within the most caudal and lateral pharyngeal segments as development proceeds, suggesting a role for *Tbx1* in pharyngeal growth (Vitelli et al., 2002a). Timed cell fate mapping studies also show a progressive increase in *Tbx1* levels in the caudal pharyngeal endoderm throughout pharyngeal development (Xu et al., 2005). Experiments have recently confirmed that *Tbx1* is indeed required for pharyngeal segmentation since deletion of *Tbx1* at timepoints prior to formation of the next arch only result in segmentation defects caudal to that arch (Xu et al., 2005). *Tbx1* has been proposed to regulate expansion of endodermal cells and there is a reduction in endodermal proliferation in $Tbx1^{-/-}$ mutants (Xu et al., 2005). In addition to the pharyngeal endoderm, *Tbx1* expression within the mesoderm also participates in the segmentation process (Zhang et al., 2006). Proliferation is also downregulated in this tissue and may be necessary for pharyngeal formation (Zhang et al., 2006). However, it is not clear as yet whether *Tbx1* also plays a role in regulating the patterning and morphogenetic events required for segmentation of the pharyngeal arches.

1.7.3 *Tbx1* and heart development

Defects in the growth, alignment and septation of the outflow tract and formation and remodelling of the aortic arch arteries are the main heart malformations which occur in *Tbx1*$^{-/-}$ mice (Vitelli et al., 2002a). In DGS patients, the aortic arch and OFT defects can occur together or in isolation. Similarly, these defects are separable in mice and have distinct time, tissue and dose requirements for *Tbx1* (Arnold et al., 2006b; Hu et al., 2004; Jerome and Papaioannou, 2001; Liao et al., 2004; Lindsay et al., 2001; Merscher et al., 2001; Xu et al., 2004; Zhang et al., 2005; Zhang et al., 2006). In addition, mouse studies suggest that the high incidence of heart abnormalities in DiGeorge patients may be explained by the fact that arch artery and OFT development are more sensitive to altered *Tbx1* dosage than other pharyngeal arch derivatives (Hu et al., 2004; Zhang and Baldini, 2007).

In particular, development of the fourth PAAs is very sensitive to reduced *Tbx1* dosage. Arch artery defects occur even when *Tbx1* is expressed at 70% of normal levels and gradually increase in penetrance and severity as *Tbx1* levels decrease (Table 1.2) (Zhang and Baldini, 2007). The particular sensitivity of fourth arch arteries to altered *Tbx1* levels may reflect the unique vascular morphology of these vessels (Bergwerff et al., 1999). Analysis of the fourth PAAs of *Df1/+* heterozygotes has shown that initial tube formation and endothelial cell differentiation are normal but at E10.5 there is a lack of NC-derived vascular smooth muscle (VSM) lining the arch arteries (Lindsay and Baldini, 2001). NC migration appears to be normal, therefore, fourth arch artery defects were originally thought to occur as a result of the non cell-autonomous effects of *Tbx1* within the endoderm or mesoderm on NC differentiation (Lindsay and Baldini, 2001). However, recent studies indicate that ectodermal *Tbx1* plays the major role in fourth arch artery development (Table 1.1) (Arnold et al., 2006b; Zhang et al., 2005). Expression within the pharyngeal ectoderm correlates with the time requirement for *Tbx1* in PAA development between approximately E7.5 and E9.0 (Figure 1.12) (Xu et al., 2004; Zhang et al., 2005). Surprisingly, this means that *Tbx1* is necessary prior to fourth PAA formation, which occurs after E9.5. Given that *Tbx1* cells also contribute to the endothelia of the fourth arch arteries (Xu et al., 2005), it is possible that *Tbx1* expression within the ectoderm and/or endothelial precursor cells may affect the ability of endothelial cells to signal to NC, or alter the ability of NC to respond and differentiate later in development.

The most common cardiovascular malformations found in DGS patients involve aberrant development of the OFT of the heart (Momma, 2007; Robin and Shprintzen, 2005). *Tbx1* is essential for normal OFT development and is required cell-autonomously within the mesoderm for OFT growth, alignment and septation mediated in part by regulation of SHF expansion (Table 1.1) (Xu et al., 2004; Zhang et al., 2006). Analysis of SHF markers in *Tbx1*$^{-/-}$ embryos reveals that there is a reduction or loss of a subpopulation of SHF precursors (Kelly and Papaioannou, 2007). Endodermal deletion of *Tbx1* also results in OFT defects (Arnold et al., 2006b) implying that interaction between the mesoderm and endoderm is important for cardiac development. *Tbx1* is expressed within the SHF from the cardiac crescent stage and contributes cells to the OFT, right ventricle and even parts of the atria (Brown et al., 2004; Huynh et al., 2007; Maeda et al., 2006; Xu et al., 2005; Xu et al., 2004). However, to date, only OFT defects have been identified in *Tbx1*$^{-/-}$ mutants (Jerome and Papaioannou, 2001; Lindsay et al., 2001). Timed-deletion experiments show that *Tbx1* is required for normal OFT development between E8.5 and E9.5 (Figure 1.12) (Xu et al., 2005), coinciding with expression of *Tbx1* within the pharyngeal and splanchnic mesoderm (Chapman et al., 1996; Lindsay et al., 2001). Cell fate mapping studies show that *Tbx1*-expressing precursors contribute extensively to the OFT specifically within this narrow time window, not only to the myocardial layer but also to the underlying endothelium of the OFT (Xu et al., 2005; Zhang and Baldini, 2007). *Tbx1* is only weakly expressed in part of the myocardial layer of the distal OFT at this stage (Vitelli et al., 2002a; Zhang and Baldini, 2007). Therefore, the results suggest that *Tbx1*-expressing SHF precursors may give rise to both myocardial and endothelial tissues of the OFT (Zhang and Baldini, 2007). This theory is supported by recent experiments demonstrating that multipotential *Isl1*+ progenitor cells contained within the SHF can contribute to myocardial, endothelial and VSM cells of the heart (Moretti et al., 2006).

OFT alignment appears to be more sensitive to altered *Tbx1* dosage than OFT septation (Lindsay et al., 1999; Zhang and Baldini, 2007). Defects such as overriding aorta occur in heterozygous *Tbx1* mutants (Liao et al., 2004; Lindsay et al., 1999) whereas aortopulmonary septation defects become prevalent when *Tbx1* levels fall below 20% of wild type (Table 1.2) (Zhang and Baldini, 2007). SHF proliferation may be more sensitive to a reduction in *Tbx1* expression which would lead to a shorter OFT, looping defects and aberrant OFT alignment. The role of *Tbx1* in regulating OFT septation is less clear. NC distribution is abnormal within the pharyngeal arches of *Tbx1* mutants

with OFT septation defects (Vitelli et al., 2002a; Xu et al., 2004; Zhang et al., 2006). However, it is not clear whether fewer NC cells invade the OFT or if *Tbx1* affects NC function within the endocardial cushions. In addition, defects in aortic sac morphogenesis have been identified in *Tbx1* mutants which may also contribute to a failure in OFT septation (Xu et al., 2004).

DGS patients exhibit a highly variable heart phenotype even though most patients have the same 22q11 deletion (Sullivan, 2004). Interestingly, $Tbx1^{Neo2/Neo}$ hypomorphic mouse mutants which express *Tbx1* at 20% of wild type levels exhibit a very variable OFT phenotype ranging from no defects, to alignment defects, to complete PTA (Table 1.2) (Zhang and Baldini, 2007). These results suggest that variability is affected by stochastic or epigenetic factors and this mouse mutant represents a better model for the OFT phenotype of DGS patients (Zhang and Baldini, 2007).

1.7.4 *Tbx1* and endocrine gland development

Thymus and parathyroid hypoplasia with associated immunodeficiency and hypocalcemia, respectively are common features of DGS. Hypothyroidism also occurs in patients with this syndrome (Robin and Shprintzen, 2005). The structures affected in DGS, the thymus, parathyroid and thyroid glands all derive from the pharyngeal endoderm. The thymus and parathyroid develop from a common primordium within the endoderm of the third pharyngeal pouch. The thyroid gland arises from endoderm lining the second arch which fuses with ultimobranchial bodies that form as outpocketings form the fourth pharyngeal pouch (Hilfer and Brown, 1984). In addition to the endoderm, NC also contributes to the connective tissue of the thymus and parathyroid glands from E11.5 and is required for correct thymic morphogenesis (Jiang et al., 2000; Le Lievre and Le Douarin, 1975; Waldo et al., 1996; Yamazaki et al., 2005).

In $Tbx1^{-/-}$ mice, development of all three endoderm-derived glands is affected. The thymus and parathyroid do not develop due to a failure in pharyngeal segmentation and patterning (Jerome and Papaioannou, 2001; Zhang and Baldini, 2007). The thyroid gland is hypoplastic in $Tbx1^{-/-}$ mice and does not form symmetrical lobes (Fagman et al., 2007; Liao et al., 2004). *Tbx1* is not expressed in the thyroid itself but appears to be required non cell-autonomously to regulate its growth and position (Fagman et al.,

2007). Defects in thymus and parathyroid gland morphogenesis also occur in *Tbx1* heterozygotes although penetrance of glandular defects depends on genetic background (Taddei et al., 2001). The thymus gland has been the most well studied of the endocrine organs affected by *Tbx1* mutations. Normal thymic development requires *Tbx1* early between E7.5 and E8.5 to regulate pharyngeal segmentation and thymic induction (Figure 1.12). *Tbx1* also plays another role later between E10.5 and E11.5 in thymic morphogenesis (Xu et al., 2005). Tissue-specific deletion experiments indicate that *Tbx1* functions in both the mesoderm and endoderm for normal thymus development (Table 1.1) (Arnold et al., 2006b; Zhang et al., 2006). In addition, the penetrance and severity of thymic defects varies over a wide range of *Tbx1* doses (70 to 20% of wild type levels) demonstrating the acute sensitivity of the thymus to altered *Tbx1* expression (Table 1.2) (Zhang and Baldini, 2007).

1.7.5 *Tbx1* and craniofacial development

DGS patients exhibit a range of craniofacial malformations including facial bone deformities, ear malformations and skeletal muscle hypotonia (Robin and Shprintzen, 2005). Many of the structures affected derive from the pharyngeal arches which give rise to bones, muscles and connective tissue of the head and neck (Graham, 2003).

Pharyngeal mesoderm gives rise to branchiomeric muscles including the muscles of mastication (pharyngeal arch one), facial expression muscles (pharyngeal arch two) and muscles of the pharynx and larynx (caudal arches) (Couly et al., 1992; Hacker and Guthrie, 1998; Noden, 1983; Trainor et al., 1994). In *Tbx1*$^{-/-}$ embryos, expression of the myogenic determination genes, *Myf5* and *MyoD* is sporadically activated within the pharyngeal mesoderm resulting in random, aberrant development of muscles derived from the first arch (Kelly et al., 2004). The caudal branchiomeric muscles fail to form in *Tbx1*$^{-/-}$ mutants (Kelly et al., 2004). Therefore, *Tbx1* is required for robust activation of branchiomeric myogenesis, a process which is relatively dosage-insensitive since pharyngeal derived muscles appear normally in hypomorphic mice expressing *Tbx1* at 10% of wild type levels (Arnold et al., 2006b). Endoderm and mesoderm-specific deletion of *Tbx1* both cause defective *MyoD* expression and abnormal development of pharyngeal-derived muscles suggesting that *Tbx1* may be required to regulate interactions between the endoderm and mesoderm for normal muscle development (Table 1.1) (Arnold et al., 2006b; Dastjerdi et al., 2007).

Bones derived from the pharyngeal arches including those of the jaw, middle and outer ear and cartilages of the throat are all affected in *Tbx1*$^{-/-}$ mutants (Jerome and Papaioannou, 2001). In addition, non-pharyngeal derived craniofacial bones are also abnormal consistent with expression of *Tbx1* within the head mesenchyme as well as the pharyngeal arches (Jerome and Papaioannou, 2001). Craniofacial malformations occur in *Tbx1*$^{neo/neo}$ mice expressing 25% of wild type *Tbx1* levels however, they are less severe than *Tbx1*$^{-/-}$ mice (Hu et al., 2004). In addition, cleft palate is particularly insensitive to altered *Tbx1* levels. Expression of as little as 4% of *Tbx1* wild type expression is sufficient to rescue palate defects (Table 1.2) (Zhang and Baldini, 2007).

1.7.6 *Tbx1* and ear development

DGS patients often exhibit external ear defects and hearing loss, of which a proportion is of the sensorineural type (Digilio et al., 1999; Reyes et al., 1999). There is one reported case of a patient with a *TBX1* mutation who also has a hearing impairment (Yagi et al., 2003). *Tbx1*$^{-/-}$ mice exhibit malformations of the outer, middle and inner ear ((Jerome and Papaioannou, 2001; Vitelli et al., 2003). Loss of *Tbx1* within the pharyngeal endoderm affects expansion of the first pharyngeal pouch and formation of pharyngeal arch one and two-derived middle and outer ear bones (Table 1.1) (Arnold et al., 2006b). *Tbx1* is also expressed within the otocyst and periotic mesenchyme of the inner ear (Raft et al., 2004; Vitelli et al., 2003). In *Tbx1*$^{-/-}$ mice, the otic vesicle is small and the vestibular and cochlear structures do not form (Jerome and Papaioannou, 2001; Moraes et al., 2005; Raft et al., 2004; Vitelli et al., 2003). Tissue-specific ablation studies have revealed that *Tbx1* plays a cell-autonomous role for contribution, proliferation and cell fate determination of a subpopulation of otic epithelial cells (Arnold et al., 2006a; Xu et al., 2007b). *Tbx1* may act to delimit the neurogenic domain in the otocyst by suppressing Delta-Notch signalling and *Ngn1*-mediated neural fate determination (Xu et al., 2007b). *Tbx1* also plays a non cell-autonomous role within the periotic mesenchyme for cochlear morphogenesis (Table 1.1) (Xu et al., 2007a; Xu et al., 2007b). Mesoderm-specific deletion of *Tbx1* causes reduced cell proliferation within the periotic mesenchyme affecting formation of the pericochlear capsule and subsequently, cochlear development (Xu et al., 2007a).

1.7.7 Summary

Studies on multiple mouse mutants have revealed the precise dose, tissue and time requirements for *Tbx1* in development of different pharyngeal structures. These experiments have led to a better understanding of why certain malformations such as thymic and cardiovascular defects occur more frequently in DGS patients and the underlying mechanisms through which *Tbx1* functions during embryogenesis. Proliferation defects have been found in nearly all pharyngeal tissues in which *Tbx1* is expressed representing a common cellular process regulated by *Tbx1*. Differentiation and cell fate determination are other processes regulated by *Tbx1*. It still remains to be determined whether *Tbx1* also functions through additional mechanisms to control pharyngeal and heart development. In particular, given that NC plays an important role in the development of nearly all the structures affected in *Tbx1* mutants, a better analysis of the role of *Tbx1* in regulating NC function is required.

1.8 MODIFIERS OF DIGEORGE SYNDROME

The developmental defects exhibited by *Tbx1* mutants, and the identification of *TBX1* mutations in DGS patients without a deletion, strongly suggests that this gene plays a major role in the aetiology of DGS. However, some of the defects exhibited by DGS patients such as renal and skeletal abnormalities are not present in *Tbx1* mutant mice (Robin and Shprintzen, 2005; Sullivan, 2004). Also, there are numerous DGS patients with rare 22q11 deletions that do not include *TBX1* (Amati et al., 1999; Rauch et al., 1999; Rauch et al., 2005; Saitta et al., 1999; Weksberg et al., 2006). One possible explanation is that adjacent deletions may affect *TBX1* regulatory elements or cause changes in chromatin structure affecting *TBX1* expression. Alternatively, DGS may be a contiguous gene syndrome in which multiple genes within the region contribute to the phenotype.

The likelihood that DGS is a contiguous disorder is supported by findings implicating a role for the adaptor protein, Crkl. Mice homozygous for a mutation in the murine homologue, *Crkl* exhibit cardiovascular anomalies, thymic and parathyroid defects reminiscent of DGS (Guris et al., 2001). *CRKL* is contained within the typical 3Mb 22q11 deleted region but not the 1.5Mb deletion of DGS patients so it may not be critical for the phenotype. However, double heterozygous $Crkl^{+/-};Tbx1^{+/-}$ mice display more severe cardiovascular defects than $Tbx1^{+/-}$ mice indicating an important role for *Crkl* in modifying the effects of *Tbx1* haploinsufficiency (Guris et al., 2006). Double heterozygous mutants exhibit an increased penetrance and severity of thymic, parathyroid, fourth PAA and OFT defects resulting from abnormal pharyngeal segmentation and patterning (Guris et al., 2006). These malformation may at least partly be caused by locally upregulated RA levels within the pharyngeal arches due to decreased expression of the RA metabolising enzymes, *Cyp26a1* and *Cyp26b1* which are regulated in a dose-dependent manner by *Crkl* and/or *Tbx1* (Guris et al., 2006). In addition, Crkl mediates Fgf8 signalling through binding to Fgf receptors, Fgfr1 and Fgfr2 (Moon et al., 2006). Double mutants ($Crkl1^{+/-};Fgf8^{+/-}$ and $Crkl1^{-/-};Fgf8^{+/-}$) exhibit more severe cardiovascular, craniofacial and skeletal abnormalities than single mutants ($Fgf8^{+/-}$, $Crkl^{+/-}$ or $Crkl^{-/-}$) providing further evidence that haploinsufficiency of *CRKL* may contribute to the pathogenesis of DGS especially in the context of heterozygous *TBX1* expression.

Other genes contained within the 3Mb TDR may also influence the clinical outcome in DGS patients. Neural crest-specific knockdown of chick *Hira*, a histone chaperone or *Ufd1l*, a gene proposed to be involved in ubiquitin-mediated protein degradation, causes OFT septation defects (Farrell et al., 1999; Yamagishi et al., 2003a). In addition, attenuating *Dgcr6* expression in chick neural crest results in DGS-like fourth PAA and OFT alignment defects and also appears to alter expression of *Tbx1*, *Hira* and *Ufd1l* within the pharyngeal arches and heart (Hierck et al., 2004).

Furthermore, mouse mutants have implicated multiple 22q11 genes in the neurobehavioral phenotype of DGS. *Df1/+* mouse mutants (Paylor et al., 2001) as well as *Tbx1* (Paylor et al., 2006), *Prodh* (Gogos et al., 1999), *Zdhhc8* (Mukai et al., 2004) and *Gnb1l* mutants (Paylor et al., 2006) all exhibit deficits in prepulse inhibition (PPI), a sensorimotor gating defect associated with schizophrenia and found in 22q11 deletion syndrome patients (Sobin et al., 2005). In addition, *Comt* mouse mutants exhibit other behavioural phenotypes such as increased aggressiveness and anxiety (Gogos et al., 1998).

These studies demonstrate that additional genes on chromosome 22q11 may contribute to the physical and neurological symptoms of DGS patients. However, in terms of the pharyngeal and cardiovascular defects, *Tbx1* is the only gene that has been shown to be haploinsufficient in both animal models and human patients and is therefore still the best candidate for the major clinical features in DGS patients.

1.9 *TBX1* REGULATORS AND TARGETS

The importance of *Tbx1* in development has been well studied using numerous mouse models. However, the genetic pathways through which *Tbx1* functions have just begun to be elucidated. Determining the upstream regulators and downstream effectors of *Tbx1* is important not only for understanding the role of *Tbx1* in pharyngeal and heart development, but also, for determining which genes may act as modifiers of the extremely variable DGS phenotype in humans.

1.9.1 Potential *Tbx1* regulators

Studies of animal models with DGS-like phenotypes have led to the identification of potential *Tbx1* regulators. *Shh* is a signalling molecule which is expressed in the pharyngeal endoderm and ectoderm/endodermal boundaries (Helms et al., 1997; Wall and Hogan, 1995) and when disrupted results in pharyngeal and heart defects which are similar to $Tbx1^{-/-}$ mice (Chiang et al., 1996; Litingtung et al., 1998; Washington Smoak et al., 2005). These defects include a single outflow tract arising from the right ventricle, great vessel anomalies and thymic hypoplasia (Fagman et al., 2004; Moore-Scott and Manley, 2005; Washington Smoak et al., 2005). *Tbx1* is down-regulated in the pharyngeal endoderm and mesoderm of $Shh^{-/-}$ mutants at E10.5 and ectopic expression of *Shh* is sufficient to induce *Tbx1* expression in chick (Garg et al., 2001). More recent studies have shown that *Shh* is required for maintenance of *Tbx1* expression rather than induction and may regulate *Tbx1* through Fox transcription factors (Goddeeris et al., 2007; Hu et al., 2004; Maeda et al., 2006; Yamagishi et al., 2003b).

Two conserved *Fox* transcription factor binding sites located upstream of *Tbx1* are necessary to direct expression of a lacZ transgene to the pharyngeal endoderm, mesoderm, head mesenchyme and OFT domains (Hu et al., 2004; Maeda et al., 2006; Yamagishi et al., 2003b). *In vitro* experiments suggest that *Foxa2*, *Foxc1* and *Foxc2* can bind to these consensus enhancer elements and regulate *Tbx1* expression (Maeda et al., 2006; Yamagishi et al., 2003b). All three *Fox* genes are downregulated in $Shh^{-/-}$ mutants and are expressed in overlapping domains with *Tbx1* in the pharyngeal mesoderm (Hu et al., 2004; Seo and Kume, 2006; Yamagishi et al., 2003b). *Foxa2* is also expressed in the pharyngeal endoderm (Hu et al., 2004; Yamagishi et al., 2003b).

Foxc1 and *Foxc2* mutants have overlapping functions and exhibit OFT and arch artery defects similar to *Tbx1*$^{-/-}$ mice (Kume et al., 1998; Kume et al., 2001; Seo and Kume, 2006; Winnier et al., 1999). *Tbx1* is downregulated within the pharyngeal mesoderm of single and double *Fox* mutants and may play a role downstream in expansion of the SHF for contribution to the OFT (Seo and Kume, 2006; Yamagishi et al., 2003b). In addition, *Foxa2* is downregulated in the pharyngeal mesoderm of *Tbx1* hypomorphic mice suggesting that a reinforcing autoregulatory loop may normally function in the SHF to amplify *Tbx1* expression (Hu et al., 2004). Together, these studies provide strong evidence that *Fox* transcription factors act upstream of *Tbx1* within the mesoderm. However, it remains to be determined whether *Foxa2* also regulates *Tbx1* expression in the pharyngeal endoderm and what role this pathway may play in development.

Chordin, a *Bmp* antagonist secreted by the endoderm may also act upstream of *Tbx1* in development. *Chordin*$^{-/-}$ mice recapitulate the *Tbx1*$^{-/-}$ phenotype; the caudal arches do not form and embryos have a small otic vesicle at E9.5 (Bachiller et al., 2003). Later in development, *Chordin*$^{-/-}$ mutants have persistent truncus arteriosus, great vessel defects, craniofacial defects including cleft palate and hypo or aplastic thymus and parathyroid glands (Bachiller et al., 2003). All domains of *Tbx1* expression are downregulated in these mutants and *Chordin* is also sufficient to induce *Tbx1* expression ectopically in Xenopus (Bachiller et al., 2003). This data suggests that *Bmp* signalling plays a vital role upstream of *Tbx1* in development. However, the molecular mechanisms through which this pathway may regulate *Tbx1* are unknown.

Alterations in RA homeostasis can also lead to a DGS-like phenotype (Roberts et al., 2006; Vermot et al., 2003) and recent studies have indicated that RA represses *Tbx1* expression (Roberts et al., 2005). *In vitro* experiments show that downregulation of *Tbx1* by RA is partly dependent on new protein synthesis suggesting that RA acts both directly and indirectly to regulate *Tbx1* (Roberts et al., 2005). Downstream effectors of RA in this pathway have yet to be identified and it remains to be confirmed if RA response elements (RAREs) identified upstream of *Tbx1* play a role in mediating the effects of RA (Roberts et al., 2005).

Vascular endothelial growth factor (*Vegf*), is an important signalling molecule required for cardiovascular development (Lambrechts and Carmeliet, 2004). Loss of a specific

isoform in mice, *Vegf*^{164} leads to craniofacial, cardiovascular and glandular defects reminiscent of DGS (Stalmans et al., 2003). Evidence for a genetic interaction between *Vegf* and *Tbx1* comes from experiments which show that *Tbx1* is downregulated in *Vegf*^{164}-deficient mice. In zebrafish, decreasing *vegf* levels enhance the PAA and cartilage defects induced by *tbx1* knockdown (Stalmans et al., 2003). In humans, specific promoter haplotypes of *VEGF* appear to correlate with increased risk of heart defects in DGS patients (Stalmans et al., 2003). These results suggest that *VEGF* may modulate the effects of *TBX1* disruption and contribute to the variability in expressivity observed in DGS.

1.9.2 Potential *Tbx1* targets

The signalling ligand, *Fgf8* is one of the most well studied potential *Tbx1* targets. It is expressed within the pharyngeal endoderm, ectoderm and splanchnic mesoderm during mouse development, in domains overlapping with *Tbx1* (Hu et al., 2004; Lewandoski et al., 1997; Meyers et al., 1998; Park et al., 2006). *Fgf8* is downregulated in the pharyngeal endoderm and splanchnic mesoderm of *Tbx1*$^{-/-}$ mice (Hu et al., 2004; Vitelli et al., 2002b; Zhang et al., 2006). Interestingly, Fgf8 is also downregulated in *Foxc1*$^{-/-}$*;Foxc2*$^{-/-}$ double mutants and *Chrd*$^{-/-}$ mice, genes which potentially act upstream of *Tbx1* (Bachiller et al., 2003; Seo and Kume, 2006). *Fgf8* hypomorphs exhibit a range of defects reminiscent of *Tbx1*$^{-/-}$ mutants and DGS including caudal pharyngeal hypoplasia, OFT and PAA defects, craniofacial abnormalities and small or absent thymus glands (Abu-Issa et al., 2002; Frank et al., 2002). Cre-mediated deletion of *Fgf8* within *Tbx1* expression domains of the pharyngeal endoderm and mesoderm recapitulates the OFT defects exhibited by Fgf8 hypomorphs (Brown et al., 2004). Also, *Tbx1* can regulate enhancer elements located upstream of *Fgf8* in tissue culture assays (Hu et al., 2004). Together, these experiments suggest that *Fgf8* represents a good candidate for a direct target gene acting downstream of *Tbx1* in pharyngeal and heart development. However, subsequent studies have indicated that *Tbx1* and *Fgf8* may only interact in PAA development.

Tbx1$^{+/-}$;*Fgf8*$^{+/-}$ compound heterozygotes exhibit an increased penetrance of fourth PAA defects compared to single heterozygotes (Vitelli et al., 2002b). Notably, no other cardiovascular, craniofacial or glandular defects are present in these double mutants (Vitelli et al., 2002b). In addition, *Fgf8* knocked into the *Tbx1* locus only alters the

PAA phenotype (Vitelli et al., 2006). Tamoxifen-induced ablation of *Fgf8* within the pharyngeal endoderm of *Tbx1* heterozygotes (*Tbx1*$^{mcm/+}$;*Fgf8*$^{flox/+}$) at E9.5 also increases the penetrance of PAA defects (Vitelli et al., 2006). These experiments have led to the conclusion that the endoderm is the site of *Tbx1* and *Fgf8* interaction in arch artery development. However, recent studies examining the tissue and time specific requirements for these genes in PAA development suggest that the interaction between *Tbx1* and *Fgf8* in this process is more complex (Macatee et al., 2003; Park et al., 2006; Vitelli et al., 2006; Xu et al., 2005; Zhang et al., 2005). Firstly, conditional mutants have demonstrated that ectodermal *Fgf8* is specifically required for fourth PAA development although a role for endodermal *Fgf8* has not been ruled out (Macatee et al., 2003; Park et al., 2006). *Tbx1* is also required within the pharyngeal ectoderm for PAA development (Arnold et al., 2006b; Zhang et al., 2005). However, *Fgf8* is robustly expressed in the ectoderm of *Tbx1*$^{-/-}$ mutants demonstrating it is unlikely that these two genes interact in this tissue (Arnold et al., 2006b; Zhang et al., 2005). In addition, *Tbx1* is required early in development, between E7.5 and E8.5, for development of the fourth arch artery (Xu et al., 2005). In contrast, reduction of *Fgf8* expression within the endoderm of *Tbx1* heterozygotes at E9.5 is sufficient to increase PAA defects (Vitelli et al., 2006). Thus, it is still unclear whether *Fgf8* is directly regulated by *Tbx1*.

In addition to *Fgf8*, a number of other *Fgf* ligands are downregulated in *Tbx1*$^{-/-}$ mutants. *Fgf10* expression is diminished in the SHF domain and *Fgf3* is downregulated in the pharyngeal endoderm of *Tbx1*$^{-/-}$ embryos (Aggarwal et al., 2006; Hu et al., 2004; Kelly et al., 2004; Kochilas et al., 2002; Vitelli et al., 2002b). Even though *Fgf10* appears to be directly regulated by *Tbx1* in cell culture experiments (Xu et al., 2004), there is no evidence as yet to suggest an *in vivo* genetic interaction between *Fgf10* and *Tbx1* (Aggarwal et al., 2006; Kelly and Papaioannou, 2007). A combination of double and triple knockout mutants between *Tbx1*, *Fgf8* and *Fgf10* in the mesoderm and *Tbx1*, *Fgf8* and *Fgf3* in the endoderm has not revealed any genetic interaction in pharyngeal or heart development (Aggarwal et al., 2006; Kelly and Papaioannou, 2007). Considering that additional *Fgf* family members are also expressed in the pharyngeal region, for example *Fgf15* (Vincentz et al., 2005), *Fgf4* (Niswander and Martin, 1992) and *Fgf16* (Wright et al., 2003), it is possible that functional redundancy among *Fgf*s may have affected analyses of epistasis with *Tbx1*. Furthermore, the *Fgf* receptor, *Fgfr1* has recently been identified as downregulated in the pharyngeal endoderm and mesenchyme of *Tbx1*$^{+/-}$ and *Tbx1*$^{-/-}$ mutants and has been implicated in OFT development (Park et al.,

2006). Overall, these studies suggest that Fgf signalling plays an important role downstream of *Tbx1* in development. However, the precise functions of each *Fgf* ligand and receptor are still being investigated.

The transcription factor, *Pitx2* represents another downstream target of *Tbx1* (Nowotschin et al., 2006). *Pitx2* in involved in signalling pathways mediating left-right asymmetry during development and is left-asymmetrically expressed during development of the heart (Kitamura et al., 1999; Liu et al., 2002; Schweickert et al., 2000). Mouse knockouts of *Pitx2c*, the left-asymmetrically expressed isoform of *Pitx2*, exhibit PAA abnormalities, VSD, atrial septal defects (ASD), atrioventricular (AV) valve and OFT alignment defects (Kitamura et al., 1999; Liu et al., 2001; Liu et al., 2002). Analysis of the expression of *Tbx1* and *Pitx2* during development has demonstrated that both genes are asymmetrically expressed in the left SHF and *Pitx2* is downregulated in this domain in $Tbx1^{-/-}$ mutants (Nowotschin et al., 2006). *Tbx1* and *Pitx2* appear to genetically interact during cardiovascular development with $Tbx1^{+/-}$;$Pitx2^{+/-}$ double heterozygotes exhibiting more severe OFT alignment defects, VSD, ASD and AV valve defects than either heterozygote, alone. Furthermore, *in vitro* experiments show that *Tbx1* and *Nkx2.5* synergistically activate a *Pitx2* enhancer suggesting that *Pitx2* is a direct target of *Tbx1* (Nowotschin et al., 2006). In contrast to the SHF, *Tbx1* appears to act downstream of *Pitx2* during muscle development within the first pharyngeal arch (Shih et al., 2007). It is not known whether branchiomeric myogenesis is abnormal in $Tbx1^{+/-}$;$Pitx2^{+/-}$ mutants. However, these results highlight the fact that different interactions can occur between the same genes, depending on the tissue.

In order to identify additional targets of *Tbx1*, a microarray was carried out in our lab comparing the gene expression profile of *Tbx1*-null mutants to wild type embryos. This study identified a number of potential downstream *Tbx1* targets including *Gbx2*, *Gcm2*, *Pax9* and the RA-catabolizing enzymes, *Cyp26a1*, *b1* and *c1* (Ivins et al., 2005; Roberts et al., 2006).

Knockout mouse mutants of the transcription factor, *Gbx2* display pharyngeal and heart defects reminiscent of DGS including craniofacial, great vessel and outflow tract anomalies (Byrd and Meyers, 2005). *Gbx2* is down-regulated in both $Tbx1^{-/-}$ mice and *Fgf8* hypomorphs and *Tbx1* and *Gbx2* appear to genetically interact in PAA

development (A. Calmont and S. Ivins, pers.comm., (Byrd and Meyers, 2005)). In addition, compound *Gbx2*$^{+/-}$;*Fgf8*$^{+/-}$ heterozygotes display PAA defects not seen in single heterozygotes and also exhibit thymic anomalies (Byrd and Meyers, 2005). Altogether these results imply that *Fgf8* and *Gbx2* interact genetically and may be downstream of *Tbx1*.

RA is very important for pharyngeal development and dysregulation of RA levels recapitulates the DGS phenotype (see section 1.2.2). The *Cyp26* family of retinoic acid metabolising enzymes consist of three genes, *Cyp26a1*, *Cyp26b1* and *Cyp26c1* which encode enzymes required to catabolize the active retinoic acid metabolite to an inactive form (Fujii et al., 1997; White et al., 1996). In *Tbx1*$^{-/-}$ mutants, expression of the *Cyp26* genes is dysregulated in the pharyngeal region (Guris et al., 2006; Ivins et al., 2005; Roberts et al., 2006). Inhibition of *Cyp26* enzyme function in the chick phenocopies DGS and results in caudal pharyngeal arch and arch artery defects, a hypoplastic otic vesicle and OFT defects similar to *Tbx1*$^{-/-}$ mice which are considered to occur as a result of the subsequent increase in RA levels within these embryos (Roberts et al., 2006). These results suggest that the *Cyp26* genes act downstream of *Tbx1* in pharyngeal development however, it is unclear as yet whether they are direct or indirect targets.

1.10 AIMS AND OVERVIEW

Animal models of gene present on homologous regions of 22q11 have revealed that several of these genes contained within chromosome 22q11 may function in pharyngeal and heart development, the main processes affected in DGS patients. Considering the highly variable phenotype and lack of a critical minimally deleted region, these findings suggest that DGS is a contiguous gene syndrome. However, the role of *Tbx1* in DGS appears to be particularly important. It is the only gene in this region that has been shown to be dose-sensitive in mouse development and the only gene in which mutations have been associated with DGS in humans. The extremely variable DGS phenotype can also be at least partly explained by the dosage effects of *Tbx1* and sequence variations in *Tbx1* regulators and downstream genes. While the developmental role of *Tbx1* has been extensively studied, the genetic pathways which lie downstream have yet to be fully characterised and may reveal additional genes which modify the DGS phenotype.

The overall aim of this project was to identify and characterise genes important in the development of structures affected in DGS, namely the pharyngeal apparatus and heart. Multiple approaches were taken in order to achieve this aim. First, a microarray analysis of *Tbx1*-expressing cells was carried out to identify downstream targets of *Tbx1* (Chapter 3). This experiment required a novel technique to be optimised for isolation of *Tbx1-lacZ* expressing cells. To complement these studies, BAC recombineering experiments were also undertaken to generate a GFP-labelled *Tbx1* allele enabling easier isolation of *Tbx1* cells for future experiments (Chapter 4). One of the genes identified by microarray as a potential *Tbx1* target, *Hes1*, was further characterised. This revealed a previously unknown defect in craniofacial and cardiovascular development (Chapter 5). Finally, in a different approach to finding novel genes which may cause or modify a DGS-like phenotype, DGS patients without the typical deletion were investigated. FISH was used to map the breakpoint in DGS patients with t(11;22) translocations. This led to the identification of a potentially disrupted gene, *HIC2*, whose function was analysed using gene trap mouse models and which was shown to play a role in heart development (Chapter 6).

CHAPTER 2. METHODS

2.1 REAGENTS

All reagents were of AnalaR grade and supplied by Sigma Aldrich or BDH unless otherwise stated. Solutions were made using milliQ water and autoclaved where appropriate.

2.2 STOCK SOLUTIONS

20 x SSC	3 M NaCl, 0.3 M sodium citrate pH 7.0
FISH hybridisation buffer	50% FA, 10% dextran sulfate, 2 x SSC, 1 x PBS
ST buffer	0.05% Tween 20, 2 x SSC
TE pH 8.0	10 mM Tris-HCl ph 8.0, 1 mM EDTA pH8.0
LB broth	1% Bactotryptone, 0.5% Bactoyeast, 1% NaCl
LB agar	2% Bactoagar, 1% Bactotryptone, 0.5% Bactoyeast, 1% NaCl
NB buffer (10 x) (Bioline)	100mM Tris-HCl, 400 mM NaCl, 15 mM $MgCl_2$, 2.5 mM spermidine
10mM dNTP	10 mM dATP, 10 mM dCTP, 10 mM dGTP, 10 mM dTTP
TAE buffer (10 x)	0.4 M Tris-acetate, 10 mM EDTA pH 8.0
DNA ladder	50 ng/µl DNA ladder in 1 x loading buffer
Loading buffer (6 x)	10 mM Tris-HCl pH 7.5, 50 mM EDTA pH 8.0, 10% Ficoll 400, 0.4% Orange G
Tail lysis buffer	100 mM Tris-HCl pH 8.5, 5 mM EDTA pH 8.0, 0.2% SDS, 200 mM NaCl, 100 µg/ml proteinase K (added immediately prior to use)
TBE buffer (5 x)	0.45 M Tris-borate, 0.01 M EDTA pH 8.0
Prehybridisation buffer	50% formamide, 1.3 x 20xSSC, 5 mM EDTA pH 8, 50µg/ml yeast RNA, 0.002% Tween 20, 0.5% CHAPS, 100 µg/ml heparin in water.
PBTX	0.1% TritonX-100 in PBS
TBTX	50 mM Tris-HCl pH 7.5, 150 mM NaCl, 0.1% TritonX-100, water.

X-gal buffer	20 mM $K_3Fe(CN)_6$, 20 mM $K_4Fe(CN)_6$-$3H_2O$, 5 mM EGTA, 2 mM $MgCl_2$, 0.02% NP40, 0.01% Deoxycholate, PBS. 1 mg/ml X-gal is added immediately prior to use.

2.3 MOUSE STRAINS, BREEDING AND GENOTYPING

2.3.1 Mouse strains

Df1 and *Tbx1* mice were obtained from Antonio Baldini, Baylor college of medicine, Houston, Texas, USA. The *Df1* mice contain a 1.2 Mb deletion of chromosome 16 (Lindsay et al., 1999) and the *Tbx1* mice contain a non-functional *Tbx1* allele which was generated by knocking in a lacZ reporter gene into exon 5 of *Tbx1* (Lindsay et al., 2001). The mice were maintained on a C57Bl/6 background.

Hes1 mice were obtained from Francois Guillemot, National Institute for Medical Research, London, UK. The *Hes1* mouse was generated by replacing the first three exons with a PGK-*neo* cassette (Ishibashi et al., 1995). The mice were maintained on a MF1 background.

Hic2 gene trap (RRN127) mice were obtained from BayGenomics, University of California, San Francisco, USA, originally on a 129P2 background. The mice were crossed to a C57Bl/6 background. *Hic2* gene trap mice were generated by random integration of a pGT0Lxf gene trap vector into intron 2 of *Hic2*.

TgTbx1floxGFP mice were generated by Genoway (France) through pronuclear injection of fertilized C57Bl/6 oocytes with a modified *Tbx1*-containing RP23-35B9 BAC. Mice were maintained on a C57Bl/6 background.

Adult mice were paired overnight and the females were checked in the morning for the presence of a copulation plug. At midday, females with a copulation plug were considered to be at embryonic day (E) 0.5. Pregnant females were killed by cervical dislocation and the uterus was placed in DMEM + 25 mM HEPES for further dissection.

2.3.2 DNA extraction

2.3.2.1 Tail biopsies

DNA was extracted from tail tips taken from pups aged approximately 10 days for genotyping. 3 mm tail tips were digested with 4 µl 10 mg/ml proteinase K (Roche) in 400 µl tail lysis buffer (see stock solutions) at 55°C overnight. For DNA precipitation, 400 µl 100% isopropanol was added and samples were spun at 12 000 x g for 30 minutes at 4°C. The DNA pellet was washed in 70% ethanol and spun at 12 000 x g for 10 minutes at 4°C and finally the DNA pellet was resuspended in 200 µl TE pH 8.0. 2-4 µl was used for PCR.

2.3.2.2 Yolk sacs

As embryos were collected, corresponding yolk sacs were collected and mixed with 50 µl PBS and 2 µl 10 mg/ml proteinase K (Roche) and incubated at 55°C overnight. The following day, the yolk sac DNA mix was heated at 100°C for 5 minutes to inactivate the proteinase K and then spun down at 12 000 x g for 5 minutes. 2µl was used for PCR.

2.3.3 Genotyping

Genotyping of embryos was carried out by PCR analysis of yolk sac or tail tip genomic DNA using the following primers.

Table 2.1 Mouse mutant genotyping primers

Mouse line	Primer name	Sequence	Notes
Tbx1 (Lindsay et al. 2001)	TbxWTF3	AGTCTGGGGACTCTGGAAGG	wt allele
	TbxWTR3	AAGGCAGATCCTGCTACACC	
	TbxWTF3	AGTCTGGGGACTCTGGAAGG	mutant allele
	TbxTAR2R	TCGACTAGAGCTTGCGGAAC	
Df1 (Lindsay et al. 1999)	UFDTAR2F	TCTTTGTCAGCAGTTCCCTTT	mutant allele
	UFDTAR2R	TGGGCAATTGTTTAATCTTCC	
Hes1 (Ishibashi et al. 1995)	Hes1WT-F	CCCCTTTGCAGTCATCAAAG	wt allele
	Hes1WT-R	GCATTGCTCACTTACATCTTTC	
	Hes1polyA-F	GGGAGGATTGGGAAGACAAT	mutant allele
	Hes1intron3-R	GGCGGAAGTCTGGAAGAAAT	
Hic2	EN2-F	AACAAACTTGGCCTCACCAG	mutant allele
	EN2-R	GCCAAGGCCATACAAGTGTT	
TgTbx1floxGFP	GFPend_F	CCACTACCTGAGCACCCAGT	transgenic allele
	Tbx1intron1-R	GCCTGGAGAAAATCCACAGA	

2.4 DNA AMPLIFICATION BY POLYMERASE CHAIN REACTION

2.4.1 Primer design

Primers were designed using the Primer3 program (http://primer3.sourceforge.net/) and ordered through Sigma. Forward and reverse PCR primers were designed on the following criteria: GC content approximately 50-60%, length between 20-30bp, absence of repeat sequences and similar melting temperatures (Tm). Primers were checked on the Sigma ordering website to ensure they would not anneal to one another.

2.4.2 PCR primers

Table 2.2 Analysis of FACS-enrichment of *Tbx1* cells

Label	Primer name	Sequence (5' to 3')	Product size (bp)
GAPDH	mGAPDH-F	TGCACCACCAACTGCTTAG	175
	mGAPDH-R	GATGCAGGGATGATGTTC	
Tbx1-lacZ	IRESLACZ-F	TCGGTGCACATGCTTTACAT	166
	IRESLACZ-R	GTTTTCCCAGTCACGACGTT	
Tbx1-wt	Ex4-F	TTTGTGCCCGTAGATGACAA	238
	Tbx1ex6-R	AATCGGGGCTGATATCTGTG	

Table 2.3 BAC Recombineering primers

Primer label	Primer name	Sequence (5' to 3')	Product size (bp)
a	GFP-F	ACGTAAACGGCCACAAGTTC	186
b	GFP-R	AAGTCGTGCTGCTTCATGTG	
c	Iresgfp1880-F	GAGCAAAGACCCCAACGAGAA	1344 (-Kan), 3490 (+Kan)
d	mTbx1exon1-2-R	TGTCATCTACGGGCACAAAG	
e	mTbx1exon1-2-F	TGAAGAAGAACCCGAAGGTG	271
f	Exon4-IRES-R	AGACCCCTAGGAATGCTCGT	
g	GFPend-F	CCACTACCTGAGCACCCAGT	587
h	Tbx1intron1-R	GCCTGGAGAAAATCCACAGA	
i	SNP55Kbup-F	CACAATGGTGAGGTCTGTCG	212
j	SNP55Kbup-R	GACCTGGGTCCTTGTGAGAA	
k	SNP10Kbup-F	CACATTCACCTCACAGGCTCT	242
l	SNP10Kbup-R	CCTTTGCTGTCTGCATCTGA	
m	SNP50Kbdown-F	CTGTGATATCAATGTTCAAGCAAG	240
n	SNP50Kbdown-R	GAAACAGAGAGCAAGCACCTC	
o	pBACeamp-F	CGATATCCCGCAAGAGGCCCGGCA GTACCGGCATAACCAAGCCTATGC	
p	pBACeamp-R	CTTCTTAGACGTCAGGTGGCAC GGTGTGCGGTTGTATGCCTGCTGT GGATTGCTGCTGTGTCCTGCTTATC CCTCACGTTAAGGGATTTTGGTC	1121

2.4.3 PCR

Reactions were carried out in a final volume of 25 µl in PCR tubes. The following PCR mix and conditions were used for the majority of PCRs:

20-50 ng genomic DNA

1 x NB buffer

200 µM each dNTP

1.5mM $MgCl_2$

0.8 µM forward primer

0.8 µM reverse primer

1 U Taq Polymerase (Bioline)

In sterile, distilled water

The standard program used for most PCRs was 94°C for 2 minutes, followed by 30 cycles of 94°C for 30 seconds, an annealing temperature dependent on the primers used (typically between 55-65°C) for 30 seconds and an elongation step of 72°C for 30 seconds. An aliquot of each sample was checked by agarose gel electrophoresis.

2.4.4 Agarose gel electrophoresis

DNA was separated on a 1-2% agarose gel containing 0.5µg/ml ethidium bromide in 1 x TAE. An appropriate 100 bp or 1 Kb DNA ladder (Invitrogen) was also loaded. Samples were run in a 1/6th volume of loading buffer and gels were electrophoresed at 50-150V until the fragments had separated sufficiently. DNA was visualised by UV illumination.

2.5 SEQUENCING

2.5.1 Cycle sequencing

Cycle sequencing reactions were set up using BigDye Terminator v3.1 (Applied Biosystems) for running on the MegaBACE (Amersham Biosciences) which uses thedideoxynucleotide chain termination method for sequencing. Sequencing reactions were carried out in 10 µl reaction volumes as follows: 3 µl miniprep plasmid DNA, 5pmol forward or reverse primer and sterile water were heated to 95°C for 5 minutes then 2 µl dilution buffer and 1 µl BigDye premix was added. The sequencing program used consisted of a denaturation step of 95°C for 5 minutes then 36 cycles of 95°C for

20 seconds, 50°C for 10 seconds and 60°C for 3 minutes. The reaction volume was topped up to 20 μl with sterile water.

Samples were sequenced by an in house sequencing facility. Files from the MegaBACE were downloaded in ABD format and checked using the Sequencher v4.2 program.

2.6 REVERSE-TRANSCRIPTION-POLYMERASE CHAIN REACTION

2.6.1 RNA extraction

RNA was extracted from tissues using 1ml Trizol reagent (Invitrogen). The tissue was homogenized by passing the sample twice through a 25-gauge needle then the sample was left to sit at room temperature for 5 minutes to allow complete dissociation of nucleoprotein complexes. 200 µl of 49:1 chloroform:isoamyl alcohol was added to each sample and vortexed for 30 seconds. The samples were then left for 2 minutes at room temperature before being spun at 12 000 x g for 5 minutes at 4°C to separate the aqueous, RNA-containing phase from the organic phase. The aqueous phase was collected into another eppendorf tube and 500 µl ice-cold isopropanol was added and the samples incubated at -20°C for 1 hour to overnight. The sample was then centrifuged at 12 000 x g for 30 minutes at 4°C to pellet the RNA and subsequently the pellet was washed with 1 ml of 70% ethanol and spun again at 12 000 x g for 10 minutes. Finally, the RNA pellet was resuspended in 50 µl RNAse-free water.

2.6.2 Reverse transcription (RT) and RT-PCR

cDNA was synthesized using 1-5 µg total RNA which was added to 0.5 µl 500 ng/µl random primers (Promega), 1 µl 10 mM dNTP and water to a final volume of 12 µl. This mixture was incubated at 65°C for 5 minutes then placed on ice. 4 µl 5 x reverse transcriptase buffer and 2 µl 100 mM DTT were added to the mix which was then heated to 25°C for 2 minutes. 1 µl 200 Units/µl Superscript reverse transcriptase II (Invitrogen) and water were added to a total volume of 20 µl and the mixture was incubated at 25°C for 10 minutes, 42°C for 50 minutes and finally, 70°C for 15 minutes to inactivate the reaction.

2.7 CLONING

2.7.1 Plasmid mini-preps

IMAGE clone plasmid DNA was received as a culture streaked onto an agar slope (Geneservice, UK). On arrival, bacteria were streaked out onto LB plates containing the appropriate antibiotic and left to grow overnight at 37°C. A culture of 3ml LB broth containing the appropriate antibiotic was inoculated with one colony and incubated at 37°C, shaking overnight. 15% glycerol stocks were prepared and stored at -80°C. Purified plasmid DNA was isolated using the Spin miniprep kit microcentrifuge protocol (Qiagen). Plasmid DNA was eluted in either water or Buffer EB. Bacterial artificial chromosomes (BACs) were received as either stab cultures (BAC PAC) or glycerol stocks (Invitrogen).

2.7.2 Digests

Digests of plasmid DNA were carried out in a total volume of 30 µl using 1-2 µg plasmid DNA, 3 µl 10 x enzyme buffer, 0.3 µl 100 x BSA, 1-2 units of enzyme and water. The plasmids were digested at the appropriate temperature for optimal enzyme activity for 2 hours and then run on an agarose gel for analysis.

Digests of BAC DNA were carried out in a total volume of 50 µl using 20 µl BAC miniprep DNA, 5 µl 10 x enzyme buffer, 0.5 µl 100 x BSA, 1-2 units of enzyme and water. BACs were digested at the appropriate temperature for optimal enzyme activity for at least 2 hours and then run on an agarose gel for analysis.

2.7.3 Gel extraction

Gel extraction was carried out to isolate and purify DNA fragments from agarose gels. The Qiagen QIAquick gel extraction kit was used following the manufacturer's instructions and DNA was eluted from the column in 30 µl water.

2.7.4 De-phosphorylation of plasmids

Digested plasmids were de-phosphorylated to remove the phosphate groups from the 5'-ends to prevent self-ligation of the vector. The following components were mixed together: 30 µl gel-purified, digested plasmid DNA vector, 5 µl 10 x SAP buffer (USB), 0.5 units Shrimp Alkaline phosphatase (SAP) (USB) and water to make a total volume of 50 µl. The mixture was incubated at 37°C for 1 hour, then at 65°C for a further 15 minutes to inactivate SAP.

2.7.5 Oligonucleotide annealing

To ligate oligonucleotides (oligos) into a vector, oligo ligation was carried out according to the following protocol: 2.5 μM each of two complementary oligos was added to 10 mM $MgCl_2$ and 20 mM Tris-HCl pH7.5 in a final volume of 100 μl. The oligos were denatured at a few degrees below their melting temperature for 5 minutes and allowed to cool to room temperature for at least 10 minutes to allow annealing of the complementary oligos.

2.7.6 Ligation

Ligation of the plasmid vector and the annealed oligos was carried out by mixing together the following components: 100ng plasmid, 1 μl 10 x ligation buffer (Promega), 0.25-3 μl annealed oligos, 3 units T4 DNA ligase (Promega) and water to make a total volume of 10 μl. The vector and oligo were allowed to ligate overnight at 4°C.

2.7.7 Transformation

Transformation of the plasmid DNA into subcloning efficiency DH5α competent cells (>10^7 cfu/μg DNA, Gibco BRL) was carried out according to the following protocol: 3 μl ligation reaction (from 2.7.6) or 1-10 ng plasmid DNA was added to 30 μl thawed DH5α competent cells and incubated on ice for 20 minutes. The cells were heat shocked by incubating at 37°C for 20 seconds and then placed back on ice. 900 μl LB broth was added and the cells were incubated at 37°C, shaking for 1 hour for expression. After expression, the cells were plated onto LB agar plates containing the appropriate antibiotic and incubated at 37°C overnight.

2.8 BAC RECOMBINEERING

2.8.1 Preparation of BAC DNA

2.8.1.1 BAC Maxiprep

Bacterial artificial chromosomes (BACs) were received as either stab cultures (BAC PAC) or glycerol stocks (Invitrogen). On arrival, bacteria were streaked out onto LB plates containing the appropriate antibiotic, either 20 μg/μl chloramphenicol or 15 μg/μl kanamycin and left to grow overnight at 37°C. A starter culture of 3ml LB broth with the appropriate antibiotic as above was inoculated with one colony and incubated at

37°C, shaking overnight. 1 ml of the starter culture was transferred to a 2 L flask containing 500 ml LB broth with the appropriate antibiotic and incubated at 37°C, shaking overnight. 15% glycerol stocks were prepared and stored at -80°C.

Cells were harvested and the DNA was isolated using the maxiprep plasmid purification kit protocol for the isolation of low copy number plasmids (Qiagen), following manufacturer's instructions. The final DNA pellet was dissolved in 100µl TE pH 8.0. Quality and quantity of the BAC DNA was determined by spectrophotometric measurement of OD_{260}/OD_{280} values.

2.8.1.2 BAC Miniprep

A culture of 2ml LB broth containing the appropriate antibiotic was inoculated with one colony and incubated at 32°C or 37°C, shaking overnight. The following day the culture was spun for 10 minutes at 400 x g and the pellet resuspended by vortexing in 0.3 ml P1 solution (see stock solutions). The DNA was lysed using 0.3 ml P2 solution in which the mixture was gently shaken and allowed to sit for 5 minutes at room temperature. Renaturation of BAC DNA was carried out by the slow addition of 0.3 ml P3 solution. The mixture was incubated on ice for 5 minutes then spun at 8000 x g for 10 minutes at 4°C. The supernatant was transferred to another eppendorf tube containing 0.8 ml ice-cold isopropanol, mixed and incubated on ice for 5 minutes. The mixture was then spun for at 12000 x g for 15 minutes at 4°C. The DNA pellet was washed with 0.5 ml 70% ethanol and spun at 12000 x g for 5 minutes at 4°C. BAC DNA was resuspended by addition of 40 µl TE pH 8 without pipetting to prevent DNA shearing.

2.8.2 Making electrocompetent cells

EL250 or SW105 bacterial cells are modified BAC host strains that carry a defective prophage supplying functions which protect and recombine electroporated, linear DNA (Lee et al., 2001). These functions are under tight control of the temperature-sensitive λ repressor so recombination functions can be transiently supplied by increasing the temperature to 42°C (Lee et al., 2001). EL250 cells were therefore maintained at 32°C.

To prepare electrocompetent cells, 2 ml overnight LB broth cultures were grown at 32°C and then diluted 50-fold in LB broth and grown to an OD_{600} 0.5-0.7. 10 ml cultures were induced for recombination gene expression by shifting the cells to 42°C

for 15 minutes and then chilled on ice for 20 minutes. Cells were then spun at 5500 x g for 5 minutes at 4°C and washed with 1.5 ml ice-cold, sterile water which was repeated three times. Finally, cells were resuspended in 50 µl ice-cold, sterile water and electroporated. For electroporation of BACs, the induction step was omitted.

2.8.3 Electroporation into EL250/SW105 cells

Transformation of DNA into EL250/SW105 cells was carried out by electroporating 300 ng BAC DNA or linearised, plasmid DNA into 50 µl of ice-cold, competent cells in 0.1 cm cuvettes in a Bio-Rad gene pulser set at 1.8kV. 1 ml of LB broth was added after electroporation and the cells were grown for 1.5 hours, shaking at 32°C and then plated onto LB agar plates containing the appropriate antibiotic.

2.8.4 Removal of the kanamycin/neomycin resistance genes

Prior to pronuclear injection of the recombined BAC into oocytes to generate transgenic mice, the kanamycin/neomycin selectable markers were removed. 2 ml LB broth overnight cultures were prepared from individual colonies, diluted 50-fold in LB medium and grown at 32°C to an OD_{600} of 0.5. *flpe* expression in EL250/SW105 cells was induced by addition of 0.1% L-arabinose in LB medium and cells were incubated for 1 hour, shaking at 32°C. The bacterial cells were then diluted 10-fold in LB medium, grown for another hour and then serial dilutions were plated onto LB agar with 20 µg/µl chloramphenicol. The plates were incubated overnight at 32°C and the next day colonies were replica-plated onto LB agar plates containing 15 µg/µl kanamycin to test for loss of kanamycin resistance and on chloramphenicol plates to allow recovery of kan-sensitive colonies.

2.8.5 Field Inversion Gel Electrophoresis (FIGE)

FIGE was used to separate large fragments of DNA obtained after digesting BAC DNA. FIGE works on the principle that by altering the electric field between spatially distinct electrodes, large DNA fragments are able to reorient and move at different speeds through the agarose gel allowing for better separation of large DNA molecules. There is a net downward migration of the DNA through the gel by using an asymmetric voltage. BAC DNA fragments were resolved by running the DNA in a 1% agarose gel containing 0.5 µg/µl ethidium bromide in 0.5 x TBE for 16 hours with a switch time of

0.1-0.4 seconds, a 21% linear switch time ramp, a forward voltage of 180V and a reverse voltage of 120V. DNA fragments were visualised by UV illumination.

2.9 FLUORESCENT *IN SITU* HYBRIDISATION (FISH)

2.9.1 Mammalian cell culture

Epstein Barr Virus (EBV)-transformed patient B-cell lymphoblastoid cell lines were cultured in RPMI 1640 medium with glutamax (Gibco) supplemented with 10% fetal calf serum and 1% penicillin/streptomycin (Gibco). Cells were maintained at 37°, 5% CO_2 in a humidified atmosphere. Patient cell lines FN and FY1198 were obtained from ECACC, Porton Down, UK and Dr James Lespinase, respectively.

2.9.2 Preparation of metaphase spreads

Metaphase spreads were prepared from 50ml patient cell cultures. Cells were spun down and resuspended in fresh culture medium 24 hours before harvesting. Mitotic arrest was induced by incubating a uniform cell suspension with colcemid (10 μg/μl) (Gibco) to a final concentration of 0.1 ml/10 ml for one hour at 37°C, 5% CO_2. Cells were subsequently spun down at 500 x g for 8 minutes and the supernatant removed. The cell pellet was resuspended in 25-30 ml hypotonic 75 mM KCl to spread out the chromosomes and incubated at 37°C, 5% CO_2 for 10 minutes. Cells were again spun at 500 x g for 8 minutes, supernatant discarded and cells were suspended in 25-30 ml fresh fixative solution (3:1 methanol:glacial acetic acid). This fixative wash step was repeated for a total of three times. The cell pellet was then resuspended in 3-5 ml fixative solution and stored at -20°C.

To make metaphase spreads, 1 ml of the cell suspension was spun at 2000 x g for 1 minute and resuspended in 300 μl fresh fixative and dropped from 20-30cm onto glass slides that had been kept at -20°C and subsequently humidified. This enabled the chromosomes to spread out when the cells burst as they are dropped from above. Slides were then dried and a diamond marker was used to locate the drop. Finally the slides were flooded with fresh fix solution, left to dry and the metaphase spreads were stored at 4°C.

2.9.3 Nick translation and precipitation of BAC probes

To obtain 300-500 bp labelled DNA fragments suitable for FISH, purified BAC DNA was nick translated using a nick translation kit (Vysis). The nick translation reaction incorporates a fluorescent label into the DNA probes by nicking the DNA using deoxyribonuclease I (DNase I) and then incorporating the fluorescent nucleotide into the DNA strand as it repairs the nicks using E. Coli DNA polymerase I.

Reactions were carried out in a total volume of 50 µl containing: 1 µg BAC DNA, 0.5 nM dTTP, 1nM each of dATP, dCTP, dGTP, 1 x nick translation buffer, 5 units nick translation enzyme and nuclease-free water. The component were added in the above order, mixed by pipetting and incubated at 15°C for 8 hours then stopped by heating to 70°C for 10 minutes.

Probes were precipitated using human Cot-1 DNA (Invitrogen) and herring testes DNA (Promega) in order to suppress cross-hybridisation to human repetititve DNA and remove unincorporated nucleotides. 20 µl of nick translated DNA was added to 6 µg Cot-1, 12 µg herring testes DNA and water to a total volume of 50 µl, mixed by pipetting and then 4 µl 3 M sodium acetate and 112 µl 100% ethanol were added. The mixture was put at -80°C for at least 40 minutes then centrifuged at 12 000 x g for 30 minutes at 4 °C. The supernatant was removed and the pellet resuspended in 40 µl hybridisation buffer and incubated at 37°C for at least 2 hours. Probes were stored at -20°C.

2.9.4 Fluorescence *in situ* hybridisation, washes and detection

Metaphase spread slides were incubated in 2 x SSC for 1 hour at 4°C then dehydrated in 70% ethanol, 90% ethanol and 100% ethanol for 5 minutes each and left to air dry. 5 µl each of the precipitated, nick translated BAC probes were mixed with the 5 µl of the control BAC probe and pipetted onto the centre of the slide. A 22 x 22 mm coverslip was applied and sealed with a thick layer of vulcronising rubber solution (Weldtite). Slides were placed in a hybridisation chamber and denatured at 72°C for 2 minutes then incubated at 37 °C overnight in the dark.

After incubation, the slides were kept in the dark, the coverslip was removed and slides were washed in ST buffer for 5 minutes at room temperature, 0.4 x SSC, 0.3% NP-40 at 72°C for 2 minutes and then washed again in ST buffer twice for 5 minutes each. Slides were left to dry before applying vectastain mounting medium containing DAPI (Vector Labs) to stain chromosomal DNA. Coverslips were applied and sealed with nail polish. Slides were viewed under a Zeiss Axioskop fluorescent microscope and images were taken using a Photometrics camera with Smartcapture software.

2.10 MICROARRAY

2.10.1 Fluorescent Activated Cell Sorting (FACS)

2.10.1.1 CMFDG labelling of a single cell suspension

E9.5 embryos were dissected out in DMEM + 25 mM HEPES containing 10% FCS. The embryos were staged by somite counting and *Df1/Tbx1*^{lacZ} embryos were separated from *Df1/+*, *Tbx1*$^{+/lacZ}$ and wild type embryos. CMFDG loading was carried out using the Detectagene green CMFDG lacZ gene expression kit (Molecular Probes). In order to reduce background fluorescence by blocking endogenous lysosomal β-galactosidase activity, the embryos were incubated in 0.3mM chloroquine diluted in DMEM + 25 mM HEPES containing 5% FCS and incubated at 37°C, 5% CO_2 for 30 minutes. Following three rinses in PBS, embryos were incubated in 0.25% trypsin (Gibco) in PBS for approximately 30 minutes during which the embryos were dissociated into a single cell suspension by trituration every 5-10 minutes using plastic pipettes, starting with larger tips and moving down to smaller tips. The single cell suspension was spun down at 300 x g for 3 minutes and resuspended in pre-warmed (10 minutes at 37°C) 50 μM CMDFG, 200 μM verapamil in 5% FCS/DMEM + 25 mM HEPES and incubated for 30 minutes at 37°C, 5% CO_2. The verapamil was used to inhibit efflux of the fluorescent, CMFDG-glutathione adduct from the cells. Following incubation, the cells were placed on ice and diluted to approximately 1-3 million cells/mL with 5%FCS/DMEM + 25 mM hepes. 1 mM PETG was added to stop the reaction and 1.5 μM propidium iodide was added to identify dead cells. Cells were flow-sorted as soon as possible.

2.10.1.2 FACS analysis

Single cell suspensions were sorted using the Beckman Coulter Epics Altra cell sorter (High Wycombe) and analysed using the Expo2 software (Beckman Coulter) or using the MoFlo cell sorter (Dakocytomation,Fort Collins, Colorado) and analysed using the Summit v4.11 software (Dakocytomation). Cells were gated on the basis of forward scatter and side scatter characteristics to exclude debris. Propidium Iodide (PI) was used as a viability stain to exclude all dead cells. Cells which were fluorescent for FDG above background were collected into 10%FCS/DMEM + 25 mM HEPES and placed on ice. At least 50000 events were acquired for analysis.

Sorted cells were immediately spun down at 300 x g for 4 minutes and resuspended in 800 µl Trizol (Gibco BRL). The cells were then homogenized by passing them twice through a 25-gauge needle and stored at -80°C.

2.10.2 Microarray

2.10.2.1 RNA extraction

Sorted cell samples in Trizol were thawed and 250 µg/ml glycogen (Roche) or 50 µg/mL Glycoblue (Ambion) was added as an RNA co-precipitant to improve yield. The sample was then vortexed at high speed for 10 seconds and the genomic DNA was sheared by passing the sample twice again through a 25-gauge needle. 160 µl of 49:1 chloroform:isoamyl alcohol was added to each sample and vortexed for 30 seconds. The samples were then spun at 12 000 x g for 5 minutes at 4°C to separate the aqueous, RNA-containing phase from the organic phase. The aqueous phase was collected into another eppendorf tube and 400 µl ice-cold isopropanol was added and the samples incubated at -20°C for 1 hour to overnight. The sample was then centrifuged at 12 000 x g for 30 minutes at 4°C to pellet the RNA and subsequently the pellet was washed with 200 µl 70% ethanol and spun again at 12 000 x g for 10 minutes. Finally, the RNA pellet was resuspended in 30 µl RNAse-free water.

2.10.2.2 RNA amplification

The Microarray Target Amplification kit (Roche) was used for the PCR-based random amplification of cDNA from small amounts of RNA, while still maintaining the relative

gene expression profile of transcripts between samples. This protocol works by using a unique Target Amplification Sequence (TAS) primer with no known homology to any sequence in public databases to reverse-transcribe the total RNA population and also for the subsequent PCR amplification of cDNA.

2.10.2.2.1 First strand cDNA synthesis

RNA was amplified according to the instructions provided in the microarray target amplification kit. For first strand cDNA synthesis, the RNA sample or 50 ng control RNA was added to 50 pmol of the TAS-T7 Oligo $(dT)_{24}$ primer and water to a final volume of 10.5 µl and incubated at 70°C for 10 minutes. The samples were then placed on ice and the following components added: 1 x reverse transcriptase buffer, 10 mM DTT, 1 mM dNTP mix and 25 units of reverse transcriptase enzyme mix to a total volume of 20 µl. Samples were vortexed and spun down in a centrifuge and then incubated in a thermal cycler at 42°C for 60 minutes.

2.10.2.2.2 Second-strand cDNA synthesis

The RNA:DNA hybrid was then denatured at 95°C for 5 minutes and the sample placed on ice. For second-strand cDNA synthesis, the following components were added: 0.5 mM dNTP mix, 500 pmol TAS-$(dN)_{10}$ primer, 1 x Klenow reaction buffer, 13.5 µl water and 8 units Klenow enzyme to a total volume of 50 µl. The sample was vortexed and spun down in a centrifuge and then incubated in a thermal cycler at 37°C for 30 minutes.

2.10.2.2.3 Purification of double-stranded cDNA

To purify the double-stranded cDNA, the Microarray Target Purification kit (Roche) was used. 1.25 µl carrier RNA and 50 µl double-distilled water was added to each sample. 400 µl Binding Buffer + 4 µl β-mercaptoethanol (Sigma) and 200 µl 100% ethanol was then added and the sample was mixed before adding it to a High Pure filter tube and spinning at 6000 x g for 15 seconds. The flowthrough was discarded and 500 µl wash buffer was added before spinning again at 6000 x g for 15 seconds. 300 µl wash buffer was then added and the samples were spun at 12 000 x g for 1 minute. After discarding the wash buffer, the filter tube was put into a new collection tube and spun again at 12 000 x g for 1 minute to remove any residual wash buffer. Finally, the filter tube was placed in a new collection tube and the purified double-stranded cDNA

was eluted with 50 µl Elution buffer B by incubating for 1 minute at room temperature and then spinning at 6000 x g for 1 minute.

2.10.2.2.4 First PCR (Optimisation) and second PCR (random amplification of entire mRNA population)

To determine the optimal number of cycles for amplification of each cDNA sample to ensure the reaction is in the exponential phase, an optimisation PCR was carried out. The PCR reaction contained the following components: 12.5 µl purified ds cDNA, 50 pmol TAS primer, 0.2 mM dNTP mix, 73 µl double distilled water, 1 x Expand PCR buffer and 5.25 units Expand enzyme mix to make a total volume of 100 µl. The following PCR conditions were used: the samples were denatured at 95°C for 2 minutes followed by 30 cycles of amplification consisting of a denaturation at 95°C for 30 seconds, annealing at 55°C for 30 seconds and elongation at 72°C for 3 minutes. 10 µl samples were removed at 16, 18, 21, 24, 27 and 30 cycles for analysis by agarose gel electrophoresis on a 1.2% agarose gel. The optimum cycle for amplification of each sample (in which the reaction was in the exponential phase) was determined as the cycle at which a visible smear of DNA could be seen within a range of 0.7 to 2.2 Kb. Following determination of optimal cycle number for each sample, PCR amplification was carried out as outlined in the protocol above.

2.10.2.2.5 Purification of PCR product

The amplified PCR product was purified using the microarray target purification kit as outlined above for the purification of double-stranded cDNA. Purification was initiated by addition of 400 µl Binding buffer + 4 µl β-mercaptoethanol to the PCR product. The purified PCR product was eluted in 50 µl Elution buffer B. The concentration and purity of the PCR product was determined by measuring the absorbance at 260 nm on a Nanodrop spectrophotometer (Labtech International).

2.10.2.3 In vitro transcription

The Microarray RNA Target Synthesis kit (Roche) was used to generate Biotin-UTP labelled transcripts at a labelling density of 1:3. In a sterile tube, *in vitro* transcription components were added in the following order: Sterile, RNAse-free water, 4 µl NTP mix A (1:3 label density consisting of 25 mM ATP, 25 mM CTP, 25 mM GTP and 16.7 mM UTP), 1.67 mM Biotin-UTP (Roche), 10 mM DTT, 300 ng purified, amplified

PCR product, 1 x transcription buffer and 3 µl transcription enzyme blend to make a total of 20 µl. *In vitro* transcription was carried out by incubating at 37°C for 3 hours.

2.10.2.3.1 Purification of Biotin-UTP labelled cRNA

The Affymetrix GeneChip sample cleanup module (Qiagen) was used to purify the Biotin-UTP labelled cRNA according to the following protocol: 60 µl of RNAse-free water was added to the cRNA and mixed by vortexing for 3 seconds. Then 350 µl IVT cRNA Binding buffer was added to the sample and mixed by vortexing followed by the addition of 250 µl 100% ethanol. The sample was added to the IVT cRNA Cleanup Spin column and centrifuged for 15 seconds at 8 000 x g. The spin column was then transferred to a new collection tube, washed with 500 µl IVT cRNA Wash buffer and spun for 15 seconds at 8 000 x g. The flow-through was discarded and the column washed with 500 µl 80% ethanol and then spun again for 15 seconds at 8 000 x g. After the flow-through was again discarded, the spin column was centrifuged for 5 minutes at 12 000 x g to remove any residual wash buffer. Finally, the spin column was put into a new collection tube and the purified cRNA was eluted by spinning at 12 000 x g for 1 minute after the addition of 11 µl of RNAse-free water to the spin column and spinning again after the addition of 10 µl RNAse-free water. The concentration and purity of the cRNA samples was determined by measuring the absorbance at 260 nm on a Nanodrop spectrophotometer (Labtech International).

2.10.2.4 Microarray hybridisation

Six *Df1/Tbx1*^{lacZ} samples and six *Tbx1*$^{+/lacZ}$ samples were hybridised onto MOE430 v2 oligonucleotide array chips (Affymetrix) consisting of over 45000 probe sets representing over 34000 mouse genes. Purified, biotin-UTP labelled cRNA was fragmented and hybridised onto MOE430 v2 microarray chips according to Affymetrix protocols and this was carried out by the ICH Gene Microarray Centre (London UK). Arrays were scanned using the Affymetrix GeneChip Scanner and array images were captured using the Microarray Analysis Suite v5 software package (MAS, Affymetrix). The report files were examined to establish quality of the hybridisation.

2.10.2.5 Genespring analysis

Genespring software version 4.2.1 (Silicon Genetics) was used for the comparison of *Df1/Tbx1*^{lacZ} and *Tbx1*$^{+/lacZ}$ microarrays. Per chip normalisation used the 50th percentile

of all measurements as a positive control for each sample. Measurements for each gene were divided by this synthetic positive control. The bottom tenth percentile was used as a test for correct background subtraction. Per gene normalisation was then carried out, for which all *Tbx1*$^{+/lacZ}$ samples were normalised to 1 and all *Df1/Tbx1*^{lacZ} samples were normalised to the *Tbx1*$^{+/lacZ}$ samples. The data from the mouse MOE430 v.2 microarray chips was then filtered to exclude genes with signals below the raw value of 22. Seventeen out of twenty *Df1* genes represented on the chip were expressed above threshold levels. Iterative analyses were then carried out on the normalised data to determine the appropriate filters to apply to identify the majority of hemizygously-expressed *Df1* genes. Fourteen out of 17 *Df1* genes were downregulated to 0.83 in 5 out of 6 chips hybridised with the *Df1/Tbx1*^{lacZ} target. The resulting gene list was statistically analysed using the non-parametric t-test (Wilcoxon-Mann-Whitney/Kruskal-Wallis test) with a p-value cutoff of 0.05 and the Benjamini and Hochberg False Discovery Rate multiple testing correction was applied. In addition, the reciprocal analysis was conducted on the filtered, normalised data to identify genes showing relative, normalised expression of 1.17 or more in 5 out of 6 chips hybridised with the *Df1/Tbx1*^{lacZ} target. The resulting gene list was statistically analysed using the same t-test and multiple testing correction as above.

2.10.3 Quantitative Real Time PCR

RNA used for quantitative real time PCR was obtained from an independent pool of *Tbx1*$^{+/lacZ}$ and *Df1/Tbx1*^{lacZ} cells isolated from 10 E9.5 *Df1/Tbx1*^{lacZ} embryos and 26 E9.5 *Tbx1*$^{+/lacZ}$ embryos, ranging in somite number from 18 to 24. RNA collected from pools of *Tbx1*$^{+/lacZ}$ and *Df1/Tbx1*^{lacZ} cells was extracted, amplified and *in vitro* transcribed as per sections (see Microarray sections 2.10.2.1, 2.10.2.2 and 2.10.2.3). However, for *in vitro* transcription, 200 ng purified, amplified PCR product was used with NTP mix D (25 mM ATP, 25 mM CTP, 25 mM GTP and 25 mM UTP (Roche)). The cRNA was purified according to section 2.10.2.3.1.

2.10.3.1 cDNA synthesis

cDNA was synthesized using 500 ng PCR-amplified *Tbx1*$^{+/lacZ}$ and *Df1/Tbx1*^{lacZ} cRNA which was added to 0.5 µl 500 ng/µl random primers (Promega), 1 µl 10 mM dNTP and water to a final volume of 12 µl. This mixture was incubated at 65°C for 5 minutes then placed on ice. 4 µl 5 x reverse transcriptase buffer and 2 µl 100 mM DTT were added to

the mix, which was then heated to 25°C for 2 minutes. 1 µl 200 units/µl Superscript reverse transcriptase II (Invitrogen) and water were added to a total volume of 20 µl and the mixture was incubated at 25°C for 10 minutes, 42°C for 50 minutes and finally, 70°C for 15 minutes to inactivate the reaction. 230 µl of water was added to dilute the cDNA.

2.10.3.2 Quantitative real time PCR

PCR primers were designed to span one or more exons. Some primer sequences were obtained from Primerbank (http://pga.mgh.harvard.edu/primerbank/index.html), a public database of PCR primers specifically designed for use in real time PCR (Wang and Seed 03). Primers were synthesized by Sigma-Aldrich (UK) and sequences are included below (Table 2.4)

Reactions were carried out using MicroAmp™ (Applied Biosystems) optical strips and caps. Each amplification reaction contained 12.5 µl 2 x SYBR green PCR master mix (QIAGEN), 0.4 µl 20 µm forward and reverse primers, 5µl diluted cDNA and water in a total volume of 25µl. PCR conditions were 95°C for 15 minutes, followed by 40 cycles of 95°C for 15s and 60°C for 1 min at which stage fluorescence measurements were taken. . All reactions were performed in triplicate on an ABI PRISM 7000 Sequence Detection System (Applied Biosystems). Product specificity was determined by analysing dissociation curves. These curves highlight the melting temperature of the double-stranded product and the presence of primer dimers. The PCR products were also run on an agarose gel to check that the correct sized product was amplified. Expression values were determined using the DART-PCR analysis excel software which takes into account the amplification efficiency of each gene to obtain relative quantities (Peirson et al., 2003). Relative changes in gene expression were calculated by comparing the normalised expression values in *Df1/Tbx1*^{lacZ} samples to the normalised expression values in *Tbx1*$^{+/lacZ}$ samples. Expression values for each gene were normalised to *Gapdh* expression. Each gene was analysed in 3 separate experiments and values were reported as the mean fold change in *Df1/Tbx1*^{lacZ} cells relative to *Tbx1*$^{+/lacZ}$ cells which were designated a value of 1.

2.10.3.3 qRT-PCR primers

Table 2.4 qRT-PCR primers

Gene	Primer name	Sequence (5' to 3')	Product size (bp)	PrimerBank accession number
Plek	PLEK-F	ACAGCAGGACCACTTCTTCC	168	na
	PLEK-R	AGATACAAAGCCCCCAAGTC		
Gbx2*	GBX2-F	ACAATTTGCCTGGTCAGACTG	236	6753952a3
	GBX2-R	CACCTCGCTGAGTTTGAGGG		
Six2	SIX2-F	CGTGCTTGATGAAGCGGTGTG	129	na
	SIX2-R	GATACCGAGCAGACCATTGTC		
Dab2	DAB2-F	GATGCCAATCAACTGTTGAACA	166	na
	DAB2-R	GGATCAGAAGATGCAGGCTG		
Cyp26a1	CYP26A1-F	CTCATCCAGAGGATGCTTCC	119	na
	CYP26A1-R	CAATCACAGTGCCTAGCCAG		
Cyp26b1	CYP26B1-F	CTACCGCACTGTGCTGCAGA	159	na
	CYP26B1-R	ATCCTCACTGCGTGCCTGAC		
Cyp26c1	KCYP26C1-F	CAGCCATCACCAAAATCCAG	233	na
	KCYP26C1-R	AACCGTCCAGTTCAAAGGTG		
Nkx2.6*	NKX2-6-F	CTTTCTCGGTAGCTGACATTCTC	142	3098520a1
	NKX2-6-R	TCGCTGCTCTCAAACCATCC		
Cxcl4*	CXCL4-F	AGCTCATAGCCACCCTGAAG	175	na
	CXCL4-R	CATCGGAAGATTGCAGTTACA		
Smad7	SMAD7-F	GGCCGGATCTCAGGCATTC	153	6678778a1
	SMAD7-R	TTGGGTATCTGGAGTAAGGAGG		
Cdh1	CDH1-F	CAGGTCTCCTCATGGCTTTGC	175	6753374a1
	CDH1-R	CTTCCGAAAAGAAGGCTGTCC		
Notch3	NOTCH3-F	CCACAGGTGTGAACTGTGAA	153	na
	NOTCH3-R	GATGCACACTCATTGATCTCC		
Hes1	HES1-F	CCTCTGAGCACAGAAAGTCATC	151	na
	HES1-R	CAGAATGTCTGCCTTCTCTAGC		
Ndufa13*	NDUFA13-F	ACGGCCCCATCGACTACAA	120	12963633a1
	NDUFA13-R	CCTGGTTCCACCTCATCATTCT		
Crb3*	CRB3-F	CACCGGACCCTTTCACAAATA	130	29244038a1
	CRB3-R	CCCACTGCTATAAGGAGGACT		
Sema3c	SEMA3C-F	GGAGGAAGGAGGTTAAACTG	191	na
	SEMA3C-R	ACCACTTGTCTGTCACAACG		
Slit2*	SLIT2-F	GGCAGACACTGTCCCTATCG	154	30794374a1
	SLIT2-R	GTGTTGCGGGGGATATTCCT		
Lztfl1	LZTFL1-F	GGATTTGCTAAAGGCCCAAGA	134	15277319a3
	LZTFL1-R	GTTTGGCTGCTGCTAGGTTCT		
Isl1	ISL1-F	GACATGATGGTGGTTTACAGGC	209	31543007a3
	ISL1-R	GCTGTTGGGTGTATCTGGGAG		
Dsg2	DSG2-F	CTGGTCAAGCAGCTAAAGTAACA	154	22779879a2
	DSG2-R	GCCACAACCTTTGCAGTGTA		
Bmpr1a*	BMPR1A-F	CTCGTCGTTGTATTACAGGAGGA	169	6753194a3
	BMPR1A-R	ACTTGGCTCCAACTTACTTCATC		

Gene	Primer name	Sequence (5' to 3')	Product size (bp)	PrimerBank accession number
Tbx18	TBX18-F	ACCGTCTTCACAACTGTCACT	115	31560050a3
	TBX18-R	CCAAACCCATTCTGTTCCTCC		
Tle4*	TLE4-F	TTTACAGGCTCAATACCACAGTC	166	33859646a1
	TLE4-R	TGCACAGATAGCATTTAGTCGTT		
Daam1	DAAM1-F	GTAGAGACGGAGCTGGAGTATC	203	na
	DAAM1-R	GAAGAACTCATCTGGCTGGA		
Gsk3b	GSK3B-F	TGGCAGCAAGGTAACCACAG	189	9790077a1
	GSK3B-R	CGGTTCTTAAATCGCTTGTCCTG		
Pitx1*	PITX1-F	GAATCGTCCGACGCTGATCTG	153	6755070a2
	PITX1-R	GCTTGTGAAGTGAGTGCGTTG		
Scml2*	SCML2-F	TGGAGCCAGGTTACGTCTAC	90	18875336a3
	SCML2-R	CCAACAGGTTGTATGTCTGATGA		
FoxP1	FOXP1-F	CAATGCAGCTTTACAGGCTTC	151	na
	FOXP1-R	TGTCACTCTCGTTGCTGTTG		
Socs3	SOCS3-F	GGAGCCCCTTTGTAGACTTC	237	na
	SOCS3-R	GGAAACTTGCTGTGGGTGAC		
Lrr16	LRRC16-F	CAGGATCACCTCAACTCCTTAC	237	na
	LRRC16-R	AATCCTTCAGTTGTTCATCCAC		
Tmeff1	TMEFF1-F	GAGAACGTTGGGTGTGTATG	168	na
	TMEFF1-R	CATCTGTGTCTGTGCAGTGG		
Fstl1	FSTL1-F	ATGACCTGTGATGGAAAGAATC	212	na
	FSTL1-R	GCTGCAGACTCTGTGTGTACTG		
Efnb2	EPHRINB2-F	GTGCCAGACAAGAGCCATGAA	169	31542597a2
	EPHRINB2-R	GGTGCTAGAACCTGGATTTGG		
Tbx20*	TBX20-F	AAACCCCTGGAACAATTTGTGG	171	12082750a1
	TBX20-R	CATCTCTTCGCTGGGGATGAT		
Pafah1b2*	PAFAH1B2-F	GCAGCTATTCCACATGCCG	156	6679199a1
	PAFAH1B2-R	CCGCCATATCTCGTACTGCT		
Dkk1*	DKK1-F	CTCATCAATTCCAACGCGATCA	105	31542557a1
	DKK1-R	GCCCTCATAGAGAACTCCCG		
Cxcl12*	CXCL12-F	TGCATCAGTGACGGTAAACCA	166	28386193a3
	CXCL12-R	TGCACACTTGTCTGTTGTTGTT		
Suv39h2*	SUV39H2-F	ATCTACGAATGCAACTCAAGGTG	110	31543790a1
	SUV39H2-R	CCACAGCCATTGCTAGTTCTAA		
Prickle1*	PRICKLE1-F	CAACATCACAGGGGCATCAG	138	na
	PRICKLE1-R	GTGCAGCATGGAAGAGTTCA		
Numb	NUMB-F	GATGCCAAGAAAGCTGAGAC	216	na
	NUMB-R	TCTTCTGGCTAAGAGCAGGA		
Rhbdl1*	RHBDL1-F	TTGCCCAGATCATCGTGTTCC	182	21450189a3
	RHBDL1-R	GGCATTGAACCCTAGCTGCT		
Gapdh	mGAPDH-F	TGCACCACCAACTGCTTAG	175	
	mGAPDH-R	GATGCAGGGATGATGTTC		
	mGAPDHb-F	CATGTTCCAGTATGACTCCACTC	136	6679937a2
	mGAPDHb-R	GGCCTCACCCCATTTGATGT		
	mGAPDHc-F	TGACCACAGTCCATGCCATC	203	6679937a3
	mGAPDHc-R	GACGGACACATTGGGGGTAG		

na: not applicable

*qRT-PCR experiments carried out by K. Pearce.

2.11 EMBRYO ANALYSIS

2.11.1 Magnetic Resonance Imaging

Embryos were dissected out at E15.5 and fixed for at least 3 days in 4% formaldehyde and 2 mM gadolinium-diethylenetriamine pentaacetic anhydride (Gd-DTPA Magnevist, Schering UK) in PBS at 4°C. Embryos were imaged by Shoumo Bhattacharya's group at the Wellcome Trust Centre for Human Genetics, Oxford, UK. Multi-embryo magnetic resonance imaging (MRI) was carried out as described (Schneider et al., 2004). Briefly, embryos were embedded in 1% agarose containing 2 mM Gd-DTPA in 28mM nuclear magnetic resonance tubes. MRI measurements were performed using an 11.7 Tesla (500 MHz) vertical magnet (Magnex Scientific, Oxon, UK) interfaced to a Bruker Avance console (Bruker Medical, Ettlingen, Germany) with a maximal gradient strength of 548 mTesla/m (Magenx Scientific, Oxon, UK), and quadrature-driven birdcage type coils with an inner diameter of 28 mm (Rapid Biomedical, Wurzburg, Germany). A 3D spoiled echo sequence (echo time 10 ms), a $\pi/2$ excitation pulse with rectangular pulse shape, ($\pi/2$ = 100 μs) was used with a short repetition time (30 ms) to obtain strong T_1 contrast. The field of view was 26 x 26 x 50 mm with a matrix size of 608 x 608 x 1408 (bandwidth: 130 Hz/pixel), resulting in an experimental resolution of 43 x 43 x 36 μm. The total experimental time was ~ 12.3 hours for 32 embryos with each phase encoding step being averaged four times (Schneider et al., 2004). Data was analysed using Amira 3.1 (TGS Europe, Merignac Cedex, France).

2.11.2 Whole Mount *in situ* Hybridisation

2.11.2.1 Dissection

Embryos for whole mount *in situ* hybridisation were dissected out into cold PBS and fixed overnight in 4% formaldehyde in PBS at 4°C. The next day, embryos were washed in 100% MeOH several times and stored at -20°C in 100% MeOH.

2.11.2.2 Generation of labelled riboprobe

2.11.2.2.1 Preparation of the DNA template

1μg of plasmid was digested with an appropriate enzyme to give a 5' overhang and 50ng was run on a 1% agarose gel to check digestion was complete. The digest was purified by diluting to 200 μl with H_2O, adding an equal volume of phenol/chloroform (49:1 $CHCl_3$:IAA), vortexing and spinning in a centrifuge at 12000 x g for 5 minutes at 4°C. The aqueous, upper layer was removed and placed in a new tube and an equal volume of chloroform:IAA (49:1) was added. The solution was then spun again as above, the upper layer removed and placed in a new tube. $1/10^{th}$ volume of 3M NaOAc (pH 5.2) and 2.5 volumes of ice-cold 100% EtOH was added and the DNA was left to precipitate on ice for 30 minutes. The solution was spun in a centrifuge at 12 000 x g, 4°C for 20 minutes and the DNA pellet was washed with ice-cold 70% EtOH and spun again at 12000 x g for 5 minutes. The DNA pellet was resuspended in 11.5μl H_2O of which 1μl was run on a 1% agarose gel to check the template before proceeding to the transcription reaction.

2.11.2.2.2 Probe Transcription

To generate DIG-labelled RNA transcripts the following components were added to an eppendorf tube in the following order: 4μl 5 X transcription buffer (Promega), 2μl 0.1M DTT, 2μl DIG-labelled NTPs, 10.5μl (1μg) linearised plasmid, 0.5μl Ribonuclease inhibitor (40U/μl) and 2μl SP6, T7 or T3 RNA polymerase (10U/μl) (Promega). *In vitro* transcription was carried out by incubating for 2 hours at 37°C (or 40°C for SP6). 1μl of the probe was run on a 1% agarose gel to check synthesis. An RNA band of approximately 10-fold greater intensity than the plasmid band indicated that approximately 10μg probe had been synthesised.

To purify the probe, the solution was diluted to 50μl with H_2O, and the probe precipitated by adding $1/10^{th}$ volume 3M sodium acetate (pH 5.2) and 2.5 volumes ice-cold 100% ethanol and incubating on ice for 30 minutes. The RNA probe was spun down at 12 000 x g for 5 minutes at 4°C, washed with ice-cold 70% ethanol, air-dried and resuspended in 100μl H_2O. 2μl probe was run on a 1% agarose gel to check purification and estimate concentration by comparing to a known concentration of DNA ladder.

2.11.2.3 Pretreatment of Embryos

Embryos for whole mount *in situ* hybridisation were dissected out into cold PBS and fixed overnight in 4% formaldehyde in PBS at 4°C. The next day embryos were washed in 100% MeOH several times and stored at -20°C in 100% MeOH. Embryos were then rehydrated by taking them back through a methanol series, washing in each solution for 20 minutes at room temperature. The embryos were then washed 3 x in PBTX for 10 minutes each and treated with 10μg/ml proteinase K in PBTX for 2-35 minutes depending on the stage of embryo. Afterwards, embryos were washed 2 x in PBTX and re-fixed in 4% formaldehyde/0.2% glutaraldehyde in PBTX for 20 minutes at room temperature. Embryos were washed again 2 x in PBTX for 10 minutes each and finally transferred into 1-1.5 ml prehybridisation buffer. Embryos were stored at -20°C until required.

2.11.2.4 Probe Hybridisation

Embryos were incubated in prehybridisation solution (see stock solutions, section 2.2) at 68°C for at least 2 hours to overnight. 0.2-1.0 μg/ml DIG-labelled probe was added to the prehybridisation solution and the embryos were incubated at 68°C, rocking overnight.

2.11.2.5 Post-hybridisation washes and Antibody Incubation

The probe was removed and embryos were rinsed in pre-warmed, prehybridisation buffer 2 x and washed 3 x in prehybridisation buffer at 68°C for at least 30 minutes each. The embryos were then washed in 1:1 prehybridisation buffer:TBTX for 20 minutes at 68°C and rinsed 3 x in room temperature TBTX. TBTX washes were then carried out at room temperature 3 x for at least 30 minutes each. Embryos were then blocked in 20% sheep serum in TBTX for 2 -3 hours at room temperature and incubated in 1/2000 anti-DIG antibody (Boehringer) in 20% sheep serum/TBTX overnight at 4°C, rocking.

2.11.2.6 Post-Antibody Washes

The antibody solution was removed and the embryos washed 5 x with TBTX for at least 1 hour each. The last wash was carried out overnight at 4°C.

2.11.2.7 Histochemistry

The embryos were washed twice in TBST for 15 minutes each then washed 3 x in freshly made NTMT for 10 minutes each. The colour reaction was started by incubating the embryos in NBT/BCIP solution (Roche) or BM Purple staining solution (2ml BM Purple (Roche), 20µl 100 x levamisol, 20µl 10% Tween 20) in the dark. After colour had developed, the embryos were washed 2 x in TBTX, fixed in 4% formaldehyde in PBS for 1 hour at room temperature and stored in 0.1% formaldehyde in PBS at 4°C. Embryos were visualised and pictures taken using a Zeiss Stereo Lumar.V12 microscope.

2.11.2.8 In situ probes

Table 2.5 In situ probes

Gene	Source
Cyp26c1	In house probe. Roberts *et al.* 2006
Dab2	IMAGE clone 3587226, Geneservice, UK
Gbx2	Gift from Alex Joyner, Sloan-Kettering Institute, NY, USA
Gcm2	Gift from Nancy Manley, University of Georgia, GA, USA
Gm603	IMAGE clone 6366969, Geneservice, UK
Hes1	PCR 552bp probe using primers Hes1IS-F GAGAGGCTGCCAAGGTTTTT and Hes1IS-R GTAATACGACTCACTATAGGGTCAAATAAACTTCCCCAAA
Hic2	IMAGE clone 6851068, Geneservice, UK
Nkx2.6	In house probe
Pax1	Gift from Peter Gruss, Max-Planck Society, Munich, Germany
Raldh2	Gift from Ursula Drager, Eunice Kennedy Shriver centre for Mental Retardation, Waltham, MA, USA

2.11.3 X-gal staining of embryos

Embryos were dissected out and fixed for 30 to 60 minutes in 1% formaldehyde, 0.2% glutaraldehyde in PBS with 2 mM $MgCl_2$ at room temperature. Embryos were then washed twice in PBS with 2 mM $MgCl_2$ and incubated in X-gal buffer (see stock solutions, section 2.2) with 1 mg/ml X-gal (Promega) at 37°C until the stain developed. Embryos were then rinsed in PBS and fixed overnight in 4% formaldehyde in PBS.

2.11.4 Intracardiac ink injection

Indian Ink (Pelikan) was injected into the outflow tract or aorta of embryos using a microinjection needle to visualise the pharyngeal arch arteries or great vessels of the heart.

2.11.5 Embedding and sectioning

2.11.5.1 Wax embedding and sectioning

Embryos were fixed overnight in 4% formaldehyde in PBS at 4°C. Following fixation, embryos were dehydrated to 100% ethanol by taking them through washes in 50% PBS:50% ethanol, 70% ethanol and 90% ethanol in H_2O where each wash was at least 30 minutes long. Embryos were then washed twice in Histoclear (Raymond A Lamb, Hull, UK) for 30 minutes each, then 50% Histoclear:50% wax for 20 minutes at 60°C and finally 3 x 40 minute (or longer) washes in wax at 60°C before embedding in wax and allowed to set. Sections were cut at 10 μm and placed on superfrost slides coated with Tespa. To remove the wax, sections were incubated in histoclear , then re-hydrated through an ethanol series (2 x Histoclear for 10 minutes each, then 10 minute washes in 100% ethanol, 90%, 70%, 50%, 30% ethanol and finally H_2O). Coverslips were mounted onto slides using DPX mounting media. Sections were visualised and pictures taken using a Zeiss Axiophot2 microscope.

2.11.5.2 OCT embedding and sectioning

Embryos were fixed in 4% formaldehyde in PBS for 2-3 hours, rinsed in PBS then left to equilibrate in 20% sucrose in PBS overnight at 4°C. Embryos were transferred to 50% sucrose, 50% Optimal Cutting Temperature compound (OCT) and then frozen in 100% OCT on dry ice. OCT-embedded embryos were sectioned on a cryostat set at approximately 22°C. Sections were cut at 10 μm thickness, collected onto Superfrost+

glass slides and allowed to dry. GFP fluorescent TgTbx1floxGFP sections were visualised and pictures taken using a Zeiss Stereo Lumar.V12 microscope.

2.11.6 Hematoxylin and eosin staining

Wax embedded sections were stained with hematoxylin and eosin to enable visualisation of the nuclei and cytoplasm. After removal of the wax as per section 2.10.5.1, sections were stained in 100% hematoxylin (Raymond Lamb) solution until the desired stain was achieved. The sections were then rinsed in tap water and stained in eosin solution (Raymond Lamb), rinsed in tap water again and allowed to air dry. Coverslips were mounted onto slides using DPX mounting media.

CHAPTER 3. MICROARRAY ANALYSIS OF *TBX1*-EXPRESSING CELLS

3.1 INTRODUCTION

Since the discovery of *TBX1* as the major candidate gene responsible for the primary symptoms of DGS, researchers have come a long way towards understanding the spatial and temporal requirement for *Tbx1* in development. However, the molecular pathways downstream of *Tbx1* have not yet been clearly defined. Some of the potential direct targets of *Tbx1* include the *Fgf* ligands, *Fgf8* and *Fgf10* (Hu et al., 2004; Xu et al., 2004)and the transcription factor, *Pitx2c* (Nowotschin et al., 2006).

In order to characterise the transcriptional networks downstream of *Tbx1* in development, a microarray was carried out in our lab comparing the genetic profile of dissected pharyngeal arches and adjacent tissues from E9.5 *Df1/Tbx1*^{lacZ} compound heterozygous embryos (also referred to as *Tbx1*-null) to wild type embryos (Ivins et al., 2005). A number of altered genes were identified giving an indication of the pathways potentially downstream of *Tbx1* and which could represent direct *Tbx1* targets. However, since the tissues compared contained a number of different cell types, not all of which express *Tbx1*, the more subtle effects of altered *Tbx1* expression could have been masked by the gene expression profile of unaffected/non *Tbx1*-expressing cells. Conversely, tissue loss may have resulted in apparent changes in gene expression due to absence of cells/anatomical differences between *Tbx1* null and wild type embryos. To minimise these problems, studies have used flow-sorting to obtain specific cell populations for microarray analysis (Bouchard et al., 2005; Kalajzic et al., 2005; Kamath et al., 2005; Prall et al., 2007; Takasato et al., 2004), and experiments have shown this to be a valid method for analysing the genetic profile of defined cell subpopulations (Szaniszlo et al., 2004). Therefore, to try to overcome the limitations of the previous microarray, enrich for cell-autonomous effects and further define targets and downstream pathways important in pharyngeal and heart development, a method was optimised for isolating *Tbx1*-expressing cells from *Df1/Tbx1*^{lacZ} and *Tbx1*$^{+/lacZ}$ embryos for comparison by microarray.

The *Tbx1* non-functional allele was generated by knocking a *lacZ* reporter gene into exon 5, which encodes the T-box DNA binding domain and therefore cells expressing this allele can be identified by using lacZ substrates. Fluorescent, lacZ substrates have been used previously to mark living cells for flow sorting (Brachvogel et al., 2005; Laugwitz et al., 2005). However, this method has never been used to isolate cells for whole genome analysis. The fluorescent lacZ substrate, CMFDG was used to label and flow-sort *Tbx1*-expressing cells from E9.5 compound heterozygous *Df1/Tbx1*^{lacZ} and *Tbx1*$^{+/lacZ}$ embryos and the gene expression profile of these two cell populations was compared by microarray analysis.

3.2 RESULTS

3.2.1 Isolation of *Tbx1*-expressing cells

In order to isolate *Tbx1*-expressing cells from *Tbx1-lacZ* embryos, a single cell suspension was generated from the appropriate embryos. A procedure for the optimal labelling of *Tbx1-lacZ* cells was then developed using a fluorescent, lacZ substrate. C_{12}FDG is a non-toxic, fluorogenic β-galactosidase substrate that has been used in numerous studies to label *lacZ*-expressing cells (Jasin and Zalamea, 1992; Peng et al., 1993). C_{12}FDG contains a 12-carbon lipophilic moiety covalently attached to Fluorescein Digalactoside (FDG), which allows for direct loading into cells by adding the substrate to the aqueous medium. The suitability of C_{12}FDG as a fluorogenic substrate was tested in a single cell suspension of E9.5 embryonic cells. However, results were not consistent when using this substrate, since analysis by fluorescent activated cell sorting (FACS) often failed to demonstrate fluorescence above background levels. In addition, C_{12}FDG gave high background fluorescence in control wild type cells that do not contain the *lacZ* gene.

An alternative fluorogenic substrate, 5-chloromethylfluorescein di-β-D-galactopyranoside (CMFDG) was therefore tested. CMFDG can also be directly loaded into cells, but once cleaved by β-galactosidase, it reacts with glutathione to form a membrane-impermeant adduct which means it is better retained within cells. CMFDG consistently showed high fluorescence above background (as analysed by FACS) when tested as a substrate in a single cell suspension made from mouse embryos. Therefore CMFDG was used to isolate *Tbx1*-expressing cells (*Df1/Tbx1*^{lacZ} and *Tbx1*$^{+/lacZ}$) by FACS.

E9.5 embryos were chosen for collection and analysis due to strong expression of *Tbx1* at this stage in the pharyngeal arches and surrounding tissues, and the requirement for *Tbx1* in development of the pharyngeal arch arteries and outflow tract at this timepoint (Xu et al., 2005). E9.5 embryos obtained from *Df1*/+male x $Tbx1^{+/lacZ}$ female matings were collected and $Df1/Tbx1^{lacZ}$ embryos were separated by phenotype from the $Tbx1^{+/lacZ}$;*Df1*/+;wild type embryo pool for subsequent dissociation into a single cell suspension. After staining with the fluorescent substrate, CMFDG, cells were collected based on fluorescence intensity (above background) and cell viability. FACS analysis showed that these cells constituted, on average, less than 1% of the total cell population obtained from E9.5 embryos (Figure 3.1A, B). Cells which were gated as FDG-negative were run back through the cell sorter for re-analysis, confirming that no fluorescent cells were present in this population (Figure 3.1C). Due to the small sample size, the FDG-positive cells collected could not be re-analysed.

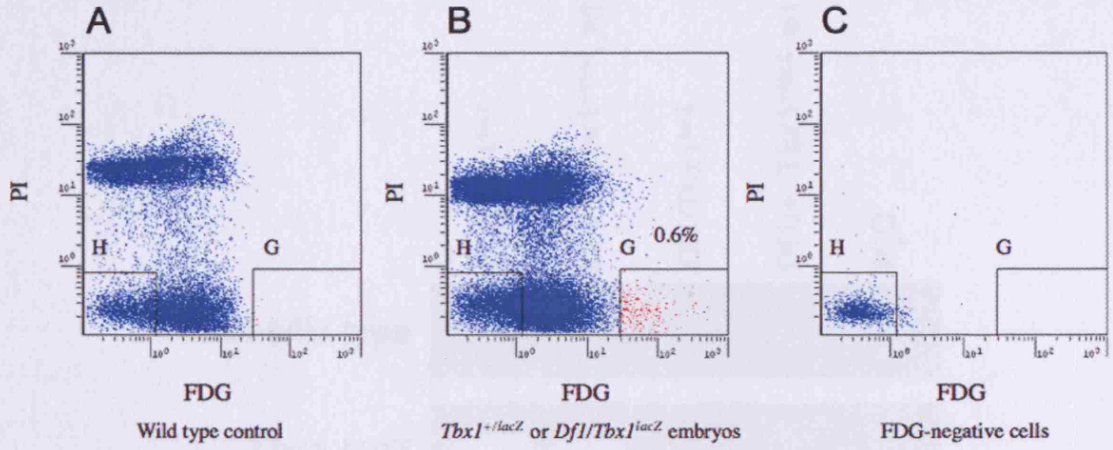

Figure 3.1 Isolating *Tbx1-lacZ* expressing cells by FACS
After cells from E9.5 embryos were loaded with the fluorescent substrate, CMFDG, *Tbx1-lacZ* expressing cells were collected by FACS. Cells from a wild type embryo (**A**) were used as a background control and subsequently, cells from $Tbx1^{+/lacZ}$ or $Df1/Tbx1^{lacZ}$ embryos were flow-sorted to isolate fluorescent, *Tbx1-lacZ* expressing cells which constituted approximately 0.6% of the total cell population (**B** - box G) . FDG-negative cells (**B** - box H) were re-anlaysed to ensure that no fluorescent cells were contained in this population (**C**). PI (Propidium Iodide) measures the amount of cell death and FDG is a measure of the fluorescence intensity.

To analyse for enrichment of *Tbx1-lacZ* cells, FDG-negative cells were collected from the combined $Tbx1^{+/lacZ}$;*Df1/+;*wild type flow sort and also from the $Df1/Tbx1^{lacZ}$ flow sort to compare to the FDG-positive cells (which should only be $Df1/Tbx1^{lacZ}$ and $Tbx1^{+/lacZ}$ cells). RNA was extracted, reverse-transcribed and amplified, then analysed for the presence of the *Tbx1* wild type and *Tbx1-lacZ* alleles. The *Tbx1* wild type allele was detected in the FDG-positive cell population containing $Tbx1^{+/-}$ cells and in the FDG-negative cell population containing $Tbx1^{+/lacZ}$, *Df1/+* and wild type cells (Figure 3.2). In contrast, the *Tbx1-lacZ* allele was only detected in FDG-positive cells (Figure 3.2). These results indicate that the FDG-positive cells collected were the *Tbx1-lacZ* expressing cells of interest consisting of $Tbx1^{+/lacZ}$ and $Df1/Tbx1^{lacZ}$ cells. Subsequently, RNA was extracted from these cells, amplified, labelled and hybridised onto microarray chips for gene expression analysis.

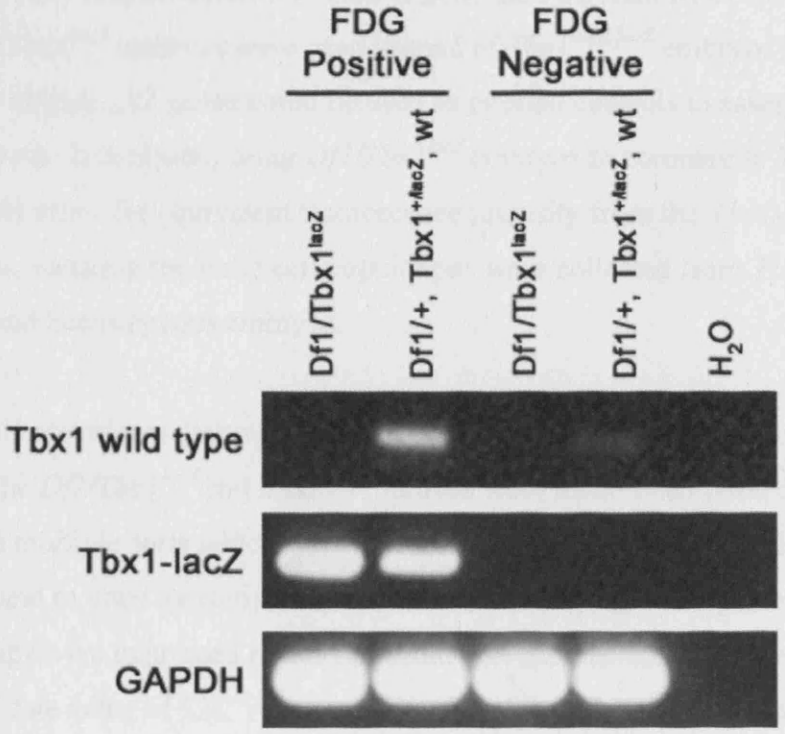

Figure 3.2 Analysis of *Tbx1-lacZ* cell enrichment
The wild type *Tbx1* allele is present in both FDG-positive and FDG-negative cell populations. The *Tbx1-lacZ* allele representing $Df1/Tbx1^{lacZ}$ cells and $Tbx1^{+/lacZ}$ cells is only present in FDG-positive cell populations.

3.2.2 Microarray results

Microarray experiments were carried out using Affymetrix mouse MOE430 v2.0 arrays consisting of over 34 000 well characterised mouse genes, represented by over 45 000 probe sets. Analysis of the microarray experiments was conducted using Genespring v4.2.1. Six replicate microarray experiments were carried out in total using RNA extracted from 3 pools of *Df1/Tbx1*^{lacZ} cells and 3 pools of *Tbx1*$^{+/lacZ}$ cells. Each pool of cells was obtained from a group of E9.5 embryos ranging in somite number from 17s to 25s. Pools of cells were used to minimise variation due to staging differences. Altogether, RNA was extracted from 38004 *Df1/Tbx1*^{lacZ} cells sorted from a total of 71, E9.5 embryos and 57563 *Tbx1*$^{+/lacZ}$ cells sorted from a total of approximately 89, E9.5 embryos. The average number of cells obtained per embryo was 535 cells per *Df1/Tbx1*^{lacZ} embryo and 646 cells per *Tbx1*$^{+/lacZ}$ embryo. Due to the limited number of cells obtained, PCR amplification was used to generate sufficient RNA for microarray analysis. *Df1/Tbx1*^{lacZ} embryos were used instead of *Tbx1*$^{lacZ/lacZ}$ embryos so that the hemizygously deleted *Df1* genes could be used as internal controls to assess the quality of the experiment. In addition, using *Df1/Tbx1*^{lacZ} embryos to compare to *Tbx1*$^{+/lacZ}$ embryos should allow for equivalent fluorescence intensity from the *Tbx1-lacZ* allele in both genotypes, ensuring the same cell populations were collected from *Tbx1* homozygous and heterozygous embryos.

Initially, 3 replicate microarrays were carried out for preliminary analysis of gene expression. The *Df1/Tbx1*^{lacZ} and *Tbx1*$^{+/lacZ}$ probes were made from pooled RNA collected from multiple sorts which were divided into 3 equal aliquots for RNA amplification and in vitro transcription. 17 out of the 20 *Df1* genes represented on the microarray chips were expressed above threshold detection levels (Genespring evaluated raw data value of 22). After applying filtering and statistical analyses to the data (Non-parametric t-test with a p value cutoff of 0.5 + the Benjamini and Hochberg False Discovery Rate multiple testing correction), 13 out of the 17 *Df1* genes were significantly down-regulated to 0.6 fold in 2 out of 3 *Df1/Tbx1*^{lacZ} chips compared to *Tbx1*$^{+/lacZ}$ chips indicating that the correct cells were isolated and that the microarray experiment was sensitive enough to detect down-regulation of genes expressed from only 1 allele in *Tbx1*$^{+/lacZ}$ cells compared to *Df1/Tbx1*^{lacZ} cells.

Subsequently, 3 further microarrays were carried out to make a total of 6 replicate microarrays. The *Df1/Tbx1*^{lacZ} and *Tbx1*$^{+/lacZ}$ probes for the 4th microarray experiment were made from pooled RNA collected from multiples sorts. The 4th microarray experiment was kept separate from the last 2 experiments because cells were collected using a different machine, the MoFlo, which resulted in fewer cells per embryo (Dakocytomation - Ely Cambridge).

For the 5th and 6th microarray experiments, the *Df1/Tbx1*^{lacZ} and *Tbx1*$^{+/lacZ}$ probes were made from pooled RNA collected from multiple sorts carried out on the Beckman Coulter Epics Altra machine. The pooled RNA was divided into 2 equal aliquots for subsequent RNA amplification and in vitro transcription to make microarray probes.

3.2.2.1 Df1 Genes

After combining all microarray chips into one Genespring experiment and applying filtering and statistical analyses to the data, 17 out of the 20 *Df1* genes represented on the MOE430v2.0 chips were expressed above threshold levels (Table 3.1). Iterative analyses were then carried out to determine the appropriate filters to apply to identify the majority of hemizygously-expressed *Df1* genes. Fourteen out of those 17 *Df1* genes were down-regulated to at least 0.83 in 5 out of 6 *Df1/Tbx1*^{lacZ} arrays compared to *Tbx1*$^{+/lacZ}$ arrays, the filtering cut off applied to extract the majority of *Df1* genes. On average, these 14 genes were downregulated to 0.594 ± 0.09 indicating the sensitivity of the experiment in detecting downregulated genes (Table 3.1). In addition, the upregulation of *Es2el* is a known artifact resulting from ectopic activation of part of the gene located at the end of the *Df1* deletion (Ivins et al., 2005).

Table 3.1 *Df1* genes analysed by microarray

Gene	Relative expression in *Df1/Tbx1*^{lacZ} vs. *Tbx1*$^{+/lacZ}$ cells
Dgcr6	0.517 ± 0.068
Zdhhc8	0.663 ± 0.140
Ranbp1	0.598 ± 0.095
Htf9c	0.549 ± 0.104
D16h22s680e	0.563 ± 0.267
Arvcf	0.490 ± 0.165
Comt	0.601 ± 0.118
Txnrd2	0.531 ± 0.054
Septin 5	0.568 ± 0.167
Ufd1l	0.459 ± 0.091
Slc25a1	0.639 ± 0.097
Cdc45l	0.694 ± 0.206
Prodh	0.632 ± 0.205
Dgcr8	0.807 ± 0.153
*Cldn5**	0.752 ± 0.478
*Gnb1l**	0.706 ± 0.325
Vpreb2 (L)	0.749 ± 0.704
Rtn4r (L)	0.977 ± 0.631
Tbx1 (L)	0.324 ± 0.344
Es2el	1.459 ± 0.238

L indicates low signal strength

*These genes did not pass the filtering and statistical analysis applied

3.2.2.2 Dysregulated genes

Applying the same filtering and statistical analyses to the combined microarray as that used to identify 14 out of 17 hemizygous *Df1* genes resulted in a total of 1553 unique sequences which were downregulated to at least 0.83 in 5 out of 6 *Df1/Tbx1*^{lacZ} arrays compared to *Tbx1*$^{+/lacZ}$ arrays. Classification of these genes into gene ontology (GO) categories revealed that the ratio of genes within each functional class was maintained in the dysregulated gene data set relative to genes across the entire microarray data set suggesting that there was no particular functional class which was more sensitive to altered *Tbx1* dosage (Table 3.2). Genes involved in translation comprised the only category which was perhaps overrepresented in the downregulated gene group (7% of downregulated genes vs. 4% of all microarray genes) (Table 3.2).

In comparison to the number of downregulated genes identified in the microarray, fewer genes were found to be upregulated in *Df1/Tbx1*^{lacZ} cells. When applying the reciprocal analysis to identify upregulated genes, only 171 genes passed the statistical filters used, increasing in expression to 1.17 in 5 out of 6 *Df1/Tbx1*^{lacZ} chips. GO annotation showed that there appeared to be fewer genes associated with regulation of transcription while genes involved in transport and cell death were more predominant among upregulated genes in comparison to the microarray data as a whole (Table 3.2).

Table 3.2 Classification of genes into GO categories

	MOE430v2 transcripts	**Downregulated transcripts**	**Upregulated transcripts**
Unique	39000	1553	171
GO-annotated	27393	1029	109
GO category			
Metabolic process	16636 (61%)	662 (64%)	67 (61%)
Signal transduction	5675 (21%)	204 (20%)	24 (22%)
Transcriptional regulation	4987 (18%)	197 (19%)	15 (14%)
Transport	5454 (20%)	190 (18%)	29 (27%)
Translation	1134 (4%)	73 (7%)	2 (2%)
Cell cycle	1766 (6%)	71 (7%)	6 (5.5%)
Cell adhesion	1438 (5%)	61 (6%)	4 (4%)
Cell death	1547 (6%)	51 (5%)	10 (9%)
Cytoskeleton organisation and biogenesis	1207 (4%)	46 (4%)	6 (5.5%)

% values represent the number of genes in each GO category as a percentage of total GO-annotated transcripts

3.2.3 Validation of downregulated genes by qRT-PCR

The primary aim was to identify *Tbx1* targets, particularly genes which could be important in pharyngeal or heart development. Validation focused on downregulated genes because *Tbx1* has been demonstrated to be a transcriptional activator (Ataliotis et al., 2005; Stoller and Epstein, 2005; Xu et al., 2004). Quantitative, real-time PCR (qRT-PCR) was carried out to confirm gene expression changes using RNA amplified from an independent pool of *Df1/Tbx1*^{lacZ} and *Tbx1*$^{+/lacZ}$ cells collected by FACS from 10, E9.5 *Df1/Tbx1*^{lacZ} embryos and 26, E9.5 *Tbx1*$^{+/lacZ}$ embryos, ranging in somite number from 18 to 24. *Gapdh* expression was not altered in *Df1/Tbx1*^{lacZ} cells relative to *Tbx1*$^{+/lacZ}$ cells in the microarray (1.019 ± 0.279) indicating that overall transcription was not changed. Gene expression levels were therefore normalised to *Gapdh* for subsequent qRT-PCR analysis. A proportion of the qRT-PCR experiments were carried out by Kerra Pearce, a research assistant in the lab (see section 2.10.3.3).

Previous microarray experiments carried out in the lab have compared the expression profile of E9.5 *Df1/Tbx1*^{lacZ} embryos to wild type embryos by dissecting out the pharyngeal region and adjacent tissues corresponding to the major sites of *Tbx1* expression (Ivins et al., 2005). A number of genes identified as downregulated in *Df1/Tbx1*^{lacZ} embryos by the previous microarray (Ivins et al., 2005; Roberts et al., 2006) were chosen for further analysis to determine whether they were also downregulated specifically in *Tbx1*-expressing cells. Seven genes were chosen based on their demonstrated role in pharyngeal and/or heart development (*Gbx2*, *Six2*, *Cyp26a1*, *Cyp26b1* and *Cyp26c1*) (Abu-Abed et al., 2001; Byrd and Meyers, 2005; Kutejova et al., 2005; Roberts et al., 2006) or because they were significantly downregulated in both microarray experiments (*Plek* and *Dab2*). Most of these genes did not pass the filtering used in the present microarray experiment to identify downregulated genes (except for *Plek* and *Dab2*). However, more detailed analysis revealed that *Gbx2*, *Six2* and *Cyp26b1* also appeared to be downregulated in *Df1/Tbx1*^{lacZ} cells but the changes were not statistically significant. qRT-PCR is a more sensitive method of identifying small expression changes and was therefore used for analysis of the above genes. *Plek*, *Gbx2*, *Six2*, *Cyp26a1* and *Cyp26b1* were verified as downregulated in *Df1/Tbx1*^{lacZ} *cells* by this method (Figure 3.3). *Dab2* expression was also downregulated in *Tbx1* null cells. However, the difference just failed to pass statistical significance ($p = 0.059$). *Cyp26c1* is downregulated in the pharyngeal region

of *Df1/Tbx1*^{lacZ} embryos as analysed by qRT-PCR and *in situ* hybridisation (Roberts et al., 2006). However, the expression of this gene was not changed in *Df1/Tbx1*^{lacZ} cells in comparison to *Tbx1*$^{+/lacZ}$ cells (Figure 3.3) suggesting possibly that alterations in the expression of this gene in *Tbx1* mutants may be due to expression changes not cell-autonomous to *Tbx1* cells.

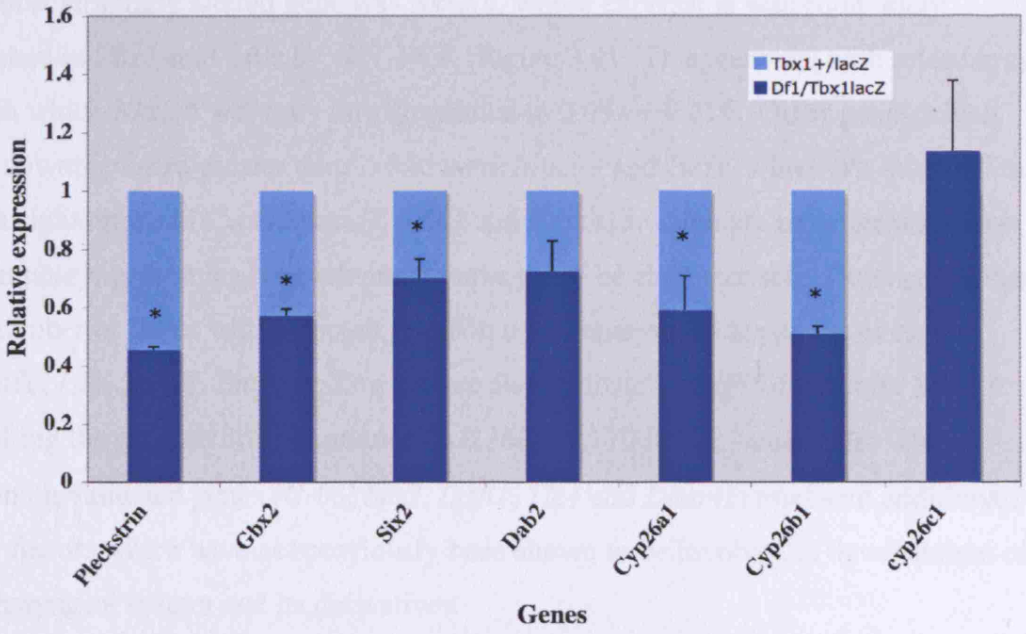

Figure 3.3 Quantitative real time PCR of potential *Tbx1* targets
Average changes in gene expression *in Df1/*^{Tbx1lacZ} vs. *Tbx1*$^{+/lacZ}$ cells. Error bars represent the standard error of n=3 experiments (except for *Gbx2* where n=2). *$P<0.05$.

Additional genes were selected for independent validation by qRT-PCR based on their expression pattern, known or potential function in pharyngeal or heart development and significant downregulation in the microarray experiments. Altogether, 34 putative, downstream *Tbx1* targets were analysed by qRT-PCR; 18 (53%) showed significant ($p < 0.05$) downregulation in *Df1/Tbx1*^{lacZ} cells, consistent with the microarray results (Figure 3.4). *Pitx1* expression also appeared to be downregulated, but this difference was not statistically significant (p=0.078). In contrast to the microarray data, *Rhbdl2* was noted to be upregulated by qRT-PCR and 15 genes showed no appreciable changes in expression (Figure 3.4).

The most strikingly altered gene was *Nkx2.6*, whose expression was completely abolished in *Tbx1*-null cells by qRT-PCR (Figure 3.4). This contrasts with microarray data in which *Nkx2.6* was only downregulated to 0.694 ± 0.219. Other genes which were downregulated greater than 3-fold were *Notch3* and *Hes1*, which are involved in Notch signalling and *Cxcl4*, *Smad7*, *Cdh1* and *Ndufa13* which are novel genes whose role in pharyngeal or heart development have yet to be characterised. Downregulation of a number of genes with a known function in the pharyngeal apparatus or heart (*Sema3c*, *Isl1*, *Tbx18*, *Bmpr1a*, *Dsg2*) were also validated by qRT-PCR with *Sema3c* exhibiting the greatest downregulation to 0.360 ± 0.170 in *Tbx1*-null cells. The remaining validated genes (*Crb3*, *Slit2*, *Lztfl1*, *Tle4* and *Daam1*) represent additional, novel factors which have not previously been shown to be involved in development of the pharyngeal system and its derivatives.

In general, qRT-PCR results of validated, downregulated genes revealed similar or slightly greater expression changes between *Df1/Tbx1*^{lacZ} cells and *Tbx1*$^{+/lacZ}$ cells (Figure 3.5) consistent with reported studies of significantly greater fold changes by qRT-PCR vs. microarray (Dallas et al., 2005).

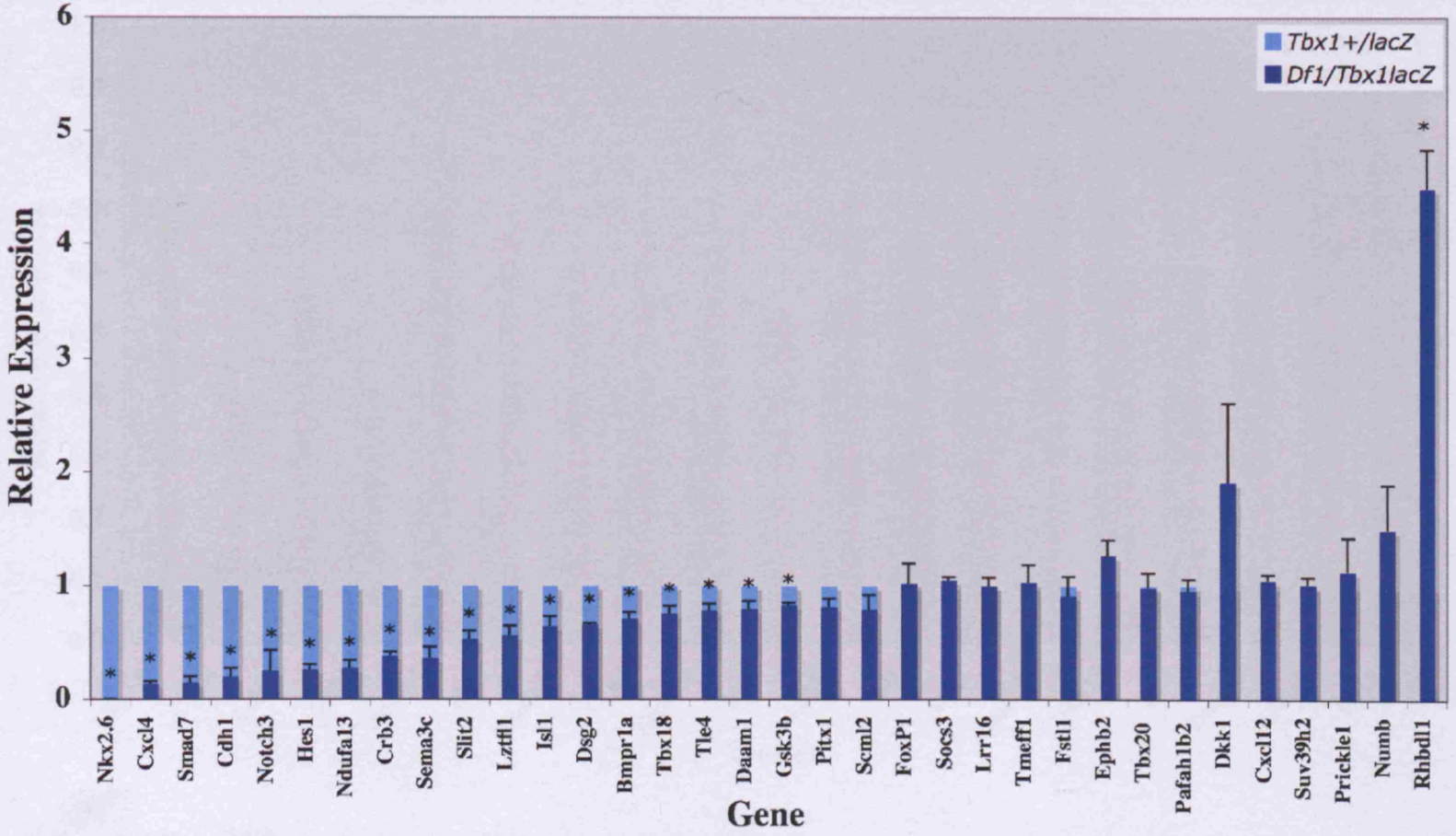

Figure 3.4 Quantitative real-time PCR analysis of gene expression

Average changes in gene expression in *Df1/Tbx1*^{lacZ} vs. *Tbx1*$^{+/lacZ}$ cells. Error bars represent the standard error of n=3 experiments (except for Dsg2 where n=2). *$P<0.05$.

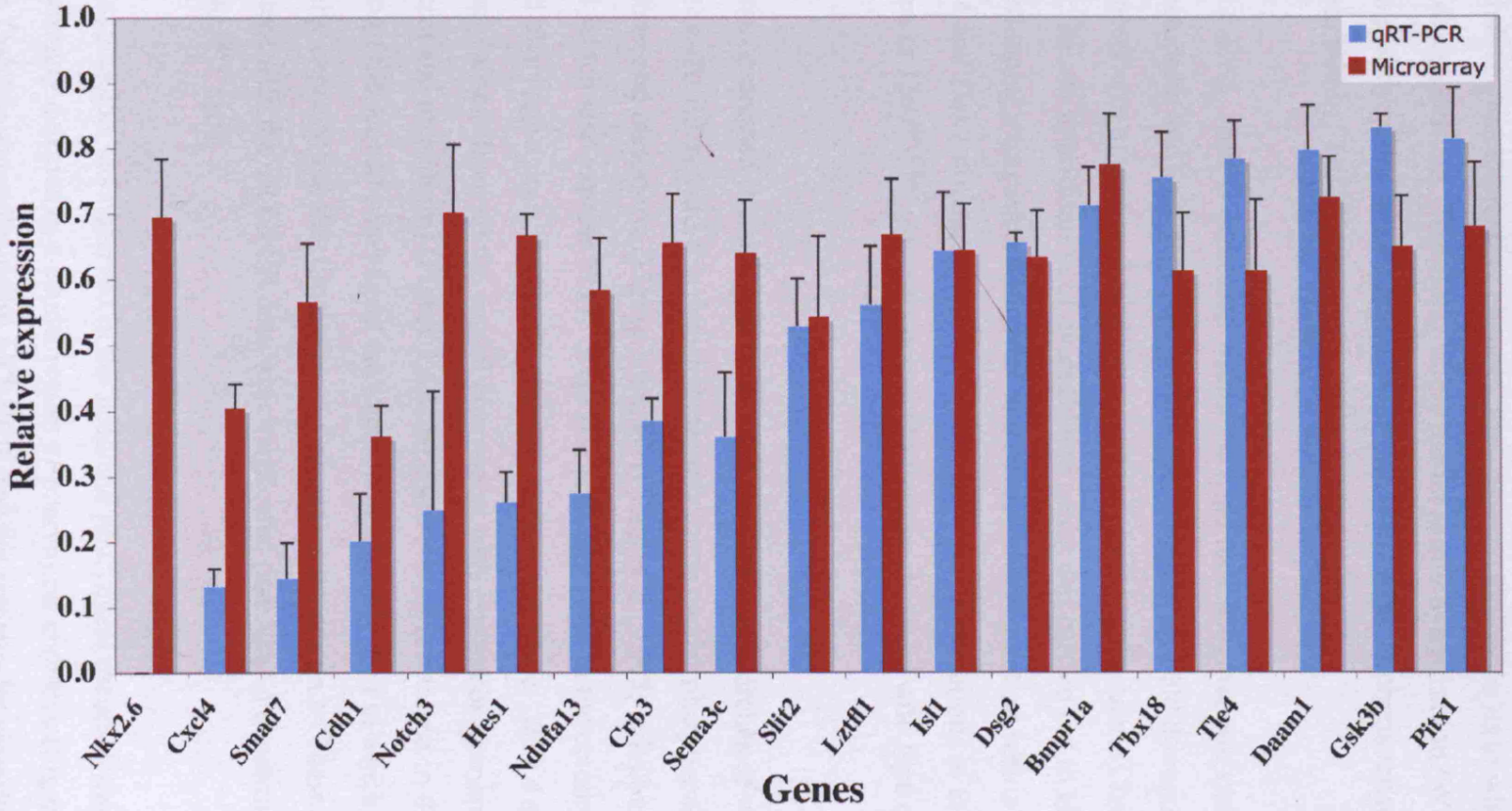

Figure 3.5 Quantitative real time PCR results compared to microarray results
Average changes in gene expression in *Df1/Tbx1*^{lacZ} vs. *Tbx1*$^{+/lacZ}$ cells. Error bars represent the standard error of n=3 experiments for qRT-PCR and n=6 for microarray experiments.

3.2.4 Whole mount in situ analysis of downregulated genes

While the microarray and qRT-PCR analyses of *Tbx1*-expressing cells revealed quantitative gene expression changes, they gave no indication as to where in the embryo these changes occur. Therefore, whole mount *in situ* hybridisation (WISH) was carried out on putative *Tbx1* targets identified by the microarray to characterise the expression changes within $Tbx1^{-/-}$ embryos.

At E9.0-E9.5, *Tbx1* is expressed within the head mesenchyme, otic vesicle, pharyngeal arch ectoderm and endoderm, and within the second heart field domain consisting of the core mesoderm of each arch and the mesoderm dorsal to the heart (Chapman et al., 1996). *In situ* hybridisation of dysregulated genes was carried out to identify the areas of overlapping expression with *Tbx1* and assess downregulation within these domains. *Nkx2.6* and *Dab2* were analysed by WISH and showed alterations in their expression patterns in $Tbx1^{lacZ/lacZ}$ embryos compared to stage-matched wild type embryos (Figure 3.6).

Nkx2.6 is expressed in a restricted pattern in the pharyngeal arches of wild type embryos. At E9.5, *Nkx2.6* is detected strongly in the caudal pharyngeal arch ectoderm, endoderm and mesoderm (Figure 3.6A, B) (Biben et al., 1998; Nikolova et al., 1997), tissues which also express *Tbx1*. *Nkx2.6* is also expressed in the ectoderm overlying the second pharyngeal arch. In $Tbx1^{-/-}$ embryos at the same stage, *Nkx2.6* expression is strikingly absent from all the caudal pharyngeal arch expression domains (endoderm, ectoderm and mesoderm) (Figure 3.6A, B). However, it is retained in the anterior portion of the second pharyngeal arch ectoderm, the only area in which *Tbx1* in not normally expressed at this timepoint (A.Calmont, pers. comm.). These results are consistent with the qRT-PCR data which indicated that *Nkx2.6* expression is lost in $Df1/Tbx1^{lacZ}$ cells.

Dab2 expression was observed in the head and pharyngeal mesenchyme at E9.5 and is most strongly detected in a caudal region of pharyngeal arch two (Figure 3.6C). Even though *Dab2* downregulation by qRT-PCR was not statistically significant, *in situ* hybridisation revealed that $Tbx1^{-/-}$ homozygotes exhibit loss of *Dab2* expression, particularly within the second pharyngeal arch (Figure 3.6C).

Preliminary WISH analysis of potential *Tbx1* targets identified by microarray has led to a better qualitative characterisation of the precise expression domains in which each gene is dysregulated. Further characterisation of other downregulated genes is currently underway in our lab and should give a better indication as to what role these genes may play in pharyngeal and heart development.

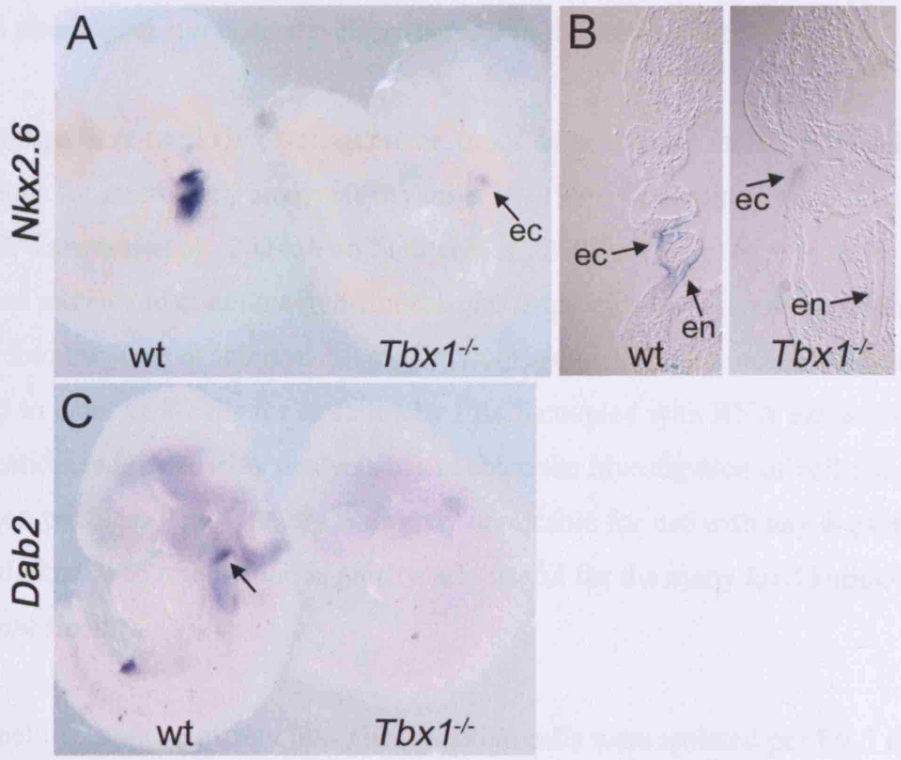

Figure 3.6 Expression analysis of *Nkx2.6* and *Dab2*
(**A**) *Nkx2.6* expression at E9.5 is lost in the pharyngeal arches of *Tbx1*$^{-/-}$ mutants except in the pharyngeal ectoderm overlying pharyngeal arch two. (**B**) Coronal sections of the wild type and *Tbx1*$^{-/-}$ embryos in (**A**). (**C**) *Dab2* expression at E9.5 in the second pharyngeal arch (arrow) of a wild type embryo and absent expression in *Tbx1*$^{-/-}$ mice. Abbreviations: ec, ectoderm; en, endoderm.

In summary, CMFDG-labelling of *Tbx1-lacZ* cells was effectively used to isolate *Df1/Tbx1*^{lacZ} and *Tbx1*$^{+/lacZ}$ cells from E9.5 embryos. Microarray analysis of PCR-amplified RNA extracted from these cell populations has led to the identification of dysregulated genes representing potential *Tbx1* targets important in development of the pharyngeal apparatus and heart.

3.3 DISCUSSION

3.3.1 Technical considerations

In this project, fluorescent labelling of *lacZ*-positive cells was optimised to isolate *Tbx1*-expressing cells. Comparison of the gene expression profile of $Tbx1^{+/lacZ}$ vs. $Df1/Tbx1^{lacZ}$ cells has led to the identification of potential *Tbx1* targets which may play a role in pharyngeal and heart development and in the etiology of DGS.

Many groups have used GFP transgenic or knock-in animals to isolate pure cell populations for microarray analysis (Bryant et al., 1999; Covassin et al., 2006; Prall et al., 2007; Takasato et al., 2004; Von Stetina et al., 2007). However, it is more common for mouse mutants to contain a non-fluorescent, ß-galactosidase reporter which has been inserted into the gene of interest. Using the fluorogenic ß-galactosidase substrate, CMFDG to label *lacZ* cells for isolation by FACS coupled with RNA extraction, amplification and microarray analysis has enabled the investigation of cell-specific gene expression profiles. This strategy is directly applicable for use with any ß-galactosidase transgenic/knock-in mutant and is particularly useful for the many *lacZ* knock-in gene trap mouse lines.

After labelling, approximately 600 *Tbx1*-positive cells were isolated per E9.5 embryo. In comparison, GFP-positive cells collected from similar or even smaller-sized tissues generally yield a greater number of cells per embryo (1500 Nkx2.5+ cells per 21s heart tube, 5000-10000 Pax2+ cells per 4-6s midbrain/hindbrain region) (Bouchard et al., 2005; Prall et al., 2007). This discrepancy between CMFDG-cells and GFP-cells may be due to the fluorescent labelling method used to mark *lacZ* cells, since the reagents used are known to cause cell death. For example, chloroquine is used to decrease background staining, but it has also been shown to be cytotoxic (Poot and Arttamangkul, 1997).

FACS analysis revealed that *Tbx1*-expressing cells account for less than 1% of the total cell population obtained from E9.5 $Tbx1^{+/lacZ}$ embryos or $Df1/Tbx1^{lacZ}$ embryos meaning that very small numbers of cells were collected from each flow sort. Therefore, in order to generate enough RNA for microarray analysis, samples were pooled for each condition and RNA was amplified in independent aliquots to make microarray probes. Recent studies on the effects of pooling samples for microarray

analysis demonstrate that this is advantageous if the biological variance is large, compared to the technical variance (Kendziorski et al., 2005; Kendziorski et al., 2003; Peng et al., 2003). In this microarray experiment, a combination of biological replicates and semi-technical replicates were used to assess differential gene expression. Considering the large numbers of embryos that were pooled to make microarray probes, several lines of evidence suggest that an accurate gene expression profile was maintained for *Tbx1*$^{+/lacZ}$ and *Df1/Tbx1*^{lacZ} samples.

Amplification of starting RNA amounts was required to generate enough material to make microarray probes. In this study, the PCR exponential amplification method was used since several studies have shown that it requires only very small amounts of starting material, is reproducible and preserves abundance relationships (Iscove et al., 2002; Ji et al., 2004; Klur et al., 2004). One study even concludes that it is in fact better than linear amplification, generating cRNA of higher quality (Klur et al., 2004). As discussed below, in this microarray experiment, analysis of the *Df1* genes (which act as positive controls) showed that quantitative relationships between *Tbx1*$^{+/lacZ}$ and *Df1/Tbx1*^{lacZ} samples appeared to be maintained.

3.3.2 Identification of differentially regulated genes

Compound heterozygous *Df1/Tbx1*^{lacZ} cells were used for comparison instead of *Tbx1*$^{lacZ/lacZ}$ cells so that the haploid *Df1* genes could be used as an internal control to test the sensitivity of the microarray experiment in detecting significantly down-regulated genes. Our lab has shown previously that the *Df1* genes are decreased to approximately 50% of wild type expression levels in *Df1/+* heterozygotes and they do not exhibit dosage compensation (where expression reverts to wild type levels) (Prescott et al., 2005). Also, the *Df1/+* mutant phenotype reflects *Tbx1* haploinsufficiency, *Df1/+* arch artery defects can be rescued using a *TBX1* transgene and *Df1/+;Tbx1*$^{+/-}$ compound heterozygotes are indistinguishable from *Tbx1*$^{-/-}$ homozygotes (Lindsay et al., 2001; Vitelli et al., 2002a). Thus, the heterozygous *Df1* deletion may be used to accurately represent a *Tbx1* mutant allele.

Using CMFDG-labelling to isolate *Tbx1*-expressing cells meant that only cells containing the *Tbx1-lacZ* allele could be labelled and corresponding wild type cells could not be identified. Therefore, *Df1/Tbx1*^{lacZ} cells could only be compared to

heterozygous *Tbx1*$^{+/lacZ}$ cells which potentially results in smaller gene expression changes than if compared to the relevant wild type cells. Despite these limitations, analysis of the *Df1* deleted genes demonstrated that this microarray experiment could distinguish between *Df1/Tbx1*^{lacZ} cells and *Tbx1*$^{+/lacZ}$ cells accurately. Fourteen of the 17 hemizygously deleted *Df1* genes represented on the microarray chips were significantly down-regulated, displaying a mean relative expression level of 0.594 ± 0.090 in *Df1/Tbx1*^{lacZ} cells.

In addition to the *Df1* genes, 1553 unique transcripts were also found to be downregulated in *Df1/Tbx1*^{lacZ} cells. However, relatively few upregulated genes were detected. This is most likely due to the fact that *Tbx1* is a transcriptional activator (Ataliotis et al., 2005; Stoller and Epstein, 2005; Xu et al., 2004) and thus there is a bias towards downregulation of genes when *Tbx1* function is disrupted. Also, the relatively large number of downregulated genes identified in the microarray suggests that *Tbx1* may be required for maintenance or proliferation of a subpopulation of cells in which case any genes expressed in such a population would appear downregulated.

The microarray, qRT-PCR and WISH analysis identified a number of putative *Tbx1* targets including genes from a variety of functional categories and which represent members of different signalling pathways. These genes and the potential roles they may play in pharyngeal/heart development are summarised in Table 3.3. Expression results for a proportion of the genes were obtained from *in situ* hybridisation analyses carried out by a member of the lab, Irinna Papangeli. These results were generated during her Masters course in which I helped to design the research project and supervised the experiments.

Table 3.3 Downregulated genes and their role in development

Gene	Molecular Function	Expression	Animal model/Human mutations	Potential role in development	References
Nkx2.6	transcription factor	Pharyngeal endoderm, mesoderm and ectoderm, OFT	*Nkx2.6*$^{-/-}$ mice appear phenotypically normal but *Nkx2.5*$^{-/-}$;*Nkx2.6*$^{+/-}$ double knockouts have more severe pharyngeal arch defects than *Nkx2.5* mutants alone (there is a decrease in PE cells and pharyngeal pouches do not form). *NKX2.6* mutations are associated with common arterial trunk.	*Nkx2.6* may be required for proliferation and survival of PE cells.	(Biben et al., 1998; Heathcote et al., 2005; Nikolova et al., 1997; Tanaka et al., 2001; Tanaka et al., 2000)
Cxcl4 or *Pf4*	chemokine	Liver, megakaryocytes	*Cxcl4*$^{+/-}$ and *Cxcl4*$^{-/-}$ mice exhibit increased platelet counts and reduced thrombus formation following injury.	*Cxcl4* may play a role in angiogenesis. The Cxc family member, *Cxcl12* is important for ventricular septum development.	(Gengrinovitch et al., 1995; Keith Ho et al., 2001; Nagasawa et al., 1996; Struyf et al., 2007)
Smad7	signal transduction/ transcriptional regulation	SHF and OFT[#]	*Smad7*$^{hypo/hypo}$ mice are embryonic lethal and exhibit increased Tgfβ signalling and altered B cell responses.	Embryonic lethality could indicate heart or vascular defects. *Smad6*$^{-/-}$ mutants exhibit OFT defects.	(Galvin et al., 2000; Liu et al., 2007b; Luukko et al., 2001; Zwijsen et al., 2000)
Cdh1	cell adhesion	pharyngeal endoderm[#]	*Cdh1*$^{-/-}$ mice exhibit preimplantation defects. *CDH1* mutations are associated with cleft palate and skeletal defects.	The *E-cad* homologue, *N-cad* is required in actin cables for correct pharyngeal morphogenesis.	(Frebourg et al., 2006; Quinlan et al., 2004; Riethmacher et al., 1995)
Ndufa13 or *Grim19*	NADH dehydrogenase activity	heart	*Grim19*$^{-/-}$ embryos die prior to E9.5 due to gastrulation defects.	In *Tbx1* mutants, RA-homeostasis is disrupted leading to pharyngeal defects. *Ndufa13* is induced by RA and could act downstream of this pathway in pharyngeal development.	(Angell et al., 2000; Huang et al., 2004; Kotarsky et al., 2007; Roberts et al., 2006)

Gene	Molecular Function	Expression	Animal model/Human mutations	Potential role in development	References
Crb3	cell adhesion	pharyngeal endoderm[#]	nd	*Crb3* is required for formation of epithelial tight junctions and apicobasal polarity during development which could be important for correct pharyngeal morphogenesis.	(Chalmers et al., 2005; Lemmers et al., 2004)
Sema3c	signal transduction	pharyngeal endoderm, SHF, OFT	*Sema3c*$^{-/-}$ mice exhibit OFT and PAA defects reminiscent of DGS.	*Sema3c* may act as a guidance/attraction cue for cardiac neural crest.	(Feiner et al., 2001)
Slit2	guidance cue, receptor binding	pharyngeal endoderm[#]	*Slit2*$^{-/-}$ mice exhibit perinatal lethality and defects in retinal axon guidance.	Embryonic lethality could indicate heart or vascular defects. *Slit2* acts as a guidance cue for axons and a chemorepellent during cell migration. Drosophila *slit* acts as a guide to align myocardial cells during development.	(Nguyen Ba-Charvet et al., 1999; Plump et al., 2002; Wu et al., 2001; Yuan et al., 1999)
Lztfl1	transcription factor-like	nd	nd	nd	
Isl1	transcription factor	SHF	*Isl1*$^{-/-}$ mice exhibit severe second heart field defects resulting in absence of the OFT, right ventricle and parts of the atria.	*Isl1* is required for proliferation of SHF cells prior to differentiation and regulation of genes important in heart development such as *Mef2c*, *Nkx2.5* and *Shh*.	(Cai et al., 2003a; Dodou et al., 2004; Lin et al., 2006; Takeuchi et al., 2005)
Dsg2	cell-cell adhesion	Endoderm, heart	*Dsg2*$^{-/-}$ mutants exhibit early embryonic lethality at the implantation stage, and *Dsg2*$^{-/-}$ ES cells exhibit decreased proliferation. *DSG2* mutations are associated with arrrhythmogenic right ventricular cardiomyopathy.	*Dsg2* is required for cell adhesion which may be important during pharyngeal morphogenesis and heart development.	(Awad et al., 2006; Eshkind et al., 2002; Mahoney et al., 2002; Pilichou et al., 2006)

Gene	Molecular Function	Expression	Animal model/Human mutations	Potential role in development	References
Bmpr1a	receptor/ signal transduction	ubiquitous	NC-specific knockouts exhibit OFT defects. *Isl1*-cre specific knockouts (SHF &PE) exhibit OFT and atrioventricular septal defects and results in decreased *Tbx2* and *Tbx3* in the AVC. *BMPR1A* mutations are associated with juvenile polyposis.	Mutations in *BmprII*, *Bmp4* and *Bmp7* also result in defects in OFT septation, in addition to arch artery defects, suggesting that Bmp signalling is important for OFT development.	(Delot et al., 2003; Dewulf et al., 1995; Howe et al., 2001; Liu et al., 2004; Stottmann et al., 2004; Yang et al., 2007)
Tbx18	transcription factor	head mesenchyme, splanchnic mesoderm	*Tbx18*$^{-/-}$ mice exhibit craniofacial and skeletal defects in addition to defects in anterior-posterior somite polarity. *Tbx18*$^{-/-}$ mutants also fail to form sinus horns and have defective caval veins.	*Tbx1* and *Tbx18* may interact during formation of the craniofacial skeleton since both mutants exhibit occipital bone defects. In addition, *Tbx1* and *Tbx18* could interact in the overlapping expression domain within the SHF during cardiovascular development.	(Bussen et al., 2004; Christoffels et al., 2006; Kraus et al., 2001)
Tle4	cofactor for transcription	pharyngeal pouches*	Misexpression of *Tle4* results in heart laterality defects in medaka embryos.	*Tle4* is a corepressor for transcriptional repressors eg. *Gbx2* and *Hes1* which are potential downstream targets of *Tbx1*.	(Bajoghli et al., 2007; Heimbucher et al., 2007; Koop et al., 1996; Nuthall et al., 2002)
Daam1	actin binding/actin cytoskeletal organisation	pharyngeal endoderm#	nd	*Daam1* mediates actin cytoskeletal rearrangements and is involved in the non-canonical Wnt-signalling pathway in which multiple members such as *Vangl2 and Dvl2,* exhibit roles in OFT development.	(Aspenstrom et al., 2006; Habas et al., 2001; Hamblet et al., 2002; Nakaya et al., 2004; Phillips et al., 2005; Phillips et al., 2007)
Gsk3β	signal transduction/ kinase	ubiquitous	*Gsk3β*$^{-/-}$ mice exhibit cleft palate and skeletal defects. *Gsk3β*$^{-/-}$ mice also die during midgestation prior to E14.5 due to liver degeneration.	*Gsk3β* is involved in the regulation of multiple signalling pathways, including Wnt and Shh signalling, which are important in pharyngeal and heart development.	(Hoeflich et al., 2000; Liu et al., 2007a)

Gene	Molecular Function	Expression	Animal model/Human mutations	Potential role in development	References
Notch3	receptor/ transcription factor	pharyngeal endoderm[#]	*Notch3*$^{-/-}$ adult mice exhibit defects in VSMC maturation and arterial differentiation and also have a hypoplastic thymus. Transgenic mice overexpressing *Notch3* exhibit VSMC degeneration and impaired vascular mechanotransduction. *NOTCH3* mutations are associated with CADASIL, a type of adult-onset vascular dementia.	*Tbx1* and *Notch3* may interact in development of the thymus and during vascular smooth muscle development.	(Domenga et al., 2004; Dubroca et al., 2005; Joutel et al., 1996; Kitamoto et al., 2005; Ruchoux et al., 2003)
Hes1	transcriptional repressor	pharyngeal endoderm, SHF and pharyngeal mesenchyme.	*Hes1*$^{-/-}$ mutants exhibit DGS-like OFT, AA, palate and thymic defects. *Hes1*$^{-/-}$ mice also exhibit defects in neurogenesis, ear, pituitary gland, pancreas, kidney, lung and eye development.	*Hes1* regulates multiple developmental processes including differentiation, and proliferation of progenitor cell populations.	(Ishibashi et al., 1995; Ito et al., 2000; Jensen et al., 2000; Kaneta et al., 2000; Kita et al., 2007; Ohtsuka et al., 1999; Tomita et al., 1999; Zheng et al., 2000)
Six2	transcription factor	pharyngeal arches*	*Six2*$^{-/-}$ mice exhibit renal hypoplasia and perinatal lethality. Transgenic embryos overexpressing *Six2* exhibit defects in pharyngeal arch 2-derived skeletal elements.	*Six2* is required for maintenance and proliferation of the mesenchymal progenitor cell population in kidney development. *Tbx1* and *Six2* may interact in formation of the second pharyngeal arch..	(Kutejova et al., 2005; Oliver et al., 1995; Self et al., 2006)
Dab2	cytoplasmic adaptor	pharyngeal arches, strong expression in caudal region of 2nd pharyngeal arch*	*Dab2*$^{-/-}$ mice are embryonic lethal due to extraembryonic defects in which there is decreased proliferation at E5.5. Epiblast-specific *Dab2* knockouts appear phenotypically normal but have some kidney defects.	*Dab2* acts as an adaptor protein and is involved in signal transduction and cell positioning control which may be important in pharyngeal morphogenesis.	(Hocevar et al., 2001; Morris et al., 2002; Yang et al., 2002)
Plek	signalling factor	nd	nd	*Plek* causes reorganisation of the actin cytoskeleton.	(Ma and Abrams, 1999)

Gene	Molecular Function	Expression	Animal model/Human mutations	Potential role in development	References
Cyp26a1	Retinoic acid metabolizing enzyme	pharyngeal pouches*	*Cyp26a1*$^{-/-}$ mice exhibit defects in kidney, urogenital tract, hindgut, vertebrae and brain development. Knockdown of all *Cyp26* genes in chick causes a DGS-like phenotype.	*Cyp26a1* is required to maintain the correct RA levels during development.	(Abu-Abed et al., 2001; de Roos et al., 1999; Roberts et al., 2006)
Cyp26b1	Retinoic acid metabolizing enzyme	pharyngeal endoderm and ectoderm	*Cyp26b1*$^{-/-}$ mice exhibit DGS-like palate, thymic, OFT and AA defects. Knockdown of all *Cyp26* genes in chick causes a DGS-like phenotype.	*Cyp26b1* is required to maintain the correct RA levels during development.	K. Yashiro pers comm., (MacLean et al., 2001; Roberts et al., 2006)
Gbx2	transcription factor	pharyngeal endoderm, ectoderm and mesoderm[§]	*Gbx2*$^{-/-}$ mutants exhibit DGS-like palate, OFT and PAA defects. *Tbx1*$^{+/-}$;*Gbx2*$^{+/-}$ mutants exhibit increased penetrance of PAA defects.	*Gbx2* and *Tbx1* could interact in patterning the neural crest during pharyngeal arch development.	(Byrd and Meyers, 2005)S. Ivins and A. Calmont, pers. comm.

*Expression within a specific pharyngeal tissue not yet determined

[#]Expression analysis carried out by I. Papangeli

[§]A. Calmont, pers. comm.

Abbreviations: ES, embryonic stem; NC, neural crest; nd, not determined; OFT, outflow tract; PE, pharyngeal endoderm; PAA, pharyngeal arch artery; SHF, second heart field

The primary defect in *Tbx1*$^{-/-}$ homozygous mutants is considered to be failure of pharyngeal segmentation, which leads to craniofacial, glandular and cardiovascular malformations. However, *Tbx1* is expressed in multiple tissues of the pharyngeal system within the endoderm, ectoderm, and core mesoderm which has made it difficult to determine the role that *Tbx1* plays within each tissue during pharyngeal development. Evidence from tissue-specific deletion studies suggests that *Tbx1* is required in both the mesoderm and pharyngeal epithelia for development of the majority of structures affected in *Tbx1*$^{-/-}$ mutants since deletion within either tissue recapitulates most of the *Tbx1*$^{-/-}$ phenotype (Arnold et al., 2006b; Zhang et al., 2006). However, *Tbx1* is required exclusively in the pharyngeal epithelia for secondary palate and fourth PAA development (Arnold et al., 2006b; Zhang et al., 2005; Zhang et al., 2006). Reactivation experiments have also revealed that OFT, second pharyngeal arch and third and sixth PAA development are dependent on mesodermal expression of *Tbx1* (Zhang et al., 2006). Similar "restoration of function" experiments will need to be conducted to better define the requirement for *Tbx1* in the pharyngeal endoderm and ectoderm.

It is clear from these studies that *Tbx1* plays cell-autonomous and non cell-autonomous roles in pharyngeal development, but, in order to mediate interactions between tissues, *Tbx1* may regulate the expression of genes encoding signalling factors. To date, the only characterised, downstream targets of *Tbx1* which could act in this manner are members of the Fgf signalling pathway. *Fgf3*, *Fgf8* and *Fgf10* are secreted fibroblast growth factors which are downregulated in the pharyngeal region of *Tbx1*$^{-/-}$ embryos (Aggarwal et al., 2006; Arnold et al., 2006b; Hu et al., 2004; Xu et al., 2004; Zhang et al., 2005). *Fgf8* and *Tbx1* interact genetically in development of the fourth arch artery (Vitelli et al., 2002b; Vitelli et al., 2006). However, due to possible functional redundancy between the Fgf ligands, it has been difficult to determine if they play a role in other aspects of pharyngeal development, downstream of *Tbx1* (Aggarwal et al., 2006). Tissue-specific ablation of *Fgf* signalling in *Tbx1* mutants may clarify the genetic interaction between these pathways, but other signalling factors are most likely also involved in mediating tissue interactions regulated by *Tbx1*.

In this microarray, the signalling effectors, *Sema3c* and *Slit2* were identified as dysregulated in *Tbx1* null cells. Both genes are expressed in the pharyngeal endoderm and *Sema3c* is also present in the SHF. *Slit2* and *Sema3c* have been previously demonstrated to act as guidance cues for axons (Bagnard et al., 1998; Koppel et al., 1997; Nguyen Ba-Charvet et al., 1999; Plump et al., 2002). In addition, *Slit2* can act as a chemorepellent during cell migration (Wu et al., 2001) and Drosophila *Slit* has been shown to play a role in aligning myocardial cells at the midline during heart tube development (Qian et al., 2005). It is possible that in the context of pharyngeal morphogenesis, these genes may act to regulate NC cell migration for proper arch artery and OFT development or possibly, *Slit2* could regulate endodermal cell movements in formation of the pharyngeal pouches.

One of the general mechanisms through which *Tbx1* acts to regulate development is by controlling cell proliferation. *Tbx1* has been shown to be required to maintain cell proliferation in the pharyngeal endoderm, mesoderm and otic vesicle (Vitelli et al., 2003; Xu et al., 2005; Xu et al., 2004; Zhang et al., 2006). A number of genes identified in the microarray could act downstream of *Tbx1* in this process, including *Nkx2.6*, *Gbx2*, *Isl1* and *Hes1*. Mouse mutants for these genes all show defects in cell proliferation (Cai et al., 2003a; Murata et al., 2005; Tanaka et al., 2001; Waters and Lewandoski, 2006).

In addition to proliferation, *Tbx1* may also be required for correct cell migration in the formation of the pharyngeal arches. The pharyngeal apparatus develops in a cranial to caudal manner and forms initially as outpocketings of the pharyngeal endoderm, which moves towards the surface ectoderm. These tissues come into close contact and expand along the proximodistal axis to form the pharyngeal pouches and clefts separating each pharyngeal arch (Graham and Smith, 2001). Quinlan et al. have demonstrated that the formation of actin cables within the pharyngeal endoderm linked via N-Cadherin adherens junctions plays an important role in this process (Quinlan et al., 2004). Given that cell adhesion molecules and genes involved in cytoskeletal rearrangement such as *Cdh1*, *Crb3*, *Daam1*, *Dab2* and *Plek* were verified as downregulated in *Df1/Tbx1*^{lacZ} cells, it would be interesting to investigate whether *Tbx1* also plays a direct role in mediating cell shape changes and cell migration in pharyngeal morphogenesis.

In an effort to identify transcriptional targets of *Tbx1*, a novel approach was undertaken to isolate *Tbx1*-expressing cells from mutant embryos by labelling *Tbx1-lacZ* cells with a fluorogenic, β-galactosidase substrate. Gene expression analysis of PCR-amplified RNA from these cells has led to the identification of novel *Tbx1* targets (and the elucidation of genetic pathways) which may play important roles in pharyngeal and heart development.

3.3.3 Future experiments

Microarray analysis is an excellent tool for investigating global gene expression changes caused by disruption of a transcription factor. In this project, confining the analysis to *Tbx1*-expressing cells has allowed for enrichment of cell autonomous effects. However, *Tbx1* is expressed in multiple cell types within the pharyngeal region which were all included in the microarray and this method gives no indication as to where the changes occur *in vivo* or whether dysregulated genes are primary or secondary targets.

WISH analysis of the dysregulated genes can be used to address the first issue and currently, the lab is carrying out *in situ* experiments on the potential *Tbx1* targets identified by the microarray in order to prioritise genes for further investigation. *In situ* analysis should determine whether genes are downregulated in multiple or a subset of *Tbx1* expression domains, the degree of downregulation and whether genes are also altered in adjacent non-*Tbx1*-expressing tissues such as the neural crest, which also plays an important role in pharyngeal development.

Another disadvantage of including multiple *Tbx1* cell types in the microarray analysis is that changes which occur only in a subdomain may be masked by no changes in other *Tbx1*-expressing tissues. For example, *Fgf8,* which has been shown to genetically interact with *Tbx1* (Vitelli et al., 2002b; Vitelli et al., 2006) was not identified as dysregulated in this microarray. This may be because while *Fgf8* is downregulated in the pharyngeal endoderm and SHF of $Tbx1^{-/-}$ mutants, *Fgf8* expression within the pharyngeal ectoderm, in an area overlapping with *Tbx1*, remains robust (Arnold et al., 2006b; Zhang et al., 2005; Zhang et al., 2006). Future microarrays may overcome this problem by focusing on only one *Tbx1* domain for analysis. This could be achieved if the enhancer elements required for *Tbx1* expression within a particular tissue are

discovered. Subsequently, transgenic mice expressing GFP under control of these regulatory elements could be used for isolation of homogeneous *Tbx1* cell populations. In order to distinguish between direct and indirect targets of *Tbx1*, the results from this microarray need to be combined with an experiment such as ChIP-chip, in which chromatin immunoprecipitation is coupled with microarray analysis. This method would involve using formaldehyde to crosslink Tbx1 with its genomic DNA binding sites followed by immunoprecipitation with a Tbx1 antibody. The regions bound by Tbx1 could then be used as a probe on genomic DNA microarrays. Results from ChIP-chip could be compared to the gene expression analysis to determine if any identified genomic DNA binding sites for TBX1 occur within the vicinity of dysregulated genes.

In addition to determining whether genes are direct or indirect targets of *Tbx1*, *in vivo* functional studies should be undertaken to confirm a role for potential targets in pharyngeal and/or heart development. This could be achieved by generating knockout or conditionally mutant mouse models or by using antisense morpholino oligonucleotides in zebrafish or chick. Furthermore, to test whether genes act in the same pathway as *Tbx1*, epistatic interactions will need to be analysed in animal models by crossing mouse mutants or using double morpholino injections in zebrafish. Tissue-specific roles for putative *Tbx1* targets could be examined by conditional deletion of genes and/or restoration of gene function in a mutant *Tbx1* background. These experiments would help to define the requirement for a particular gene downstream of *Tbx1* and in development.

These studies will provide the basis for investigating the molecular mechanisms through which *Tbx1* acts to regulate pharyngeal and heart development.

CHAPTER 4. *TBX1* BAC RECOMBINEERING

4.1 INTRODUCTION

At present, *Tbx1*-expressing cells can be isolated from *Tbx1-lacZ* mice using the mutant *Tbx1-lacZ* allele which can be identified by using a fluorescent *lacZ* substrate. Labelled cells can then be collected by FACS. However, there are a number of disadvantages to isolating cells by this method. Firstly, corresponding wild type cells cannot be identified because they cannot be labelled. In addition, treating the cells with CMFDG and other chemicals in this protocol may potentially interfere with normal cell function and gene expression and is also time-consuming. In fact, the chemical chloroquine, which is used to reduce background caused by lysosomal enzyme activity, has been shown to decrease cell viability (Poot and Arttamangkul, 1997).

In order to overcome these limitations, recombination-mediated genetic engineering of bacterial artificial chromosomes (BAC recombineering) was used to generate a transgenic mouse carrying a GFP-labelled *Tbx1* allele. BAC recombineering is a method of modifying large genomic fragments of DNA using phage-based homologous recombination. In the past, genetic engineering by homologous recombination required the use of restriction enzymes, ligase and large regions (hundreds of base pairs) of homology. By incorporating a prophage with recombination functions into bacterial cells, scientists developed a more efficient and simple method of modifying BACs and PACs which requires less than 50bp homology (Figure 4.1A) (Lee et al., 2001; Muyrers et al., 2001; Yu et al., 2000). Lee and colleagues introduced a defective λ prophage into the BAC host strain, DH10B for use in BAC recombineering (Lee et al., 2001). The λ prophage has the recombination genes, *gam*, *bet* and *exo* whose expression is under control of a temperature sensitive repressor, λ-cI857. *Exo* encodes an exonuclease which digests the 5' ends of linear dsDNA then *bet* attaches to the 3' overhangs and mediates annealing to complementary sequences of DNA in the host cell. *Gam* is required to prevent the RecBCD activity of the host cell which would degrade the linear targeting cassette. Normally, the cells are maintained at 32°C and the repressor is active but when the cells are shifted to 42°C for 15 minutes, the recombination genes are expressed and homologous recombination can occur between the target DNA and the BAC (Figure 4.1B) (Lee et al., 2001; Yu et al., 2000).

Additional genes including *cre*, *flpe* and the galactose operon have also been introduced into the BAC host strains to make modifying BAC DNA even easier (Lee et al., 2001; Warming et al., 2005). BAC recombineering has thus made it possible to modify large pieces of DNA efficiently and has made constructing gene targeting vectors for the production of transgenic mice much easier. Recombineering can be used to introduce reporter genes, subclone out regions of genomic DNA by gap repair and even introduce point mutations. This system was used to modify the *Tbx1* gene within a BAC.

Figure 4.1 BAC recombineering to generate a modified allele
(A) A linear targeting cassette containing 40 – 50bp homology arms is introduced into cells containing the BAC of interest. (**B**) The defective prophage contains *gam*, *bet* and *exo* genes which are under control of the P_L promoter and the temperature-sensitive repressor, *c1857*. Arabinose-inducible *Cre* or *Flp* recombinase genes are also contained in the defective prophage. Phage-mediated homologous recombination is induced by shifting the cells to 42ºC. The phage recombination exonuclease, λ-Exo, digests the 5' ends of the targeting cassette leaving 3' overhangs. λ-Beta then binds to the 3' overhangs and mediates annealing to complementary ssDNA in the cell resulting in a recombinant BAC. Modified from (Copeland et al., 2001)

4.2 RESULTS

4.2.1 BAC recombineering

The aim of this project was to generate transgenic mice carrying an additional labelled, reversible, mutant *Tbx1* allele (TgTbxlfloxGFP) by inserting a floxed IRES2-eGFP sequence into intron 1 of *Tbx1* within a BAC (Figure 4.2). Introducing an IRES2-eGFP sequence (containing a poly A signal and downstream of a splice acceptor) within the first intron of *Tbx1*, after the first coding exon should generate either a null mutant allele or at least a hypomorphic allele, much like gene trap insertions (Stanford et al., 2001).

Producing TgTbx1floxGFP mice by pronuclear injection of oocytes should generate phenotypically normal mice, depending on the insertion site, since the allele is mutant but it is contained within a BAC, which inserts randomly into the murine genome. Cells still express endogenous, wild type *Tbx1* thus negating the null phenotype of the mutant transgene. In any event, mice with an extra copy of *Tbx1* should be phenotypically normal since mice expressing up to four copies of a BAC containing *Tbx1* plus three other genes (*Gnb1l*, *Gp1bß* and *Cdcrel1)* are phenotypically normal as well (Lindsay et al., 2001; Zhang and Baldini, 2007). The rationale behind modifying a *Tbx1* BAC to make transgenic animals for future studies lies in experiments which have shown that using a 140kb PAC containing *Tbx1* is sufficient to rescue the arch artery defects present in *Df1/+* mouse mutants (Lindsay et al., 2001). This implies that the 140kb region including the *Tbx1* gene contains regulatory elements which are sufficient for normal *Tbx1* function at least in the tissues required for proper arch artery development.

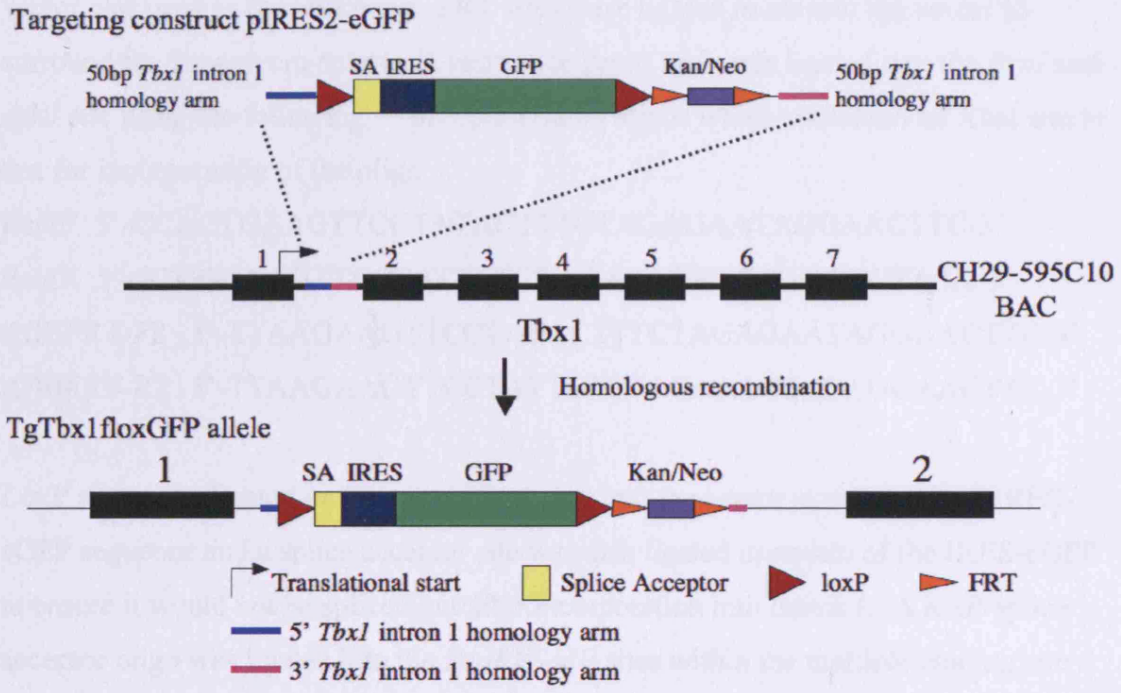

Figure 4.2 Generation of the TgTbx1floxGFP allele
The targeting construct was generated by cloning loxP sites, FRT sites and *Tbx1*-intron 1 homology arms into the pIRES2-eGFP vector. Electroporation of this vector into competent bacterial cells containing the CH29-595C10 BAC and induction of homologous recombination resulted in the recombined BAC containing a floxed IRES2-eGFP within intron 1 of *Tbx1*.

4.2.1.1 Generation of the Tbx1 targeting vector

To incorporate a floxed IRES2-eGFP into intron 1 of *Tbx1*, a targeting vector for homologous recombination was generated (Figure 4.2). The pIRES2-eGFP plasmid vector was used as the backbone. FRT sites were ligated *in cis* into the vector to surround the kanamycin/neomycin resistance genes and were ligated into the *BsaI* and *AflII* site using the following 5'-phosphorylated oligos which contained an XbaI site to test for incorporation of the oligo:

BsaIF 5'-CCACTGAAGTTCCTATACTTTCTAGAGAATAGGAACTTC-3'

BsaIR 5'-GTGGGAAGTTCCTATTCTCTAGAAAGTATAGGAACTTCA-3'

AflIIFRT-F2 5'-TTAAGAAGTTCCTATACTTTCTAGAGAATAGGAACTTC-3'

AflIIFRT-R2 5'-TTAAGAAGTTCCTATTCTCTAGAAAGTATAGGAACTTC-3'

LoxP sites were ligated in the same orientation into the vector to surround the IRES-eGFP sequence and a splice acceptor site was also ligated upstream of the IRES-eGFP to ensure it would not be spliced out after incorporation into intron 1. A loxP-splice acceptor oligo was ligated into the *EcoRI/SacII* sites within the multiple cloning site region upstream of IRES2-eGFP using the following 5'-phosphorylated oligos containing a SalI site to test for incorporation:

loxpSA-F

5'AATTATAACTTCGTATAGCATACATTATACGAAGTTATGTCGACAGGGTTT
CCTTGACAATATCATACTTATCCTGTCCCTTTTTTTTCCACAGGC-3'

loxpSA-R

5'CTGTGGAAAAAAAAGGGACAGGATAAGTATGATATTGTCAAGGAAACCC
TGTCGACATAACTTCGTATAATGTATGCTATACGAAGTTAT-3'

Another loxP site was ligated into the *NotI* site downstream of the IRES-eGFP sequence using the following 5'-phosphorylated oligos containing a *PstI* site to test for incorporation:

NotILoxP-F

5'GGCCGCATAACTTCGTATAGCATACATTATACGAAGTTATCTGCAGGC-3'

NotILoxp-R

5'GGCCGCCTGCAGATAACTTCGTATAATGTATGCTATACGAAGTTATGC-3'

The vector was sequenced using primer c, Iresgfp1880-F (Figure 4.4) to ensure the FRT sequence ligated into the *AflII* site and the loxP sequence ligated into the *NotI* site were in the correct orientation in relation to the other FRT and loxP sites.

Finally, 50bp of homologous *Tbx1* intron 1 sequences were ligated into the *BsaI* site and *NheI/XhoI* site within the multiple cloning site region to ensure the vector would be targeted into *Tbx1*. Both sets of oligos contained an *NruI* site to test for incorporation and to linearise the vector and remove unwanted vector sequence before homologous recombination into intron 1 of *Tbx1*. The following 5'-phosphorylated oligos were used for ligation:

BsaItbx1intron1-F

5'CCACACCAGCTCCGTGGCCAAGGAGGCTCAGGGCCTGTTTGCAAAGCCTT CTCGCGA-3'

BsaItbx1intron1-R

5'GTGGTCGCGAGAAGGCTTTGCAAACAGGCCCTGAGCCTCCTTGGCCACGG AGCTGGT-3'

NheItbx1intron1-F

5'CTAGCTCGCGAGAGGGAAAAAGGAACAATTGCAGATGCTCCCGATTTGAC CAGTAGACC-3'

XhoItbx1intron1-R

5'TCGAGGTCTACTGGTCAAATCGGGAGCATCTGCAATTGTTCCTTTTTCCCT CTCGCGAG-3'

The targeting vector was linearised by digesting with NruI in preparation for electroporation into the target BAC.

4.2.1.2 Tbx1 BAC Recombineering of CH29-595C10

The *Tbx1* BAC, CH29-595C10 was transfomed by electroporation into EL250 cells, a competent cell line containing temperature-inducible recombination genes and an arabinose-inducible *flpe* gene (Lee et al., 2001; Yu et al., 2000). Digestion by HindIII and NotI was carried out to determine the normal digestion pattern of the BAC (Figure 4.3A). Originally, four *Tbx1*-containing BACs, generated from different mouse strains, were obtained. CH29-595C10, generated from a NOD mouse strain, was chosen for subsequent recombineering experiments so that the transgene could potentially be distinguished from the C57Bl/6 host strain, by SNP-based PCR.

The pTamp vector (Lee et al., 2001) was used to try to remove the loxP site present in the CH29-595C10 BAC vector backbone, pTARBAC2.1. Removal of the loxP site was necessary to prevent it from interfering with the loxP sites contained within the targeting vector. BamHI digestion of the pTamp vector (Lee et al., 2001) was used to release the ampicillin cassette and pBeloBAC11 vector sequences flanking the loxP site. This linear DNA was then used as a targeting vector to replace the loxP site and was electroporated into EL250 cells containing the BAC. Subsequent recombined BACs were isolated by selecting for *amp*-resistant colonies (Lee et al., 2001).

The targeting vector was linearized by digesting with NruI. EL250 cells carrying the modified CH29-595C10 *Tbx1* BAC were shifted to 42°C for 15 minutes to induce the recombination genes, *exo*, *bet* and *gam* and then electroporated with the linearized targeting vector. Kanamycin-resistant colonies were selected the next day and HindIII and NotI restriction digests confirmed the integrity of the BAC.

The *kanamycin/neomycin* selection cassette was removed to prevent it from interfering with *Tbx1* function. To induce recombination between the FRT sites surrounding the *kan/neo* gene, Flp recombinase was activated in EL250 cells carrying the CH29-595C10 BAC, by addition of L-arabinose. Fifty chloramphenicol-resistant colonies were picked and replica-plated onto kanamycin plates to test for loss of resistance. Forty-nine out of fifty colonies were kanamycin-sensitive indicating that the *FRT* sites were functional. Restriction digest and FIGE gel electrophoresis of several clones were carried out again to assess the integrity of the BAC (Figure 4.3B). A different digest pattern was apparent for the recombined BACs compared to the original CH29-595C10 BAC.

However, this was assumed to be due to the deletions and insertions incorporated into the BAC by the above recombination steps. This recombined BAC was sent to PolyGene and used for pronuclear injection into mouse oocytes to generate transgenic mice carrying a reversible, *Tbx1*-null/hypomorphic allele.

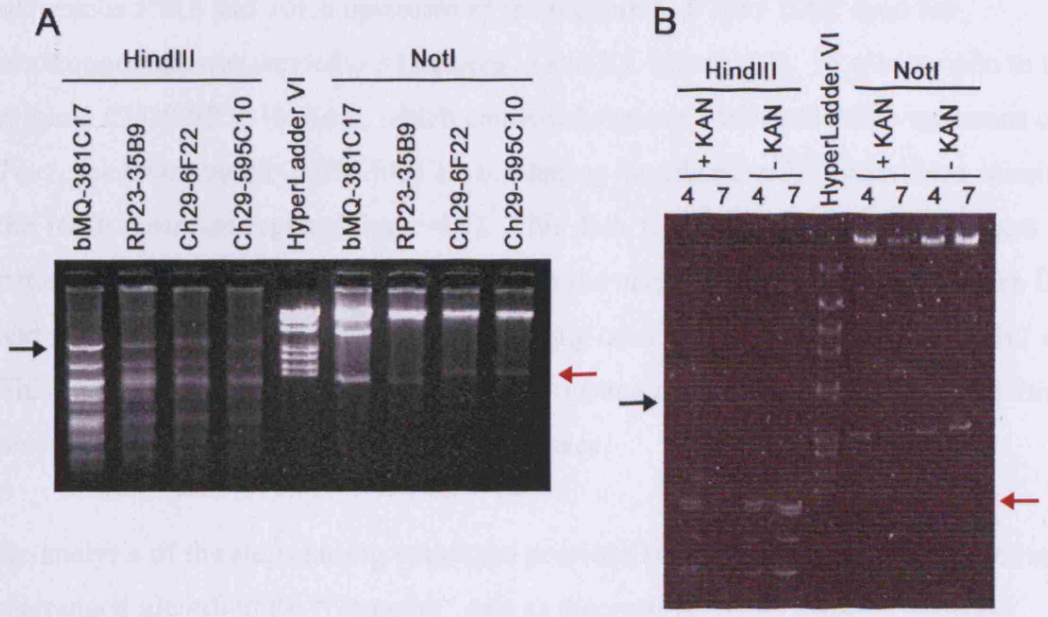

Figure 4.3 BAC recombineering of CH29-595C10
(**A**) HindIII and NotI digests of BACs containing *Tbx1* prior to recombineering. (**B**) HindIII and NotI digests of the *Tbx1*floxGFP CH29-595C10 BAC before and after removal of the *kan* selection cassette looks the same (4 and 7 are clone numbers). However, the digestion pattern of the recombined CH29-595C10 BAC (**B**) appears different to the unmodified BAC (**A**). The bands in (**A**) labelled by the black and red arrows do not appear in (**B**). Note that the gels were run for different lengths of time.

According to PolyGene, a total of 199 injected zygotes were transferred to 9 foster mothers, leading to the birth of 49 pups, from which tail biopsies were collected for genotyping. Twenty-five of the 49 pups were positive for the GFP vector sequence as analysed by PCR. Fourteen potential TgTbx1floxGFP founders were mated with C57Bl/6 wild type mice to collect litters and test for fluorescence of the transgene. Five, E9.5 litters were collected from potential TgTbx1floxGFP mice (#10, 11, 28, 42 and 44). However, none of the embryos were fluorescent within the expected *Tbx1*-expressing regions of the pharyngeal apparatus, head mesenchyme or otic vesicle. In order to determine whether the insert was being expressed, RT-PCR analysis was carried out on one of the litters obtained from TgTbx1floxGFP x wildtype matings using primers spanning the region from *Tbx1* exon 1 to the IRES sequence of the insert using primers e and f (Figure 4.4). A band of approximately 200bp was amplified.

However, the PCR should have yielded a product of 271bp, indicating that this band was either a non-specific product or that part of the insert had been deleted.
To confirm that the recombined BAC contained all of the *Tbx1* regulatory regions and to determine why the TgTbx1floxGFP mice did not fluoresce, PCR analysis of sequences 55Kb and 10Kb upstream of the recombined *Tbx1* BAC used for electroporation was carried out (primers i,j and k,l, Figure 4.4). In comparison to the original CH29-595C10 BAC, which contained regions 10Kb and 55Kb upstream of *Tbx1*, the recombined CH29-595C10 containing the IRES2-eGFP insert was missing the 10Kb upstream region (Figure 4.5). This data, together with the altered digest pattern of the recombined BAC compared to the original BAC suggested that the BAC had aberrantly rearranged at some point during construction of the modified *Tbx1* allele. This rearrangement had led to disruption of upstream regulatory sequences and this is presumably why the transgene did not fluoresce.

Re-analysis of the steps during which the previous BAC, CH29-595C10, may have rearranged identified the "Tamping" step as the most probable cause of aberrant rearrangement. Many BAC vector backbones contain a loxP site which needs to be removed to prevent it from interfering with any loxP sites contained within the targeting cassette. The pTamp vector contains an *ampicillin* gene flanked by arms homologous to pBeloBAC11 vector regions surrounding the endogenous *loxP* site. This vector can be used to replace the endogenous loxP site by gene targeting. However, the pTamp plasmid is only applicable for use with BACs contained within the vector, pBeloBAC11 (Lee et al., 2001). The BAC used for engineering (CH29-595C10) is contained within the pTARBAC2.1 vector which has different sequences flanking its *loxP* site, therefore, this is the most likely step at which rearrangement occurred.

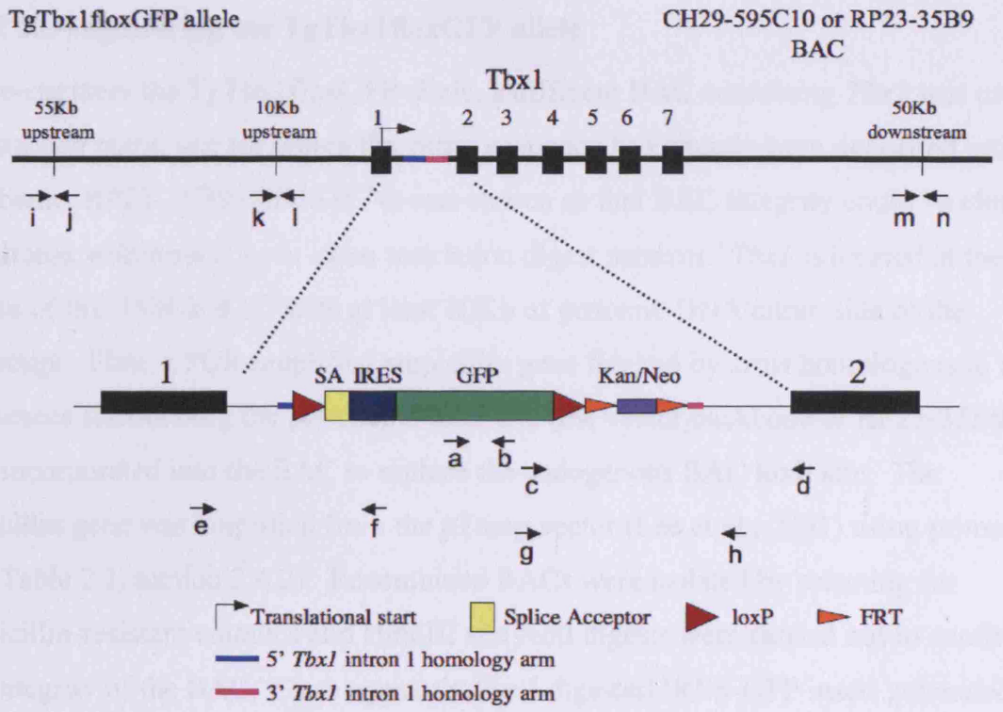

Figure 4.4 PCR primers used to assess BAC integrity
PCR primers located upstream and downstream of Tbx1 and also within the modified Tbx1 allele were used to analyse TgTbx1floxGFP BAC integrity and for genotyping. Primers are represented by the labelled black arrows. The sequences for primers a to n are located in section 2.4.2, Table 2.3.

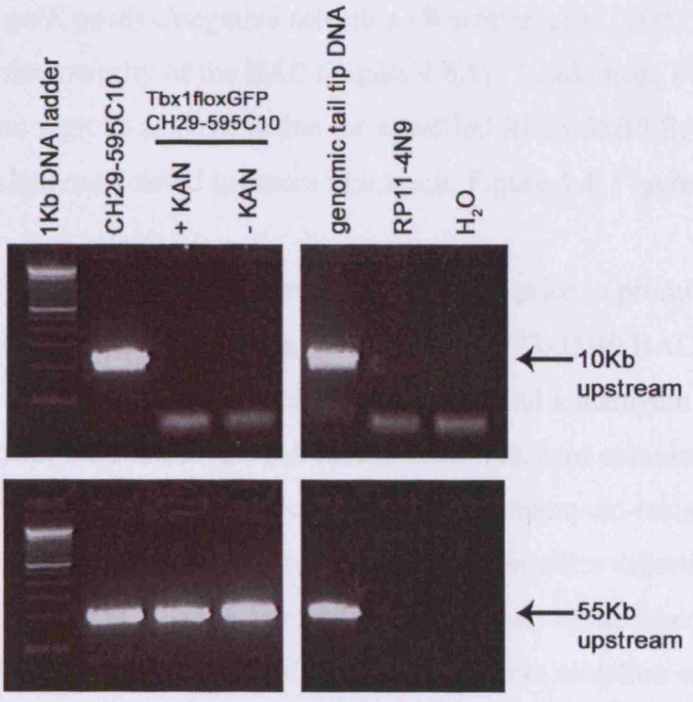

Figure 4.5 PCR analysis of genomic DNA surrounding *Tbx1*
The presence of genomic DNA 10Kb and 55Kb upstream of Tbx1 was analysed in recombined, Tbx1floxGFP CH29-595C10 BACs. The 10Kb upstream region was missing in recombined Tbx1floxGFP CH29-595C10 BACs. The 55Kb upstream region was present in all recombined BACs. Genomic tail tip DNA and the chromosome 11 BAC, RP11-4N9 were used as positive and negative controls, respectively.

4.2.2 Re-engineering the TgTbx1floxGFP allele

To re-engineer the TgTbx1floxGFP allele, a different BAC containing *Tbx1* was used as the starting point, one for which the entire sequence had already been deposited into Genbank. RP23-35B9 (AC133574) was chosen so that BAC integrity could be closely monitored with respect to *in silico* restriction digest patterns. *Tbx1* is located at the centre of this 168Kb BAC with at least 80Kb of genomic DNA either side of the transcript. First, a PCR-amplified ampicillin gene flanked by arms homologous to the sequences surrounding the pBACe3.6 loxP site (the vector backbone of RP23-35B9) was incorporated into the BAC to replace the endogenous BAC loxP site. The ampcillin gene was amplified from the pTamp vector (Lee et al., 2001) using primers o,p, Table 2.3, section 2.4.2). Recombined BACs were isolated by selecting for ampicillin-resistant colonies and HindIII and NotI digests were carried out to confirm the integrity of the BAC. Once again, the NruI-digested IRES-GFP insert generated previously was engineered into the RP23-35B9 BAC by electroporating the linearised targeting vector into the RP23-35B9 BAC contained within SW105 cells and selecting for kanamycin-resistant colonies the next day. SW105 cells were derived from the EL250 temperature inducible competent cell strain. However, they also contain a *gal* operon for use in *galK* postive/negative selection (Warming et al., 2005). A HindIII digest confirmed the integrity of the BAC (Figure 4.6A). In addition, PCR analysis of up and downstream regions of *Tbx1* within the modified RP23-35B9 BAC confirmed that these regions had not deleted (primers i,j;k,l;m,n, Figure 4.4, Figure 4.6B)

The *kanamycin/neomycin* selection cassette was removed prior to pronuclear injection by inducing *Flp* in SW105 cells carrying the modified RP23-35B9 BAC by addition of L-arabinose and cells were plated onto chloramphenicol and kanamycin plates to test for loss of kanamycin-resistance. 24 chloramphenicol-resistant colonies were then replica-plated onto kanamycin plates to confirm loss of kanamycin-resistance. A SalI digest confirmed BAC integrity, matching the predicted, *in silico* digestion pattern (Figure 4.6C). Finally, a PCR using primers spanning a part of the insert and exon 2 of *Tbx1* (primers c,d, Figure 4.4) confirmed that the kanamycin selection cassette had been removed, giving PCR products of the correct, predicted size (Figure 4.6D).

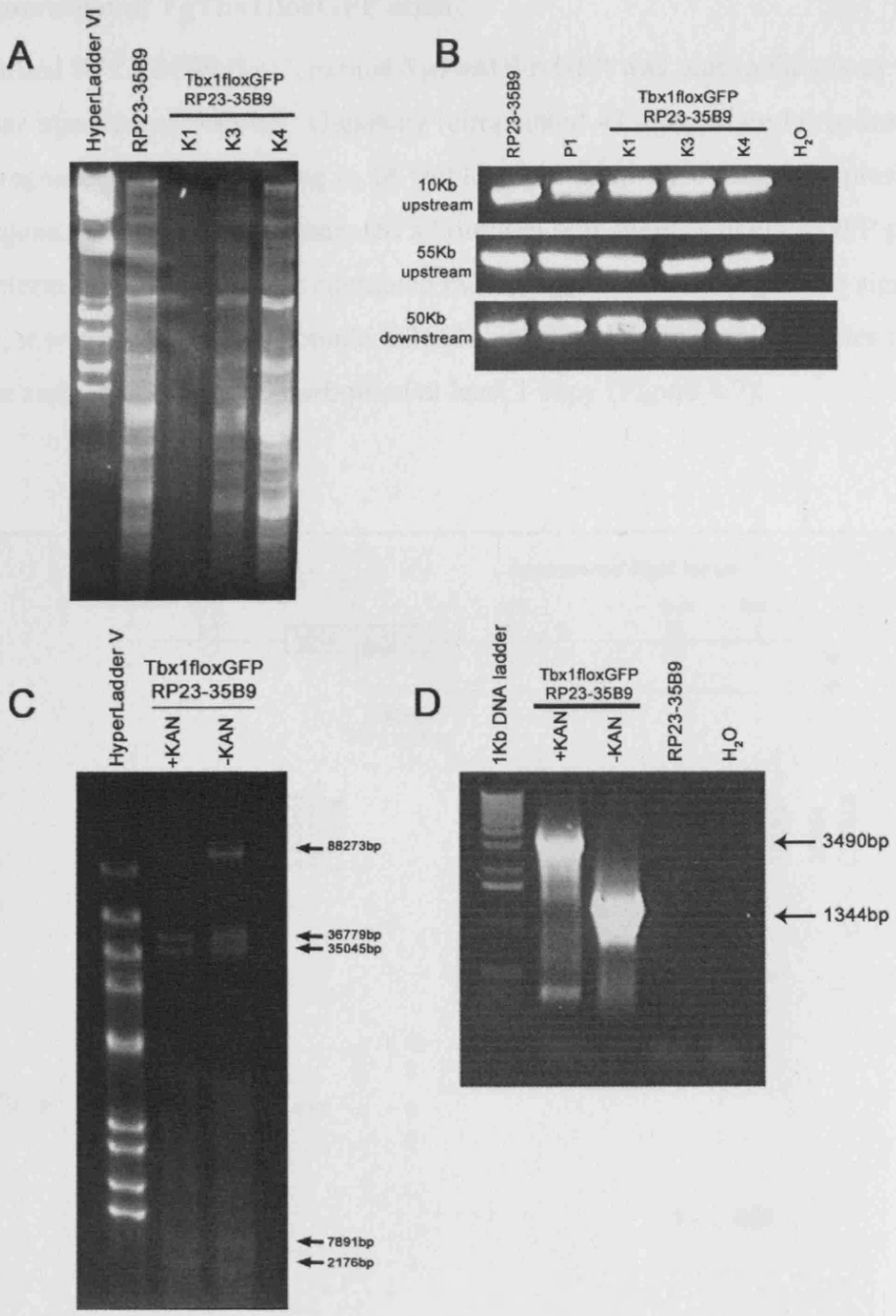

Figure 4.6 Re-engineering the modified *Tbx1* allele in RP23-35B9
(**A**) The HindIII digestion pattern of Tbx1floxGFP RP23-35B9 BACs, K1, K3 and K4 matches the original RP23-35B9 digest pattern. (**B**) PCR analysis shows that regions of genomic DNA, 10Kb and 55Kb upstream and 50Kb downstream of *Tbx1* are present in the Tbx1floxGFP BACs, K1, K3 and K4 plus another RP23-35B9 recombinant, P1. (**C**) The SalI digestion pattern of the K3 recombinant before and after removal of the *kan* selection cassette matches the predicted, *in silico* digest pattern. (**D**) PCR analysis of the Tbx1floxGFP RP23-35B9 recombinant before and after removal of the *kan* selection cassette using primers spanning the IRES sequence of the insert and *Tbx1* exon 2.

4.2.3 Generation of TgTbx1floxGFP mice

The modified RP23-35B9 BAC, named TgTbx1floxGFP was sent to Genoway for pronuclear injection of oocytes. Genoway reimplanted 47 injected embryos into 2 pseudopregnant mothers, resulting in 14 viable pups which were tested for presence of the transgene. Genoway also conducted a Southern blot analysis using a GFP probe which determined that 2 animals contained the transgene. According to the signal intensity, it was estimated that founder #36523 contained more than 10 copies of the transgene and founder #36853 harboured at least 1 copy (Figure 4.7).

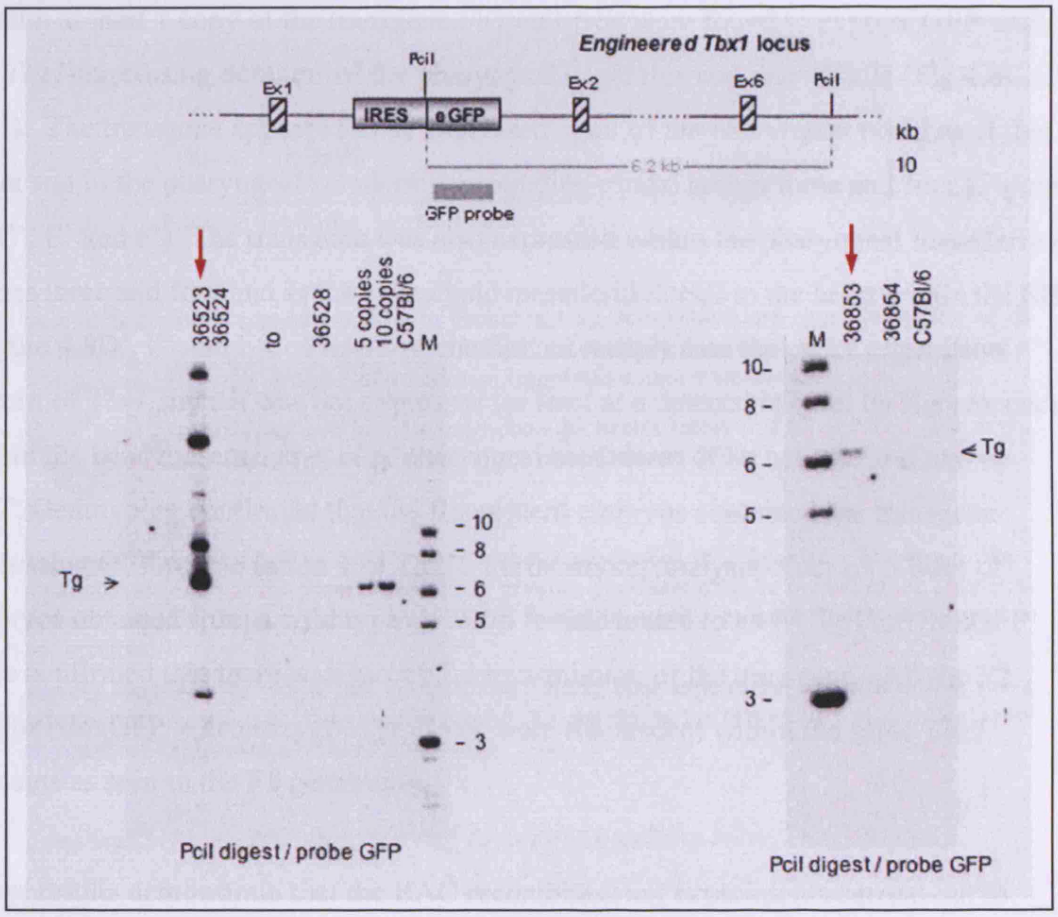

Figure 4.7 Southern blot analysis of TgTbx1floxGFP mice
After PciI digestion of genomic DNA, a GFP probe was used to detect a 6.2Kb DNA fragment containing the transgene. Fourteen potential founders were analysed but only 2, #36523 and #36853 contained the transgene (red arrows). The intensity of the signal was compared to known copies of the transgene (0, 5 and 10 copies) to determine the copy number in the founder animals. (Conducted by Genoway).

These 2 male animals, #36523 and #36853 were obtained from Genoway and mated to wild type C57Bl/6 females to assess fluorescence of the transgene in embryonic litters. Embryos were collected at E9.5, a timepoint at which *Tbx1* is normally expressed at high levels within embryonic tissues (Chapman et al., 1996). *Tbx1* is normally expressed at this stage in the head mesenchyme, otic vesicle and pharyngeal endoderm and ectoderm. It is also detected within SHF domains consisting of the core mesoderm of the pharyngeal arches and the splanchnic mesoderm and *Tbx1* is also expressed within the distal OFT (Figure 4.8A and B). Two E9.5 litters were collected from wildtype matings to founder #36523. However, none of the embryos were fluorescent. One E9.5 litter was analysed from a wildtype mating to the founder #36853, reported to contain at least 1 copy of the transgene. F1 embryos were found to express GFP within the *Tbx1*-expressing domains of the pharyngeal apparatus and otic vesicle (Fig 4.8C,C'-F,F'). The transgene appeared to be expressed in all of the pharyngeal pouches at this stage and in the pharyngeal ectoderm surrounding caudal arches three and four (Figure 4.8C', E' and F') The transgene was also expressed within the pharyngeal mesoderm of arches three and four and in the splanchnic mesoderm dorsal to the heart within the SHF (Figure 4.8D', E' and F'). The transgene did not recapitulate the entire expression pattern of *Tbx1* since it was not expressed (at least at a detectable level by fluorescence) within the head mesenchyme, core pharyngeal mesoderm of arches one and two or OFT. Genotyping confirmed that the fluorescent embryos contained the transgene expressing GFP within intron 1 of *Tbx1*. Furthermore, analysis of an E9.5 litter of embryos obtained from a wild type C57Bl/6 female mated to an F1 TgTbx1floxGFP male confirmed that there was successful transmission of the transgene. All the F2 TgTbx1floxGFP/+ heterozygous embryos were fluorescent within the same *Tbx1* domains as seen in the F1 generation.

These results demonstrate that the BAC recombineering experiments carried out to generate a *Tbx1* allele expressing GFP were successful and produced a TgTbx1floxGFP mouse which will be a valuable tool for use in future experiments to study the role of *Tbx1* in development.

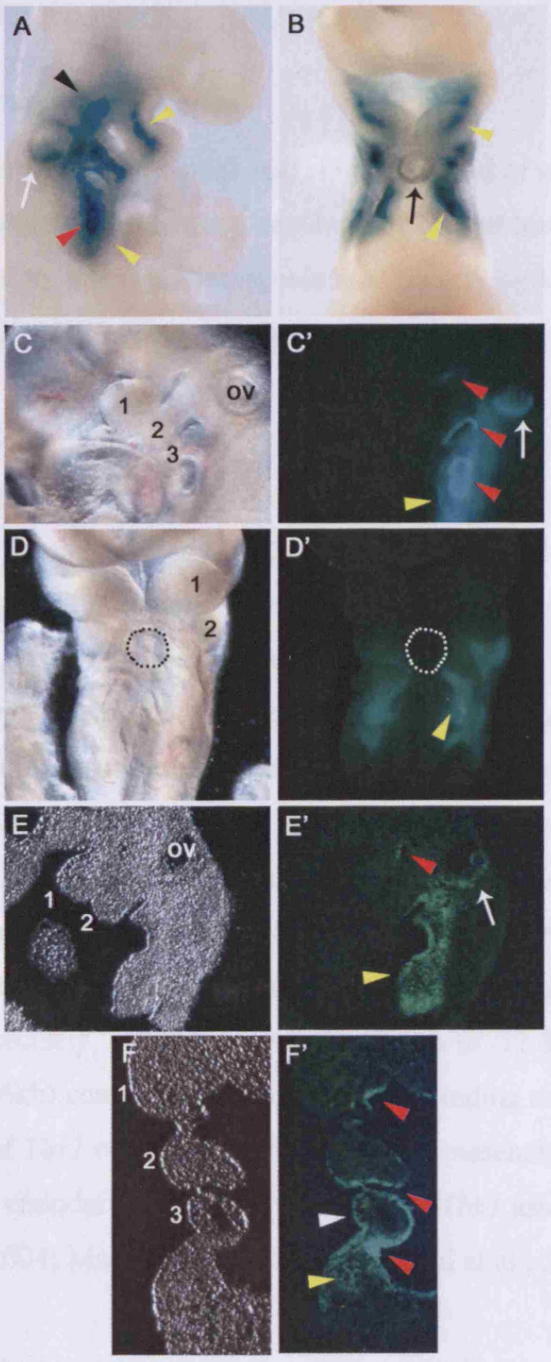

Figure 4.8 GFP expression in TgTbx1floxGFP embryos
(**A, B**) Expression of *Tbx1* at E9.5 shown by X-gal staining of *Tbx1*$^{+/lacZ}$ embryos. *Tbx1* is expressed in the head mesenchyme (black arrowhead), otic vesicle (white arrow), core pharyngeal mesoderm and splanchnic mesoderm (yellow arrowhead), pharyngeal endoderm (red arrowhead) and outflow tract (black arrow). (**C, D**) Expression of the TgTbx1floxGFP transgene detected by fluorescence at E9.5 within the otic vesicle (white arrow), splanchnic mesoderm (yellow arrowhead) and pharyngeal endoderm (red arrowhead). A lateral (**C**) and frontal (**D**) brightfield view and the corresponding view of fluorescent tissues (**C', D'**). The dotted circle represents the position of the outflow tract. (**E, F**) Cryosections of E9.5 TgTbx1floxGFP embryos. Brightfield views of sagittal (**E**) and coronal (**F**) sections and the corresponding views of fluorescent tissues (**E', F'**). Fluorescence is also detected in the pharyngeal ectoderm in coronal sections (**F'**, white arrowhead).

4.3 DISCUSSION AND FUTURE DIRECTIONS

4.3.1 Analysis of TgTbx1floxGFP mice

BAC recombineering is a relatively quick and simple method of modifying genetic loci while retaining all the regulatory elements required for correct transgene expression. This approach was used to generate a transgenic mouse carrying a modified *Tbx1* allele in which a floxed IRES2-eGFP vector was inserted into intron 1 of *Tbx1*.

One founder TgTbx1floxGFP mouse was obtained which appears to express the transgene within a subpopulation of *Tbx1*-expressing cells. At E9.5, the TgTbx1floxGFP allele is expressed in the otic vesicle, pharyngeal endoderm and ectoderm and the pharyngeal mesoderm/splanchnic mesoderm of caudal pharyngeal arches three and four. Loss of the more rostral head mesenchyme and pharyngeal mesoderm expression may have occurred secondary to positional effects of transgene integration or because the mesodermal enhancer required for this expression is located outside the BAC. However, experiments by another group have indicated that multiple *Fox cis* elements contained within the 13kb region directly upstream of the translational start site of *Tbx1* are sufficient to direct expression of a *lacZ* reporter in most endogenous *Tbx1* expression domains (Hu et al., 2004; Maeda et al., 2006; Yamagishi et al., 2003b). More precisely, a 200bp fragment (-12.8kb to -12.6kb) plus a 1.5kb fragment (-8.1kb to -6.6kb) containing 2 conserved *Fox* binding sites upstream of the translational start site of *Tbx1* could recapitulate the head mesenchyme, pharyngeal mesoderm, pharyngeal endoderm and OFT expression of *Tbx1* assessed at E9.5 by *lacZ* expression (Hu et al., 2004; Maeda et al., 2006; Yamagishi et al., 2003b).

In TgTbx1floxGFP mice, transgene expression does not fully recapitulate endogenous *Tbx1* expression, which could be due to a number of different reasons. One possibility is that the transgene could be expressed in the core pharyngeal mesoderm and head mesenchyme but at insufficient levels to be detected by fluorescence. One way of determining whether the transgene is expressed in these tissues would be to amplify the signal using the Biotin-Avidin system. A rabbit anti-GFP antibody could be used followed by a biotinylated anti-rabbit antibody and finally, a peroxidase conjugated avidin applied for detection. This series of steps provides a more sensitive method of detecting expression due to the amplification of binding sites.

The copy number of the transgene may also have affected expression within the head mesenchyme and pharyngeal mesoderm. The original founder animal tested contained only one copy of the transgene. However, additional copies may be required for detection in all *Tbx1* expression domains, as has been noted for other *Tbx1* transgenes (Maeda et al., 2006).

Alternatively, some of the *Fox* enhancer elements or other *cis*-regulatory regions identified upstream of *Tbx1* may have been lost (Hu et al., 2004; Maeda et al., 2006; Yamagishi et al., 2003b). Future experiments should determine whether these sites were lost during the injection and homologous recombination into mouse genomic DNA. Considering that the BAC DNA was injected by Genoway without first linearizing the vector, it is not clear how the BAC integrated into the genome. A proportion of the regulatory regions controlling *Tbx1* expression may have been lost. If these required *Fox* elements or other regulatory regions are found to be missing, the expression of the TgTbx1floxGFP transgene could mean that additional regulatory elements can direct *Tbx1* expression in the pharyngeal endoderm and the more caudal domains of the pharyngeal ectoderm and SHF. It is also possible that insertion of the IRES2-eGFP fragment into intron 1 of *Tbx1* disrupted an enhancer or activated a repressor element leading to an altered expression pattern. Rearrangement of the BAC during integration may also have altered the position of important regulatory elements. In addition, silencing of some *Tbx1* expression domains could have occurred depending on the integration site.

In order to distinguish between these possibilities and assess the integrity of the transgene, real-time PCR could be used to analyse the copy number of regulatory sequences surrounding *Tbx1*, which should be contained within the transgene. Also, Southern blot analysis could be used to determine if transgene fragments are missing or have rearranged. Functional studies of the TgTbx1floxGFP mice could also be carried out. TgTbx1floxGFP mice could be bred to $Tbx1^{cre}$ animals to generate $Tbx1^{cre/cre}$;TgTbx1floxGFP mice so that transgene rescue of the $Tbx1^{cre/cre}$ ($=Tbx1^{-/-}$) mutant phenotype could be assessed. The $Tbx1^{cre}$ allele was generated by knocking in an IRES-Cre construct into the T-box DNA binding domain of *Tbx1* and it is expressed in all endogenous *Tbx1* expression domains (Huynh et al., 2007). Cre-mediated recombination of the TgTbx1floxGFP allele should occur in expression domains in which both Cre and the transgene overlap. This recombination should allow removal of

the IRES2-eGFP from intron 1 of *Tbx1*, restoring full length *Tbx1* expression. Analysis of the extent of phenotypic rescue would begin to indicate if the transgene is expressed in all *Tbx1* domains. If, for example, the transgene was not expressed within the head mesenchyme and core mesoderm of the first and second pharyngeal arches then the branchiomeric myogenesis defect and second pharyngeal arch hypoplasia exhibited by $Tbx1^{-/-}$ mutants (caused by loss of *Tbx1* expression in the mesoderm) may still be present.

The loss of *Tbx1* in a sub-mesodermal domain may be quite fortuitous in that it should allow the function of *Tbx1* in the caudal mesodermal domain to be distinguished from its role in more rostral mesoderm. The difference in *Tbx1* function between these two regions is exemplified by regulation of *Pitx2* which is considered to be downstream of *Tbx1* in the SHF (Nowotschin et al., 2006) however, it is upstream of *Tbx1* in the first pharyngeal arch mesoderm (Shih et al., 2007).

4.3.2 Identification of *Tbx1* target genes

TgTbx1floxGFP mice could also be crossed to $Tbx1^{+/mcm}$ mutants to generate $Tbx1^{mcm/mcm}$;TgTbx1floxGFP mice to investigate genetic pathways downstream of *Tbx1*. The $Tbx1^{mcm}$ allele was generated by knocking in a tamoxifen-inducible Cre into the DNA binding domain of *Tbx1* (Xu et al., 2004). $Tbx1^{mcm/mcm}$;TgTbx1floxGFP embryos will effectively be homozygous null for functional *Tbx1* (equivalent in phenotype to $Tbx1^{-/-}$ or $Df1/Tbx1^{lacZ}$ embryos). GFP-positive cells (effectively $Tbx1^{-/-}$) could be isolated by FACS. Following sorting, these cells could be split into two portions, one of which is treated with tamoxifen to induce Cre-mediated recombination of the TgTbx1floxGFP allele, restoring *Tbx1* function to these cells. Comparing the gene expression profile between the tamoxifen-treated and carrier-treated *Tbx1* cells should further enrich for direct *Tbx1* targets because RNA can be extracted soon after tamoxifen induction of recombination, thus enriching for immediate early response genes. In addition, this experiment allows a within-group comparison to be carried out, reducing the effects of variability among different embryos. Results from these studies could be compared to the microarray data for further validation of potential *Tbx1* targets.

After tamoxifen treatment, time needs to be allowed for Cre-mediated recombination of the TgTbx1floxGFP allele and subsequent protein expression of functional Tbx1 to take place before RNA can be extracted for expression analysis. In order to determine the correct time to extract RNA, a preliminary experiment could be carried out in which RNA or genomic DNA is extracted from tamoxifen-treated cells at various timepoints after addition of tamoxifen. RT-PCR or PCR analysis could then be carried out to test for recombination of the transgenic allele. In addition, protein could also be extracted at various timepoints after tamoxifen injection to test for presence of the functional Tbx1 protein by Western analysis. These preliminary experiments could be used to identify the timepoint at which RNA should be extracted after Tbx1 protein production. This is important as the shorter the time after Tbx1 production, the greater the enrichment for direct *Tbx1* targets.

4.3.3 Additional *Tbx1* BACs

While this transgenic mouse enables further analysis of the role of *Tbx1* in development, other BACs/transgenic mice are being constructed in our lab which will enable even better analysis of the genetic pathways downstream of *Tbx1*. Incorporating a mutated form of the ligand binding domain of the human estrogen receptor (ER) downstream of Cre recombinase has been successfully used to control the time of recombination in various tissues (Monvoisin et al., 2006; Yajima et al., 2006). Normally, the Cre-ER fusion protein is retained in the cytoplasm within a HSP90 complex and is inactive. However, upon addition of tamoxifen, a synthetic ER ligand, the HSP90 complex is disrupted and the Cre recombinase protein is translocated to the nucleus where it can act to induce recombination at its target sites (Feil et al., 1997). BAC recombineering has been used in our lab to fuse the estrogen receptor to the last exon of *Tbx1* which should enable temporal control of Tbx1 activity. These transgenic mice will enable better identification of immediate, early response genes upon Tbx1 activation since transcription of *Tbx1* does not need to occur.

In conclusion, the generation of TgTbx1floxGFP mice will enable further direct downstream targets of *Tbx1* to be identified providing a valuable resource to study the role of *Tbx1* in development.

CHAPTER 5. FUNCTIONAL ANALYSIS OF *HES1* IN DEVELOPMENT

5.1 INTRODUCTION

The microarray of *Df1/Tbx1*^{lacZ} cells vs. *Tbx1*$^{+/lacZ}$ cells identified a number of potential *Tbx1* targets including *Notch3* and *Hes1*, genes encoding transcription factors involved in the Notch signalling pathway. *Notch3* is a receptor and transcription factor, while *Hes1 is* a transcriptional repressor and effector of Notch signalling. Both genes were significantly downregulated in *Tbx1*-null cells by greater than 3 fold to 0.249 ± 0.103 and 0.261 ± 0.093, respectively, according to qRT-PCR. *Notch3*$^{-/-}$ mutant embryos appear phenotypically normal. However, adults exhibit vascular abnormalities (Domenga et al., 2004). *Notch3* expression within the pharyngeal apparatus overlaps with other Notch receptors, thus there is a possibility that functional redundancy affects analysis of the role of *Notch3* in embryogenesis (Kitamoto et al., 2005). *Hes1*$^{-/-}$ mutants exhibit a large range of abnormalities demonstrating the importance of this gene during development. *Hes1* is required for normal neurogenesis, pituitary gland, eye, ear, thymus, lung and pancreas development (Ishibashi et al., 1995; Ito et al., 2000; Jensen et al., 2000; Kaneta et al., 2000; Raetzman et al., 2007; Tomita et al., 1999; Tomita et al., 1996; Zheng et al., 2000; Zhu et al., 2006; Zine et al., 2001).

5.2 RESULTS

5.2.1 Analysis of *Hes1* expression

Reports of *Hes1* expression during development show that *Hes1* is present within the pharyngeal arches between embryonic days E8.5 to E9.5 at least (Barsi et al., 2005; Hamada et al., 1999; Koop et al., 1996). However, the role of *Hes1* in this structure has not been well characterised. *In situ* hybridisation analysis at E9.5 revealed that *Hes1* is expressed in an overlapping fashion with *Tbx1*, in the pharyngeal mesenchyme, the endoderm lining the pharyngeal pouches and the splanchnic mesoderm within the SHF domain (Figure 5.1). *Hes1* appeared downregulated within all of these domains in *Tbx1*$^{-/-}$ mutant embryos at the same stage. These results show that *Hes1* is diminished in cell lineages important for pharyngeal and cardiovascular development suggesting that *Hes1* may play a role downstream of *Tbx1* in the morphology of structures affected in *Tbx1* mutants.

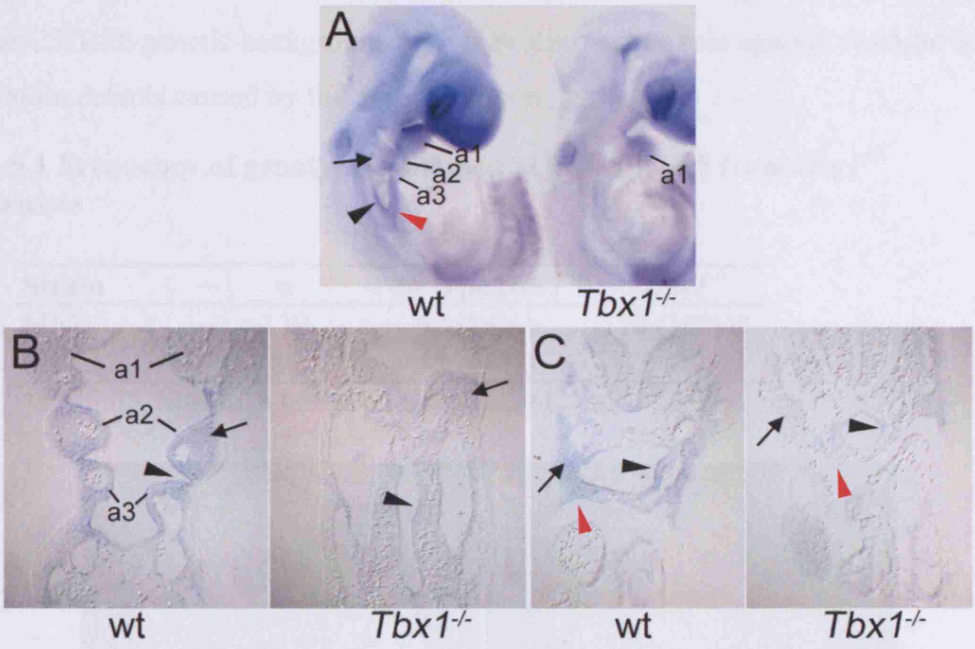

Figure 5.1 *In situ* hybridisation of *Hes1* in wild type and *Tbx1*$^{-/-}$ embryos at E9.5
(**A**) *Hes1* expression within the pharyngeal mesenchyme (black arrow), endoderm (black arrowhead) and second heart field (red arrowhead) within wild type embryos is downregulated in *Tbx1*$^{-/-}$ embryos. (**B**) Coronal sections and (**C**) transverse sections demonstrating downregulation of *Hes1* within the pharyngeal mesenchyme (black arrow), endoderm (black arrowhead) and second heart field (red arrowhead) of *Tbx1*$^{-/-}$ embryos. Abbreviations: a, arch.

5.2.2 *Hes1* and analysis of lethality

According to the original study of the *Hes1* mouse knockout phenotype, a proportion of *Hes1*$^{-/-}$ homozygotes are embryonic lethal commencing at age E12.5 (Ishibashi et al., 1995). In this study, *Hes1*$^{-/-}$ embryos collected at E14.5-E15.5 on an MF1 background were also underrepresented according to the expected Mendelian ratios (Table 5.1) and dead *Hes1*$^{-/-}$ embryos were often found at this stage which had either resorbed, or had neurulation defects as previously described (Ishibashi et al., 1995). In the analysis of embryos at earlier stages, it was noted that some *Hes1*$^{-/-}$ homozygotes exhibit haemorrhage throughout the body at E11.5 (n=2 out of 7) (Figure 5.2) which has not been previously reported. These observations suggest that vascular defects may be partly responsible for the embryonic lethality of *Hes1*$^{-/-}$ mutants from E12.5.

The phenotype of *Hes1*$^{-/-}$ mutants was also assessed on a mixed MF1;C57Bl/6 background. *Hes1*$^{-/-}$ embryos on this background were present in normal Mendelian ratios at E15.5 (Table 5.1) and brain and neural tube defects were not observed at this stage in contrast to *Hes1*$^{-/-}$ mice maintained on a pure MF1 background. This suggests that the C57Bl/6 genetic background may play a protective role against vascular and neurulation defects caused by the *Hes1* mutation.

Table 5.1 Frequency of genotypes obtained at E14.5-E15.5 from *Hes1*$^{+/-}$ intercrosses

Strain	n	wild type/*Hes1*$^{+/-}$	*Hes1*$^{-/-}$
MF1	110	92 (84%)	18 (16%)*
MF1;C57Bl/6	80	57 (71%)	23 (29%)

*$p < 0.05$ Statistics based on Chi squared test.

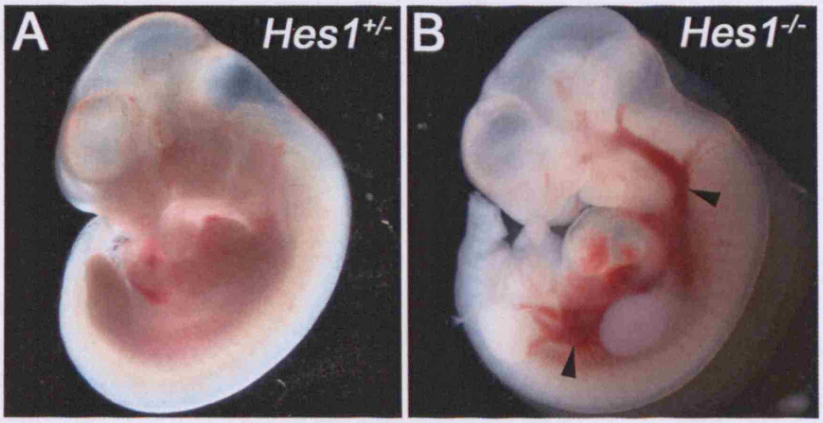

Figure 5.2 Vascular defects in *Hes1*$^{-/-}$ mouse mutants
(**A**) A control *Hes1*$^{+/-}$ embryo at E11.5 (**B**) A *Hes1*$^{-/-}$ mutant exhibiting haemorrhaging throughout the body (arrowheads in B).

5.2.3 *Hes1* mutants exhibit defects in multiple organs

The gross morphology of the whole embryo, including the cardiovascular system was investigated at E14.5 to E15.5 to determine whether *Hes1* mutants exhibited any DGS-like abnormalities. A combination of MRI scanning and conventional histological methods were used to analyse the phenotype of *Hes1* mutants on both a pure MF1 background and a mixed MF1;C57Bl6 background to determine whether strain differences would affect the phenotypes observed.

Hes1$^{-/-}$ mice have previously been shown to exhibit defects in multiple organs and MRI scanning of E15.5 *Hes1*$^{-/-}$ homozygotes detected some of the reported defects in eye, pancreas and thymus development (Jensen et al., 2000; Kaneta et al., 2000; Tomita et al., 1999; Tomita et al., 1996) (Table 5.2). All *Hes1*$^{-/-}$ embryos regardless of genetic background had absent eyes and a hypoplastic or aplastic pancreas (Figure 5.3B, D). *Hes1*$^{-/-}$ mutants also exhibited hypo/aplasia of one or both thymic lobes (n = 23/23, 100% MF1;C57Bl6 and n = 13/15, 87% MF1) (Figure 5.3F), a phenotype which is very similar to that seen in *Tbx1* mutants (Jerome and Papaioannou, 2001; Lindsay et al., 2001; Merscher et al., 2001).

Table 5.2 Developmental defects identified by MRI in E15.5 *Hes1*$^{-/-}$ mutants

Strain	Genotype	n	Eye defects	Pancreatic hypo/aplasia	Thymic hypo/aplasia
MF1	*Hes1*$^{-/-}$	15	15 (100%)	15 (100%)	13 (87%)
	Hes1$^{+/-}$	15	0	0	0
	Wild type	2	0	0	0
MF1;C57Bl/6	*Hes1*$^{-/-}$	23	23 (100%)	23 (100%)	23 (100%)
	Hes1$^{+/-}$	21	0	0	0
	Wild type	7	0	0	0

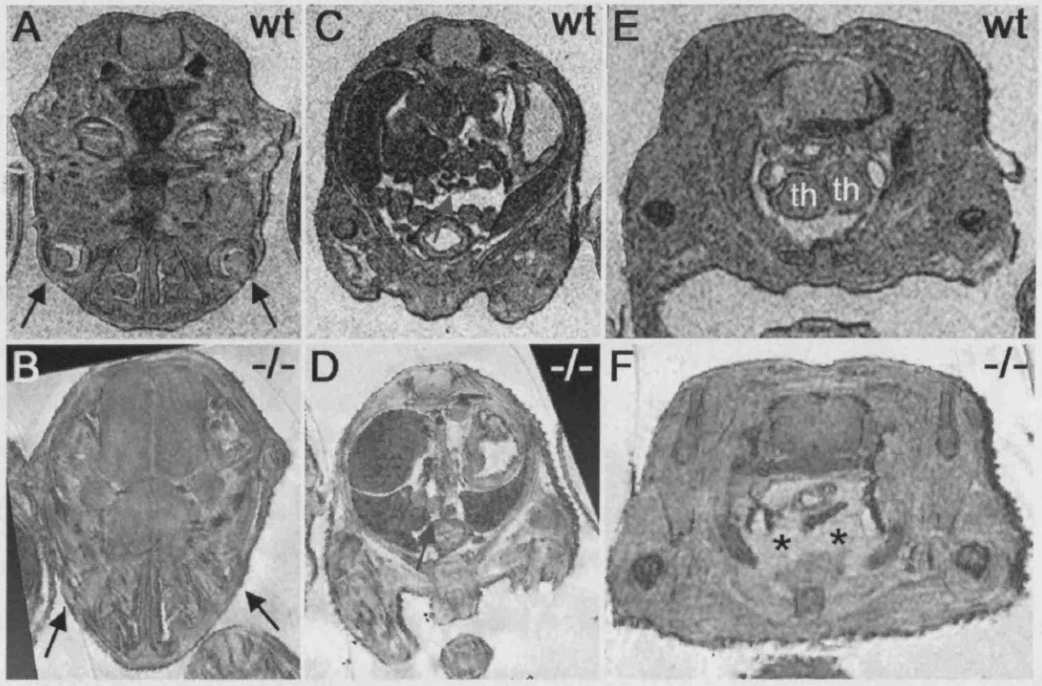

Figure 5.3 Morphological defects detected in E15.5 *Hes1*$^{-/-}$ embryos by MRI
Transverse MRI scans show that *Hes1*$^{-/-}$ mutants are missing eyes (compare black arrows in (**B**) to (**A**)), and exhibit pancreatic hypo/aplasia (small dark spots indicated by red arrow in (**D**) which are absent in (**C**)) as well as thymic hypo/aplasia (asterisks in (**F**) compared to (**E**)). Abbreviations: th, thymic lobe.

5.2.4 Analysis of pharyngeal and heart development in *Hes1* mutant embryos

5.2.4.1 Hes1 mutants exhibit pharyngeal arch artery defects

Tbx1 is required in the pharyngeal apparatus for correct growth and remodelling of the pharyngeal arch arteries. These initially form as bilaterally symmetric vessels which pass through each pharyngeal arch and remodel during embryogenesis to form part of the aorta and great vessels of the heart. To examine the potential role of *Hes1* downstream of *Tbx1* in pharyngeal development, the pharyngeal arch arteries were analysed at E10.5. At this stage, $Tbx1^{+/-}$ heterozygous embryos exhibit fourth arch artery hypo/aplasia (Jerome and Papaioannou, 2001; Lindsay et al., 2001; Merscher et al., 2001). Intracardiac ink injection was carried out to visualise the arch arteries in stage-matched wild type, $Hes1^{+/-}$ and $Hes1^{-/-}$ mutant embryos. These experiments revealed that 5/27 (19%) $Hes1^{-/-}$ embryos analysed on an MF1 background had an arch artery defect including hypo/aplasia of the fourth arch artery, persistent first and second arch arteries and hypoplastic sixth arch arteries (Figure 5.4D-F; Table 5.3). In addition, the same range of pharyngeal arch artery defects also occurred in a smaller proportion of $Hes1^{+/-}$ mutant embryos (5/42, 12%) (Figure 5.4B, C; Table 5.3), although these involved hypoplasia rather than aplasia and no sixth arch artery defects were found. In comparison, wild type control embryos (Figure 5.4A) did not exhibit pharyngeal arch artery defects except for one embryo which may possibly have had a unilateral, hypoplastic fourth arch artery (1/67, 1%) (Table 5.3).

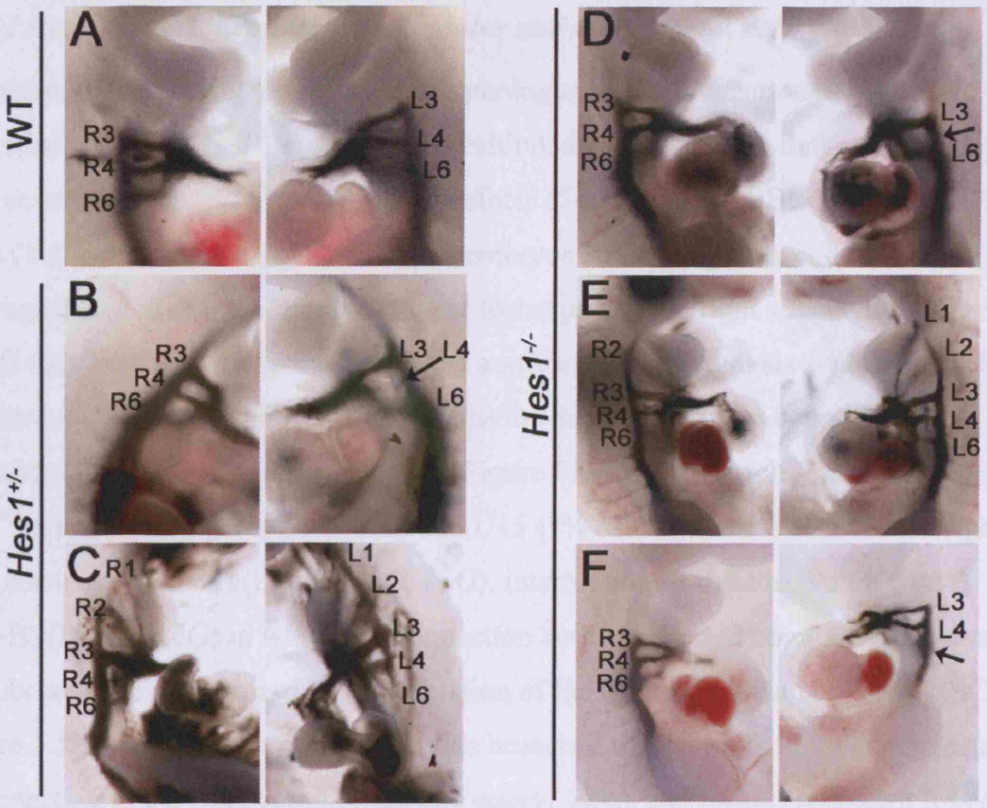

Figure 5.4 Intracardiac ink injection of E10.5 Hes1 mutants
(**A**) In wild type embryos, bilateral pairs of caudal arch arteries R3-R6 and L3-L6 are present at E10.5. A proportion of *Hes1*$^{+/-}$ mutants have hypoplasia of the fourth arch artery (arrow in **B**) and persistent first and second arch arteries (**C**). *Hes1*$^{-/-}$ mutants also exhibit fourth arch artery aplasia (arrow in **D**), persistent first and second arch arteries (**E**) and sixth arch artery hypoplasia (arrow in **F**). Abbreviations: L, left; R, right.

Table 5.3 Frequency of pharyngeal arch artery defects in E10.5 Hes1 mutants

	PAA	WT	*Hes1*$^{+/-}$	*Hes1*$^{-/-}$
Ink Injection				
Abnormal	1st	-	1 (pers)	1 (pers)
	2nd	-	1 (pers)	2 (pers)
	3rd	-	-	-
	4th	1	5 (hypo/ap)	3 (hypo/ap)
	6th	-	-	1 (hypo)
Total abnormal		1	5*	5**
Normal		66	37	22
Total embryos (93)		67	42	27
Percentage of embryos with arch artery abnormalities		1%	12%	19%

Abbreviations: PAA, pharyngeal arch artery; WT wild type
* Significantly different from WT (Fisher's exact test, $p<0.05$)
** Significantly different from WT (Fisher's exact test, $p<0.01$)

5.2.4.2 Hes1 mutants exhibit cardiovascular and craniofacial defects

In addition to the previously reported morphological defects mentioned above, a proportion of E15.5 *Hes1*$^{-/-}$ embryos also exhibited cardiovascular defects including great vessel and outflow tract alignment defects (5/23, 22% MF1;Bl6 and 2/15 (13%) MF1) (Table 5.4). Normally in wild type embryos at this stage, the right fourth pharyngeal arch artery has remodelled and forms part of the right subclavian artery and the left fourth arch artery forms part of the aortic arch. The right sixth arch artery has regressed and the left sixth arch artery forms the ductus arteriosus connecting the pulmonary trunk to the descending aorta (Figure 5.5A, B, E). Arch artery defects in *Hes1*$^{-/-}$ mutants (4/23 (17% MF1;Bl6) and 1/15 (7% MF1), Table 5.4) included right-sided aortic arch (RAA) (Figure 5.5C, F, G), interruption of the aortic arch type B (IAA-B) (Figure 5.5G) in which the connection between the left common carotid and left subclavian artery is missing, and isolation of the right subclavian artery (I-RSCA) (Figure 5.5H) in which the right subclavian branched off the pulmonary artery instead of connecting to the right common carotid artery. RAA and IAA-B represent loss of the left fourth arch artery and persistence of the right fourth arch artery and I-RSCA occurs due to aberrant remodelling of the right fourth arch artery. In addition, some embryos exhibited right-sided ductus arteriosus (Figure 5.5D, F), a manifestation of loss of the left sixth arch artery and persistence of the right sixth arch artery. The phenotype of these *Hes1*$^{-/-}$ embryos is consistent with the earlier arch artery defects observed at E10.5.

In addition to great vessel abnormalities, defects in outflow tract alignment were also observed in *Hes1*$^{-/-}$ homozygotes (2/23 (9% MF1;Bl6) and 1/15 (7% MF1)) (Table 5.4; Figure 5.6). These outflow tract defects included double outlet right ventricle (DORV) (Figure 5.6D, F) in which both the aorta and pulmonary trunk arose from the right ventricle or an overriding aorta and both of these defects were accompanied by a VSD (Figure 5.6B).

Table 5.4 Frequency of cardiovascular and craniofacial defects in E15.5 *Hes1* mutants

Strain	Genotype	n	CV defect	Great vessel defect	OFT defect	Cleft Palate
MF1	*Hes1*$^{-/-}$	15	2 (13%)	1 (7%)	1 (7%)	9 (60%)
	Hes1$^{+/-}$	15	1[a] (7%)	0	0	0
	Wild type	2	0	0	0	0
MF1;C57Bl/6	*Hes1*$^{-/-}$	23	5 (22%)	4 (17%)	2 (9%)	9 (39%)
	Hes1$^{+/-}$	21	0	0	0	1 (5%)
	Wild type	7	0	0	0	0

[a] Dextroposition of the heart

CV-cardiovascular, OFT-outflow tract

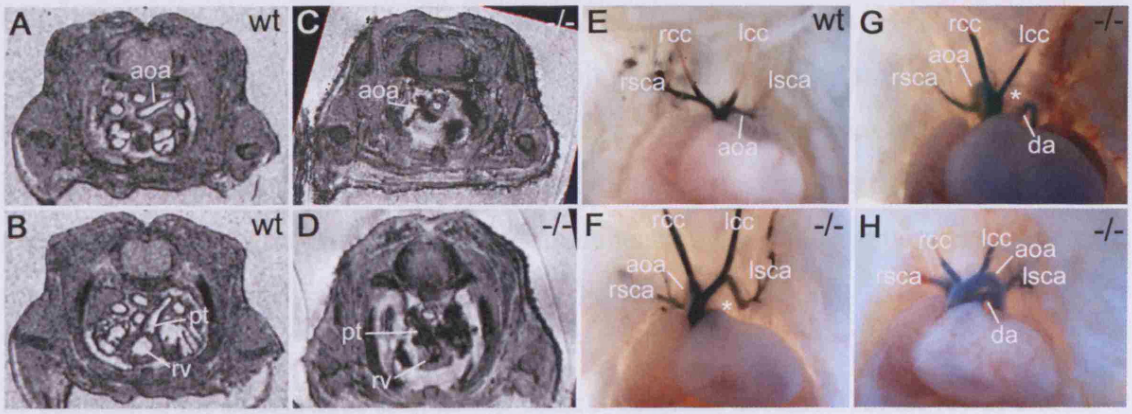

Figure 5.5 Great vessel defects in E15.5 *Hes1*$^{-/-}$ mutants
(**A-D**) Transverse MRI scans. (**E-H**) Intracardiac ink injection. (**A**, **B**) In wild type (wt) embryos, the aortic arch (**A**) and pulmonary trunk (**B**) pass to the left of the trachea. (**C**, **D**) In some *Hes1*$^{-/-}$ (-/-) mutants, the aortic arch (**C**) and pulmonary trunk (**D**) pass to the right of the trachea. (**E**) Intracardiac ink injection of a wild type embryo displaying normal great vessel morphology (**F-H**) *Hes1*$^{-/-}$ mutants with right-sided aortic arch and right-sided ductus arteriosus (**F**), interruption of the aortic arch type B and a right-sided aortic arch (**G**), and isolation of the right subclavian artery (**H**). Abbreviations: aoa, aortic arch; da, ductus arteriosus; lcc, left common carotid; lsca, left subclavian artery; pt, pulmonary trunk; rcc, right common carotid; rsca, right subclavian artery; rv, right ventricle. Asterisks denote missing segments.

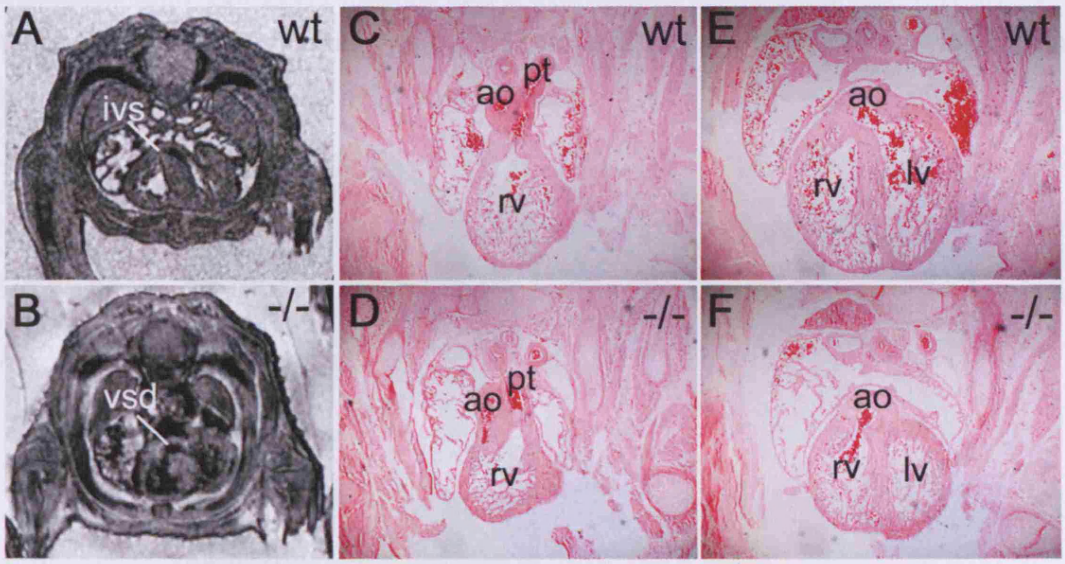

Figure 5.6 Outflow tract and ventricular septal defects in E15.5 *Hes1*$^{-/-}$ mutants
(**A-B**) Transverse MRI scans. (**C-F**) Transverse histological sections. (**A**) In wild type embryos the interventricular septum separates the right and left ventricles. (**B**) *Hes1*$^{-/-}$ mutants exhibit a ventricular septal defect. (**C**, **E**) Consecutive transverse sections of a wild type embryo in which the pulmonary trunk arises from the right ventricle (**C**) and the aorta joins the left ventricle (**E**). (**D**, **F**) Consecutive sections of a *Hes1*$^{-/-}$ embryo with DORV in which both the aorta and pulmonary trunk arise from the right ventricle. Abbreviations: ao, aorta; ivs, interventricular septum; lv, left ventricle; pt, pulmonary trunk; tv, right ventricle; vsd, ventricular septal defect.

Craniofacial abnormalities were also observed in *Hes1*$^{-/-}$ mutant embryos. A previously unreported phenotype was the presence of cleft palate in 39% (9/23) of *Hes1*$^{-/-}$ mutants on a MF1;C57Bl/6 background and 60% (9/15) of *Hes1*$^{-/-}$ embryos on an MF1 background (Table 5.4). The secondary palatal shelves appeared to have rotated but they did not meet in the midline in *Hes1*$^{-/-}$ mutants compared to wild type embryos at the same stage (Figure 5.7).

In contrast to the pharyngeal arch artery defects detected in *Hes1*$^{+/-}$ embryos at E10.5, no great vessel abnormalities were found in later stage *Hes1*$^{+/-}$ heterozygotes at E15.5 indicating that these pharyngeal arch artery defects may largely recover later in development. However, one MF1;C57Bl/6 *Hes1*$^{+/-}$ embryo was slightly growth delayed in comparison to its littermates and had a cleft palate and another, MF1 *Hes1*$^{+/-}$ embryo had dextroposition of the heart (Table 5.4) suggesting that a small proportion of *Hes1* heterozygotes may exhibit some type of phenotypic abnormality.

In conclusion, MRI and histological analysis has revealed that *Hes1*$^{-/-}$ mutants exhibit cardiovascular, thymic and secondary palate defects which are highly reminiscent of those observed in *Tbx1* mutant mice and further implicates *Hes1* as a downstream target of *Tbx1* in pharyngeal and heart development.

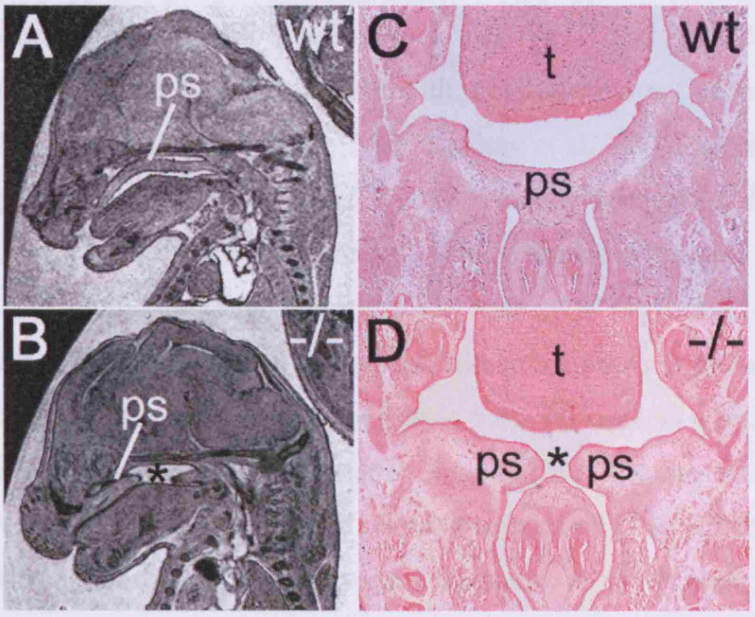

Figure 5.7 Craniofacial defects in E15.5 *Hes1*$^{-/-}$ mutants
(**A**, **B**) Sagittal MRI sections. (**C**, **D**) Transverse histological sections. (**A**, **C**) In wild type (wt) embryos the palatal shelves are fused. (**B**, **D**) *Hes1*$^{-/-}$ (-/-) mutants exhibit cleft palate where the palatal shelves do not meet in the midline. Abbreviations: ps, palatal shelf; t, tongue. Asterisks indicate missing segments.

5.2.5 Analysis of epistasis between *Tbx1* and *Hes1* in pharyngeal arch artery development

Given the evidence presented for *Hes1* as a potential *Tbx1* target, *Tbx1*$^{+/-}$ mice were crossed with *Hes1*$^{+/-}$ mice to determine whether *Tbx1* and *Hes1* interact within the same genetic pathway in pharyngeal arch artery development. Genotyping of P10 litters obtained from these matings indicated that *Tbx1*$^{+/-}$;*Hes1*$^{+/-}$ mice were slightly underrepresented according to expected Mendelian ratios but values did not reach statistical significance ($\chi 2=5.67$; $0.15>P>0.1$) (Table 5.5).

Table 5.5 Frequency of genotypes obtained from *Hes1*$^{+/-}$ x *Tbx1*$^{+/-}$ matings

Stage	Wild type	*Hes1*$^{+/-}$	*Tbx1*$^{+/-}$	*Hes1*$^{+/-}$;*Tbx1*$^{+/-}$	Total
P10	38 (30)	32 (30)	29 (30)	20 (30)	119

Numbers in parentheses indicate the expected number of mice per genotype rounded to the nearest whole number

Embryos were collected from *Tbx1*$^{+/-}$ x *Hes1*$^{+/-}$ and *Hes1*$^{+/-}$;*Tbx1*$^{+/-}$ x *Hes1*$^{+/-}$;*Tbx1*$^{+/-}$ matings at E10.5-E11.5 to examine the pharyngeal arch arteries by intracardiac ink injection on the mixed MF1;C57Bl/6 background. All *Tbx1*$^{+/-}$ embryos (5/5, 100%) had a fourth arch artery defect at E10.5 consistent with previous reports (Jerome and Papaioannou, 2001; Lindsay and Baldini, 2001; Lindsay et al., 2001; Merscher et al., 2001). In comparison, 80% (8/10) of *Hes1*$^{+/-}$;*Tbx1*$^{+/-}$ transheterozygotes exhibited a fourth pharyngeal arch artery defect (Table 5.6). There was no difference between *Tbx1*$^{+/-}$ and *Hes1*$^{+/-}$;*Tbx1*$^{+/-}$ mutants in terms of the severity of the fourth pharyngeal arch artery defect. Numbers of absent vs. hypoplastic arch arteries or the number of bilateral vs. unilateral cases were equivalent (Table 5.6). No defects were seen in development of any of the other arch arteries in *Hes1*$^{+/-}$;*Tbx1*$^{+/-}$ embryos in comparison to the *Tbx1*$^{+/-}$ or *Hes1*$^{+/-}$ embryos collected on this background (Table 5.6). All *Tbx1*$^{-/-}$ embryos exhibited a severe defect in pharyngeal formation in which none of the caudal arches or arch arteries formed. This phenotype was consistent with or without a *Hes1* heterozygous mutation (Table 5.6).

Table 5.6 Frequency of fourth arch artery defects at E10.5-E11.5

		Right fourth arch artery		Left fourth arch artery		
Genotype	Abnormal/Total[a]	hypoplastic	absent	hypoplastic	absent	Bilateral defects
Wild type	0/1	0	0	0	0	0
Hes1$^{+/-}$	0/3	0	0	0	0	0
Tbx1$^{+/-}$	5/5	1	3	0	5	4
Hes1$^{-/-}$	1/6	1	0	0	0	0
Tbx1$^{-/-}$	3/3[b]	-	-	-	-	-
Hes1$^{+/-}$;*Tbx1*$^{+/}$	8/10[c]	2	5	1	6	6
Hes1$^{+/-}$;*Tbx1*$^{-/-}$	3/3[b]	-	-	-	-	-
Hes1$^{-/-}$;*Tbx1*$^{+/-}$	0/1	0	0	0	0	0

[a]Embryos with fourth arch artery defects generated from *Hes1*$^{+/-}$ x *Tbx1*$^{+/-}$ and *Hes1*$^{+/-}$;*Tbx1*$^{+/-}$ x *Hes1*$^{+/-}$;*Tbx1*$^{+/-}$ matings

[b]All *Tbx1*$^{-/-}$ embryos were missing the caudal arch arteries

[c]One, *Hes1*$^{+/-}$;*Tbx1*$^{+/-}$ embryos which did not have a fourth arch artery defect appeared to be growth delayed

These results indicate that the incidence and severity of pharyngeal arch artery malformations is not altered in *Tbx1*$^{+/-}$ or *Tbx1*$^{-/-}$ embryos by reducing the dosage of *Hes1* by half. One *Tbx1*$^{+/-}$;*Hes1*$^{-/-}$ embryo was obtained from the above matings. It did not exhibit any pharyngeal arch artery defects despite the further reduction in *Hes1* gene dosage (Table 5.6).

Tbx1$^{+/-}$ mice exhibit a strain-dependent recovery from the fully penetrant fourth arch artery defects present at E10.5. Subsequently, depending on the genetic background, only 30-50% of *Tbx1*$^{+/-}$ mice at term exhibit a fourth arch artery-derived great vessel abnormality (Lindsay and Baldini, 2001; Taddei et al., 2001). The *Tbx1*$^{+/-}$;*Hes1*$^{-/-}$ embryo and one *Hes1*$^{+/-}$;*Tbx1*$^{+/-}$ embryo (1/10) with no arch artery defect appeared to be slightly older (~ E11.5) compared to most of the *Tbx1*$^{+/-}$ mutants analysed in the litters obtained. Therefore, strain-dependent rescue at this later stage may account for the lack of phenotype in these embryos.

To investigate the effect of *Hes1* on this recovery phenotype, the fourth pharyngeal arch arteries were examined from E10.5 to E12.5 in embryos collected from *Hes1*$^{+/-}$ x *Tbx1*$^{+/-}$ matings (Table 5.7). At E10.5, all *Tbx1*$^{+/-}$ embryos regardless of *Hes1* genotype, exhibited fourth arch artery abnormalities. By E11.5 approximately 40% (2/5) of *Hes1*$^{+/-}$;*Tbx1*$^{+/-}$ embryos had fourth arch artery hypo/aplasia compared to 25% (2/ 8) of *Tbx1*$^{+/-}$ mice (Table 5.7). At E12.5, the percentage of embryos with abnormal arch

arteries had decreased even further in both *Hes1*$^{+/-}$;*Tbx1*$^{+/-}$ and *Tbx1*$^{+/-}$ mutants to 8% (n = 1 of 12) and 14% (n = 1 of 7), respectively (Table 5.7). This data shows that decreasing the dosage of *Hes1* does not appear to significantly affect the penetrance of the pharyngeal arch artery defects in *Tbx1*$^{+/-}$ mutants during embryogenesis. However, larger numbers of embryos may be needed to clarify these results.

The penetrance of the arch artery defects in *Tbx1*$^{+/-}$ heterozygotes at E11.5 appears to be decreased compared to the reported penetrance in *Tbx1*$^{+/-}$ mice on a C57Bl6 x 129SvEvBrd background (Lindsay and Baldini, 2001). One possibility is that this may be due to the mixed MF1;C57Bl/6 background on which these embryos were analysed.

Table 5.7 Frequency of fourth arch artery defects in embryos generated from *Hes1*$^{+/-}$ x *Tbx1*$^{+/-}$ matings from E10.5 to E12.5

Genotype	E10.5	E11.5	E12.5
Wild type	0/1*	0/1	0/11
Hes1$^{+/-}$	0/2	0/5	0/8
Tbx1$^{+/-}$	4/4 (100%)	2/8 (25%)	1/7 (14%)
Hes1$^{+/-}$;*Tbx1*$^{+/-}$	3/3 (100%)	2/5 (40%)	1/12 (8%)

*Abnormal/Total

Altogether, the results so far suggest that *Hes1* and *Tbx1* do not interact genetically in development of the arch arteries. There was no change in the type or severity of cardiovascular defects apparent in *Hes1*$^{+/-}$;*Tbx1*$^{+/-}$ embryos compared to *Tbx1*$^{+/-}$ heterozygotes. Nor was there any significant increase in the penetrance of arch artery defects in double heterozygotes later in development relative to *Tbx1* heterozygotes. There appeared to be a loss of double heterozygotes neonatally, although this did not reach statistical significance. However, due to the phenotypic variability among *Hes1* and *Tbx1* mutants and the effect of genetic background, it is still possible that an epistatic interaction between *Hes1* and *Tbx1* in arch artery development was masked in the small numbers of embryos examined. Furthermore, *Tbx1* and *Hes1* may genetically interact in other biological processes such as outflow tract, thymus and/or craniofacial development which were not investigated in these experiments.

5.2.6 Analysis of pharyngeal arch patterning

To better characterise the pharyngeal phenotype of *Hes1*$^{-/-}$ mutants and begin to dissect out the mechanisms underlying the pharyngeal defects, markers of pharyngeal patterning were analysed by WISH. *Tbx1* mutants exhibit thymic, thyroid and parathyroid defects which occur due to aberrant development of the pharyngeal apparatus (Jerome and Papaioannou, 2001; Lindsay et al., 2001; Merscher et al., 2001). Thymic hypo/aplasia was clearly evident in *Hes1*$^{-/-}$ embryos at E15.5. However, parathyroid defects at this stage were difficult to assess. Expression analysis has shown that *Gcm2*, a marker of parathyroid precursor cells in third pouch endoderm is absent from the presumptive third pharyngeal pouch in *Tbx1*$^{-/-}$ mutant embryos at E10.5 (Ivins et al., 2005). Expression of this parathyroid marker was analysed in *Hes1*$^{-/-}$ mutants to assess whether there were any parathyroid defects similar to those seen in *Tbx1* mutants. *Gcm2* was not found to be downregulated in *Hes1*$^{-/-}$ mutants (n = 7) when compared to wild type embryos at E10.5 (Figure 5.8A). Thus, unlike *Tbx1*$^{-/-}$ mutants it does not appear that *Hes1*$^{-/-}$ embryos exhibit any defects in parathyroid development at E10.5.

The expression of *Pax1* was used to assess whether the pharyngeal arches were correctly patterned. *Pax1* is normally expressed within the pharyngeal pouch endoderm separating each pharyngeal arch (Neubuser et al., 1995). In *Tbx1*$^{+/-}$ heterozygotes, *Pax1* has been reported to be downregulated in the fourth pharyngeal pouch (Guris et al., 2006) and in *Tbx1*$^{-/-}$ mutants, *Pax1* expression could be detected only in the first pharyngeal pouch revealing a lack of caudal pharyngeal patterning (Guris et al., 2006; Jerome and Papaioannou, 2001). In one *Hes1*$^{-/-}$ embryos at E10.5 (1/6), expression of *Pax1* between the second and third pouches was expanded medially within the pharyngeal endoderm indicating a failure of *Pax1* to discretely localise to the lateral endoderm within the pharyngeal pouches (Figure 5.8B, C).

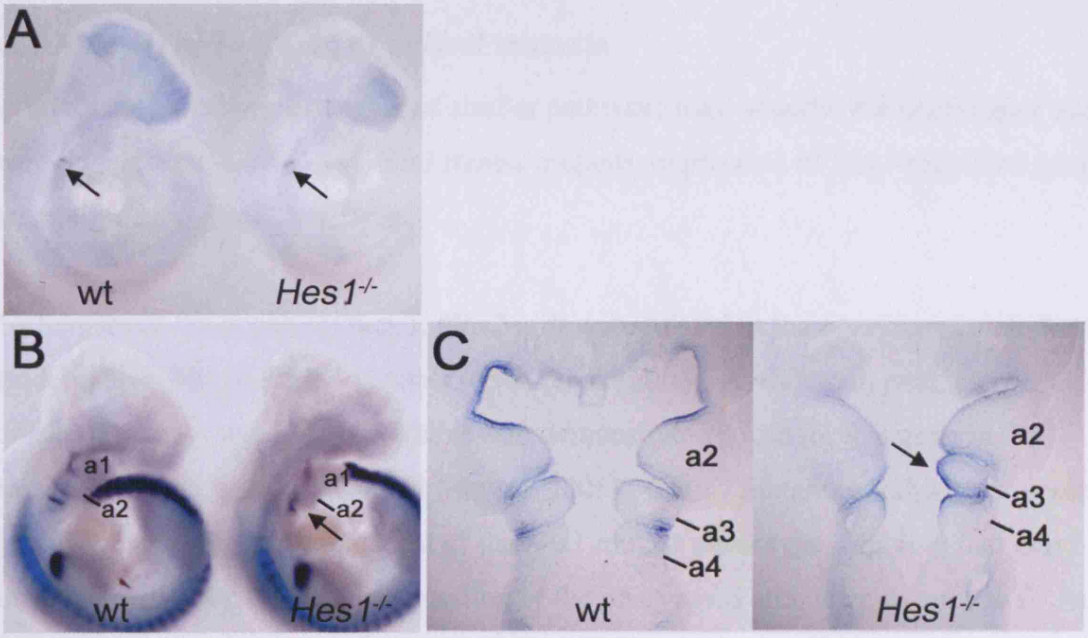

Figure 5.8 Pharyngeal patterning in *Hes1*$^{-/-}$ mutants
(**A**) Whole mount *in situ* hybridisation shows no change in expression of *Gcm2*, a marker for parathyroid precursors, between wild type (wt) and *Hes1*$^{-/-}$ (-/-) embryos at E10.5 (see arrows). (**B**, **C**) Expression of the pharyngeal pouch marker, *Pax1* is continuous between pharyngeal arches 2 and 3 in a *Hes1*$^{-/-}$ embryo (arrow in **B**). (**C**) Coronal sections of the corresponding embryos in B show that expression of *Pax1* extends medially into the endoderm lining pharyngeal arch 3 (arrow in **C**).
Abbreviations: a, arch.

5.2.7 Analysis of *Tbx1* targets in *Hes1* mutants

To investigate whether disruption of similar pathways may underlie the pharyngeal and heart defects seen in *Tbx1* and *Hes1* mouse mutants, expression of *Tbx1*-regulated genes was examined in *Hes1*$^{-/-}$ embryos.

The homeobox transcription factor, *Gbx2* is downregulated in the pharyngeal endoderm, ectoderm and SHF of *Tbx1*$^{-/-}$ mutants ((Ivins et al., 2005), A. Calmont, pers. comm.). Knockout mouse models of *Gbx2* have also demonstrated a role for this gene in pharyngeal development (Byrd and Meyers, 2005). *Gbx2*$^{-/-}$ mutants exhibit great vessel and OFT defects highly reminiscent of the *Tbx1* mutant phenotype implying that *Gbx2* may act downstream of *Tbx1* in formation of the pharyngeal arch arteries and OFT. At E9.5, *Gbx2* expression in wild type embryos was detected in the pharyngeal ectoderm overlying pharyngeal arch one and in the endoderm and ectoderm of the caudal arches (Figure 5.9A, B). However, in *Hes1*$^{-/-}$ mutants (n=2) at the same stage, expression within the caudal ectoderm was diminished (Figure 5.9A, B). Later, at E10.5, *Gbx2* expression in wild type embryos was observed within the ectoderm of the first pharyngeal arch and in the endoderm lining the caudal pharyngeal arches (Figure 5.9C, D), Ivins et al 05). In contrast, in a proportion of *Hes1*$^{-/-}$ mutants (n=2 out of 6) at the same stage, expression of *Gbx2* in the caudal pharyngeal endoderm was absent similar to that seen in *Tbx1*$^{-/-}$ embryos (Figure 5.9C, D). In addition, *Gbx2* appeared to be upregulated within the second pharyngeal arch ectoderm of *Hes1*$^{-/-}$ embryos (Figure 5.9C, D). These results suggest that *Gbx2* may lie downstream of *Tbx1* and *Hes1* in a common pathway required for proper development of the pharyngeal apparatus.

In *Tbx1*$^{-/-}$ mutants, expression of the *Cyp26* genes is dysregulated in the pharyngeal region (Guris et al., 2006; Ivins et al., 2005; Roberts et al., 2006) and knockdown of Cyp26 enzyme function in the chick phenocopies the *Tbx1* mouse mutant (Roberts et al., 2006). The *Cyp26* family of retinoic acid metabolising enzymes consist of three genes, *Cyp26a1*, *Cyp26b1* and *Cyp26c1* which encode enzymes required to catabolize the active retinoic acid metabolite to an inactive form (Fujii et al., 1997; White et al., 1996; White et al., 2000). All three *Cyp26* genes are expressed within the pharyngeal region in both complementary and overlapping domains (de Roos et al., 1999; MacLean et al., 2001; Roberts et al., 2006; Tahayato et al., 2003)and they play an important role in regulating levels of retinoic acid for normal development of the pharyngeal apparatus

and heart (Abu-Abed et al., 2001; Roberts et al., 2006; Uehara et al., 2007; Yashiro et al., 2004)(K. Yahiro, pers. comm.).

In a preliminary analysis of *Cyp26* gene expression in *Hes1*$^{-/-}$ mutants, *Cyp26c1* expression was examined. In *Tbx1*$^{-/-}$ embryos, *Cyp26c1* expression is downregulated in the peri-otic mesenchyme, otic vesicle, epibranchial placodes and pharyngeal endoderm but is expanded within the first pharyngeal arch mesenchyme (Roberts et al 06). In *Hes1*$^{-/-}$ embryos at E9.5 (n = 3), *Cyp26c1* expression was also dysregulated, but in contrast to *Tbx1*$^{-/-}$ mutants, *Cyp26c1* was expanded into the second pharyngeal arch of *Hes1*$^{-/-}$ mutant embryos and was also ectopically expressed within the caudal pharyngeal ectoderm overlying pharyngeal arches three and four (Figure 5.9E, G, H).

In addition to the *Cyp26* gene expression changes which occur in *Tbx1*$^{-/-}$ mutants, *Raldh2*, the main gene required for synthesis of retinoic acid is upregulated in the head mesenchyme of *Tbx1*$^{-/-}$ mutants and shifted anteriorly within the splanchnic mesoderm (Guris et al., 2006; Ivins et al., 2005). Analysis of *Raldh2* expression in *Hes1*$^{-/-}$ embryos at E9.5 (n = 2) did not reveal any changes in expression compared to wild type embryos (Figure 5.9F).

Examination of genes required to maintain the correct levels of retinoic acid for normal development has shown that retinoic acid levels may be altered in the pharyngeal region of *Hes1*$^{-/-}$ mouse mutants however, expression changes appear to be different to those which occur in *Tbx1*$^{-/-}$ embryos.

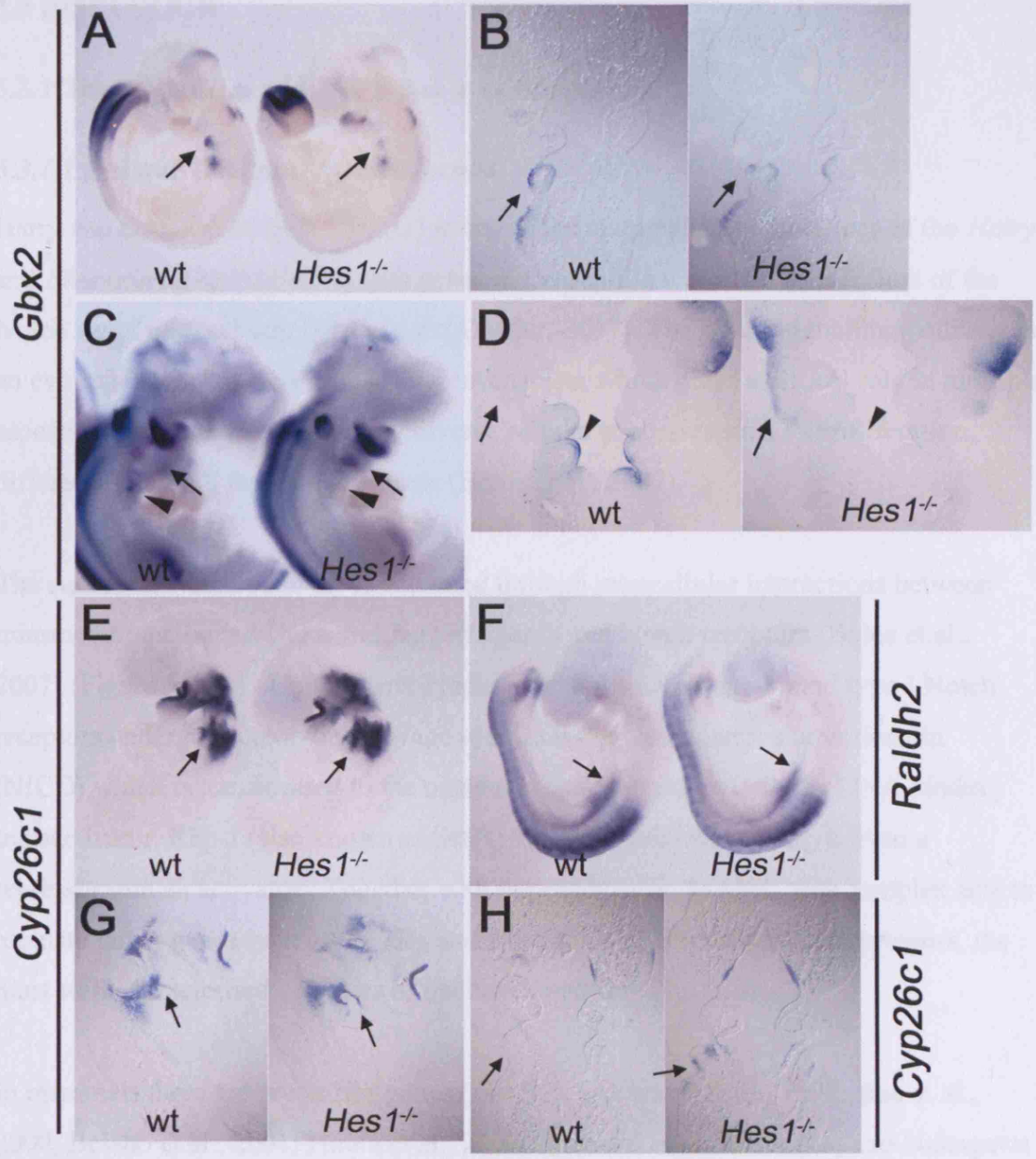

Figure 5.9 Expression of potential *Tbx1* targets in *Hes1*$^{-/-}$ mutants
(**A-D**) In a proportion of *Hes1*$^{-/-}$ mutants at E9.5, *Gbx2* expression is downregulated in the caudal pharyngeal ectoderm overlying pharyngeal arch 3 (arrows in **A** and **B**) whereas later at E10.5, *Gbx2* is lost in the caudal pharyngeal endoderm (arrowheads in **C** and **D**) but upregulated in the second arch ectoderm (arrows in **C** and **D**). (**B**, **D**) Coronal sections of the embryos in **A** and **C**, respectively. (**E**, **G**, **H**) *Cyp26c1* expression is expanded in *Hes1*$^{-/-}$ embryos at E9.5 (arrows in E) into pharyngeal arch 2 (arrows in **G**) and *Cyp26c1* is also ectopically expressed in the ectoderm overlying pharyngeal arches 3 and 4 (arrows in **H**). (**G**, **H**) Sagittal and coronal sections of *Cyp26c1 in situ* hybridisations, respectively. (**F**) *Raldh2* expression is not altered in *Hes1*$^{-/-}$ mutants at E9.5 (arrows in **F**).

5.3 DISCUSSION

5.3.1 The role of *Hes* and *Hey* genes in development

5.3.1.1 Hes and Hey transcription factors

Hairy and enhancer of split 1 (*Hes1*) is one of the mammalian homologues of the *Hairy* and *Enhancer-of-split* [*E(spl)*] type genes in Drosophila which act as effectors of the Notch signalling pathway (Fischer and Gessler, 2007). The Notch signalling pathway is an evolutionarily conserved signalling mechanism which plays a critical role in multiple aspects of development, regulating diverse cellular processes such as proliferation, differentiation, cell fate and apoptosis (Bolos et al., 2007).

The canonical Notch pathway is activated through intercellular interactions between transmembrane-bound Delta and Jagged ligands and Notch receptors (Bolos et al., 2007) (Figure 5.10A). Upon ligand binding, the transmembrane-bound type I Notch receptors undergo proteolytic cleavage to release the Notch intracellular domain (NICD) which is translocated to the nucleus where it interacts with the DNA binding transactivator, Rbp-J (also known as Su(H) in Drosophila) converting it from a repressor into an activator. Together with the coactivator, MAML, this complex acts to regulate target genes such as the *Hes* and *Hey* family of transcriptional repressors, the most well characterised effectors of the Notch pathway (Iso et al., 2003).

In mammals there are seven *Hes* genes (*Hes1-7*), (Akazawa et al., 1992; Bae et al., 2000; Bessho et al., 2001; Hirata et al., 2000; Ishibashi et al., 1993; Koyano-Nakagawa et al., 2000; Pissarra et al., 2000; Sasai et al., 1992) and three *Hey* genes (*Hey1*, *Hey2* and *HeyL*) (otherwise known as *Herp2, 1, 3*; *Hesr1, 2, 3*; *Hrt1, 2, 3* or *Chf2, 1*) (Iso et al., 2001a; Kokubo et al., 1999; Leimeister et al., 1999; Nakagawa et al., 1999; Steidl et al., 2000; Zhong et al., 2000). Both families primarily act as transcriptional repressors and are composed of three conserved domains: a basic helix-loop-helix (bHLH) DNA binding domain, an Orange domain that regulates the selection of heterodimer partners (Dawson et al., 1995; Taelman et al., 2004) and a C-terminal WRPW domain for Hes members or YRPW domain for Hey family members (Figure 5.10B) (Fischer and Gessler, 2007).

Hes and Hey family members can form homo- or heterodimers with one another (Fischer et al., 2007; Iso et al., 2001b; Leimeister et al., 2000; Van Wayenbergh et al.,

2003). Both family members function to actively repress transcription by binding to E-Box (CANNTG) consensus sites or N-box (CACNAG) sequences (Akazawa et al., 1992; Iso et al., 2003; Iso et al., 2001b; Ohsako et al., 1994; Sasai et al., 1992). In Hes family members, the C-terminal WRPW domain acts to repress transcription by recruiting Tle corepressors (Grbavec and Stifani, 1996; Paroush et al., 1994) whereas Hey family members primarily act to repress transcription through their bHLH domain and recruit different corepressors including N-CoR, mSin3A and HDAC1 (Fischer et al., 2002; Iso et al., 2001b). Hes and Hey transcription factors can also repress transcription in a passive manner by forming non-functional heterodimers with E-box binding bHLH factors, preventing DNA binding (Hirata et al., 2000; Sasai et al., 1992; Sun et al., 2001).

Figure 5.10 Notch signalling
(**A**) Transmembrane Notch ligands on neighbouring cells bind to Notch receptors, inducing proteolytic cleavage. The Notch intracellular domain (NICD) is translocated to the nucleus where it binds to the transcription factor, Rbp-J turning it from a repressor into an activator. Coactivators such as MAML are then recruited to the complex to induce transcription of targets such as *Hes* and *Hey* genes. (**B**) Hes and Hey transcription factors contain three conserved domains. Both families contain an N-terminal basic helix-loop-helix (bHLH) domain and an Orange (Or) domain. Hes and Hey family members differ in their C-terminal domains. Hes members have a WRPW (W) motif and Hey members contain a YRPW (Y) motif and a TE(I/V)GAF (T) peptide. Numbers represent the amino acid content of each domain. (Fischer and Gessler, 2007).

5.3.1.2 The roles of Hes1 in development

Hes1 is the most extensively studied member of the *Hes* gene family. *Hes1* knockout mice exhibit a multitude of defects in brain, neural tube, endocrine gland, sensory organ and gut formation, representing the diverse roles that *Hes1* plays in development, in maintaining proliferation, regulating differentiation and controlling binary cell fate decisions. Depending on the time and tissue in which *Hes1* is expressed, it can act to regulate one or more of these processes through Notch-dependent or independent pathways (Kageyama et al., 2007).

5.3.1.2.1 Hes1 regulates the maintenance of progenitors

Hes1 functions to regulate the maintenance of progenitor cell populations in development. In the nervous system, *Hes1*, with *Hes3* and *Hes5* act to maintain neural stem cells and prevent premature neurogenesis by repressing the expression of proneural genes such as *Mash1* and *Ngn2* (Hatakeyama et al., 2004; Ishibashi et al., 1993; Ohtsuka et al., 1999; Ohtsuka et al., 2001). Similarly, *Hes1* is required to maintain progenitor cells in the eye (Lee et al., 2005; Tomita et al., 1996), pituitary gland (Kita et al., 2007; Raetzman et al., 2007), pancreas (Jensen et al., 2000) and thymus (Tomita et al., 1999) by inhibiting the expression of pro-differentiation genes (Jensen et al., 2000; Kita et al., 2007; Raetzman et al., 2007; Tomita et al., 1999; Tomita et al., 1996). However, *Hes1* may also directly regulate proliferation as it has also been shown to repress expression of the cyclin-dependent kinase inhibitor, *p27(Kip1)* which was found to be upregulated in the brain and thymus of $Hes1^{-/-}$ mice (Murata et al., 2005).

Hes1 also acts to regulate boundary formation between the mid and hindbrain (Baek et al., 2006). High, persistent levels of *Hes1* within the boundary are required not only to prevent neuronal differentiation but also to suppress proliferation (Baek et al., 2006). Downregulation of proliferation in this tissue is thought to occur through repression of cell-cycle regulators such as *E2F-1* or *PCNA* (Baek et al., 2006; Castella et al., 2000; Hartman et al., 2004; Strom et al., 2000). In contrast, compartment cells express variable levels of *Hes1,* which the authors propose may be necessary for sustained proliferation (Baek et al., 2006).

5.3.1.2.2 Hes1 regulates the timing of differentiation

Hes1 also functions to regulate the timing of differentiation. In *Hes1*$^{-/-}$ mice, neural stem cells prematurely differentiate into neurons which become depleted and this occurs at the expense of later cell types such as oligodendrocytes and astrocytes (Hatakeyama et al., 2004). *Hes1* has been found to be required to maintain progenitor cells for a correct period of time during development to allow differentiation into late-arising neuronal cell lineages (Hatakeyama et al., 2004).

5.3.1.2.3 Hes1 controls binary cell fate decisions

Hes1 regulates binary cell fate decisions during development of the nervous system, pituitary gland and gut. In the nervous system, *Hes1* promotes the differentiation of neural stem cells into astrocytes over neuronal cells by repressing proneural genes and acting through the Lif signalling pathway to induce astrocyte-specific genes (Hatakeyama et al., 2004; Ishibashi et al., 1995; Kamakura et al., 2004; Ohtsuka et al., 1999; Ohtsuka et al., 2001). Throughout development of the digestive system, *Hes1* has also been found to regulate enterocyte versus non-enterocyte cell fate in the intestine (Jensen et al., 2000; Suzuki et al., 2005) and biliary epithelial cell versus hepatocyte lineage in the liver (Kodama et al., 2004). Furthermore, in addition to its role in maintenance of progenitor cells in the pituitary gland, *Hes1* also functions to specify intermediate versus anterior lobe formation in the pituitary (Kita et al., 2007; Raetzman et al., 2007).

5.3.1.2.4 Hes1 functions as a molecular oscillator

The formation of somites along the anterior-posterior axis of vertebrate embryos is precisely controlled by the segmentation clock in which synchronised, oscillatory expression of genes in the pre-somitic mesoderm (PSM) regulates the timing of somite development (Andrade et al., 2007). Both *Hes1* and *Hes7* have been shown to exhibit cyclical gene expression in the PSM (Bessho et al., 2001; Jouve et al., 2000). However, only *Hes7* appears to play an important role in regulating the segmentation clock in mice (Bessho et al., 2001; Hirata et al., 2004) since *Hes1*$^{-/-}$ mutants do not exhibit any defects in somitogenesis.

Interestingly, *Hes1* has also been found to exhibit oscillatory expression upon serum stimulation within multiple, different cell types in culture, such as fibroblasts, myoblasts and neuroblasts (Hirata et al., 2002; Kageyama et al., 2007; Yoshiura et al., 2007). This

expression is cell autonomous and requires transient negative autoregulation in which *Hes1* binds to its own promoter to repress transcription (Hirata et al., 2002). Real-time imaging analysis has shown that *Hes1* expression is often oscillatory within single cells but this expression is asynchronous between cells (Masamizu et al., 2006). However, the biological significance of this observation in relation to *Hes1* function in development is still unclear.

5.3.1.3 Hey genes and cardiovascular development

To date, a role for *Hes* genes in cardiovascular development has not been identified. In contrast, *Hey* genes have been shown to play diverse roles in formation of the heart and vasculature. In vascular development, *Hey1* and *Hey2* are required to regulate arterial-venous differentiation (Fischer et al., 2004b; Kokubo et al., 2005) while *Hey2* also plays a role in vascular maturation (Sakata et al., 2006).

Hey2$^{-/-}$ mutants exhibit a range of cardiac malformations including cardiomyopathy, VSDs, atrioventricular valve defects and tetralogy of Fallot (Donovan et al., 2002; Gessler et al., 2002; Kokubo et al., 2004; Sakata et al., 2002). *Hey1*$^{-/-}$;*HeyL*$^{-/-}$ mutants have similar VSD and atrioventricular valve anomalies (Fischer et al., 2007). *Hey1*, *Hey2* and *HeyL* have all been shown to play a critical role in regulating epithelial to mesenchymal transition (EMT) which is required for correct formation of the atrioventricular valves and the interventricular septum (Fischer et al., 2007; Kokubo et al., 2005). In addition, *Hey2*$^{-/-}$ mice have been shown to exhibit thin ventricular walls and defects in trabeculation suggesting a role for *Hey2* in cardiomyocyte maturation (Kokubo et al., 2005; Kokubo et al., 2004; Sakata et al., 2006). Indeed, recent studies have shown that *Hey2* acts to repress atrial gene expression within ventricles and promote myocardial proliferation (Koibuchi and Chin, 2007; Xin et al., 2007). Furthermore, *Hey1* and *Hey2* have also been demonstrated to regulate atrioventricular boundary formation during development (Kokubo et al., 2007; Rutenberg et al., 2006).

5.3.1.4 Summary

In conclusion, *Hes* and *Hey* genes play diverse roles in development and act as the primary effectors of Notch signalling. In particular, *Hes1* functions in development of many organs including the brain, sensory organs, endocrine glands and the gut while the *Hey* transcription factors are mainly involved in aspects of cardiovascular development.

5.3.2 *Hes1* Functions in pharyngeal and cardiovascular development

Hes1 was identified as a gene downregulated in *Tbx1*-null cells within the pharyngeal apparatus of *Tbx1*$^{-/-}$ mouse mutants. Analysis of *Hes1*$^{-/-}$ mutants revealed that a proportion of embryos exhibit DGS-like craniofacial, thymic and cardiovascular defects including great vessel and OFT anomalies reminiscent of the *Tbx1* mutant phenotype. These results suggest that *Hes1* may lie downstream of *Tbx1* in pharyngeal and heart development and may act as a modifier gene in DGS patients.

5.3.2.1 Hes1 and vascular development

In the original paper describing the *Hes1*$^{-/-}$ mouse mutant, a proportion of *Hes1*$^{-/-}$ embryos were embryonic lethal from E12.5 (Ishibashi et al., 1995). *Hes1*$^{-/-}$ mutants were found to exhibit a variable phenotype ranging from severe neural tube and brain defects to a grossly normal appearance. However, these mice still died perinatally (Ishibashi et al., 1995). Reports have since described additional defects in the *Hes1* knockout mouse such as lung and pancreatic abnormalities which could contribute to neonatal lethality (Ito et al., 2000; Jensen et al., 2000). However, the *Hes1*$^{-/-}$ malformations described to date still cannot account for embryonic lethality at E12.5. In the course of this study on the functional role of *Hes1* in pharyngeal and heart development, a proportion of *Hes1*$^{-/-}$ mutants at E11.5 were found to exhibit body haemorrhage, indicative of a possible vascular defect that could account for midgestation lethality.

Interestingly, the stage of embryonic lethality and haemorrhaging observed in *Hes1*$^{-/-}$ mice is reminiscent of the *Dll1*$^{-/-}$ mutant phenotype (Hrabe de Angelis et al., 1997). *Hes1* has been shown to be preferentially induced by the Notch ligand Dll1 in cell culture (Jarriault et al., 1998; Kuroda et al., 1999) and together, these results suggest that *Hes1* may regulate vascular development downstream of *Dll1*-induced Notch signalling. However, it still remains to be determined whether *Hes1* plays a similar role to other Notch signalling components in arterial-venous specification (Domenga et al., 2004; Duarte et al., 2004; Fischer et al., 2004b; Gale et al., 2004; Kokubo et al., 2005; Krebs et al., 2004).

5.3.2.2 Hes1 and Tbx1 in pharyngeal arch artery development

Hes1$^{-/-}$ mice exhibit great vessel anomalies similar to those observed in *Tbx1*$^{+/-}$ mice including right-sided and interrupted aortic arch, aberrant right-subclavian artery and right-sided ductus arteriosus, which occur due to defective fourth and sixth arch artery development. The most consistent pharyngeal arch artery defect found in *Hes1* mutants at E10.5 was fourth arch artery hypo/aplasia, although defects in development of the other arch arteries were also detected.

Hes1 is downregulated within *Tbx1*$^{-/-}$ mutants in the pharyngeal endoderm, a tissue in which *Tbx1* may be required for normal growth and remodelling of the fourth arch artery (Zhang et al., 2005). Considering that both *Hes1*$^{+/-}$ and *Tbx1*$^{+/-}$ mutants exhibit fourth arch artery defects, it was hypothesized that the reduced dosage of *Hes1* may play a role downstream of *Tbx1* in causing arch artery defects. Investigation of double heterozygous mice from E10.5 to E12.5 did not reveal any differences in either the severity or penetrance of the arch artery phenotype compared to single heterozygotes alone, thus demonstrating that *Hes1* and *Tbx1* do not appear to genetically interact in pharyngeal arch artery development in the mouse. However, there are several factors that may have affected the analyses including the effect of genetic modifiers, functional redundancy among related Hes/Hey proteins and phenotypic variability.

5.3.2.2.1 The influence of genetic background on phenotype

In the analysis of *Hes1*$^{-/-}$ mutants on two different strains, a pure MF1 background and a mixed MF1;C57Bl/6 background, it became obvious that the genetic background was altering the phenotype. In the MF1 strain, *Hes1*$^{-/-}$ mutants were embryonic lethal from E12.5 apparently from vascular defects, and they also presented with severe neural tube defects. On a mixed background, *Hes1*$^{-/-}$ mutants did not exhibit any neural tube defects and were present in normal mendelian ratios at E15.5. These observations indicate that modifiers within the C57Bl/6 background may rescue the severe vascular and neurulation defects in *Hes1*$^{-/-}$ mutants.

The effect of genetic background on the severity of brain defects in *Hes1*$^{-/-}$ mutants has been noted previously (Nakamura et al., 2000; Ohtsuka et al., 2001). The phenotypes of mouse mutants for other members of the Notch signalling pathway have also been shown to be affected by genetic background. *Hey2*, a *Hes*-related family member is heavily influenced by genetic modifiers (Fischer et al., 2004a; Sakata et al., 2006). The cardiovascular phenotype observed in *Hey2*$^{-/-}$ mutants independently generated on different strains ranges from fatal cardiomyopathy (Gessler et al., 2002) and cardiomyopathy with a ventricular septal defect (Sakata et al., 2002), to tetralogy of Fallot-like defects (Donovan et al., 2002) and atrioventricular valve anomalies (Kokubo et al., 2004).

Tbx1$^{+/-}$ mouse mutants also exhibit a variable phenotype depending on the genetic background which influences the penetrance of arch artery, thymic and parathyroid defects (Taddei et al., 2001). In this study only 14% of *Tbx1*$^{+/-}$ mutants on the mixed MF1;C57Bl/6 background exhibited fourth arch artery defects at E12.5 compared to 50% of *Tbx1*$^{+/-}$ mice on a C57Bl/6 background (Taddei et al., 2001) indicating that the MF1 strain causes increased recovery from pharyngeal arch artery defects.

The effect of the MF1 background on the *Tbx1*$^{+/-}$ pharyngeal arch artery phenotype, together with the recovery of *Hes1*$^{-/-}$ vascular defects on the C57Bl/6 background may have prevented the identification of an epistatic interaction between *Tbx1* and *Hes1*. In addition, relatively small numbers of embryos were examined and the *Hes1*$^{-/-}$ phenotype is not fully penetrant which also may have affected the results.

The analysis of *Hes1*$^{+/-}$;*Tbx1*$^{+/-}$ double heterozygotes did not include investigation of the palate, thymic or outflow tract, structures which are similarly defective in *Hes1*$^{-/-}$ and *Tbx1*$^{-/-}$ mutants. *Hes1* was found to be downregulated in *Tbx1*$^{-/-}$ mice within the pharyngeal endoderm and second heart field, *Tbx1* domains required for development of these structures (Arnold et al., 2006b; Xu et al., 2004; Zhang et al., 2006) suggesting that an interaction between *Tbx1* and *Hes1* during mouse development may yet exist.

5.3.2.2.2 The effect of functional redundancy on phenotype

Hes1 is a member of the hairy/enhancer of split (Hes) family which in mouse includes *Hes2*, *-3*, *-5*, *-6* and *-7* and the functionally related, *Hes*-related with YRPW (*Hey*) genes, *Hey1*, *-2* and *–L* which are also effectors of Notch signalling (Iso et al., 2003). *Hes1*, *-3*, and *-5* have been shown to compensate for one another during neural development. *Hes3*$^{-/-}$ mutants are phenotypically normal (Hirata et al., 2001) and *Hes5*$^{-/-}$ mice exhibit mild defects in central nervous system (CNS) and sensory organ development (Cau et al., 2000; Hojo et al., 2000; Ohtsuka et al., 1999; Zine et al., 2001). When these mice are crossed with *Hes1* mutants, double and triple knockout embryos have much more severe CNS defects than any single gene mutant (Cau et al., 2000; Hatakeyama et al., 2004; Hatakeyama et al., 2006; Ohtsuka et al., 1999; Ohtsuka et al., 2001).

Similarly, the *Hey* genes also act redundantly during cardiovascular development. *Hey1*$^{-/-}$ and *HeyL*$^{-/-}$ mice are viable and fertile (Fischer et al., 2004b; Fischer et al., 2007; Kokubo et al., 2005), however, a combined loss of *Hey1* and *HeyL* results in similar VSD and atrioventricular valve anomalies to *Hey2*$^{-/-}$ mutants (Fischer et al., 2007). *Hey1*$^{-/-}$;*Hey2*$^{-/-}$ mice also exhibit severe vascular defects in arterial-venous differentiation and vascular maturation not observed in either *Hey1*$^{-/-}$ or *Hey2*$^{-/-}$ mutants alone (Fischer et al., 2004b; Kokubo et al., 2005). This phenotype more closely reflects the zebrafish *gridlock* (*hey2*) mutant (Zhong et al., 2001; Zhong et al., 2000). *hey2* is the only *hey* gene family member expressed within blood vessels in the zebrafish (Winkler et al., 2003) whereas *Hey1*, *Hey2* and *HeyL* are coexpressed in mouse vasculature (Fischer and Gessler, 2003; Iso et al., 2003).

These experiments clearly show that functional redundancy among *Hes* and *Hey* genes plays an important role during development however, the question still remains as to whether *Hey* genes can compensate for loss of *Hes* genes and vice versa. In the

pharyngeal region, *Hes1* expression overlaps with members of the *Hey* gene family within the pharyngeal mesenchyme (*Hey1*, *Hey2* and *HeyL*) and pharyngeal endoderm (*Hey1* and *HeyL*) (Irinna Papangeli, pers. comm., (High et al., 2007)).

Evidence for functional redundancy among Notch effectors in pharyngeal development is provided by the analysis of $Pax3^{Cre/+}$ *DNMAML* mouse mutants in which Notch signalling was specifically ablated in NC tissues using a dominant negative form of *MAML* (High et al., 2007). $Pax3^{Cre/+}$ *DNMAML* mice exhibited OFT and arch artery defects highly reminiscent of the heart defects in $Hes1^{-/-}$ mutants (High et al., 2007). *Hey1*, *Hey2* and *HeyL* were shown to be downregulated in NC-derived cells but the cardiovascular and pharyngeal arch artery defects represented a novel phenotype which had never been detected in any type of *Hey* knockout mice (Donovan et al., 2002; Fischer et al., 2004b; Fischer et al., 2007; Gessler et al., 2002; Kokubo et al., 2005; Kokubo et al., 2004; Sakata et al., 2002). Functional redundancy among the *Hey* genes was suggested as a possible reason why great vessel defects were unique to this mouse mutant. However, *Hes1* expression was not analysed in *DNMAML* embryos and considering the phenotype, it seems likely that downregulation of *Hes1* may play the dominant role in pathogenesis of OFT and pharyngeal arch artery defects in these mice.

These results, in combination with the overlapping expression of *Hes* and *Hey* genes within *Tbx1* domains, indicate that functional redundancy between *Hes1* and *Hey* genes could have affected the penetrance of pharyngeal arch defects not only in $Hes1^{-/-}$ mutants but also in $Tbx1^{+/-};Hes1^{+/-}$ transheterozygotes. This represents another factor which may have prevented the identification of a genetic interaction between *Tbx1* and *Hes1* in mice.

The effects of genetic background, functional redundancy and the variability of the phenotype may have masked an epistatic interaction between *Tbx1* and *Hes1* in pharyngeal arch artery development. Alternatively, *Tbx1* and *Hes1* may not interact in this process and the similar defects observed in *Hes1* and *Tbx1* mutants could have been caused by disruptions to distinct developmental pathways. However, epistatic interaction studies conducted in zebrafish indicate that *tbx1* and *her6* (the zebrafish homologue of *Hes1*) interact in formation of the pharyngeal arch arteries (see Section 5.3.2.2.7).

5.3.2.2.3 Analysis of epistasis between tbx1 and her6 in zebrafish pharyngeal development

As mentioned above, a number of issues may have affected the identification of an epistatic interaction between *Tbx1* and *Hes1* in mouse development. In order to circumvent some of these issues to determine whether *Tbx1* and *Hes1* genetically interact in pharyngeal development, studies were carried out in the zebrafish. All zebrafish experiments were carried out by Catherine Roberts in our lab but the results have been included in this discussion to highlight the advantages of using the zebrafish model system to investigate epistatic interactions with *tbx1*.

Zebrafish represent an excellent model system to study developmental processes because of their small size, optical transparency, the large numbers of embryos which can be obtained from a single mating and their relatively rapid development in which most organs are formed within the first five days (Beis and Stainier, 2006). In addition, the biological function of one or multiple genes can be easily and simultaneously analysed by using a specific antisense morpholino oligonucleotide to downregulate expression of a particular gene (Heasman, 2002).

Tbx1 appears to play a similar role in pharyngeal development of the mouse and zebrafish. *van gogh* (*vgo*) zebrafish mutants exhibit pharyngeal, otic vesicle and thymic defects reminiscent of the *Tbx1*$^{-/-}$ mouse phenotype (Piotrowski et al., 2003; Piotrowski and Nusslein-Volhard, 2000). In *vgo* mutants, the posterior pharyngeal arches fail to segment because the endodermal pouches do not develop, aortic arches are reduced or absent, the otic vesicle is hypoplastic and embryos also exhibit thymic hypo/aplasia (Piotrowski et al., 2003; Piotrowski and Nusslein-Volhard, 2000). The gene mutated in *vgo* fish has been cloned and verified as the zebrafish homologue of *Tbx1* (Kochilas et al., 2003; Piotrowski et al., 2003). The similar malformations in mouse and zebrafish suggest that they may share genetic pathways downstream of *Tbx1* important for development of the pharyngeal apparatus. Therefore, the role of *her6* (the zebrafish homologue of *Hes1*) in pharyngeal development and its potential interaction with *tbx1* was investigated.

Her6 is important in zebrafish somite formation (Pasini et al., 2004) but there has been no previously reported role for *her6* in pharyngeal or heart development. Studies in our

lab have shown that *her6* is downregulated or absent from the pharyngeal apparatus in *vgo/vgo* mutants compared to *vgo/+* or wild type embryos, similar to *Hes1* downregulation in *Tbx1*$^{-/-}$ mice. Injection of high concentrations of *her6* antisense morpholino oligonucleotides recapitulates the *vgo/vgo* pharyngeal phenotype. *her6* and *tbx1* appear to genetically interact in zebrafish since injection of double morpholinos results in a statistically significant increase in the severity and penetrance of pharyngeal defects compared to either morpholino alone. Furthermore, preliminary experiments have shown that injecting *tbx1* morpholino plus full length *her6* mRNA into zebrafish embryos appears to decrease the penetrance of pharyngeal arch artery defects compared to embryos injected with *tbx1* morpholinos alone. Therefore, *her6* must play a critical role downstream of *tbx1* in zebrafish pharyngeal development.

Together, these experiments clearly support a genetic interaction between *tbx1* and *her6* in zebrafish pharyngeal development. The difference in epistasis results between mouse and zebrafish may reflect the fact that all experiments can be carried out within the same genetic background. Since *her6* morpholinos give a more highly penetrant pharyngeal arch artery phenotype than *Hes1*$^{-/-}$ mouse mutants (~60% vs, ~20%), morpholino knockdown may reduce *her6* to below 50% of wild type levels. There may also be less functional redundancy amongst the *her* and *hey* genes in zebrafish than in mouse.

5.3.3 The molecular role of *Hes1* downstream of *Tbx1* in pharyngeal development

One of the underlying cellular defects in *Tbx1*$^{-/-}$ mutants is decreased proliferation of the pharyngeal endoderm, mesoderm and otic epithelium, a process considered to play a major role in the aetiology of *Tbx1*$^{-/-}$ malformations (Vitelli et al., 2003; Xu et al., 2005; Xu et al., 2007a; Xu et al., 2004; Xu et al., 2007b; Zhang et al., 2006). *Tbx1* has been proposed to play a role in maintenance of progenitor cell populations within the SHF for contribution to the OFT (Xu et al., 2004; Zhang et al., 2005) and within the endoderm for proper expansion of cells for pharyngeal segmentation (Xu et al., 2005). In the ear, *Tbx1* is required in the otic epithelium to regulate the size of the otocyst and in the periotic mesenchyme for formation of the pericochlear capsule and part of the cochlea (Xu et al., 2007a; Xu et al., 2007b). However, the underlying mechanisms through which *Tbx1* may act to regulate proliferation are unknown.

Hes1 is also required to maintain or regulate progenitor cell populations within the thymus (Tomita et al., 1999), eye (Tomita et al., 1996), pituitary gland (Kita et al., 2007; Raetzman et al., 2007), brain (Hatakeyama et al., 2004; Ishibashi et al., 1995) and pancreas (Jensen et al., 2000). This function of *Hes1* may occur partly through direct downregulation of the cyclin-dependent kinase inhibitor, *p27(Kip1)* which was found to be upregulated in the hypoplastic thymus and brains of *Hes1*$^{-/-}$ mice (Murata et al., 2005). *Tbx1* may exert some of its effects on cell proliferation through *Hes1*.

Tissue-specific deletion experiments have demonstrated that *Tbx1* is required in both the endoderm and mesoderm for correct alignment and septation of the OFT (Arnold et al., 2006b; Zhang et al., 2006). So far, only outflow tract alignment defects have been detected in *Hes1*$^{-/-}$ mutants but *Hes1* could act downstream of *Tbx1* in either or both tissues in this aspect of development. In *Tbx1*$^{-/-}$ mice, insufficient addition of SHF precursors to the developing heart is considered to be the underlying defect resulting in a shortened OFT and subsequent alignment and septation defects (Xu et al., 2004). It is possible that in addition to decreased proliferation, the differentiation of SHF precursors could also be defective in *Tbx1*$^{-/-}$ mutants. *Hes1* may be required to maintain proliferation of SHF precursor cells and/or to prevent premature differentiation of mesodermal cells into outflow tract cardiomyocytes or endothelial cells.

In pharyngeal arch artery development, Notch signalling has been shown to regulate the differentiation of NC cells into VSM cells (High et al., 2007). Similarly, mice heterozygous for *Tbx1* also exhibit a lack of NC-derived VSM lining the fourth pharyngeal arch arteries (Kochilas et al., 2002; Lindsay and Baldini, 2001). These results suggest that *Tbx1* could regulate VSM cell differentiation through the Notch/Hes1 signalling pathway. *Tbx1* is not expressed in NC tissues but is required in the pharyngeal epithelia for correct pharyngeal arch artery formation and remodelling (Zhang et al., 2005). *Tbx1* could induce NC differentiation by activating a Notch ligand such as *Jag1* within the pharyngeal epithelia to signal to adjacent NC cells expressing Notch receptors and downstream effectors. Alternatively, direct regulation of *Hes1* by *Tbx1* within the pharyngeal epithelia could also affect Notch signalling within adjacent NC cells depending on the distribution of Notch ligands and receptors.

The role of *Tbx1* in palate development has not been well characterised. It is known that *Tbx1* is required in the pharyngeal epithelia for normal palate development and is only necessary after E11.5 for secondary palatogenesis (Arnold et al., 2006b; Xu et al., 2005; Zhang et al., 2006; Zoupa et al., 2006). Normal secondary palate development requires growth of the bilateral palatal shelves down from the maxillary processes, rotation and elevation of these shelves above the tongue and fusion of the shelves at the midline (Gritli-Linde, 2007). *Tbx1* is expressed in the palatal shelf epithelia and medial epithelial seam (Zoupa et al., 2006) and may be required to maintain proliferation of palatal epithelial cells or function in the epithelial to mesenchymal tranformation of medial epithelial seam cells for correct fusion (Gritli-Linde, 2007). *Hes1*$^{-/-}$ mutants exhibit a similar cleft palate phenotype and it is possible that *Hes1* could act in one of these processes downstream of *Tbx1* to control palate formation.

In thymic development, *Tbx1* has been demonstrated to play two distinct roles, one in thymic induction between E8.5 and E9.5 which occurs secondary to defective pouch formation and another in thymic morphogenesis between E10.5 and E11.5 (Xu et al., 2005). Development of the thymus requires *Tbx1* in both the pharyngeal epithelia and mesoderm (Arnold et al., 2006b; Zhang et al., 2006). *Hes1*$^{-/-}$ mutants exhibit a similar thymic hypo/aplasia phenotype which is at least partly due to the cell-autonomous role of *Hes1* in expansion of thymocytes (Tomita et al., 1999). *Hes1* may also play another role in thymic organogenesis downstream of *Tbx1* in which it could act in regulating

proliferation of endodermal cells, differentiation of NC cells or in the specification of thymic epithelial cells.

5.3.4 Analysis of biological pathways downstream of *Hes1* in pharyngeal development

5.3.4.1 Analysis of pharyngeal patterning in Hes1$^{-/-}$ mutants

To determine which developmental pathways and mechanisms were affected within the pharyngeal region of *Hes1*$^{-/-}$ mutants, and how closely the *Hes1*$^{-/-}$ defects resembled the *Tbx1* mutant phenotype, patterning of the pharyngeal apparatus was examined in addition to expression of other genes known to be regulated by *Tbx1*.

Pax1, a marker of pharyngeal pouch endoderm and a gene required for normal thymus and parathyroid development (Su et al., 2001; Wallin et al., 1996), was found to be aberrantly expressed within the pharyngeal endoderm between pouches two and three in a *Hes1*$^{-/-}$ embryo, demonstrating a lack of pharyngeal pouch identity. This patterning defect most closely resembles *Pax1* expression in RA-treated mouse embryos which fail to properly form arches caudal to pharyngeal arch two and exhibit thymic and parathyroid defects (Mulder et al., 1998). In contrast, *Pax1* expression is downregulated in the fourth pharyngeal pouch of *Tbx1*$^{+/-}$ heterozygotes (Guris et al., 2006) and is completely absent in the unsegmented caudal pharyngeal endoderm of *Tbx1*$^{-/-}$ mutants (Guris et al., 2006; Jerome and Papaioannou, 2001).

Altered *Pax1* expression in *Hes1*$^{-/-}$ mutants is indicative of a defect in pharyngeal patterning which could affect endocrine gland and/or pharyngeal arch artery development. Even though aberrant *Pax1* expression was only seen in one out of six *Hes1*$^{-/-}$ embryos, this incidence of altered marker expression corresponds with the low percentage of *Hes1*$^{-/-}$ embryos with pharyngeal arch artery defects at this stage. In addition, this altered expression pattern was not seen in any wild type or *Hes1*$^{+/-}$ embryos (n=5) used for controls or in any wild type embryos used in previous *Pax1 in situ* experiments (Ivins et al., 2005). Therefore, even though parathyroid abnormalities were not identified through analysis of *Gcm2* expression in *Hes1*$^{-/-}$ mutants, defects in this structure may still occur due to aberrant patterning in *Hes1*$^{-/-}$ mice since there is a close association between thymus and parathyroid development. This should be investigated with markers such as *Hoxa3*, which is important for endocrine gland

development (Manley and Capecchi, 1995; Su et al., 2001) and further analysis of parathyroid morphology.

To better characterise potential patterning abnormalities in *Hes1*$^{-/-}$ embryos, the expression of additional *Hox* genes could also be examined in the future. *Hox* genes confer anterior-posterior positional identity within the pharyngeal apparatus and each *Hox* gene paralog group (of which there are four) is segmentally expressed within the pharyngeal arches (Schilling, 1997). Although *Hox* gene expression within *Tbx1*$^{+/-}$ heterozygotes appears to be normal, *Hoxb1*, *Hoxb4* and *Hoxd4* have been found to be ectopically expressed in more anterior pharyngeal regions of *Tbx1*$^{-/-}$ embryos compared to wild type mice (Guris et al., 2006).

The similar malformations seen in *Hes1* and *Tbx1* mouse mutants and *her6* morpholino and *vgo/tbx1* zebrafish mutants suggests that similar mechanisms may underlie the defects in pharyngeal development. However, the low penetrance of cardiovascular defects in *Hes1*$^{-/-}$ mutants made it particularly difficult to determine which biological pathways or processes were affected and how closely they related to *Tbx1*$^{-/-}$ mutants. Given that the penetrance of pharyngeal defects in *her6* morpholino-injected zebrafish is much higher and a greater number of embryos can be examined simultaneously, it may be easier to dissect out the mechanisms responsible in zebrafish rather than mice.

5.3.4.2 Analysis of Tbx1 targets in Hes1$^{-/-}$ *mutants*

5.3.4.2.1 Hes1 and Gbx2 in pharyngeal and heart development

Analysis of the transcriptional profile of *Tbx1*$^{-/-}$ embryos (Ivins et al., 2005) and cells, identified dysregulated genes such as the transcription factor *Gbx2* and the *Cyp26* RA metabolizing genes which have been shown to function in pharyngeal and heart development (Byrd and Meyers, 2005; Roberts et al., 2006). Mutations of these genes results in DGS-like malformations, similar to those seen in *Tbx1*$^{-/-}$ embryos. However, it remains uncertain how the activity of these genes is integrated in pharyngeal and heart development. To investigate whether similar genetic pathways are disrupted in *Hes1* and *Tbx1* mutants, the expression of *Gbx2* and members of the RA signalling pathway were analysed in *Hes1*$^{-/-}$ embryos.

Gbx2$^{-/-}$ mutants exhibit craniofacial and cardiovascular defects including cleft palate, otic vesicle hypoplasia, great vessel and OFT alignment defects reminiscent of *Tbx1* and *Hes1* mouse mutants (Byrd and Meyers, 2005; Wassarman et al., 1997). *Gbx2* was found to be downregulated within the caudal pharyngeal ectoderm at E9.5 and the pharyngeal endoderm at E10.5 in *Hes1*$^{-/-}$ mutants similar to *Tbx1*$^{-/-}$ embryos ((Ivins et al., 2005), A. Calmont, pers. comm.). However, expression of *Gbx2* within the pharyngeal endoderm was diminished in *Tbx1*$^{-/-}$ mutants prior to that seen in *Hes1*$^{-/-}$ mice and the increased levels of *Gbx2* in the second pharyngeal arch ectoderm of *Hes1*$^{-/-}$ mutants at E10.5 has not been observed in *Tbx1*$^{-/-}$ mutants (Ivins et al., 2005).

These results suggest that *Tbx1* and *Hes1* may interact in regulating the expression of *Gbx2* in the pharyngeal arches. However, considering the timing of *Gbx2* downregulation and the fact that the only overlapping expression domain for all three genes is the pharyngeal endoderm, it appears likely that both *Tbx1* and *Hes1* also regulate *Gbx2* through independent pathways.

Recently our lab has demonstrated an epistatic interaction between *Tbx1* and *Gbx2* in fourth pharyngeal arch artery development (A. Calmont and S. Ivins, pers. comm). However, the tissue(s) in which this interaction occurs has not been defined and it still remains to be determined whether these genes interact in the development of other pharyngeal-derived structures.

These studies have demonstrated that *Tbx1* interacts with numerous genes to regulate pharyngeal arch artery development. The challenge now is to dissect out the links between downstream effectors and determine how different pathways integrate in regulating development of pharyngeal-derived structures. *Gbx2* may represent one node of convergence between *Tbx1* and *Hes1* although it is clear from expression and functional analyses that these genes also act through independent signalling pathways in pharyngeal and heart development. Reciprocal expression analyses of *Gbx2*, *Hes1* and other *Tbx1* target genes such as *Fgf8* within their respective loss of function mouse mutants will help to identify common links between pathways. In addition, conditional deletion of multiple *Tbx1* targets simultaneously within specific pharyngeal tissues at various timepoints should also help to characterise the genetic pathways acting downstream of, and in parallel to, *Tbx1*.

5.3.4.2.2 Hes1 and retinoic acid signalling in pharyngeal development

Maintenance of the correct RA levels is extremely important for normal pharyngeal development. Many studies have demonstrated that disrupting RA homeostasis during development (by either upregulating or downregulating RA levels) leads to a DGS-like phenotype (Mulder et al., 1998; Niederreither et al., 2003; Niederreither et al., 2001; Vermot et al., 2003; Wendling et al., 2000).

In *Tbx1*$^{-/-}$ mutants, regulation of RA levels is severely perturbed in the pharyngeal region due to downregulation of the RA-metabolizing enzymes, *Cyp26a1*, *Cyp26b1* and *Cyp26c1* and upregulation of *Raldh2*, the enzyme required for generating the majority of embryonic RA (Guris et al., 2006; Ivins et al., 2005; Roberts et al., 2006). The altered expression of these genes results in an overall increase in RA within the pharyngeal apparatus and head mesenchyme of *Tbx1*$^{-/-}$ mutants. This has been demonstrated by expression of the *RARE* reporter transgene which consists of a hsp68 promoter and *lacZ* gene under control of a canonical RA response element (Guris et al., 2006). Ablating the function of all the Cyp26 enzymes in chick phenocopies DGS and results in caudal pharyngeal arch and arch artery defects, a hypoplastic otic vesicle and OFT defects similar to *Tbx1*$^{-/-}$ mice. These defects are considered to occur as a result of the subsequent increase in RA levels within these embryos (Roberts et al., 2006).

As a preliminary analysis of whether RA levels are affected in *Hes1*$^{-/-}$ mutants, the expression of *Raldh2* and *Cyp26c1* was investigated. *Raldh2* expression was not altered in *Hes1*$^{-/-}$ embryos at E9.5 but *Cyp26c1* expression was expanded into the second pharyngeal arch and ectopically expressed in the caudal pharyngeal ectoderm. In contrast, *Cyp26c1* expression in *Tbx1*$^{-/-}$ mice was generally downregulated within the pharyngeal region except for expanded expression within the first arch mesenchyme (Roberts et al., 2006). Despite the different expression patterns, these results imply that RA levels may be altered in *Hes1*$^{-/-}$ mutants and suggest that further experiments should be carried out to investigate whether expression of other genes important for regulation of RA such as *Cyp26a1* and *Cyp26b1* are also dysregulated in *Hes1*$^{-/-}$ mutants. In addition, crossing *Hes1* mutants to *RARE-lacZ* transgenic mice should confirm whether the expression of RA is aberrant within the pharyngeal region.

RA has also been shown to induce or repress proliferation and differentiation by altering *Hes1* levels in different carcinoma cell lines ((Hartman et al., 2004; Muller et al., 2002;

Murata et al., 2005; Wakabayashi et al., 2000). *Hes1* is also upregulated in vitamin A-treated limb buds (Ali-Khan and Hales, 2006). There have been no reports so far demonstrating regulation of RA by *Hes1,* although in zebrafish, morpholino knockdown of the Notch signalling transcription factor *Su(H)*, the fish homologue of *Rbp-J*, causes downregulation of *cyp26a1* within the tailbud, leading to altered RA levels and defects in somitogenesis. These findings demonstrate a close link between Notch signalling and the control of RA metabolism (Echeverri and Oates, 2007).

Together, these reports and preliminary expression analysis of RA-regulating genes provide intriguing evidence that both *Tbx1* and *Hes1* regulate RA levels. Disruption of RA homeostasis could be a common mechanism through which pharyngeal and heart defects occur in $Tbx1^{-/-}$ and $Hes1^{-/-}$ mouse mutants.

5.3.5 A stochastic model for *Hes1* haploinsufficiency

The presence of the same range of pharyngeal arch artery defects in both *Hes1* heterozygotes and homozygotes at E10.5 implies that haploinsufficiency of *Hes1* is sufficient to cause pharyngeal defects and that this phenotype represents an autosomal dominant defect with incomplete penetrance. However, later in development only $Hes1^{-/-}$ mice exhibit pharyngeal arch artery malformations, suggesting that $Hes1^{+/-}$ mutants recover from the earlier defects. The effect of genetic modifiers and functional redundancy among related Hes/Hey proteins may go some way to explaining the penetrance and recovery from these defects during development. However, if the phenotype is truly dominant, these factors cannot fully account for why $Hes1^{+/-}$ mice are able to recover during development while $Hes1^{-/-}$ mutants cannot.

Haploinsufficiency is often defined as a reduction in gene dosage to approximately 50% of normal levels which is insufficient for normal function. Another mechanism by which haploinsufficiency could lead to an abnormal phenotype is through disruption to stochastic gene expression. In this model, a gene can exist in an active or inactive state due to cellular noise which affects the initiation of transcription (Kaern et al., 2005). This stochastic nature of gene expression means that gene products fluctuate around a mean level and copy number influences the probability of gene expression (Figure 5.11) (Cook et al., 1998). If one copy of a gene is mutated, the mean level of product decreases by 50% but also fluctuates below this level, meaning that it could transiently

act like a null allele (Cook et al., 1998). If a threshold level of transcription factor was required for activation of downstream targets and an "all or nothing" phenotype, haploinsufficiency could be explained in this model by the transient fluctuations of transcription factor below this threshold point leading to failure to regulate downstream targets and a subsequent phenotype (Figure 5.11) (Cook et al., 1998; Karmakar and Bose, 2006). This model may explain the presence of pharyngeal arch artery defects in *Hes1*$^{+/-}$ mice at E10.5. However, throughout development in *Hes1*$^{+/-}$ heterozygotes, the stochastic expression of the remaining *Hes1* allele may lead to sufficient activation of downstream pathways which could overcome the arch artery defect. In *Hes1*$^{-/-}$ mutants, this "rescue" could not occur although genetic modifiers and functionally redundant proteins could influence the phenotype. The finding that *Hes1* expression exhibits oscillatory behaviour in multiple cell types (Hirata et al., 2002; Kageyama et al., 2007; Yoshiura et al., 2007) lends strong support to a stochastic model of *Hes1* expression in which downregulation of *Hes1* decreases the probability of gene expression.

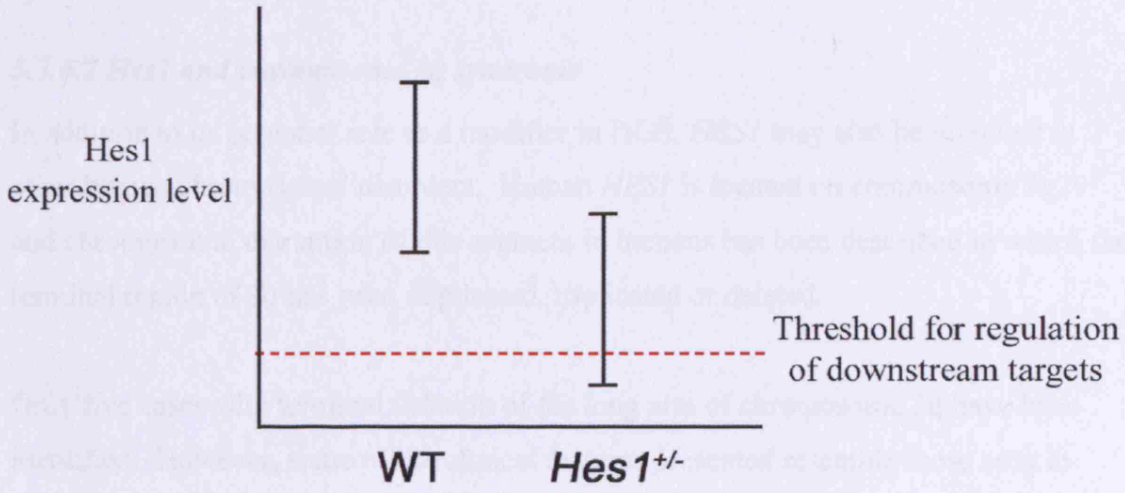

Figure 5.11 A stochastic model for *Hes1* expression in pharyngeal arch artery development
In wild type (WT) mice containing two copies of *Hes1*, the levels of Hes1 fluctuate due to stochastic gene expression but are always sufficient to maintain regulation of downstream targets. In *Hes1*$^{+/-}$ mutants, the mean levels of Hes1 decrease and sometimes fall below the threshold required to regulate downstream genes, resulting in pharyngeal arch artery defects.

5.3.6 *Hes1* and human disorders

5.3.6.1 Hes1 and DiGeorge Syndrome

Analysis of *Hes1*$^{-/-}$ mice has highlighted the importance of this gene in many aspects of development including brain, sensory organ, gut, cardiovascular and craniofacial development. *Hes1* is downregulated in *Tbx1*$^{-/-}$ embryos and *Hes1*$^{-/-}$ mutant mice exhibit all of the major features of DGS, including cleft palate, thymic hypo/aplasia and cardiovascular malformations involving the great vessels and outflow tract. An epistatic interaction between *Tbx1* and *Hes1* has yet to be described in development of these structures. However, the range of DGS-like defects in the *Hes1*$^{-/-}$ mouse, in addition to the haploinsufficient pharyngeal arch artery phenotype and the role for *Hes1* in development of many other organs, suggests that *HES1* represents a candidate modifying locus for DGS, not only in the expressivity of pharyngeal-derived defects, but also in the penetrance of less frequent DGS defects in organs such as the brain, eye and kidney.

5.3.6.2 Hes1 and chromosome 3q syndrome

In addition to its potential role as a modifier in DGS, *HES1* may also be involved in other human chromosomal disorders. Human *HES1* is located on chromosome 3q29 and chromosomal disruption of this segment in humans has been described in which the terminal region of 3q has been duplicated, triplicated or deleted.

Only five cases with terminal deletion of the long arm of chromosome 3q have been identified. However, some of the clinical features presented resemble those seen in *Hes1*$^{-/-}$ mutant mice (Alvarez Arratia et al., 1984; Brueton et al., 1989; Chitayat et al., 1996; Jokiaho et al., 1989; Sargent et al., 1985). Cardiovascular defects, micro or anopthalmia (small or absent eyes), microcephaly and small kidneys, similar to the malformations present in *Hes1*$^{-/-}$ mutants have been described for these patients suggesting that haploinsufficiency of *HES1* could be an underlying cause of these symptoms.

Duplication of chromosome 3q syndrome (Dup(3q)) is associated mainly with craniofacial defects, microcephaly, ear malformations, hand and feet anomalies, genitourinary defects, growth retardation and cardiovascular abnormalities (Aqua et al.,

1995; Faas et al., 2002; Rizzu et al., 1997; Steinbach et al., 1981). Patients with trisomy of chromosome 3q also exhibit similar clinical features (Ounap et al., 2005). Considering that precise levels of *Hes1* may be required to control such processes as proliferation, differentiation and determination of cell fate, disruption of *HES1* levels either through up or downregulation, could hypothetically lead to developmental defects in humans. An increase in *HES1* levels may be responsible for, or contribute to, some of the clinical features seen in patients with duplication and triplication of chromsome 3q such as the brain, heart and genitourinary defects which derive from structures in which *Hes1* is expressed and has been shown to play a role during development (Chen and Al-Awqati, 2005; Ishibashi et al., 1995; Iso et al., 2003; Piscione et al., 2004). It is possible that increased copies of *HES1* could affect development through aberrant increases in overall levels, or possibly by acting in a dominant negative fashion whereby increased amounts of HES1 could titrate other interacting partners.

5.4 FUTURE DIRECTIONS

5.4.1 Is *Hes1* a direct or indirect target of *Tbx1*?

Downregulation of *Hes1* within *Tbx1* expression domains in the pharyngeal apparatus and the similar range of DGS-like defects exhibited by *Hes1*$^{-/-}$ mutants suggests that *Hes1* represents an excellent potential target of *Tbx1*. However, the molecular basis of *Hes1* regulation by *Tbx1* remains to be elucidated. In order to determine if *Hes1* is a primary *Tbx1* target, similar experiments could be carried out to those suggested for other potential *Tbx1* targets (see chapter 7). These include bioinformatic analyses to identify potential *Tbx1* binding sites within regulatory regions of *Hes1* with subsequent testing by transient transfection experiments to determine if *Tbx1* can bind to these sites and induce expression. Gel shift assays could also be undertaken to analyse binding of *Tbx1*, *in vitro* or *in vivo*. Finally, ChIP experiments using a Tbx1 antibody could be analysed to find out if any DNA sequences isolated represent potential *Tbx1* binding sites contained within the regulatory regions of the *Hes1* gene.

Hes1 has been primarily described as an effector of Notch signalling, but there is evidence to suggest that *Hes1* may also act independently of the Notch pathway; its expression can still be detected in *Rbp-J* null mice and in cultured cells without addition of Rbp-J (de la Pompa et al., 1997; Iso et al., 2003). Recent studies have demonstrated that Shh, Vegf , Jnk and Ras signalling can directly regulate *Hes1* to control cell proliferation, providing strong support for a non-canonical role for *Hes1* in development (Curry et al., 2006; de la Pompa et al., 1997; Hashimoto et al., 2006; Ingram et al., 2007; Stockhausen et al., 2005). Furthermore, *Tbx* transcription factors have been shown to regulate members of the *Hes*-related family. *Tbx5* regulates expression of *Hey2* in the heart (Mori et al., 2006; Plageman and Yutzey, 2006) and *Tbx2* represses *Hey1* and *Hey2* expression independent of Notch signalling, in patterning of the atrioventricular canal (Rutenberg et al., 2006). These results suggest that a conserved regulatory pathway may exist between T-box transcription factors and members of the *Hes* family.

It is also possible that instead of, or in addition to, direct regulation of *Hes1* by *Tbx1*, *Hes1* expression could be controlled indirectly through the Notch signalling pathway. This mechanism of regulation is supported by the identification of *Notch3* as a potential *Tbx1* target in the microarray comparing *Tbx1* null cells to *Tbx1* heterozygous cells.

Notch3 is expressed in areas overlapping with *Hes1* during development such as the pharyngeal endoderm, thymus, central nervous system, kidney and lung (Chen and Al-Awqati, 2005; Felli et al., 1999; Lardelli et al., 1994; Sasai et al., 1992; Tomita et al., 1999). *In vitro* experiments have indicated that *Hes1* is most sensitive to Notch3 activation (Shimizu et al., 2002). However, *Notch3*$^{-/-}$ mice do not exhibit any gross abnormalities during development (Krebs et al., 2003) and adult mice present with small thymic lobes and defects in vascular smooth muscle cell maturation (Domenga et al., 2004; Kitamoto et al., 2005). Transgenic mice expressing a mutant form of *Notch3* exhibit vascular dysfunction and develop vascular lesions characteristic of CADASIL (cerebral autosomal dominant arteriopathy with subcortical infarcts and leukoencephalopathy), a type of adult-onset vascular dementia (Dubroca et al., 2005; Ruchoux et al., 2003).

Notch1, *-2* and *-4* are co-expressed with *Notch3* in many domains and may function redundantly. This could explain the lack of defects in *Notch3*$^{-/-}$ mice (Kitamoto et al., 2005). Proper characterisation of the role of *Notch3* in development will require *Notch3*$^{-/-}$ mice to be crossed with conditional knockouts of *Notch1*,- *2* and *-4*.

5.4.2 What are the tissue and time-specific requirements for *Hes1* in pharyngeal development?

Hes1 is expressed in multiple overlapping domains with *Tbx1* within the pharyngeal endoderm and splanchnic mesoderm, but it is also expressed within the pharyngeal mesenchyme in areas which appear to be neural crest-derived. In *Tbx1*$^{-/-}$ embryos, expression of *Hes1* within all of these domains was found to be downregulated and analysis of the *Hes1* knockout mouse has demonstrated the importance of this gene in development of pharyngeal-derived structures similar to *Tbx1*. It remains unclear what role *Hes1* plays within each tissue in pharyngeal and heart development. Conditional deletion experiments should clarify whether downregulation of *Hes1* in *Tbx1*-expressing tissues is sufficient to cause the pharyngeal defects observed in *Hes1*$^{-/-}$ mice or whether loss of *Hes1* function in NC cells is the primary cause of *Hes1*$^{-/-}$ malformations. It is possible that ablation of *Hes1* in different tissues may lead to the same range of defects as seen for *Tbx1* (Arnold et al., 2006b; Zhang et al., 2006). If this is the case then restoration of *Hes1* function in specific tissues on a *Hes1*$^{-/-}$ or *Tbx1*$^{-/-}$ background should clarify the cell-autonomous functions of *Hes1* in development.

In addition, generating compound *Hes1* and *Hey* gene mouse mutants should address the issue of functional redundancy. To better define the role of Notch signalling in cardiovascular and pharyngeal development downstream of *Tbx1*, tissue and time-specific ablation experiments should be carried out to knockdown Notch signalling within all *Tbx1* domains and specific pharyngeal tissues such as the endoderm and SHF. This could be achieved by crossing tissue-specific and tamoxifen-inducible Cre lines with *DNMAML/+* mice to downregulate Notch signalling. Combined with results obtained from conditional knockouts of *Hes1*, these experiments should lead to a clearer understanding of how *Tbx1* and *Notch/Hes1* signalling may interact in pharyngeal and heart development.

CHAPTER 6. ANALYSIS OF DGS PATIENTS WITH ATYPICAL CHROMOSOME REARRANGEMENTS

6.1 INTRODUCTION

DGS is a clinically heterogeneous syndrome associated with over 180 symptoms however the characteristic features involve craniofacial, cardiovascular, thyroid and thymic anomalies, defects in structures which derive from the pharyngeal apparatus (Robin and Shprintzen, 2005). Most DGS patients have the same 3Mb heterozygous deletion of chromosome 22q11 or a smaller, nested 1.5Mb deletion, both of which include *TBX1*. Mouse models and mutation searches have since identified haploinsufficiency of *TBX1* to be one major determinant of the clinical phenotype (Jerome and Papaioannou, 2001; Lindsay et al., 2001; Merscher et al., 2001; Yagi et al., 2003). However, there are several DGS patients with atypical deletions or translocations within and outside of the common 3Mb region that do not disrupt *TBX1* (Amati et al., 1999; Rauch et al., 1999; Rauch et al., 2005; Saitta et al., 1999; Weksberg et al., 2006; Wieser et al., 2005). Studies have shown that the severity and penetrance of the symptoms in DGS varies greatly among patients and does not correlate with the size or position of the deletion (Sullivan, 2004) suggesting that multiple genes within chromosome 22q11 may contribute to similar phenotypes. Mouse mutants of other genes within the commonly deleted 3Mb region such as *Crkl,* (Guris et al., 2006; Guris et al., 2001; Moon et al., 2006) and on other chromosomes such as *Fgf8* and *Vegf* (Abu-Issa et al., 2002; Frank et al., 2002; Stalmans et al., 2003; Vitelli et al., 2002b) have been shown to exhibit DGS-like defects in pharyngeal and heart development. In order to identify additional genes which may contribute to the DGS phenotype, DGS patients with atypical chromosome rearrangements were analysed.

FY1198 was one such DGS patient who was negative for the common deletion but exhibited features reminiscent of the disorder. FY1198 presented with pulmonary stenosis and an atrial septal defect and also exhibited other developmental abnormalities including primary hypothyroidism, cleft palate, small stature, delayed menarche, bilateral fifth finger clinodactyly, toe webbing, neck webbing, beaked nose, low columella, bilateral ptosis and learning difficulties. It was discovered that this patient had an apparently balanced t(11;22)(q23.3;q11.2) translocation. The parents and sister of FY1198 also carried the translocation but did not exhibit any obvious phenotype.

Subsequent investigation of the Mendelian Cytogenetics Network Database (MCDB) (http://www.mcndb.org/) identified another patient with a t(11;22) translocation, FN who exhibited a partial atrioventricular canal defect,

. The mother of FN also carried the translocation and had the same heart malformation.

The t(11;22) translocation is the most common non-Robertsonian translocation to occur in humans. Carriers of this balanced translocation are phenotypically normal. However, their offspring are at risk of having der(22) syndrome due to 3:1 meiotic non-disjunction events (Fraccaro et al., 1980; Zackai and Emanuel, 1980). The breakpoints on chromosome 11 and 22 in t(11;22) translocation carriers have been well characterised and occur within a low copy repeat, LCR-B on chromosome 22 and within markers, D11S1340 and APOC3 on chromosome 11 (Edelmann et al., 2001a; Edelmann et al., 1999c; Funke et al., 1999).

The aim of this study was to determine where the t(11;22) breakpoints occurred in patients FN and FY1198, whether the breakpoints were the same between the two patients, and whether the breakpoint locations were identical to the common t(11;22) translocation. If the translocation breakpoints in FY1198 and FN were different to the recurrent t(11;22) translocation, this would strongly suggest that the new breakpoint disrupts a gene important in heart development. Therefore, FISH analysis was undertaken to map the translocation breakpoints and determine which gene(s) may be disrupted and cause the developmental defects.

6.2 RESULTS

6.2.1 Mapping the chromosome 22 translocation breakpoint

YPEL1 is a gene which localises to human chromosome 22q11 and was identified as part of a screen for genes involved in craniofacial development (Farlie et al., 2001) Mouse *Ypel1* is expressed in the branchial arches and heart (Farlie et al., 2001) and was therefore considered to be a potential candidate gene for the defects seen in these patients. BACs were obtained surrounding this 22q11 region, fluorescently labelled and hybridised to metaphase spreads of the patients' and control cell lines. BACs containing the *YPEL1* gene, RP11- 47L18 and RP11-794K20 did not appear to hybridise over the breakpoint and the probe signal was located only on chromosome 22 and the derivative chromosome 11. Subsequently, BAC probes were chosen which localised to more centromeric regions. BACs, CTD-2295P14 and CTD-2589K18 hybridised over the breakpoint in both the FY1198 and FN cell line (Figure 6.1C, D). CTD2589K18 appeared to hybridise more strongly on the derivative chromosome 22 whereas the CTD2295P14 signal was stronger on the derivative chromosome 11 suggesting that the breakpoint on chromosome 22 occurred closer to the *LOC440804* gene as mapped by Ensembl (Figure 6.2).

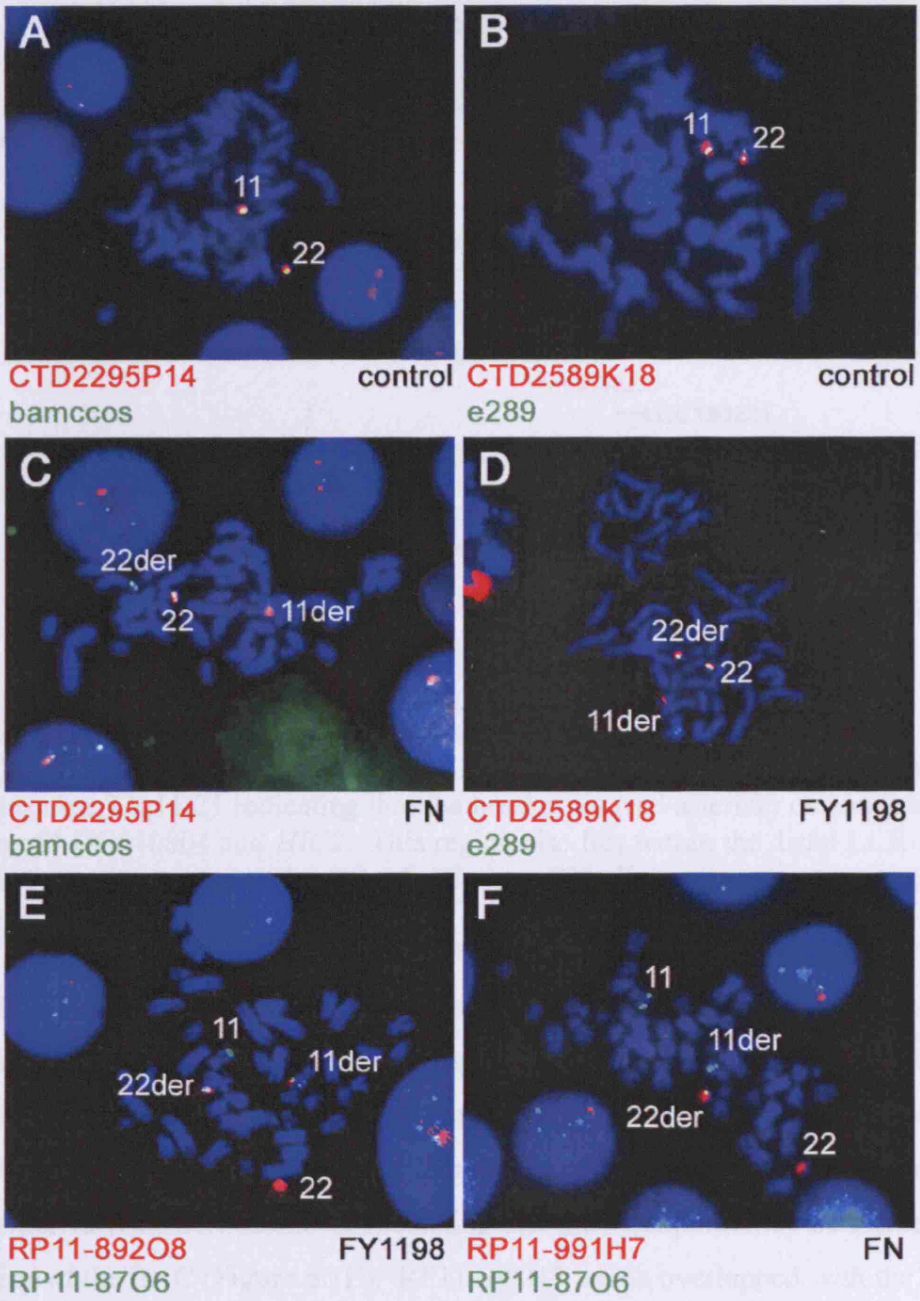

Figure 6.1 FISH mapping studies of the chromosome 22 breakpoint
(**A,B**) In control patients' cell lines, BACs CTD2295P14 and CTD2589K18 hybridised only to chromosome 22 along with the chromosome 22 control probes, bamccos and e289. (**C, D**) In both FY1198 and FN patients' cell line, these BACs hybridised over the breakpoint on chromosome 22 giving a signal on chromosome 22, 22-derivative and 11-derivative. (**E**) BAC, RP11-892O8 also hybridised over the chromosome 22 breakpoint. (**F**) RP11-991H7 was centromeric to the breakpoint giving a signal only on chromosome 22 and 22-derivative. (**E, F**) Control probe RP11-87O6 hybridised over the chromosome 11 breakpoint giving a signal on chromosome 11, 11-derivative and 22-derivative.

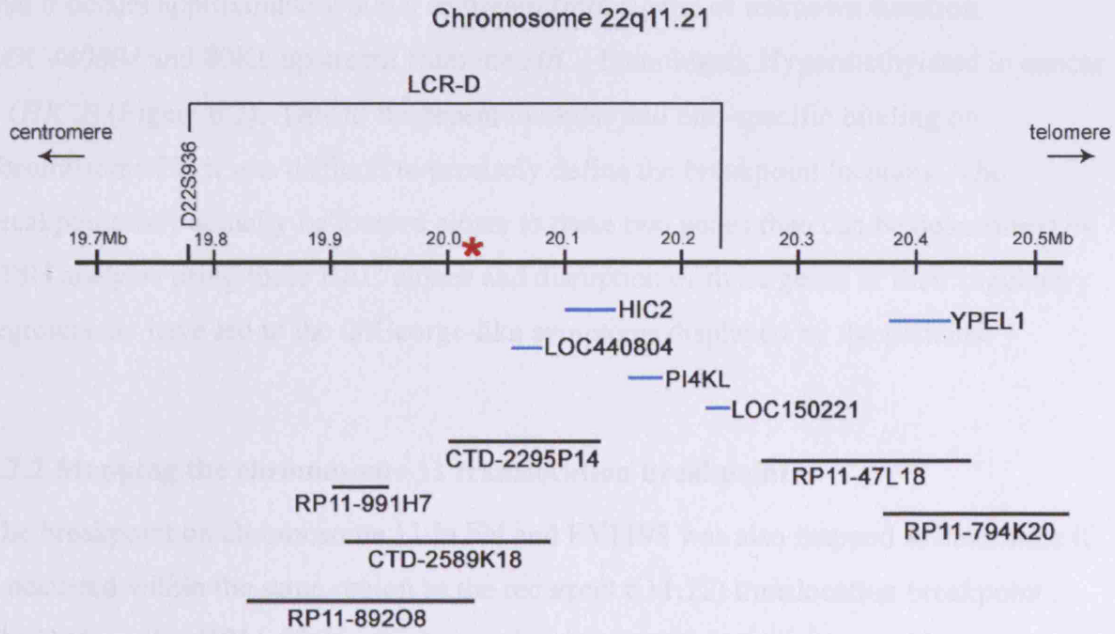

Figure 6.2 Mapping the chromosome 22 breakpoint in FY1198 and FN
BACs CTD-2295P14, CTD-2589K18 and RP11-892O8 hybridised over the breakpoint on chromosome 22q11.21 indicating that the breakpoint (red asterisk) occurs just upstream of LOC440804 and *HIC2*. This region also lies within the distal LCR-D which mediates the common 3Mb 22q11 deletion. Blue lines represent genes and black lines represent BAC clones.

Further BACs were chosen to investigate more centromeric regions and confirm that the breakpoint did indeed disrupt the region located within BACs CTD-2295P14 and CTD-2589K18. RP11-892O8 which overlapped with CTD-2589K18 and the 5' end of CTD-2295P14 hybridised over the breakpoint in both patients but only gave a very faint signal on derivative chromosome 11 indicating that the breakpoint may be located at the more 3'end of the BAC (Figure 6.1E). RP11-991H7 which overlapped with the 5' end of RP11-892O8 did not appear to hybridise over the breakpoint in either patient, only giving a signal on chromosome 22 and derivative chromosome 22 (Figure 6.1F). However, both of these BACs, RP11-892O8 and RP11-991H7 also often seemed to bind non-specifically to the metaphase spreads. LCRs are regions of high sequence homology which are present in multiple sites on chromosome 22 and which mediate aberrant recombination events (Edelmann et al., 1999a; Edelmann et al., 1999b). The breakpoint in these patients appears to occur within LCR-D which mediates the typical 3Mb deletion which may explain the non-specific binding. The chromosome 22 control probe, bamccos also hybridises to these repeat elements which is why it sometimes appeared to bind to the derivative chromosome 11 (containing part of chromosome 22). The location of the breakpoint as characterised by the above FISH experiments revealed

that it occurs approximately 60Kb upstream from a gene of unknown function, *LOC440804* and 80Kb upstream from the *HIC1* homologue, Hypermethylated in cancer 2 (*HIC2*) (Figure 6.2). Due to the repeat modules and non-specific binding on chromosome 22, it was difficult to precisely define the breakpoint location. The breakpoint may actually be located closer to these two genes than can be determined by FISH analysis using these BAC clones and disruption of these genes or their regulatory regions may have led to the DiGeorge-like symptoms displayed by the patients.

6.2.2 Mapping the chromosome 11 translocation breakpoint

The breakpoint on chromosome 11 in FN and FY1198 was also mapped to determine if it occurred within the same region as the recurrent t(11;22) translocation breakpoint.. The BAC probe, RP11-87O6 which contains the recurrent, chromosome 11 translocation breakpoint region, also hybridised over the breakpoint in the patients' cell lines (Figure 6.3A). BAC RP11-4N9 was telomeric to the breakpoint (Figure 6.3B) demonstrating that the translocation breakpoint in patients FN and FY1198 was identical or at least very similar to the constitutional t(11;22) translocation breakpoint. It is therefore unlikely that genes contained within this region are responsible for the patients' phenotype since carriers of this translocation are phenotypically normal. However, the genes which could have been directly disrupted include NP_116114.1, *ZNF259, APOA4* and *APOA5*. Alternatively, the regulatory regions of genes *APOC3*, *APOA1* and NP_079440.2 may have been affected (Figure 6.4).

Therefore, in comparison to the common t(11;22) translocation, the chromosome 11 breakpoint in patients FN and FY1198 was similar however, the chromosome 22 breakpoint occurred in a different region.

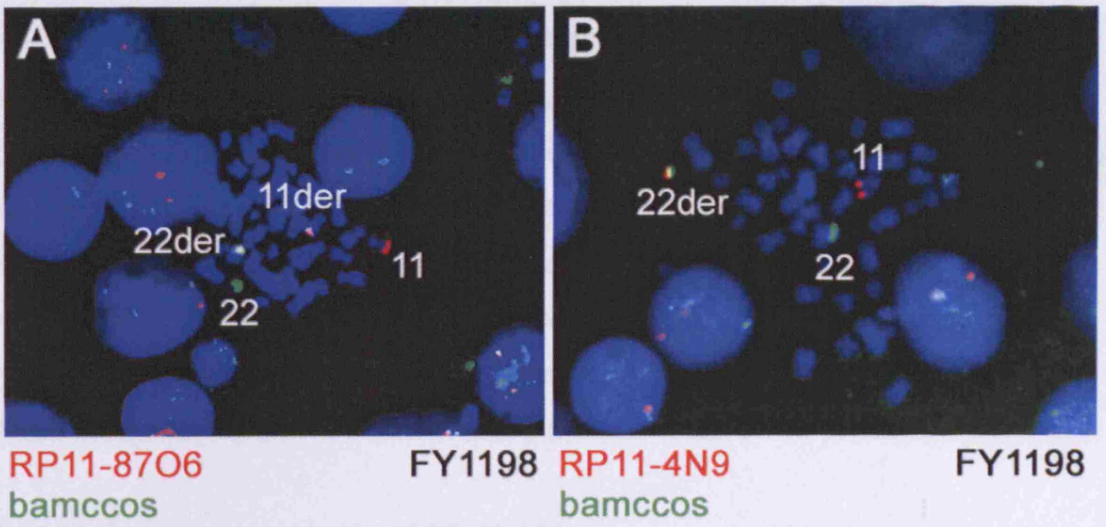

Figure 6.3 FISH mapping studies of the chromosome 11 breakpoint
(**A**)The chromosome 11 BAC, RP11-87O6 (red) localises over the breakpoint, hybridising on chromosome 11, 11-derivative and 22-derivative whereas the chromosome 22 control probe, bamccos (green) hybridises to chromosome 22, 22-derivative and also to chromosome 11-derivative. (**B**) RP11-4N9 (red) is telomeric to the breakpoint hybridising to chromosome 11 and chromosome 22-derivative and the chromosome 22 control probe, bamccos (green) hybridises to chromosome 22 and 22-derivative.

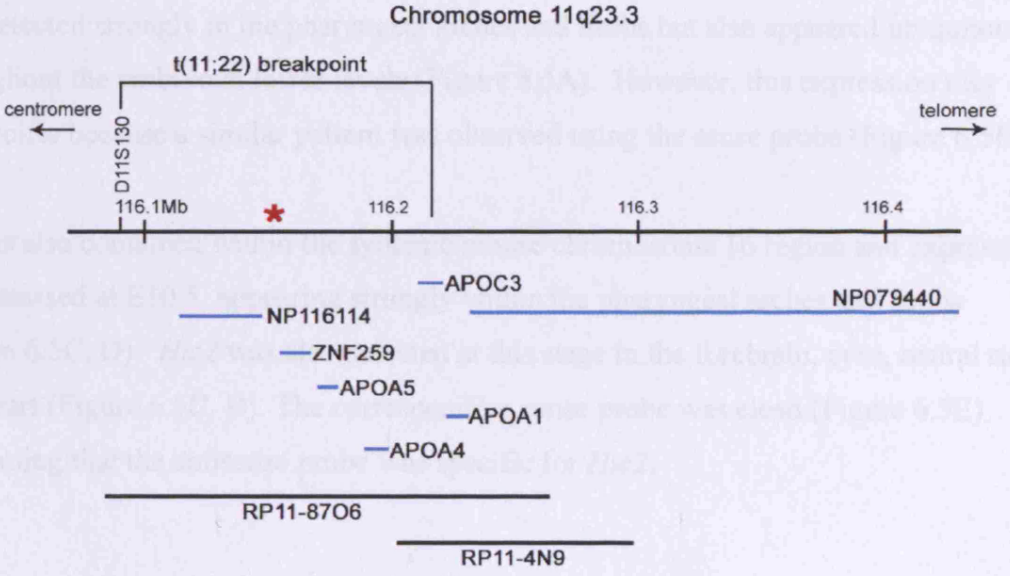

Figure 6.4 Mapping the chromosome 11 breakpoint in FY1198 and FN
BAC RP11-87O6 hybridises over the breakpoint on chromosome 11q23 whereas RP11-4N9 is telomeric to the breakpoint. This breakpoint region (red asterisk) corresponds to the location of the constitutional t(11;22) non-Robertsonian translocation breakpoint which occurs between markers D11S1340 and *APOC3*. The genes which map around this breakpoint are shown in blue.

6.2.3 Analysis of *Gm603* and *Hic2* expression patterns

The genes potentially disrupted on chromosome 22 were investigated further because this region is associated with DGS patients who have atypical 22q11 deletions (Amati et al., 1999; Rauch et al., 1999; Rauch et al., 2005; Saitta et al., 1999; Weksberg et al., 2006; Wieser et al., 2005). The human genes, *LOC440804* and *HIC2* occurred closest to the breakpoint and expression of their mouse homologues, *Gm603* and *Hic2*, respectively were analysed during development to determine whether either gene may be a candidate for the heart defects occurring in the translocation patients.

Gm603, the mouse homologue of *LOC440804* is contained within the syntenic region of mouse chromosome 16 and Ensembl revealed that *Gm603* was also the homologue of *LOC150221* which appears to be a copy of *LOC440804*. *LOC150221* occurs 160Kb telomeric to *LOC440804* (Figure 6.2) and these genes share 99% amino acid identity. They are contained within LCR-D on chromosome 22 and represent replicated genes or pseudogenes which occur in many regions of chromosome 22q11 (Collins et al., 1997; Edelmann et al., 1999a; Edelmann et al., 1999b; Edelmann et al., 2001b; Heisterkamp and Groffen, 1988; Shaikh et al., 2000). *Gm603* expression was analysed at E9.5 and was detected strongly in the pharyngeal arches and limbs but also appeared ubiquitously throughout the embryo at lower levels (Figure 6.5A). However, this expression may not be specific because a similar pattern was observed using the sense probe (Figure 6.5B).

Hic2 is also contained within the syntenic mouse chromosome 16 region and expression was assessed at E10.5, appearing strongly within the pharyngeal arches and limbs (Figure 6.5C, D). *Hic2* was also detected at this stage in the forebrain, eyes, neural tube and heart (Figure 6.5C, D). The corresponding sense probe was clean (Figure 6.5E) confirming that the antisense probe was specific for *Hic2*.

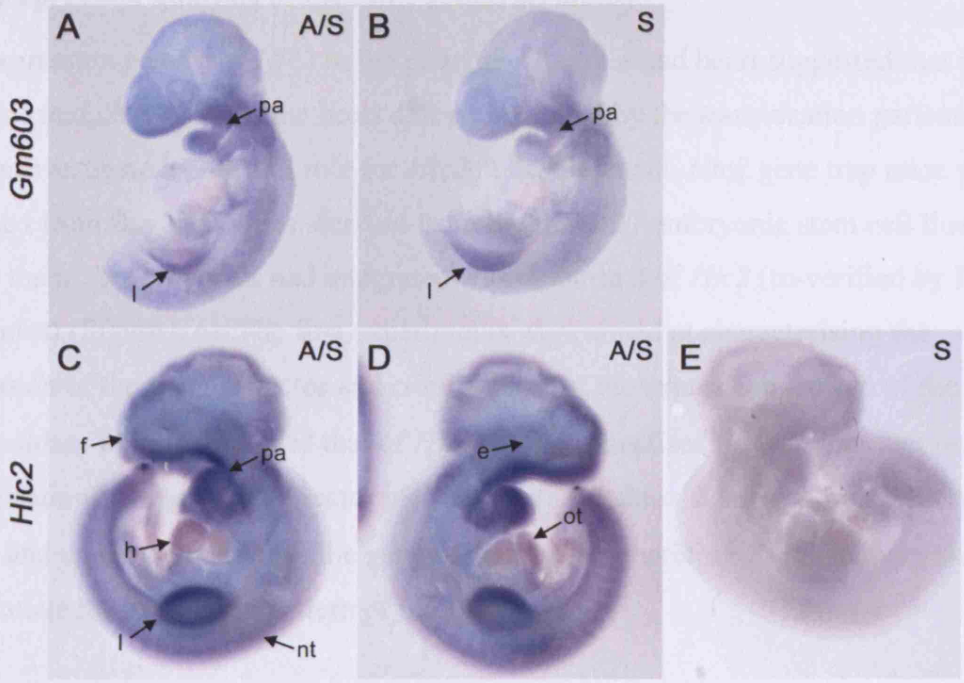

Figure 6.5 Whole mount *in situ* hybridisation of *Gm603* and *Hic2*
Gm603 expression at E9.5 (**A**) and the negative control sense probe (**B**). Hic2 expression at E10.5 (**C, D**) and the negative control sense probe (**E**). Abbreviations: e, eye; f, forebrain; h, heart; l, limb; pa, pharyngeal arches; nt, neural tube; ot, outflow tract.

6.2.4 Expression analysis of the *Hic2* genetrap mouse

The expression pattern of *Hic2* in the pharyngeal arches and heart suggested that it was the best candidate gene for the heart defects exhibited by the translocation patients. To further investigate a potential role for *Hic2* in development, *Hic2* gene trap mice were obtained from Bay Genomics, derived from the RRN127 embryonic stem cell line in which the pGT0Lxf vector had integrated within intron 2 of *Hic2* (re-verified by Bay Genomics) (Figure 6.6). The first experiments were aimed at characterising the expression of the trapped vector and confirming that the expression pattern of the β-galactosidase reporter matched that of *Hic2* mRNA visualised by whole mount *in situ* hybridisation. The gene trap vector incorporates a β-galactosidase reporter within an intron and under the control of the gene of interest and therefore X-gal staining should recapitulate the expression pattern of the gene.

Figure 6.6 The *Hic2* gene trap allele
The pGT0lxf gene trap vector integrated within intron 2 of *Hic2*. The unfilled boxes represent the 5' and 3' untranslated regions and the filled boxes represent the coding exons of *Hic2*. The blue arrow represents a loxP site, the green arrow, Lox71 and the red arrow, a FRT site. Abbreviations: En2 intr1, mouse *En2* intron 1; SA, splice acceptor of mouse *En2* exon 2; β-geo, fusion of β-galactosidase and neomycin transferase; pA, SV40 polyadenylation signal. Modified from http://www.sanger.ac.uk/PostGenomics/genetrap/vectors/pGT0lxf-500.png.

X-gal staining of *Hic2*$^{+/RRN127}$ heterozygous embryos (hereafter referred to as *Hic2*$^{+/GT}$) collected at multiple stages throughout development demonstrated that at the earliest stages examined, the *Hic2* genetrap allele was primarily expressed in extra-embryonic tissues. At E7.0, *Hic2* was expressed within the posterior amniotic fold and extraembryonic ectoderm. *Hic2* was also detected in the extraembryonic mesoderm and visceral endoderm and contiguous portions of the embryonic mesoderm and endoderm (Figure 6.7A, I). At E7.5, staining was observed in the chorionic ectoderm, yolk sac mesoderm, amnion, visceral endoderm and allantois, all extraembryonic tissues (Figure 6.7B, J). *Hic2* was not detected at this stage within the cardiac crescent but slightly later at E7.75 just prior to formation of the linear heart tube, *Hic2* began to be expressed in the more anterior regions of the cardiac crescent and was also expressed in the adjoining mesoderm just medial to the cardiac crescent which comprises part of the second heart field (Figure 6.7C, K). In addition, *Hic2* was detected in the developing neural tube. At E8.0, *Hic2* was expressed in the myocardium of the linear heart tube and also in the second heart field mesoderm just dorsal to the heart. *Hic2* was also detected in the pericardial mesothelium at this stage and also in the head folds (Figure 6.7E, L). At E8.5, the looping stage of heart development, *Hic2* was expressed throughout the myocardium in the proximal outflow tract and developing ventricles and atria and continued to be expressed in the neural tube and forebrain (Figure 6.7F, M). Later, at E10.5, *Hic2* was observed in the myocardium of both ventricles and atria, including the ventricular trabeculae and was still present in the proximal outflow tract (Figure 6.7G, N). *Hic2* continued to be expressed in the heart until E12.5, the last stage examined (Figure 6.7H).

At E10.5, *Hic2* was also present in other embryonic tissues throughout the body. Expression was observed in the pharyngeal arches, limb buds, forebrain, eyes and neural tube (Figure 6.7G, O, R). In addition, *Hic2* was expressed in the midgut, foregut and developing lungs (Figure 6.7P, Q). The expression pattern of the gene trap allele at this stage of development matched the expression pattern of *Hic2* mRNA confirming that the gene trap recapitulated endogenous *Hic2* expression. The only differences apparent between the gene trap allele and *Hic2* mRNA concerned the levels of expression in certain tissues, namely the heart, pharyngeal arches and limbs. The *Hic2* β-geo reporter appeared to be expressed at a higher level in the heart than *Hic2* mRNA whereas *Hic2* mRNA was stronger in the pharyngeal arches and limbs than the *Hic2* gene trap allele.

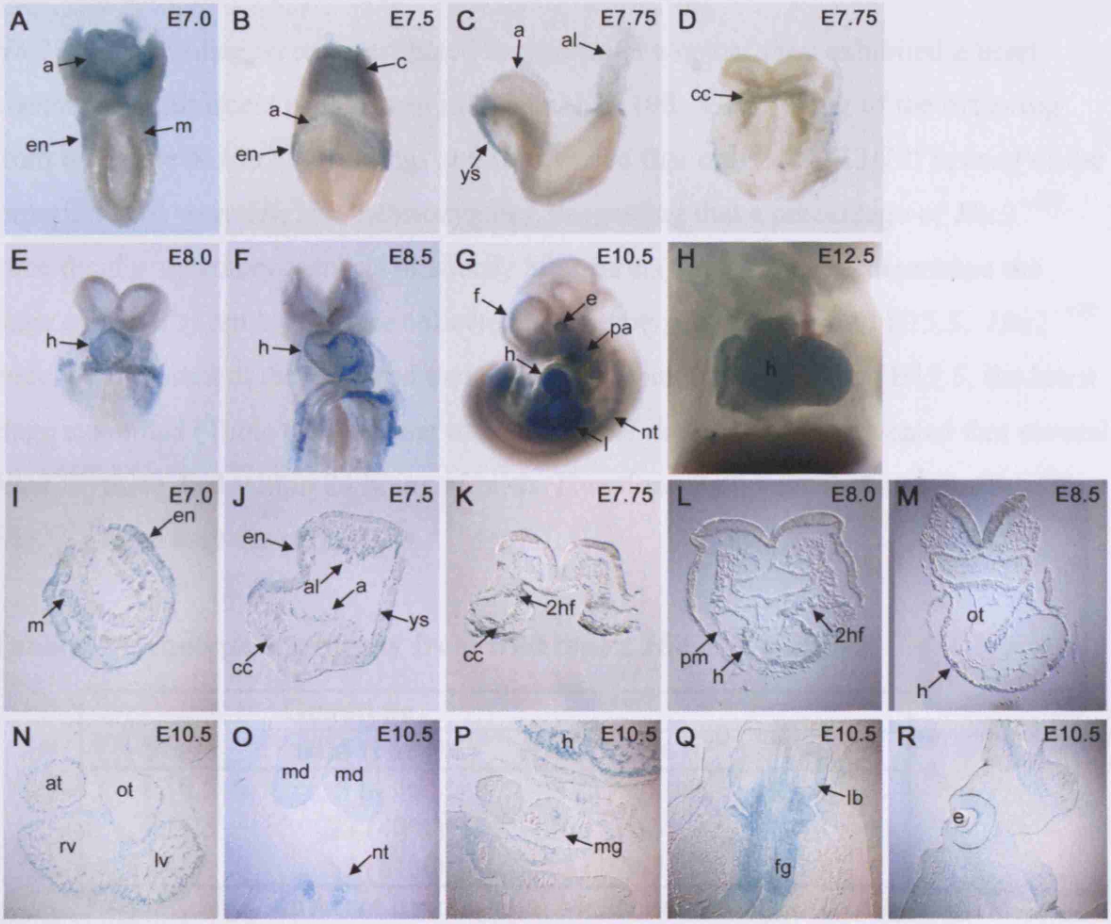

Figure 6.7 Expression of the *Hic2* gene trap by X-gal staining at a range of gestational ages

(**A-H**) Whole embryos. (**I-R**) Transverse sections. Abbreviations: 2hf, second heart field; a, amnion; al, allantois; at; atria; c, chorion; cc, cardiac crescent; e, eye; en, endoderm; f, forebrain; fg, foregut; h, heart; l, limb; lb, lung buds; lv, left ventricle; m, mesoderm; md, mandible; mg, midgut; nt, neural tube; ot, outflow tract; pa, pharyngeal arches; rv, right ventricle; ys, yolk sac.

6.2.5 Analysis of the phenotype of *Hic2* genetrap mice

Hic2 gene trap mice were investigated to determine whether they exhibited a heart phenotype reminiscent of that seen in FN and FY1198. Genotyping of the offspring from wild type X $Hic2^{+/GT}$ matings at P10 revealed that only 19% (13/70) instead of the expected 50% were $Hic2^{+/GT}$ heterozygotes, suggesting that a percentage of $Hic2^{+/GT}$ mice die during embryogenesis or shortly after birth (Table 6.1). To determine the stage of lethality, embryos were collected and genotyped at E10.5 and E15.5. $Hic2^{+/GT}$ mice were present at the expected mendelian ratios until and including E15.5, the latest stage examined (Table 6.1). Closer examination of newborn litters revealed that several $Hic2^{+/GT}$ mice died within 24 hours of birth. Therefore, it appears that a proportion of $Hic2^{+/GT}$ mice may die perinatally.

Table 6.1 Genotype of progeny from wild type x $Hic2^{+/GT}$ matings

	Genotype		
Stage	**wild type (%)**	**$Hic2^{+/GT}$ (%)**	**Total**
E10.5	6 (43%)	8 (57%)	14
E15.5	23 (47%)	26 (53%)	49
P10*	57 (81%)	13 (19%)	70

*Significantly different from normal Mendelian ratios ($P<0.001$, statistics based on Chi-squared test)

In order to determine the cause of the heterozygous lethality, E14.5 to E15.5 litters were collected from matings between wildtype and $Hic2^{+/GT}$ mice for MRI and histological analysis. Analysis of the $Hic2^{+/GT}$ embryos by MRI revealed that approximately 24% had a ventricular septal defect (n = 8/34) (Figure 6.8D) and transverse histological sections through the hearts of these embryos confirmed the MRI results (Figure 6.8H). Two of these $Hic2^{+/GT}$ embryos also appeared to have an overriding aorta accompanying the VSD (Figure 6.8C, G). No DGS-like arch artery abnormalities were identified in $Hic2^{+/GT}$ heterozygotes nor were any defects in palate formation or thymic development, structures which are affected in DGS and derive from the pharyngeal apparatus. All other organs appeared to be normal. However, there may be subtle morphological or physiological changes which were not detected in this study.

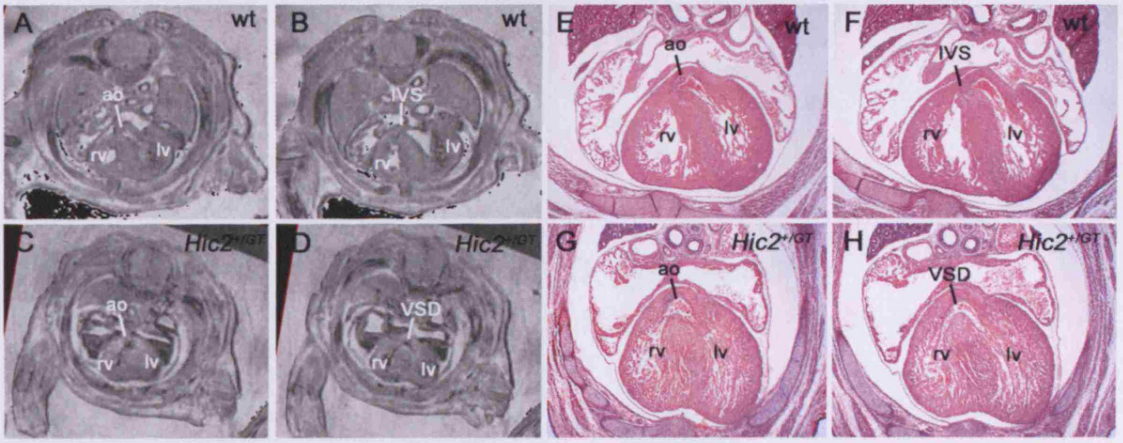

Figure 6.8 Cardiovascular defects in E15.5 *Hic2*$^{+/GT}$ mutant embryos
Transverse, MRI scans (**A-D**) and H and E-stained heart sections (**E-H**) from E15.5 embryos. (**A**, **B**, **E**, **F**) A wild type heart showing the aorta arising from the left ventricle and the interventricular septum separating the left and right ventricles. (**C**, **D**, **G**, **H**) A, *Hic2*$^{+/GT}$ mutant heart with an overriding aorta and a ventricular septal defect. Abbreviations: ao, aorta; ivs, interventricular septum; lv, left ventricle; rv right ventricle; vsd, ventricular septal defect; wt; wild type.

Hic2$^{+/GT}$ heterozygous mating pairs were also set up to determine if homozygous mutant mice would be born in mendelian ratios. Out of 3 pairs of *Hic2*$^{+/GT}$ heterozygous intercrosses set up over 2 -3 months only one litter of two pups were born and survived until weaning. There was evidence that small litters were born (3-4 pups compared to 6-8 pups from wild type C57Bl/6 matings) but it appeared that several pups died within the first 24 hours and the rest of the litter was cannibalized. To determine whether the *Hic2* mutation was embryonically lethal, embryos were collected at midgestation from *Hic2*$^{+/GT}$ intercrosses. Due to difficulty in determining the exact position of the genetrap vector within the intron, it was not possible to distinguish homozygotes from heterozygotes. However, from preliminary analysis of embryos collected at E10.5, some resorptions were noticed. One possible *Hic2*$^{GT/GT}$ embryo was identified by stronger *lacZ* staining, delayed growth compared to wild type embryos, and an enlarged heart that had not turned properly (Figure 6.9B, D). These results suggest that *Hic2*$^{GT/GT}$ homozygotes may die during embryogenesis prior to E10.5. Examination of litters collected from *Hic2*$^{+/GT}$ intercrosses after this stage revealed multiple resorptions, presumably representing *Hic2*$^{GT/GT}$ homozygotes, and providing further evidence suggesting that disruption of *Hic2* is embryonically lethal.

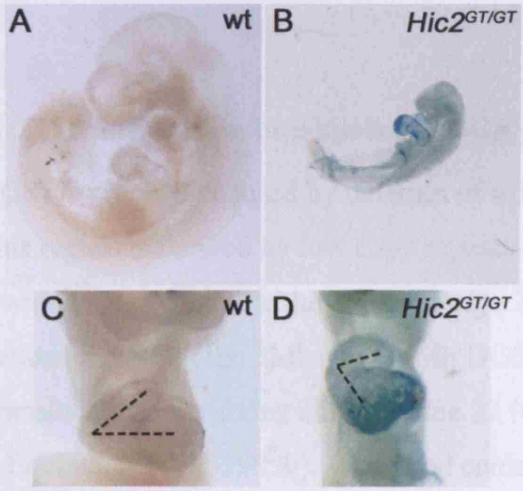

Figure 6.9 A potential *Hic2*$^{GT/GT}$ embryo
(**A**) An E10.5 wild type embryo in comparison to (**B**) a growth-delayed, potential *Hic2*$^{GT/GT}$ embryo. Ventral views of (**C**) a wild type and (**D**) a *Hic2*$^{GT/GT}$ heart which does not appear to have undergone correct looping (compare dashed lines in (**C**) to (**D**).

In conclusion, the analysis of DGS patients with atypical t(11;22) translocations has led to the identification of *HIC2*, a gene potentially disrupted by the breakpoint on chromosome 22. Expression analysis and functional characterisation of *Hic2* gene trap mice has demonstrated a role for *Hic2* in heart development suggesting that mutations in this gene may contribute to the phenotype of DGS patients.

6.3 DISCUSSION

6.3.1 Mapping the t(11;22) translocation breakpoint in DGS patients

DiGeorge syndrome (DGS) is primarily caused by deletion of a 3Mb region of chromosome 22q11. This region is flanked by low copy repeats (LCRs), highly homologous sequences which are common within chromosome 22 and mediate rearrangements and deletions including the 3Mb and 1.5Mb DGS deletion and are also sites of breakpoints in translocations involving chromosome 22 (Carlson et al., 1997; Edelmann et al., 1999a; Edelmann et al., 1999b). The most common 3Mb and 1.5Mb deletions contain *TBX1*, the main candidate gene for DGS however there have been multiple reports of DGS patients who have atypical deletions of chromosome 22 which do not include *TBX1* suggesting that additional genes on chromosome 22q11 may be involved in the aetiology of the disease. *Crkl*, a cell adaptor protein located within the 3Mb, 22q11 deletion has since been shown to also contribute to the pathophysiology of DGS (Guris et al., 2006; Guris et al., 2001; Moon et al., 2006). $Crkl^{-/-}$ mouse mutants have DGS-like craniofacial, heart and glandular defects and $Tbx1^{+/-};Crkl^{+/-}$ compound heterozygotes exhibit aortic arch, thymic and parathyroid defects with significantly increased penetrance and expressivity compared to either heterozygote alone demonstrating that *Tbx1* and *Crkl* interact within the same genetic pathway in pharyngeal development (Guris et al., 2006). Haploinsufficiency of *CRKL* may contribute to the development of malformations in some of the DGS patients with atypical deletions but it is not deleted in all atypical deletions of chromosome 22 suggesting that additional 22q11 genes may be involved in heart and/or pharyngeal development.

In order to identify genes on chromosome 22q11 which could play a role in pharyngeal or heart development, DGS patients who exhibited atypical rearrangements of chromosome 22 were investigated. Two such patients presented with an apparently balanced t(11;22)(q23.3;q11.2) translocation and exhibited some features reminiscent of DGS. In particular, both patients had cardiovascular anomalies.

The chromosome 11 breakpoint in these patients occurred in the same location as the breakpoint in phenotypically normal carriers of the constitutional t(11;22) translocation. It is therefore it is unlikely that disruption of any of the genes within or surrounding this region contributed to the heart phenotype observed. In addition, investigation of the

potential function of these genes does not support any role in pharyngeal or heart development. ZNF259 interacts with the SMN protein which when mutated leads to spinal muscular atrophy (Gangwani et al., 2001) and *Znf259*$^{-/-}$ mice exhibit axonal defects (Gangwani et al., 2005). APOA1, APOA5 and APOC3 are involved in lipoprotein metabolism (Lai et al., 2005) and the function of NP_116114.1 and NP_079440.2 is yet to be characterised.

The chromosome 22 breakpoint in FN and FY1198 occurs within LCR-D and distinguishes these patients from carriers of the common t(11;22) translocation. Therefore, the potentially disrupted chromosome 22 genes were characterised in more detail. Disruption of the genes, *LOC440804* and Hypermethylated in cancer 2 (*HIC2*) or their regulatory regions may be the cause of the heart defects presented by these patients. The gene closest to the breakpoint on chromosome 22 was *LOC440804* or *KIAA1666* which is predicted to contain several protein-protein interaction domains including SH3 and fibronectin type III domains. Chromosome 22q11 contains several low copy repeat regions comprised of replicated genes such as *DGCR6*, *BCR* AND *GGT* (Collins et al., 1997; Edelmann et al., 1999a; Edelmann et al., 1999b; Edelmann et al., 2001b; Heisterkamp and Groffen, 1988; Shaikh et al., 2000). *LOC440804* also appears to be a duplicated gene or pseudogene and another copy, named *LOC150221* can be found on chromosome 22. These genes are contained within LCR-D and it is possible that they may participate in mediating aberrant recombination events. There is little information on the expression or function of *LOC440804*. However, RT-PCR analysis has revealed that this gene is detected in fetal tissue and in many adult, human tissues including the heart, brain, lung and testis (http://www.kazusa.or.jp/huge/gfpage/KIAA1666/). Whole mount *in situ* hybridisation of the mouse homologue, *Gm603*, did not reveal a specific expression pattern for this gene. Further analysis using probes against different regions of *Gm603* may yield more information regarding its potential role in development.

HIC2 is located approximately 80Kb telomeric to the chromosome 22 breakpoint and its expression may have been affected by the translocation. To date, there has been little information concerning the expression or function of *HIC2*. RT-PCR analysis has shown that *HIC2* (annotated as KIAA1020) is expressed in fetal tissue and a variety of adult, human tissues including the brain, ovary, testis, liver, lung and heart (http://www.kazusa.or.jp/huge/gfpage/KIAA1020/). The zebrafish orthologue, *hrg22* is

expressed in brain, retina, somite borders, spinal cord, pectoral fin buds and branchial arches during development (Bertrand et al., 2004). The expression of mouse *Hic2* has been characterised through whole mount *in situ* hybridisation and X-gal staining of a *Hic2* gene trap allele. These methods demonstrate an overlapping expression pattern in mouse which is highly reminiscent of the zebrafish *hrg22* expression pattern (Bertrand et al., 2004). While the similar localisation of the *Hic2* ß-geo reporter and *Hic2* mRNA in embryos confirms that the gene trap recapitulates the endogenous *Hic2* expression pattern, levels of expression of *Hic2* were slightly different between the two methods, particularly in the heart, pharyngeal arches and limb buds. Other groups have also reported differences in expression between gene trap alleles and endogenous mRNA (Koshiba-Takeuchi et al., 2006; Pennisi et al., 2007). This may occur due to differences in detection sensitivity between X-gal staining and *in situ* hybridisation, differences in protein and RNA stability or alternatively, the gene trap insert may have disrupted an intronic regulatory element. Nevertheless, the expression patterns exhibited by the *Hic2* gene trap and *Hic2* mRNA were very similar and together give a clear profile of the expression pattern of *Hic2* throughout development.

The presence of *Hic2* in both the first and second heart fields just prior to heart tube formation and subsequently, the persistent expression in the myocardium of the ventricles, atria and proximal OFT strongly suggests that *Hic2* may play an important role in heart development.

6.3.2 *Hic2* mutants exhibit heart defects

Analysis of $Hic2^{+/GT}$ heterozygotes revealed that a proportion were perinatal lethal indicating that they exhibit a haploinsufficient phenotype. MRI and histology revealed that $Hic2^{+/GT}$ embryos have VSDs which could contribute to their mortality and a smaller proportion of embryos had an overriding aorta accompanying the VSD. These heart defects exhibited by $Hic2^{+/GT}$ heterozygotes phenocopy those seen in DGS patients where OFT abnormalities are the most prevalent heart defects and VSDs also account for a significant proportion (13-18%) (Momma, 2007).

The ventricular septum closes through fusion of the interventricular septum with the atrioventricular cushions and outflow tract (Gruber and Epstein, 2004). Defects in the development of any of these structures can lead to VSDs which are the most common

congenital heart malformation in humans occurring at a frequency of 1 in 300 births (Hoffman and Kaplan, 2002). Mutations in many genes have been associated with VSDs in mouse development including transcription factors such as *Tbx1*, *Nkx2.5* and *Hey2*, signalling factors and receptors such as *Fgf8*, *Fgfr2* and *Bmpr1a* and cell adhesion molecules such as *Vcam1* (Abu-Issa et al., 2002; Gaussin et al., 2002; Jerome and Papaioannou, 2001; Kwee et al., 1995; Lindsay et al., 2001; Marguerie et al., 2006; Merscher et al., 2001; Prall et al., 2007; Sakata et al., 2002). The VSD exhibited by $Hic2^{+/GT}$ mutants may occur as a result of malalignment of the OFT in a proportion of embryos with the defect. However, VSDs also appear to occur in isolation in $Hic2^{+/GT}$ mice suggesting that *Hic2* may also function in other aspects of septum formation.

The $Hic2^{+/GT}$ mice examined did not exhibit any other DGS-like heart defects such as great vessel anomalies nor were any defects in atrial septation or valve morphogenesis detected despite both translocation patients exhibiting atrioventricular canal defects. However, subtle abnormalities in atrioventricular development are difficult to identify at E15.5, the stage examined. In addition, the type of heart defects exhibited by *Hic2* mutants may depend on the mouse strain. Nevertheless, these studies have demonstrated that *Hic2* is dose-sensitive in heart development which strongly suggests that disruption of *HIC2* in humans may predispose individuals to heart defects, the type and penetrance of which may depend on genetic background.

6.3.3 The function of *Hic2* in development

Little is known about the functional role of *HIC2* in development or the molecular pathways in which *HIC2* interacts. However, clues as to its function, interacting partners and target genes can be obtained from analysis of its better characterised homologue, *HIC1*.

HIC1 and HIC2 are both members of the BTB/POZ (Broad complex, Tramtrack, Brick à brac (BTB) or poxvirus and zinc finger (POZ)) family of transcription factors which all contain the conserved BTB/POZ, N-terminal protein interaction domain (Kelly and Daniel, 2006). In addition to the BTB/POZ domain, HIC1 and HIC2 also share two other highly conserved domains, a C-terminal DNA-binding domain consisting of five, Krüppel-like C2H2 zinc fingers and another internal protein interaction domain, the evolutionarily conserved GLDLSKK/R motif (Deltour et al., 1999; Deltour et al., 2002).

The original BTB/POZ transcription factors were discovered in Drosophila and all play important roles in development. *BR-C* is required for central nervous system development in Drosophila (Karim et al., 1993; Restifo and White, 1991). *TtK* plays a role in compound eye development (Xiong and Montell, 1993) and *Bab* is important for ovary and limb development (Sahut-Barnola et al., 1995). The vertebrate members of the POZ domain family are also required for correct development including *Plzf* which is important for limb and skeletal formation (Barna et al., 2000) and *Miz1* and *Kaiso* which are both required for gastrulation (Adhikary et al., 2003; Park et al., 2005).

Similarly, *HIC1* has been proposed to play a major role in the developmental disorder, Miller-Dieker syndrome (MDS) (Carter et al., 2000). *HIC1* is located within the 350Kb critical region on chromosome 17p13.3 which is deleted in most patients with Miller-Dieker syndrome, characterised by lissencephaly, craniofacial and limb defects and omphalocele (Hirotsune et al., 1997; Wales et al., 1995). Haploinsufficiency of *LIS1* is considered to be the main cause of the lissencephaly and mental retardation phenotype (Chong et al., 1996; Hirotsune et al., 1998; Paylor et al., 1999; Pilz et al., 1999). However, the cause of other developmental anomalies which are part of the aetiology of Miller-Dieker syndrome could be attributed to loss of *HIC1* function since *Hic1*$^{-/-}$ null mice have defects highly reminiscent of the disease, exhibiting craniofacial, limb and ventral body wall defects (Carter et al., 2000).

HIC1, like the majority of other BTB/POZ transcription factors, acts as a transcriptional repressor (Deltour et al., 1999) and mediates this activity through two, distinct domains. The BTB/POZ domain acts to repress trancription in a Histone Deacetylase (HDAC)-independent manner (Deltour et al., 1999) whereas the GLDLSKK/R motif interacts with the co-repressor, CtBP and recruits HDACs to repress downstream targets (Deltour et al., 1999; Deltour et al., 2002). These two domains are highly conserved between HIC1 and HIC2, showing greater than 80% homology between the BTB/POZ domains and 100% homology in the GLDLSKK/R motif (Deltour et al., 2001) suggesting that HIC2 may also act as a transcriptional repressor and could interact with and regulate the expression of similar proteins.

HIC1 and HIC2 both localise to nuclear bodies within the cell (Deltour et al., 2001) and HIC1 has been shown to recruit mCtBP1 to these nuclear dots through binding to its GLDLSKK/R motif (Deltour et al., 2002), a mechanism by which HIC1 acts to repress

the activity of proteins such as TCF-4 and ß-catenin, effectors of Wnt signalling (Valenta et al., 2006). HIC1 also represses transcription by binding to the sequence specific site, 5'-C/GNGC/GGGGCAC/ACC-3'and requires multiple sites for optimal binding (Pinte et al., 2004). HIC2 shares over 80% homology with the HIC1 zinc fingers indicating that it may bind to similar sequences. Therefore, the identification of genes containing putative HIC1 binding sites may actually/also represent HIC2 targets.

The signalling pathways that may interact with *Hic1* are also starting to be characterised. In addition to repression of the Wnt signalling mediators, Tcf-4 and ß-catenin, *Hic1* has also been proposed to regulate *Fgfbp1* in response to Tgfß signalling, a process important in angiogenesis (Briones et al., 2006). In addition, the Hic1;CtBP repressor complex acts to downregulate *Sirt-1* expression (Chen et al., 2005; Zhang et al., 2007) particularly in response to redox changes in the environment (Zhang et al., 2007). Most of these potential *Hic1* target genes have been identified through *in vitro* experiments however the actual role that *Hic1* may play *in vivo* in regulating these genes is unknown. Furthermore, *mCtBP1*, *mCtBP2* and *Sirt-1* knockout mice exhibit heart and/or vascular defects (Cheng et al., 2003; Hildebrand and Soriano, 2002) and in particular, $Sirt1^{-/-}$ mice have VSDs and ASDs reminiscent of the phenotype exhibited by $Hic2^{+/GT}$ mice (Cheng et al., 2003). The close similarity in structure between HIC1 and HIC2 and the results from this study revealing a role for *Hic2* in heart development strongly suggest that *Hic2* may interact with at least some of these potential *Hic1* target genes.

6.3.4 *Hic2* and its role in DGS

FISH mapping studies determined that the breakpoint in patients, FN and FY1198 occurs within the LCR-D region on chromosome 22 in approximately the same location as the distal breakpoint of the common 3Mb deletion. LCR-D is approximately 250Kb in length and is defined by the markers D22S936 and D22S801 (Figure 6.10) (Shaikh et al., 2000). *HIC2* is located within LCR-D surrounded by repeated modules that mediate aberrant recombination events. Most studies have used FISH mapping to define the endpoint of the deletions in DGS patients however recently, studies using high density tiling oligonucleotide arrays and quantitative real time PCR have been able to more clearly define the breakpoints at the nucleotide level revealing that there are some variations of the deletion endpoints among patients with the common 3Mb deletion

(Jalali et al., 2007; Urban et al., 2006; Weksberg et al., 2006). Weksberg and colleagues (2006) showed that in a cohort of 44 patients with 22q11DS, most patients had the approximate 3Mb deletion (41/44, 93%) and of these, most deletions occurred within and including the markers *PRODH* and D22S936, in which the distal endpoint occurred just proximal to *HIC2*. However, 7 of these 3Mb deletion patients had variable proximal and distal deletion endpoints including 2 patients whose deletion included *HIC2* (2/41, 5%) (Weksberg et al., 2006) (Figure 6.10). This suggests that a proportion of patients with the 3Mb deletion may be haploinsufficient for *HIC2*. Indeed, this proportion could be even higher if transcription of *HIC2* is found to be controlled by a long-range *cis* regulatory element. In addition, there are numerous reports of DGS patients with atypical deletions of 22q11 which do not include *TBX1* but which include *HIC2* (Figure 6.10) (Amati et al., 1999; Jalali et al., 2007; Rauch et al., 1999; Rauch et al., 2005; Saitta et al., 1999; Weksberg et al., 2006; Wieser et al., 2005). Therefore, hemizygous expression of *HIC2* may contribute to the heart phenotype not only in DGS patients with atypical rearrangements of chromosome 22q11 but also in a proportion of patients with the common 3Mb deletion. This is supported by evidence in this study demonstrating that *Hic2* is dosage sensitive and is the only gene on chromosome 22q11 apart from *TBX1* which results in a heterozygous heart phenotype in mice.

Figure 6.10 DGS patients with atypical deletions
Most patients with DGS have the typical 3Mb or 1.5Mb deletion of chromosome 22q11. A proportion of patients with the 3Mb deletion have atypical distal deletion endpoints which include *HIC2* (red asterisk on 3Mb atypical). Some DGS patients have atypical 22q11 deletions which also include *HIC2* (red asterisk on blue lines). Modified from (Shaikh et al., 2007).

6.4 FUTURE DIRECTIONS

6.4.1 *Hic2* and long range transcriptional regulation

The expression of *Hic2* in the heart and the phenotype of *Hic2*$^{+/GT}$ mice provides strong support for disruption of *HIC2* as the underlying mechanism causing the heart defects in DGS patients with atypical 22q11 deletions and in t(11;22) patients FN and FY1198. However, FISH experiments map the breakpoint on chromosome 22 to an intergenic region approximately 80Kb upstream of *HIC2* suggesting that long-range *cis* regulatory elements may be disrupted by the translocation.

Further experiments need to be carried out to determine whether the breakpoint disrupts *HIC2* expression. A number of experiments could be conducted to assess *HIC2* expression in the patients' cell lines. These include real-time quantitative PCR or an allele-specific PCR to more precisely determine if *HIC2* expression from the disrupted chromosome 22 is altered. However, *in vitro* experiments on transformed cell lines may not accurately represent the *in vivo* expression of *HIC2*. In addition, disruption to regulatory elements may not affect gene expression in the same way as coding sequence mutations (see below).

Position effects caused by chromosomal rearrangements often occur as the result of disruption to long-range *cis* regulatory elements and become apparent when the phenotype caused by disruption of the regulatory element is the same or similar to the phenotype caused by intragenic mutations. Many of the genes which are regulated in this manner are important in developmental control and include *TWIST*, *POU3F4*, *PITX2*, *SOX9*, *SHH* and *MAF* which are regulated by enhancers located up to 1Mb away (Cai et al., 2003b; de Kok et al., 1996; Jamieson et al., 2002; Lettice et al., 2002; Pfeifer et al., 1999; Trembath et al., 2004).

These genes are expressed in a complex spatiotemporal pattern during development requiring a complex mode of regulation which long-range *cis* regulatory elements may provide. *Hic2* is expressed in multiple tissues during embryogenesis and disruption of *Hic2* leads to a heterozygous heart phenotype in mice and more severe developmental defects in homozygous nulls indicating that *Hic2* is an important developmental gene. It is therefore a good candidate for control by long-range regulation.

Long-range *cis* elements are often contained within evolutionarily conserved sequences in non-coding regions of the genome (Kleinjan and van Heyningen, 2005) and future experiments should aim to determine if any such conserved sequences are contained within the breakpoint region upstream of *HIC2*. Transgenic mouse studies could then be carried out to characterise any putative *cis*-regulatory elements and determine if disruption leads to a similar heart phenotype as that seen in *Hic2* genetrap mutants. However, it is important to note that defects caused by disruption to regulatory regions may be different to those caused by mutation within a gene's coding region. Mutations within regulatory elements may disrupt only certain tissues and/or lead to aberrant up or down-regulation of genes. Disruption to a *cis* regulatory element contained more than 1Mb upstream from *Shh* leads to misregulation of *Shh* only in the limbs and causes preaxial polydactyly but doesn't affect *Shh* expression in any other tissues (Lettice et al., 2003; Lettice et al., 2002). It would be interesting to determine how a *cis*-acting regulator contained within the translocation breakpoint region may affect expression of *Hic2* in the heart.

6.4.2 Further characterisation of the role for *Hic2* in development

These studies have shown that $Hic2^{+/GT}$ mice exhibit heart defects reminiscent of DGS. $Hic2^{GT/GT}$ mutants may exhibit more severe developmental abnormalities, which may be due to defects in the embryo itself or to defects in extraembryonic development since the yolk sac also expresses *Hic2*. In order to better characterise the spatial and temporal role of *Hic2* in development, conditional knockouts need to be generated.

Hic2 gene trap mice could also be used to investigate the tissue-specific role for *Hic2* in development. The *Hic2* genetrap allele was constructed to contain *loxP* sites flanking the splice-acceptor-ß-galactosidase insert. Theoretically, Cre-mediated excision of the vector should be possible, which would restore normal splicing and function of the trapped gene. It would be useful to restore function of *Hic2* in all extra-embryonic tissues using an extra-embryonic, tissue specific Cre line in order to define the role of *Hic2* in the embryo proper while circumventing any extra-embryonic defects. The *Cyp19*-Cre line is restricted to the extra-embryonic ectoderm and ectoplacental cone and all derivatives of the trophoblast stem cells (Wenzel and Leone, 2007). However, it is not expressed within the extraembryonic mesoderm which gives rise to the amnion or the primitive endoderm which contributes to cells of the yolk sac, both tissues which

express *Hic2*. Alternatively, the *Mox2*-Cre (MORE) line is restricted to epiblast derivatives including the embryo proper and extraembryonic mesoderm (Tallquist and Soriano, 2000) therefore restoring function of *Hic2* to these tissues should reveal whether the early embryonic lethality of $Hic2^{GT/GT}$ homozygotes is due to an extraembryonic requirement for *Hic2*.

Chimeric embryo studies could also be undertaken to distinguish between the extra-embryonic and embryonic requirement for *Hic2* in development by introducing mutant ES cells into wild type embryos or vice-versa. In the resulting chimeric embryo, the epiblast will be a mixture of wild type and mutant cells however, ES cells only give rise to epiblast derivatives which include the embryo proper and the extra-embryonic mesoderm but do not contribute to extraembryonic cells of the primitive endoderm or trophectoderm which will only be derived from the diploid embryo (Tam and Rossant, 2003). Therefore, mutant ES cell;diploid wild type embryo chimeras could be used to determine the effect of knocking out *Hic2* only in embryonic tissues. The reciprocal experiment, making wild type ES-cell;diploid mutant embryo chimeras would reveal the role of *Hic2* in extra-embryonic tissues.

CHAPTER 7. GENERAL DISCUSSION AND FUTURE DIRECTIONS

7.1 OVERVIEW

My thesis work involved using multiple tools to investigate pharyngeal and heart development, the major processes affected in DiGeorge syndrome. Haploinsufficiency of *TBX1*, which encodes a T-box transcription factor is considered to be the major underlying cause of this syndrome. I optimised a novel method to isolate embryonic *Tbx1*-expressing cells from transgenic mice, by using a fluorogenic lacZ substrate to label and flow-sort *Tbx1-lacZ* cells, thereby enabling cell-autonomous effects of *Tbx1* to be analysed by microarray. This work has led to the identification of a number of novel target genes that are dependent on *Tbx1* activity. In addition, I have conducted BAC recombineering experiments to generate a transgenic mouse line carrying a GFP-labelled, mutant *Tbx1* allele. This transgenic mouse will enable further direct downstream targets of *Tbx1* to be identified in future experiments, providing a valuable resource to study the role of *Tbx1* in development.

The microarray experiment identified *Hes1* as a potential *Tbx1* target. Analysis of the *Hes1* mouse mutant demonstrated an important, novel role for this gene in craniofacial, PAA and OFT development. These results suggest that *Hes1* may act downstream of *Tbx1* in development and potentially may act as a genetic modifier of DGS, (in the context of *TBX1* haploinsufficiency).

In addition to focusing on the developmental pathways downstream of *Tbx1,* this work also identified other pathways important in heart development. The analysis of DGS patients with atypical chromosome rearrangements has led to the identification of *HIC2*, a novel candidate gene on chromosome 22 involved in cardiovascular development and human disease. Examination of *Hic2* gene trap mice has revealed a dose-sensitive role for *Hic2* in heart development, strongly suggesting that *HIC2* may act as a modifier of the DGS phenotype.

Overall, these experiments have led to the elucidation of novel genes and genetic pathways which may cause or modify the DGS phenotype and function in pharyngeal apparatus and heart development. These studies will provide the basis for future

investigations into the molecular and developmental mechanisms which regulate these processes.

7.2 IDENTIFICATION OF DIRECT *TBX1* TARGETS

The microarray analysis of *Tbx1*-expressing cells identified a number of potential downstream targets, including *Hes1*, but it is unclear whether these genes represent direct or indirect targets of *Tbx1*. This is important in order to define the transcriptional networks governing pharyngeal and heart development. The TgTbx1floxGFP mice generated in this project should help to enrich for direct targets in future microarray experiments. Full length *Tbx1* expression is inducible in cells carrying this mutant allele, allowing control of the precise timepoint at which *Tbx1* is activated. Thus, FACS-sorted cells can be induced in culture and RNA isolated shortly after *Tbx1* is translated.

In order to distinguish direct from indirect targets identified in microarray analyses, a number of approaches are possible. Bioinformatic analyses could be used to identify putative T-half sites in the genomic sequence surrounding potential *Tbx1* target genes. Tools such as rVISTA (http://rvista.dcode.org/) and Mulan (http://mulan.dcode.org/) use multiple sequence alignment to identify DNA binding elements within evolutionarily conserved regions of the genome (Loots and Ovcharenko, 2004; Ovcharenko et al., 2005). These conserved regions have been shown to correlate with functionally important DNA sequences such as exons and regulatory elements. Thus, such regions are more likely to contain biologically relevant T-box binding sites (Elnitski et al., 2001; Gilligan et al., 2002; Loots et al., 2000; Pennacchio and Rubin, 2001). Considering that T-box proteins interact with other transcription factors such as Nkx2.5 and Gata4, to synergistically regulate target genes (Naiche et al., 2005; Nowotschin et al., 2006; Stennard et al., 2003), the identification of T-half sites in close proximity to Nkx2.5 or Gata binding elements may indicate that these regions are good candidate binding sequences for Tbx1.

To subsequently test whether putative binding sites are functionally relevant, *in vitro* experiments such as luciferase reporter and electrophoretic mobility shift assays (EMSAs) could be carried out. A putative DNA regulatory element (from a potential *Tbx1* target) could be cloned upstream of a bioluminescent expression reporter, such as

luciferase, to examine whether Tbx1 binds to the site and activates transcription. EMSAs could also be used to test whether Tbx1 protein directly binds to a specific, putative binding sequence (Garner and Revzin, 1981). However, these *in vitro* experiments may not accurately reflect the *in vivo* situation and interactions between Tbx1 and a target gene are likely to depend on factors such as the tissue analysed and the presence of coactivators.

Chromatin immunoprecipitation (ChIP) experiments could be used to analyse the *in vivo* interactions between Tbx1 and genomic DNA. ChIP involves using formaldehyde to crosslink proteins to their genomic DNA binding sites *in vivo*, followed by shearing of the chromatin into DNA fragments. Crosslinked Tbx1 protein-DNA fragment complexes could then be immunoprecipitated using an antibody to Tbx1. The bound DNA fragments can be analysed in multiple ways. PCR can be used to amplify specific sequences (representing putative binding sites for potential target genes) to determine if these DNA fragments were isolated by ChIP. This relies on knowing, or predicting the binding site sequence in the first place. Alternatively, a more high-throughput method of analysing the isolated DNA fragments (which does not require prior knowledge of binding sites), would be to combine ChIP with a microarray, a method termed ChIP-chip. Following ChIP, the DNA is labelled and hybridised to a microarray containing genomic DNA sequences. Results from ChIP-chip could be compared to the gene expression microarray to determine if any identified genomic DNA binding sites for Tbx1 occur within the vicinity of dysregulated genes. These ChIP experiments would be extremely helpful for identifying multiple, direct *Tbx1* targets. Moreover, these studies should help to determine whether *Hes1* is directly regulated by *Tbx1* or whether it functions downstream of Notch signalling.

The usefulness of ChIP-chip is limited by the genomic regions included on the microarray. Even whole genome oligonucleotide tiling arrays do not cover repetitive sequences (Kim et al., 2005; Lee et al., 2006). Therefore, recent studies have used ChIP followed by high-throughput sequencing in an effort to circumvent the limitations of microarray platforms (Bhinge et al., 2007; Johnson et al., 2007; Robertson et al., 2007; Wei et al., 2006). Further experiments, such as *in vitro* expression assays and the analysis of regulatory elements in transgenic animal models, will determine the functional effect of binding and confirm which gene the binding site regulates. Combining gene expression data with ChIP analysis should enable the prioritisation of

genes, which likely act as direct downstream *Tbx1* targets for further functional analysis.

7.3 *IN VIVO* FUNCTIONAL ANALYSIS OF GENES

To investigate the *in vivo* function of *Tbx1* targets and their role in pharyngeal and/or heart development, phenotypic analysis of animal mutants is required. This could be rapidly achieved by using antisense morpholino oligonucleotides in zebrafish to knockdown gene expression. *Tbx1* plays a similar role in both mouse and zebrafish pharyngeal development, suggesting that downstream effectors important in this process are conserved between species. *Her6* morpholino injections have already been carried out and demonstrate that *her6*, the zebrafish homologue of *Hes1* also functions in pharyngeal development. The developmental role of other *Tbx1* targets such as *Gbx2* and the *Cyp26* genes are currently being investigated in zebrafish. Knockout mouse mutants should also be generated, or gene trap mouse models obtained, to investigate the biological function of *Tbx1* target genes in an organism which more closely resembles the human condition.

For genes proposed to act downstream of *Tbx1* in development, genetic interactions with *Tbx1* should also be investigated in animal models. The analysis of epistatic interactions with *Tbx1* is important not only for defining downstream genetic pathways but also for determining whether genes may act as genetic modifiers of DGS. Double morpholino injections in zebrafish have been used to investigate such epistasis in our lab and have already shown that *tbx1* and *her6* interact genetically in development of the pharyngeal arches. In mice, conventional knockouts for *Tbx1* and potential target genes could be intercrossed to examine whether they act in the same pathway during development. However, heterozygous and homozygous mouse phenotypes may not accurately reflect the human situation, being too mild or too severe, respectively. This is the case for $Tbx1^{+/-}$ and $Tbx1^{-/-}$ mouse mutants, which may make it difficult to establish precise epistatic interactions. The recent characterisation of a series of hypomorphic *Tbx1* alleles has demonstrated the acute dosage sensitivity of structures such as the PAAs to altered *Tbx1* levels (Zhang and Baldini, 2007). These studies have also demonstrated that the $Tbx1^{Neo2/Neo}$ hypomorphic mouse more closely resembles the variable OFT phenotype exhibited by human DGS patients. Therefore, hypomorphic *Tbx1* mouse mutants may be better suited for epistasis experiments, for example, to

study the effect of *Hes1* mutations on the OFT phenotype. Another way to investigate epistasis with *Tbx1* involves crossing $Tbx1^{+/Cre}$ mice with conditional, floxed mouse mutants for potential downstream genes. In this way, the complete loss of target gene expression from *Tbx1* expression domains can be analysed in the presence of hemizygous *Tbx1* expression. Conducting the above epistasis experiments with *Hes1* may reveal an interaction with *Tbx1* in mouse development.

During the course of this project, the chromosome 22q11 gene, *HIC2* was identified as a potential modifier of the heart phenotype in DGS patients as evidenced by the presence of OFT alignment and ventricular septal defects in $Hic2^{+/-}$ mouse mutants. *Hic2* and *Tbx1* are both expressed in the SHF at the cardiac crescent stage of mouse development and mouse mutants for these genes exhibit similar heart defects. Thus, it is possible that they may interact in heart development.

7.4 CONDITIONAL GENE INACTIVATION

The investigate the spatial and temporal role of novel pharyngeal and heart development genes identified during this project, conditional mouse mutants will need to be generated so that gene function can be knocked out or reactivated in specific tissues, at precise timepoints. This could be achieved by crossing conditional mouse mutants (expressing floxed genes) to mouse lines expressing tissue-specific and/or tamoxifen inducible Cre-drivers. For potential *Tbx1* targets, suitable Cre-lines which could be used include *Tbx1-Cre* (Huynh et al., 2007) and the tamoxifen-inducible Cre, *Tbx1-mcm* (Xu et al., 2004) as well as drivers for specific tissues where *Tbx1* is known to be functionally active, such as the pharyngeal endoderm (*Foxa2-mcm*) (A. Moon, pers. comm.), mesoderm (*Mesp1-Cre*) (Saga et al., 1999), ectoderm (*Ap2α-Cre*) (Macatee et al 03) and the secondary heart field (*Isl1-Cre*) (Yang et al., 2006) and (*Mef2c-Cre*) (Verzi et al., 2005). Furthermore, to investigate the role of *Hic2* in the heart, myocardial Cre-drivers such as *αMHC-Cre* (Agah et al., 1997) and *Nkx2.5-Cre* (Moses et al., 2001) could be used.

These studies will help to characterise the specific roles of genes acting downstream of *Tbx1* in development and will be especially informative in the context of what is already known concerning the time, tissue and dose-requirements for *Tbx1* and the cellular processes which *Tbx1* regulates.

7.5 MICROARRAY EXPERIMENTS

Further insight into the role of downstream *Tbx1* targets in development will require gene expression microarrays to be carried out for the most relevant genes, such as *Hes1*. The TgTbx1floxGFP mice can be used to label *Tbx1*-expressing cells in target gene mouse mutants so that their role, specifically in *Tbx1*-expressing cells, can be examined. *Hic2,* a transcriptional repressor, represents a potential modifier of DGS and a novel gene involved in cardiovascular development. However, there is very little known about the transcriptional network acting downstream of *Hic2*. A microarray will therefore, be particularly useful for characterising the role of *Hic2* in heart development.

In conclusion, the genomic and transcriptomic approaches I have taken during my thesis work, have led to the identification of a number of novel *Tbx1* targets and genetic modifiers of DGS. The future work outlined above would allow these genes to be investigated to further increase our understanding of the genetic cascade regulated by *Tbx1* and to elucidate the gene network governing the DGS phenotype and pharyngeal and heart development.

REFERENCES

Abu-Abed, S., Dolle, P., Metzger, D., Beckett, B., Chambon, P. and Petkovich, M. (2001). The retinoic acid-metabolizing enzyme, CYP26A1, is essential for normal hindbrain patterning, vertebral identity, and development of posterior structures. *Genes Dev* **15**, 226-40.

Abu-Issa, R., Smyth, G., Smoak, I., Yamamura, K. and Meyers, E. N. (2002). Fgf8 is required for pharyngeal arch and cardiovascular development in the mouse. *Development* **129**, 4613-25.

Adhikary, S., Peukert, K., Karsunky, H., Beuger, V., Lutz, W., Elsasser, H. P., Moroy, T. and Eilers, M. (2003). Miz1 is required for early embryonic development during gastrulation. *Mol Cell Biol* **23**, 7648-57.

Agah, R., Frenkel, P. A., French, B. A., Michael, L. H., Overbeek, P. A. and Schneider, M. D. (1997). Gene recombination in postmitotic cells. Targeted expression of Cre recombinase provokes cardiac-restricted, site-specific rearrangement in adult ventricular muscle in vivo. *J Clin Invest* **100**, 169-79.

Aggarwal, V. S., Liao, J., Bondarev, A., Schimmang, T., Lewandoski, M., Locker, J., Shanske, A., Campione, M. and Morrow, B. E. (2006). Dissection of Tbx1 and Fgf interactions in mouse models of 22q11DS suggests functional redundancy. *Hum Mol Genet.*

Ai, D., Liu, W., Ma, L., Dong, F., Lu, M. F., Wang, D., Verzi, M. P., Cai, C., Gage, P. J., Evans, S. et al. (2006). Pitx2 regulates cardiac left-right asymmetry by patterning second cardiac lineage-derived myocardium. *Dev Biol* **296**, 437-49.

Akazawa, C., Sasai, Y., Nakanishi, S. and Kageyama, R. (1992). Molecular characterization of a rat negative regulator with a basic helix-loop-helix structure predominantly expressed in the developing nervous system. *J Biol Chem* **267**, 21879-85.

Ali-Khan, S. E. and Hales, B. F. (2006). Novel retinoid targets in the mouse limb during organogenesis. *Toxicol Sci* **94**, 139-52.

Alvarez Arratia, M. C., Rivera, H., Moller, M., Valdivia, A., Vigueras, A. and Cantu, J. M. (1984). De novo del(3)(q2800). *Ann Genet* **27**, 109-11.

Amati, F., Conti, E., Novelli, A., Bengala, M., Diglio, M. C., Marino, B., Giannotti, A., Gabrielli, O., Novelli, G. and Dallapiccola, B. (1999). Atypical deletions suggest five 22q11.2 critical regions related to the DiGeorge/velo-cardio-facial syndrome. *Eur J Hum Genet* **7**, 903-9.

Andrade, R. P., Palmeirim, I. and Bajanca, F. (2007). Molecular clocks underlying vertebrate embryo segmentation: A 10-year-old hairy-go-round. *Birth Defects Res C Embryo Today* **81**, 65-83.

Angell, J. E., Lindner, D. J., Shapiro, P. S., Hofmann, E. R. and Kalvakolanu, D. V. (2000). Identification of GRIM-19, a novel cell death-regulatory gene induced by the interferon-beta and retinoic acid combination, using a genetic approach. *J Biol Chem* **275**, 33416-26.

Aqua, M. S., Rizzu, P., Lindsay, E. A., Shaffer, L. G., Zackai, E. H., Overhauser, J. and Baldini, A. (1995). Duplication 3q syndrome: molecular delineation of the critical region. *Am J Med Genet* **55**, 33-7.

Arnold, J. S., Braunstein, E. M., Ohyama, T., Groves, A. K., Adams, J. C., Brown, M. C. and Morrow, B. E. (2006a). Tissue-specific roles of Tbx1 in the development of

the outer, middle and inner ear, defective in 22q11DS patients. *Hum Mol Genet* **15**, 1629-39.

Arnold, J. S., Werling, U., Braunstein, E. M., Liao, J., Nowotschin, S., Edelmann, W., Hebert, J. M. and Morrow, B. E. (2006b). Inactivation of Tbx1 in the pharyngeal endoderm results in 22q11DS malformations. *Development* **133**, 977-87.

Aspenstrom, P., Richnau, N. and Johansson, A. S. (2006). The diaphanous-related formin DAAM1 collaborates with the Rho GTPases RhoA and Cdc42, CIP4 and Src in regulating cell morphogenesis and actin dynamics. *Exp Cell Res* **312**, 2180-94.

Ataliotis, P., Ivins, S., Mohun, T. J. and Scambler, P. J. (2005). XTbx1 is a transcriptional activator involved in head and pharyngeal arch development in Xenopus laevis. *Dev Dyn* **232**, 979-91.

Awad, M. M., Dalal, D., Cho, E., Amat-Alarcon, N., James, C., Tichnell, C., Tucker, A., Russell, S. D., Bluemke, D. A., Dietz, H. C. et al. (2006). DSG2 mutations contribute to arrhythmogenic right ventricular dysplasia/cardiomyopathy. *Am J Hum Genet* **79**, 136-42.

Bachiller, D., Klingensmith, J., Shneyder, N., Tran, U., Anderson, R., Rossant, J. and De Robertis, E. M. (2003). The role of chordin/Bmp signals in mammalian pharyngeal development and DiGeorge syndrome. *Development* **130**, 3567-78.

Bae, S., Bessho, Y., Hojo, M. and Kageyama, R. (2000). The bHLH gene Hes6, an inhibitor of Hes1, promotes neuronal differentiation. *Development* **127**, 2933-43.

Baek, J. H., Hatakeyama, J., Sakamoto, S., Ohtsuka, T. and Kageyama, R. (2006). Persistent and high levels of Hes1 expression regulate boundary formation in the developing central nervous system. *Development* **133**, 2467-76.

Bagnard, D., Lohrum, M., Uziel, D., Puschel, A. W. and Bolz, J. (1998). Semaphorins act as attractive and repulsive guidance signals during the development of cortical projections. *Development* **125**, 5043-53.

Bajoghli, B., Aghaallaei, N., Soroldoni, D. and Czerny, T. (2007). The roles of Groucho/Tle in left-right asymmetry and Kupffer's vesicle organogenesis. *Dev Biol* **303**, 347-61.

Bamshad, M., Le, T., Watkins, W. S., Dixon, M. E., Kramer, B. E., Roeder, A. D., Carey, J. C., Root, S., Schinzel, A., Van Maldergem, L. et al. (1999). The spectrum of mutations in TBX3: Genotype/Phenotype relationship in ulnar-mammary syndrome. *Am J Hum Genet* **64**, 1550-62.

Bamshad, M., Lin, R. C., Law, D. J., Watkins, W. C., Krakowiak, P. A., Moore, M. E., Franceschini, P., Lala, R., Holmes, L. B., Gebuhr, T. C. et al. (1997). Mutations in human TBX3 alter limb, apocrine and genital development in ulnar-mammary syndrome. *Nat Genet* **16**, 311-5.

Barna, M., Hawe, N., Niswander, L. and Pandolfi, P. P. (2000). Plzf regulates limb and axial skeletal patterning. *Nat Genet* **25**, 166-72.

Barsi, J. C., Rajendra, R., Wu, J. I. and Artzt, K. (2005). Mind bomb1 is a ubiquitin ligase essential for mouse embryonic development and Notch signaling. *Mech Dev* **122**, 1106-17.

Basch, M. L. and Bronner-Fraser, M. (2006). Neural crest inducing signals. *Adv Exp Med Biol* **589**, 24-31.

Basson, C. T., Bachinsky, D. R., Lin, R. C., Levi, T., Elkins, J. A., Soults, J., Grayzel, D., Kroumpouzou, E., Traill, T. A., Leblanc-Straceski, J. et al. (1997). Mutations in human TBX5 [corrected] cause limb and cardiac malformation in Holt-Oram syndrome. *Nat Genet* **15**, 30-5.

Begbie, J., Brunet, J. F., Rubenstein, J. L. and Graham, A. (1999). Induction of the epibranchial placodes. *Development* **126**, 895-902.

Beis, D. and Stainier, D. Y. (2006). In vivo cell biology: following the zebrafish trend. *Trends Cell Biol* **16**, 105-12.

Bergwerff, M., DeRuiter, M. C., Hall, S., Poelmann, R. E. and Gittenberger-de Groot, A. C. (1999). Unique vascular morphology of the fourth aortic arches: possible implications for pathogenesis of type-B aortic arch interruption and anomalous right subclavian artery. *Cardiovasc Res* **44**, 185-96.

Bertrand, S., Pinte, S., Stankovic-Valentin, N., Deltour-Balerdi, S., Guerardel, C., Begue, A., Laudet, V. and Leprince, D. (2004). Identification and developmental expression of the zebrafish orthologue of the tumor suppressor gene HIC1. *Biochim Biophys Acta* **1678**, 57-66.

Bessho, Y., Miyoshi, G., Sakata, R. and Kageyama, R. (2001). Hes7: a bHLH-type repressor gene regulated by Notch and expressed in the presomitic mesoderm. *Genes Cells* **6**, 175-85.

Bhinge, A. A., Kim, J., Euskirchen, G. M., Snyder, M. and Iyer, V. R. (2007). Mapping the chromosomal targets of STAT1 by Sequence Tag Analysis of Genomic Enrichment (STAGE). *Genome Res* **17**, 910-6.

Biben, C., Hatzistavrou, T. and Harvey, R. P. (1998). Expression of NK-2 class homeobox gene Nkx2-6 in foregut endoderm and heart. *Mech Dev* **73**, 125-7.

Black, B. L. (2007). Transcriptional pathways in second heart field development. *Semin Cell Dev Biol* **18**, 67-76.

Bockman, D. E. and Kirby, M. L. (1984). Dependence of thymus development on derivatives of the neural crest. *Science* **223**, 498-500.

Bockman, D. E., Redmond, M. E. and Kirby, M. L. (1989). Alteration of early vascular development after ablation of cranial neural crest. *Anat Rec* **225**, 209-17.

Bockman, D. E., Redmond, M. E., Waldo, K., Davis, H. and Kirby, M. L. (1987). Effect of neural crest ablation on development of the heart and arch arteries in the chick. *Am J Anat* **180**, 332-41.

Bolos, V., Grego-Bessa, J. and de la Pompa, J. L. (2007). Notch signaling in development and cancer. *Endocr Rev* **28**, 339-63.

Bongers, E. M., Duijf, P. H., van Beersum, S. E., Schoots, J., Van Kampen, A., Burckhardt, A., Hamel, B. C., Losan, F., Hoefsloot, L. H., Yntema, H. G. et al. (2004). Mutations in the human TBX4 gene cause small patella syndrome. *Am J Hum Genet* **74**, 1239-48.

Botta, A., Lindsay, E. A., Jurecic, V. and Baldini, A. (1997). Comparative mapping of the DiGeorge syndrome region in mouse shows inconsistent gene order and differential degree of gene conservation. *Mamm Genome* **8**, 890-5.

Bouchard, M., Grote, D., Craven, S. E., Sun, Q., Steinlein, P. and Busslinger, M. (2005). Identification of Pax2-regulated genes by expression profiling of the mid-hindbrain organizer region. *Development* **132**, 2633-43.

Brachvogel, B., Moch, H., Pausch, F., Schlotzer-Schrehardt, U., Hofmann, C., Hallmann, R., von der Mark, K., Winkler, T. and Poschl, E. (2005). Perivascular cells expressing annexin A5 define a novel mesenchymal stem cell-like population with the capacity to differentiate into multiple mesenchymal lineages. *Development* **132**, 2657-68.

Briones, V. R., Chen, S., Riegel, A. T. and Lechleider, R. J. (2006). Mechanism of fibroblast growth factor-binding protein 1 repression by TGF-beta. *Biochem Biophys Res Commun* **345**, 595-601.

Brown, C. B., Wenning, J. M., Lu, M. M., Epstein, D. J., Meyers, E. N. and Epstein, J. A. (2004). Cre-mediated excision of Fgf8 in the Tbx1 expression domain reveals a critical role for Fgf8 in cardiovascular development in the mouse. *Dev Biol* **267**, 190-202.

Brown, D. D., Martz, S. N., Binder, O., Goetz, S. C., Price, B. M., Smith, J. C. and Conlon, F. L. (2005). Tbx5 and Tbx20 act synergistically to control vertebrate heart morphogenesis. *Development* **132**, 553-63.

Brueton, L. A., Barber, J. C., Huson, S. M. and Winter, R. M. (1989). Partial monosomy 3q in a boy with short stature, developmental delay, and mild dysmorphic features. *J Med Genet* **26**, 729-30.

Bruneau, B. G., Nemer, G., Schmitt, J. P., Charron, F., Robitaille, L., Caron, S., Conner, D. A., Gessler, M., Nemer, M., Seidman, C. E. et al. (2001). A murine model of Holt-Oram syndrome defines roles of the T-box transcription factor Tbx5 in cardiogenesis and disease. *Cell* **106**, 709-21.

Bryant, Z., Subrahmanyan, L., Tworoger, M., LaTray, L., Liu, C. R., Li, M. J., van den Engh, G. and Ruohola-Baker, H. (1999). Characterization of differentially expressed genes in purified Drosophila follicle cells: toward a general strategy for cell type-specific developmental analysis. *Proc Natl Acad Sci U S A* **96**, 5559-64.

Buckingham, M., Meilhac, S. and Zaffran, S. (2005). Building the mammalian heart from two sources of myocardial cells. *Nat Rev Genet* **6**, 826-35.

Bussen, M., Petry, M., Schuster-Gossler, K., Leitges, M., Gossler, A. and Kispert, A. (2004). The T-box transcription factor Tbx18 maintains the separation of anterior and posterior somite compartments. *Genes Dev* **18**, 1209-21.

Byrd, N. A. and Meyers, E. N. (2005). Loss of Gbx2 results in neural crest cell patterning and pharyngeal arch artery defects in the mouse embryo. *Dev Biol.*

Cai, C. L., Liang, X., Shi, Y., Chu, P. H., Pfaff, S. L., Chen, J. and Evans, S. (2003a). Isl1 identifies a cardiac progenitor population that proliferates prior to differentiation and contributes a majority of cells to the heart. *Dev Cell* **5**, 877-89.

Cai, J., Goodman, B. K., Patel, A. S., Mulliken, J. B., Van Maldergem, L., Hoganson, G. E., Paznekas, W. A., Ben-Neriah, Z., Sheffer, R., Cunningham, M. L. et al. (2003b). Increased risk for developmental delay in Saethre-Chotzen syndrome is associated with TWIST deletions: an improved strategy for TWIST mutation screening. *Hum Genet* **114**, 68-76.

Carlson, C., Sirotkin, H., Pandita, R., Goldberg, R., McKie, J., Wadey, R., Patanjali, S. R., Weissman, S. M., Anyane-Yeboa, K., Warburton, D. et al. (1997). Molecular definition of 22q11 deletions in 151 velo-cardio-facial syndrome patients. *Am J Hum Genet* **61**, 620-9.

Carlson, H., Ota, S., Campbell, C. E. and Hurlin, P. J. (2001). A dominant repression domain in Tbx3 mediates transcriptional repression and cell immortalization: relevance to mutations in Tbx3 that cause ulnar-mammary syndrome. *Hum Mol Genet* **10**, 2403-13.

Carter, M. G., Johns, M. A., Zeng, X., Zhou, L., Zink, M. C., Mankowski, J. L., Donovan, D. M. and Baylin, S. B. (2000). Mice deficient in the candidate tumor suppressor gene Hic1 exhibit developmental defects of structures affected in the Miller-Dieker syndrome. *Hum Mol Genet* **9**, 413-9.

Castella, P., Sawai, S., Nakao, K., Wagner, J. A. and Caudy, M. (2000). HES-1 repression of differentiation and proliferation in PC12 cells: role for the helix 3-helix 4 domain in transcription repression. *Mol Cell Biol* **20**, 6170-83.

Cau, E., Gradwohl, G., Casarosa, S., Kageyama, R. and Guillemot, F. (2000). Hes genes regulate sequential stages of neurogenesis in the olfactory epithelium. *Development* **127**, 2323-32.

Chalmers, A. D., Pambos, M., Mason, J., Lang, S., Wylie, C. and Papalopulu, N. (2005). aPKC, Crumbs3 and Lgl2 control apicobasal polarity in early vertebrate development. *Development* **132**, 977-86.

Chapman, D. L., Garvey, N., Hancock, S., Alexiou, M., Agulnik, S. I., Gibson-Brown, J. J., Cebra-Thomas, J., Bollag, R. J., Silver, L. M. and Papaioannou, V. E. (1996). Expression of the T-box family genes, Tbx1-Tbx5, during early mouse development. *Dev Dyn* **206**, 379-90.

Chen, L. and Al-Awqati, Q. (2005). Segmental expression of Notch and Hairy genes in nephrogenesis. *Am J Physiol Renal Physiol* **288**, F939-52.

Chen, W. Y., Wang, D. H., Yen, R. C., Luo, J., Gu, W. and Baylin, S. B. (2005). Tumor suppressor HIC1 directly regulates SIRT1 to modulate p53-dependent DNA-damage responses. *Cell* **123**, 437-48.

Cheng, H. L., Mostoslavsky, R., Saito, S., Manis, J. P., Gu, Y., Patel, P., Bronson, R., Appella, E., Alt, F. W. and Chua, K. F. (2003). Developmental defects and p53 hyperacetylation in Sir2 homolog (SIRT1)-deficient mice. *Proc Natl Acad Sci U S A* **100**, 10794-9.

Chiang, C., Litingtung, Y., Lee, E., Young, K. E., Corden, J. L., Westphal, H. and Beachy, P. A. (1996). Cyclopia and defective axial patterning in mice lacking Sonic hedgehog gene function. *Nature* **383**, 407-13.

Chitayat, D., Babul, R., Silver, M. M., Jay, V., Teshima, I. E., Babyn, P. and Becker, L. E. (1996). Terminal deletion of the long arm of chromosome 3 [46,XX,del(3)(q27-->qter)]. *Am J Med Genet* **61**, 45-8.

Chong, S. S., Tanigami, A., Roschke, A. V. and Ledbetter, D. H. (1996). 14-3-3 epsilon has no homology to LIS1 and lies telomeric to it on chromosome 17p13.3 outside the Miller-Dieker syndrome chromosome region. *Genome Res* **6**, 735-41.

Christoffels, V. M., Habets, P. E., Franco, D., Campione, M., de Jong, F., Lamers, W. H., Bao, Z. Z., Palmer, S., Biben, C., Harvey, R. P. et al. (2000). Chamber formation and morphogenesis in the developing mammalian heart. *Dev Biol* **223**, 266-78.

Christoffels, V. M., Hoogaars, W. M., Tessari, A., Clout, D. E., Moorman, A. F. and Campione, M. (2004). T-box transcription factor Tbx2 represses differentiation and formation of the cardiac chambers. *Dev Dyn* **229**, 763-70.

Christoffels, V. M., Mommersteeg, M. T., Trowe, M. O., Prall, O. W., de Gier-de Vries, C., Soufan, A. T., Bussen, M., Schuster-Gossler, K., Harvey, R. P., Moorman, A. F. et al. (2006). Formation of the venous pole of the heart from an Nkx2-5-negative precursor population requires Tbx18. *Circ Res* **98**, 1555-63.

Coll, M., Seidman, J. G. and Muller, C. W. (2002). Structure of the DNA-bound T-box domain of human TBX3, a transcription factor responsible for ulnar-mammary syndrome. *Structure* **10**, 343-56.

Collins, J. E., Mungall, A. J., Badcock, K. L., Fay, J. M. and Dunham, I. (1997). The organization of the gamma-glutamyl transferase genes and other low copy repeats in human chromosome 22q11. *Genome Res* **7**, 522-31.

Compernolle, V., Brusselmans, K., Franco, D., Moorman, A., Dewerchin, M., Collen, D. and Carmeliet, P. (2003). Cardia bifida, defective heart development and abnormal neural crest migration in embryos lacking hypoxia-inducible factor-1alpha. *Cardiovasc Res* **60**, 569-79.

Conlon, F. L., Fairclough, L., Price, B. M., Casey, E. S. and Smith, J. C. (2001). Determinants of T box protein specificity. *Development* **128**, 3749-58.

Cook, D. L., Gerber, A. N. and Tapscott, S. J. (1998). Modeling stochastic gene expression: implications for haploinsufficiency. *Proc Natl Acad Sci U S A* **95**, 15641-6.

Copeland, N. G., Jenkins, N. A. and Court, D. L. (2001). Recombineering: a powerful new tool for mouse functional genomics. *Nat Rev Genet* **2**, 769-79.

Couly, G., Creuzet, S., Bennaceur, S., Vincent, C. and Le Douarin, N. M. (2002). Interactions between Hox-negative cephalic neural crest cells and the foregut endoderm in patterning the facial skeleton in the vertebrate head. *Development* **129**, 1061-73.

Couly, G. F., Coltey, P. M. and Le Douarin, N. M. (1992). The developmental fate of the cephalic mesoderm in quail-chick chimeras. *Development* **114**, 1-15.

Covassin, L., Amigo, J. D., Suzuki, K., Teplyuk, V., Straubhaar, J. and Lawson, N. D. (2006). Global analysis of hematopoietic and vascular endothelial gene expression by tissue specific microarray profiling in zebrafish. *Dev Biol* **299**, 551-62.

Crump, J. G., Maves, L., Lawson, N. D., Weinstein, B. M. and Kimmel, C. B. (2004). An essential role for Fgfs in endodermal pouch formation influences later craniofacial skeletal patterning. *Development* **131**, 5703-16.

Curry, C. L., Reed, L. L., Nickoloff, B. J., Miele, L. and Foreman, K. E. (2006). Notch-independent regulation of Hes-1 expression by c-Jun N-terminal kinase signaling in human endothelial cells. *Lab Invest* **86**, 842-52.

Dallas, P. B., Gottardo, N. G., Firth, M. J., Beesley, A. H., Hoffmann, K., Terry, P. A., Freitas, J. R., Boag, J. M., Cummings, A. J. and Kees, U. R. (2005). Gene expression levels assessed by oligonucleotide microarray analysis and quantitative real-time RT-PCR -- how well do they correlate? *BMC Genomics* **6**, 59.

Dastjerdi, A., Robson, L., Walker, R., Hadley, J., Zhang, Z., Rodriguez-Niedenfuhr, M., Ataliotis, P., Baldini, A., Scambler, P. and Francis-West, P. (2007). Tbx1 regulation of myogenic differentiation in the limb and cranial mesoderm. *Dev Dyn* **236**, 353-63.

Davenport, T. G., Jerome-Majewska, L. A. and Papaioannou, V. E. (2003). Mammary gland, limb and yolk sac defects in mice lacking Tbx3, the gene mutated in human ulnar mammary syndrome. *Development* **130**, 2263-73.

David, N. B., Saint-Etienne, L., Tsang, M., Schilling, T. F. and Rosa, F. M. (2002). Requirement for endoderm and FGF3 in ventral head skeleton formation. *Development* **129**, 4457-68.

Dawson, S. R., Turner, D. L., Weintraub, H. and Parkhurst, S. M. (1995). Specificity for the hairy/enhancer of split basic helix-loop-helix (bHLH) proteins maps outside the bHLH domain and suggests two separable modes of transcriptional repression. *Mol Cell Biol* **15**, 6923-31.

de Kok, Y. J., Vossenaar, E. R., Cremers, C. W., Dahl, N., Laporte, J., Hu, L. J., Lacombe, D., Fischel-Ghodsian, N., Friedman, R. A., Parnes, L. S. et al. (1996). Identification of a hot spot for microdeletions in patients with X-linked deafness type 3 (DFN3) 900 kb proximal to the DFN3 gene POU3F4. *Hum Mol Genet* **5**, 1229-35.

de la Cruz, M. V., Sanchez Gomez, C., Arteaga, M. M. and Arguello, C. (1977). Experimental study of the development of the truncus and the conus in the chick embryo. *J Anat* **123**, 661-86.

de la Pompa, J. L., Wakeham, A., Correia, K. M., Samper, E., Brown, S., Aguilera, R. J., Nakano, T., Honjo, T., Mak, T. W., Rossant, J. et al. (1997). Conservation of the Notch signalling pathway in mammalian neurogenesis. *Development* **124**, 1139-48.

de Roos, K., Sonneveld, E., Compaan, B., ten Berge, D., Durston, A. J. and van der Saag, P. T. (1999). Expression of retinoic acid 4-hydroxylase (CYP26) during mouse and Xenopus laevis embryogenesis. *Mech Dev* **82**, 205-11.

Delot, E. C., Bahamonde, M. E., Zhao, M. and Lyons, K. M. (2003). BMP signaling is required for septation of the outflow tract of the mammalian heart. *Development* **130**, 209-20.

Deltour, S., Guerardel, C. and Leprince, D. (1999). Recruitment of SMRT/N-CoR-mSin3A-HDAC-repressing complexes is not a general mechanism for BTB/POZ transcriptional repressors: the case of HIC-1 and gammaFBP-B. *Proc Natl Acad Sci U S A* **96**, 14831-6.

Deltour, S., Pinte, S., Guerardel, C. and Leprince, D. (2001). Characterization of HRG22, a human homologue of the putative tumor suppressor gene HIC1. *Biochem Biophys Res Commun* **287**, 427-34.

Deltour, S., Pinte, S., Guerardel, C., Wasylyk, B. and Leprince, D. (2002). The human candidate tumor suppressor gene HIC1 recruits CtBP through a degenerate GLDLSKK motif. *Mol Cell Biol* **22**, 4890-901.

Dewulf, N., Verschueren, K., Lonnoy, O., Moren, A., Grimsby, S., Vande Spiegle, K., Miyazono, K., Huylebroeck, D. and Ten Dijke, P. (1995). Distinct spatial and temporal expression patterns of two type I receptors for bone morphogenetic proteins during mouse embryogenesis. *Endocrinology* **136**, 2652-63.

Digilio, M. C., Pacifico, C., Tieri, L., Marino, B., Giannotti, A. and Dallapiccola, B. (1999). Audiological findings in patients with microdeletion 22q11 (di George/velocardiofacial syndrome). *Br J Audiol* **33**, 329-33.

Dodou, E., Verzi, M. P., Anderson, J. P., Xu, S. M. and Black, B. L. (2004). Mef2c is a direct transcriptional target of ISL1 and GATA factors in the anterior heart field during mouse embryonic development. *Development* **131**, 3931-42.

Domenga, V., Fardoux, P., Lacombe, P., Monet, M., Maciazek, J., Krebs, L. T., Klonjkowski, B., Berrou, E., Mericskay, M., Li, Z. et al. (2004). Notch3 is required for arterial identity and maturation of vascular smooth muscle cells. *Genes Dev* **18**, 2730-5.

Donovan, J., Kordylewska, A., Jan, Y. N. and Utset, M. F. (2002). Tetralogy of fallot and other congenital heart defects in Hey2 mutant mice. *Curr Biol* **12**, 1605-10.

Duarte, A., Hirashima, M., Benedito, R., Trindade, A., Diniz, P., Bekman, E., Costa, L., Henrique, D. and Rossant, J. (2004). Dosage-sensitive requirement for mouse Dll4 in artery development. *Genes Dev* **18**, 2474-8.

Dubroca, C., Lacombe, P., Domenga, V., Maciazek, J., Levy, B., Tournier-Lasserve, E., Joutel, A. and Henrion, D. (2005). Impaired vascular mechanotransduction in a transgenic mouse model of CADASIL arteriopathy. *Stroke* **36**, 113-7.

Dunwoodie, S. L. (2007). Combinatorial signaling in the heart orchestrates cardiac induction, lineage specification and chamber formation. *Semin Cell Dev Biol* **18**, 54-66.

Dupe, V., Ghyselinck, N. B., Wendling, O., Chambon, P. and Mark, M. (1999). Key roles of retinoic acid receptors alpha and beta in the patterning of the caudal hindbrain, pharyngeal arches and otocyst in the mouse. *Development* **126**, 5051-9.

Echeverri, K. and Oates, A. C. (2007). Coordination of symmetric cyclic gene expression during somitogenesis by Suppressor of Hairless involves regulation of retinoic acid catabolism. *Dev Biol* **301**, 388-403.

Edelmann, L., Pandita, R. K. and Morrow, B. E. (1999a). Low-copy repeats mediate the common 3-Mb deletion in patients with velo-cardio-facial syndrome. *Am J Hum Genet* **64**, 1076-86.

Edelmann, L., Pandita, R. K., Spiteri, E., Funke, B., Goldberg, R., Palanisamy, N., Chaganti, R. S., Magenis, E., Shprintzen, R. J. and Morrow, B. E. (1999b). A common molecular basis for rearrangement disorders on chromosome 22q11. *Hum Mol Genet* **8**, 1157-67.

Edelmann, L., Spiteri, E., Koren, K., Pulijaal, V., Bialer, M. G., Shanske, A., Goldberg, R. and Morrow, B. E. (2001a). AT-rich palindromes mediate the constitutional t(11;22) translocation. *Am J Hum Genet* **68**, 1-13.

Edelmann, L., Spiteri, E., McCain, N., Goldberg, R., Pandita, R. K., Duong, S., Fox, J., Blumenthal, D., Lalani, S. R., Shaffer, L. G. et al. (1999c). A common breakpoint on 11q23 in carriers of the constitutional t(11;22) translocation. *Am J Hum Genet* **65**, 1608-16.

Edelmann, L., Stankiewicz, P., Spiteri, E., Pandita, R. K., Shaffer, L., Lupski, J. R. and Morrow, B. E. (2001b). Two functional copies of the DGCR6 gene are present on human chromosome 22q11 due to a duplication of an ancestral locus. *Genome Res* **11**, 208-17.

Elnitski, L., Li, J., Noguchi, C. T., Miller, W. and Hardison, R. (2001). A negative cis-element regulates the level of enhancement by hypersensitive site 2 of the beta-globin locus control region. *J Biol Chem* **276**, 6289-98.

Epstein, J. A., Li, J., Lang, D., Chen, F., Brown, C. B., Jin, F., Lu, M. M., Thomas, M., Liu, E., Wessels, A. et al. (2000). Migration of cardiac neural crest cells in Splotch embryos. *Development* **127**, 1869-78.

Eshkind, L., Tian, Q., Schmidt, A., Franke, W. W., Windoffer, R. and Leube, R. E. (2002). Loss of desmoglein 2 suggests essential functions for early embryonic development and proliferation of embryonal stem cells. *Eur J Cell Biol* **81**, 592-8.

Faas, B. H., De Vries, B. B., Van Es-Van Gaal, J., Merkx, G., Draaisma, J. M. and Smeets, D. F. (2002). A new case of dup(3q) syndrome due to a pure duplication of 3qter. *Clin Genet* **62**, 315-20.

Fagman, H., Grande, M., Gritli-Linde, A. and Nilsson, M. (2004). Genetic deletion of sonic hedgehog causes hemiagenesis and ectopic development of the thyroid in mouse. *Am J Pathol* **164**, 1865-72.

Fagman, H., Liao, J., Westerlund, J., Andersson, L., Morrow, B. E. and Nilsson, M. (2007). The 22q11 deletion syndrome candidate gene Tbx1 determines thyroid size and positioning. *Hum Mol Genet* **16**, 276-85.

Farin, H. F., Bussen, M., Schmidt, M. K., Singh, M. K., Schuster-Gossler, K. and Kispert, A. (2007). Transcriptional repression by the T-box proteins Tbx18 and Tbx15 depends on Groucho corepressors. *J Biol Chem* **282**, 25748-59.

Farlie, P., Reid, C., Wilcox, S., Peeters, J., Reed, G. and Newgreen, D. (2001). Ypel1: a novel nuclear protein that induces an epithelial-like morphology in fibroblasts. *Genes Cells* **6**, 619-29.

Farrell, M. J., Stadt, H., Wallis, K. T., Scambler, P., Hixon, R. L., Wolfe, R., Leatherbury, L. and Kirby, M. L. (1999). HIRA, a DiGeorge syndrome candidate gene, is required for cardiac outflow tract septation. *Circ Res* **84**, 127-35.

Feil, R., Wagner, J., Metzger, D. and Chambon, P. (1997). Regulation of Cre recombinase activity by mutated estrogen receptor ligand-binding domains. *Biochem Biophys Res Commun* **237**, 752-7.

Feiner, L., Webber, A. L., Brown, C. B., Lu, M. M., Jia, L., Feinstein, P., Mombaerts, P., Epstein, J. A. and Raper, J. A. (2001). Targeted disruption of semaphorin 3C leads to persistent truncus arteriosus and aortic arch interruption. *Development* **128**, 3061-70.

Felli, M. P., Maroder, M., Mitsiadis, T. A., Campese, A. F., Bellavia, D., Vacca, A., Mann, R. S., Frati, L., Lendahl, U., Gulino, A. et al. (1999). Expression pattern of notch1, 2 and 3 and Jagged1 and 2 in lymphoid and stromal thymus components: distinct ligand-receptor interactions in intrathymic T cell development. *Int Immunol* **11**, 1017-25.

Fischer, A. and Gessler, M. (2003). Hey genes in cardiovascular development. *Trends Cardiovasc Med* **13**, 221-6.

Fischer, A. and Gessler, M. (2007). Delta-Notch--and then? Protein interactions and proposed modes of repression by Hes and Hey bHLH factors. *Nucleic Acids Res* **35**, 4583-96.

Fischer, A., Klamt, B., Schumacher, N., Glaeser, C., Hansmann, I., Fenge, H. and Gessler, M. (2004a). Phenotypic variability in Hey2 -/- mice and absence of HEY2 mutations in patients with congenital heart defects or Alagille syndrome. *Mamm Genome* **15**, 711-6.

Fischer, A., Leimeister, C., Winkler, C., Schumacher, N., Klamt, B., Elmasri, H., Steidl, C., Maier, M., Knobeloch, K. P., Amann, K. et al. (2002). Hey bHLH factors in cardiovascular development. *Cold Spring Harb Symp Quant Biol* **67**, 63-70.

Fischer, A., Schumacher, N., Maier, M., Sendtner, M. and Gessler, M. (2004b). The Notch target genes Hey1 and Hey2 are required for embryonic vascular development. *Genes Dev* **18**, 901-11.

Fischer, A., Steidl, C., Wagner, T. U., Lang, E., Jakob, P. M., Friedl, P., Knobeloch, K. P. and Gessler, M. (2007). Combined loss of Hey1 and HeyL causes congenital heart defects because of impaired epithelial to mesenchymal transition. *Circ Res* **100**, 856-63.

Fraccaro, M., Lindsten, J., Ford, C. E. and Iselius, L. (1980). The 11q;22q translocation: a European collaborative analysis of 43 cases. *Hum Genet* **56**, 21-51.

Franco, D., Meilhac, S. M., Christoffels, V. M., Kispert, A., Buckingham, M. and Kelly, R. G. (2006). Left and right ventricular contributions to the formation of the interventricular septum in the mouse heart. *Dev Biol* **294**, 366-75.

Frank, D. U., Fotheringham, L. K., Brewer, J. A., Muglia, L. J., Tristani-Firouzi, M., Capecchi, M. R. and Moon, A. M. (2002). An Fgf8 mouse mutant phenocopies human 22q11 deletion syndrome. *Development* **129**, 4591-603.

Frebourg, T., Oliveira, C., Hochain, P., Karam, R., Manouvrier, S., Graziadio, C., Vekemans, M., Hartmann, A., Baert-Desurmont, S., Alexandre, C. et al. (2006). Cleft lip/palate and CDH1/E-cadherin mutations in families with hereditary diffuse gastric cancer. *J Med Genet* **43**, 138-42.

Fujii, H., Sato, T., Kaneko, S., Gotoh, O., Fujii-Kuriyama, Y., Osawa, K., Kato, S. and Hamada, H. (1997). Metabolic inactivation of retinoic acid by a novel P450 differentially expressed in developing mouse embryos. *Embo J* **16**, 4163-73.

Funke, B., Edelmann, L., McCain, N., Pandita, R. K., Ferreira, J., Merscher, S., Zohouri, M., Cannizzaro, L., Shanske, A. and Morrow, B. E. (1999). Der(22) syndrome and velo-cardio-facial syndrome/DiGeorge syndrome share a 1.5-Mb region of overlap on chromosome 22q11. *Am J Hum Genet* **64**, 747-58.

Funke, B., Epstein, J. A., Kochilas, L. K., Lu, M. M., Pandita, R. K., Liao, J., Bauerndistel, R., Schuler, T., Schorle, H., Brown, M. C. et al. (2001). Mice

overexpressing genes from the 22q11 region deleted in velo-cardio-facial syndrome/DiGeorge syndrome have middle and inner ear defects. *Hum Mol Genet* **10**, 2549-56.

Gale, N. W., Dominguez, M. G., Noguera, I., Pan, L., Hughes, V., Valenzuela, D. M., Murphy, A. J., Adams, N. C., Lin, H. C., Holash, J. et al. (2004). Haploinsufficiency of delta-like 4 ligand results in embryonic lethality due to major defects in arterial and vascular development. *Proc Natl Acad Sci U S A* **101**, 15949-54.

Galvin, K. M., Donovan, M. J., Lynch, C. A., Meyer, R. I., Paul, R. J., Lorenz, J. N., Fairchild-Huntress, V., Dixon, K. L., Dunmore, J. H., Gimbrone, M. A., Jr. et al. (2000). A role for smad6 in development and homeostasis of the cardiovascular system. *Nat Genet* **24**, 171-4.

Gangwani, L., Flavell, R. A. and Davis, R. J. (2005). ZPR1 is essential for survival and is required for localization of the survival motor neurons (SMN) protein to Cajal bodies. *Mol Cell Biol* **25**, 2744-56.

Gangwani, L., Mikrut, M., Theroux, S., Sharma, M. and Davis, R. J. (2001). Spinal muscular atrophy disrupts the interaction of ZPR1 with the SMN protein. *Nat Cell Biol* **3**, 376-83.

Garcia-Martinez, V. and Schoenwolf, G. C. (1993). Primitive-streak origin of the cardiovascular system in avian embryos. *Dev Biol* **159**, 706-19.

Garg, V., Kathiriya, I. S., Barnes, R., Schluterman, M. K., King, I. N., Butler, C. A., Rothrock, C. R., Eapen, R. S., Hirayama-Yamada, K., Joo, K. et al. (2003). GATA4 mutations cause human congenital heart defects and reveal an interaction with TBX5. *Nature* **424**, 443-7.

Garg, V., Yamagishi, C., Hu, T., Kathiriya, I. S., Yamagishi, H. and Srivastava, D. (2001). Tbx1, a DiGeorge syndrome candidate gene, is regulated by sonic hedgehog during pharyngeal arch development. *Dev Biol* **235**, 62-73.

Garner, M. M. and Revzin, A. (1981). A gel electrophoresis method for quantifying the binding of proteins to specific DNA regions: application to components of the Escherichia coli lactose operon regulatory system. *Nucleic Acids Res* **9**, 3047-60.

Gaussin, V., Van de Putte, T., Mishina, Y., Hanks, M. C., Zwijsen, A., Huylebroeck, D., Behringer, R. R. and Schneider, M. D. (2002). Endocardial cushion and myocardial defects after cardiac myocyte-specific conditional deletion of the bone morphogenetic protein receptor ALK3. *Proc Natl Acad Sci U S A* **99**, 2878-83.

Gavalas, A., Trainor, P., Ariza-McNaughton, L. and Krumlauf, R. (2001). Synergy between Hoxa1 and Hoxb1: the relationship between arch patterning and the generation of cranial neural crest. *Development* **128**, 3017-27.

Gengrinovitch, S., Greenberg, S. M., Cohen, T., Gitay-Goren, H., Rockwell, P., Maione, T. E., Levi, B. Z. and Neufeld, G. (1995). Platelet factor-4 inhibits the mitogenic activity of VEGF121 and VEGF165 using several concurrent mechanisms. *J Biol Chem* **270**, 15059-65.

Gessler, M., Knobeloch, K. P., Helisch, A., Amann, K., Schumacher, N., Rohde, E., Fischer, A. and Leimeister, C. (2002). Mouse gridlock: no aortic coarctation or deficiency, but fatal cardiac defects in Hey2 -/- mice. *Curr Biol* **12**, 1601-4.

Ghosh, T. K., Packham, E. A., Bonser, A. J., Robinson, T. E., Cross, S. J. and Brook, J. D. (2001). Characterization of the TBX5 binding site and analysis of mutations that cause Holt-Oram syndrome. *Hum Mol Genet* **10**, 1983-94.

Gilligan, P., Brenner, S. and Venkatesh, B. (2002). Fugu and human sequence comparison identifies novel human genes and conserved non-coding sequences. *Gene* **294**, 35-44.

Gitler, A. D., Lu, M. M. and Epstein, J. A. (2004). PlexinD1 and semaphorin signaling are required in endothelial cells for cardiovascular development. *Dev Cell* **7**, 107-16.

Gitler, A. D., Lu, M. M., Jiang, Y. Q., Epstein, J. A. and Gruber, P. J. (2003). Molecular markers of cardiac endocardial cushion development. *Dev Dyn* **228**, 643-50.

Goddeeris, M. M., Schwartz, R., Klingensmith, J. and Meyers, E. N. (2007). Independent requirements for Hedgehog signaling by both the anterior heart field and neural crest cells for outflow tract development. *Development* **134**, 1593-604.

Gogos, J. A., Morgan, M., Luine, V., Santha, M., Ogawa, S., Pfaff, D. and Karayiorgou, M. (1998). Catechol-O-methyltransferase-deficient mice exhibit sexually dimorphic changes in catecholamine levels and behavior. *Proc Natl Acad Sci U S A* **95**, 9991-6.

Gogos, J. A., Santha, M., Takacs, Z., Beck, K. D., Luine, V., Lucas, L. R., Nadler, J. V. and Karayiorgou, M. (1999). The gene encoding proline dehydrogenase modulates sensorimotor gating in mice. *Nat Genet* **21**, 434-9.

Gottlieb, P. D., Pierce, S. A., Sims, R. J., Yamagishi, H., Weihe, E. K., Harriss, J. V., Maika, S. D., Kuziel, W. A., King, H. L., Olson, E. N. et al. (2002). Bop encodes a muscle-restricted protein containing MYND and SET domains and is essential for cardiac differentiation and morphogenesis. *Nat Genet* **31**, 25-32.

Graham, A. (2003). Development of the pharyngeal arches. *Am J Med Genet A* **119**, 251-6.

Graham, A., Begbie, J. and McGonnell, I. (2004). Significance of the cranial neural crest. *Dev Dyn* **229**, 5-13.

Graham, A. and Smith, A. (2001). Patterning the pharyngeal arches. *Bioessays* **23**, 54-61.

Grammatopoulos, G. A., Bell, E., Toole, L., Lumsden, A. and Tucker, A. S. (2000). Homeotic transformation of branchial arch identity after Hoxa2 overexpression. *Development* **127**, 5355-65.

Grbavec, D. and Stifani, S. (1996). Molecular interaction between TLE1 and the carboxyl-terminal domain of HES-1 containing the WRPW motif. *Biochem Biophys Res Commun* **223**, 701-5.

Gritli-Linde, A. (2007). Molecular control of secondary palate development. *Dev Biol* **301**, 309-26.

Gruber, P. J. and Epstein, J. A. (2004). Development gone awry: congenital heart disease. *Circ Res* **94**, 273-83.

Gu, C., Rodriguez, E. R., Reimert, D. V., Shu, T., Fritzsch, B., Richards, L. J., Kolodkin, A. L. and Ginty, D. D. (2003). Neuropilin-1 conveys semaphorin and VEGF signaling during neural and cardiovascular development. *Dev Cell* **5**, 45-57.

Guris, D. L., Duester, G., Papaioannou, V. E. and Imamoto, A. (2006). Dose-dependent interaction of Tbx1 and Crkl and locally aberrant RA signaling in a model of del22q11 syndrome. *Dev Cell* **10**, 81-92.

Guris, D. L., Fantes, J., Tara, D., Druker, B. J. and Imamoto, A. (2001). Mice lacking the homologue of the human 22q11.2 gene CRKL phenocopy neurocristopathies of DiGeorge syndrome. *Nat Genet* **27**, 293-8.

Habas, R., Kato, Y. and He, X. (2001). Wnt/Frizzled activation of Rho regulates vertebrate gastrulation and requires a novel Formin homology protein Daam1. *Cell* **107**, 843-54.

Habets, P. E., Moorman, A. F., Clout, D. E., van Roon, M. A., Lingbeek, M., van Lohuizen, M., Campione, M. and Christoffels, V. M. (2002). Cooperative action of

Tbx2 and Nkx2.5 inhibits ANF expression in the atrioventricular canal: implications for cardiac chamber formation. *Genes Dev* **16**, 1234-46.

Hacker, A. and Guthrie, S. (1998). A distinct developmental programme for the cranial paraxial mesoderm in the chick embryo. *Development* **125**, 3461-72.

Hamada, Y., Kadokawa, Y., Okabe, M., Ikawa, M., Coleman, J. R. and Tsujimoto, Y. (1999). Mutation in ankyrin repeats of the mouse Notch2 gene induces early embryonic lethality. *Development* **126**, 3415-24.

Hamblet, N. S., Lijam, N., Ruiz-Lozano, P., Wang, J., Yang, Y., Luo, Z., Mei, L., Chien, K. R., Sussman, D. J. and Wynshaw-Boris, A. (2002). Dishevelled 2 is essential for cardiac outflow tract development, somite segmentation and neural tube closure. *Development* **129**, 5827-38.

Hartman, J., Muller, P., Foster, J. S., Wimalasena, J., Gustafsson, J. A. and Strom, A. (2004). HES-1 inhibits 17beta-estradiol and heregulin-beta1-mediated upregulation of E2F-1. *Oncogene* **23**, 8826-33.

Hasegawa, S., Sato, T., Akazawa, H., Okada, H., Maeno, A., Ito, M., Sugitani, Y., Shibata, H., Miyazaki Ji, J., Katsuki, M. et al. (2002). Apoptosis in neural crest cells by functional loss of APC tumor suppressor gene. *Proc Natl Acad Sci U S A* **99**, 297-302.

Hashimoto, T., Zhang, X. M., Chen, B. Y. and Yang, X. J. (2006). VEGF activates divergent intracellular signaling components to regulate retinal progenitor cell proliferation and neuronal differentiation. *Development* **133**, 2201-10.

Hatakeyama, J., Bessho, Y., Katoh, K., Ookawara, S., Fujioka, M., Guillemot, F. and Kageyama, R. (2004). Hes genes regulate size, shape and histogenesis of the nervous system by control of the timing of neural stem cell differentiation. *Development* **131**, 5539-50.

Hatakeyama, J., Sakamoto, S. and Kageyama, R. (2006). Hes1 and Hes5 regulate the development of the cranial and spinal nerve systems. *Dev Neurosci* **28**, 92-101.

He, M., Wen, L., Campbell, C. E., Wu, J. Y. and Rao, Y. (1999). Transcription repression by Xenopus ET and its human ortholog TBX3, a gene involved in ulnar-mammary syndrome. *Proc Natl Acad Sci U S A* **96**, 10212-7.

Heasman, J. (2002). Morpholino oligos: making sense of antisense? *Dev Biol* **243**, 209-14.

Heathcote, K., Braybrook, C., Abushaban, L., Guy, M., Khetyar, M. E., Patton, M. A., Carter, N. D., Scambler, P. J. and Syrris, P. (2005). Common arterial trunk associated with a homeodomain mutation of NKX2.6. *Hum Mol Genet* **14**, 585-93.

Heimbucher, T., Murko, C., Bajoghli, B., Aghaallaei, N., Huber, A., Stebegg, R., Eberhard, D., Fink, M., Simeone, A. and Czerny, T. (2007). Gbx2 and Otx2 interact with the WD40 domain of Groucho/Tle corepressors. *Mol Cell Biol* **27**, 340-51.

Heisterkamp, N. and Groffen, J. (1988). Duplication of the bcr and gamma-glutamyl transpeptidase genes. *Nucleic Acids Res* **16**, 8045-56.

Helms, J. A., Kim, C. H., Hu, D., Minkoff, R., Thaller, C. and Eichele, G. (1997). Sonic hedgehog participates in craniofacial morphogenesis and is down-regulated by teratogenic doses of retinoic acid. *Dev Biol* **187**, 25-35.

Herrmann, B. G., Labeit, S., Poustka, A., King, T. R. and Lehrach, H. (1990). Cloning of the T gene required in mesoderm formation in the mouse. *Nature* **343**, 617-22.

Hierck, B. P., Molin, D. G., Boot, M. J., Poelmann, R. E. and Gittenberger-de Groot, A. C. (2004). A chicken model for DGCR6 as a modifier gene in the DiGeorge critical region. *Pediatr Res* **56**, 440-8.

High, F. A., Zhang, M., Proweller, A., Tu, L., Parmacek, M. S., Pear, W. S. and Epstein, J. A. (2007). An essential role for Notch in neural crest during cardiovascular development and smooth muscle differentiation. *J Clin Invest* **117**, 353-63.

Hildebrand, J. D. and Soriano, P. (2002). Overlapping and unique roles for C-terminal binding protein 1 (CtBP1) and CtBP2 during mouse development. *Mol Cell Biol* **22**, 5296-307.

Hilfer, S. R. and Brown, J. W. (1984). The development of pharyngeal endocrine organs in mouse and chick embryos. *Scan Electron Microsc*, 2009-22.

Hirata, H., Bessho, Y., Kokubu, H., Masamizu, Y., Yamada, S., Lewis, J. and Kageyama, R. (2004). Instability of Hes7 protein is crucial for the somite segmentation clock. *Nat Genet* **36**, 750-4.

Hirata, H., Ohtsuka, T., Bessho, Y. and Kageyama, R. (2000). Generation of structurally and functionally distinct factors from the basic helix-loop-helix gene Hes3 by alternative first exons. *J Biol Chem* **275**, 19083-9.

Hirata, H., Tomita, K., Bessho, Y. and Kageyama, R. (2001). Hes1 and Hes3 regulate maintenance of the isthmic organizer and development of the mid/hindbrain. *Embo J* **20**, 4454-66.

Hirata, H., Yoshiura, S., Ohtsuka, T., Bessho, Y., Harada, T., Yoshikawa, K. and Kageyama, R. (2002). Oscillatory expression of the bHLH factor Hes1 regulated by a negative feedback loop. *Science* **298**, 840-3.

Hiroi, Y., Kudoh, S., Monzen, K., Ikeda, Y., Yazaki, Y., Nagai, R. and Komuro, I. (2001). Tbx5 associates with Nkx2-5 and synergistically promotes cardiomyocyte differentiation. *Nat Genet* **28**, 276-80.

Hirotsune, S., Fleck, M. W., Gambello, M. J., Bix, G. J., Chen, A., Clark, G. D., Ledbetter, D. H., McBain, C. J. and Wynshaw-Boris, A. (1998). Graded reduction of Pafah1b1 (Lis1) activity results in neuronal migration defects and early embryonic lethality. *Nat Genet* **19**, 333-9.

Hirotsune, S., Pack, S. D., Chong, S. S., Robbins, C. M., Pavan, W. J., Ledbetter, D. H. and Wynshaw-Boris, A. (1997). Genomic organization of the murine Miller-Dieker/lissencephaly region: conservation of linkage with the human region. *Genome Res* **7**, 625-34.

Hocevar, B. A., Smine, A., Xu, X. X. and Howe, P. H. (2001). The adaptor molecule Disabled-2 links the transforming growth factor beta receptors to the Smad pathway. *Embo J* **20**, 2789-801.

Hoeflich, K. P., Luo, J., Rubie, E. A., Tsao, M. S., Jin, O. and Woodgett, J. R. (2000). Requirement for glycogen synthase kinase-3beta in cell survival and NF-kappaB activation. *Nature* **406**, 86-90.

Hoffman, J. I. and Kaplan, S. (2002). The incidence of congenital heart disease. *J Am Coll Cardiol* **39**, 1890-900.

Hojo, M., Ohtsuka, T., Hashimoto, N., Gradwohl, G., Guillemot, F. and Kageyama, R. (2000). Glial cell fate specification modulated by the bHLH gene Hes5 in mouse retina. *Development* **127**, 2515-22.

Hoogaars, W. M., Barnett, P., Moorman, A. F. and Christoffels, V. M. (2007). T-box factors determine cardiac design. *Cell Mol Life Sci* **64**, 646-60.

Howe, J. R., Bair, J. L., Sayed, M. G., Anderson, M. E., Mitros, F. A., Petersen, G. M., Velculescu, V. E., Traverso, G. and Vogelstein, B. (2001). Germline mutations of the gene encoding bone morphogenetic protein receptor 1A in juvenile polyposis. *Nat Genet* **28**, 184-7.

Hrabe de Angelis, M., McIntyre, J., 2nd and Gossler, A. (1997). Maintenance of somite borders in mice requires the Delta homologue DII1. *Nature* **386**, 717-21.

Hu, T., Yamagishi, H., Maeda, J., McAnally, J., Yamagishi, C. and Srivastava, D. (2004). Tbx1 regulates fibroblast growth factors in the anterior heart field through a reinforcing autoregulatory loop involving forkhead transcription factors. *Development* **131**, 5491-502.

Huang, G., Lu, H., Hao, A., Ng, D. C., Ponniah, S., Guo, K., Lufei, C., Zeng, Q. and Cao, X. (2004). GRIM-19, a cell death regulatory protein, is essential for assembly and function of mitochondrial complex I. *Mol Cell Biol* **24**, 8447-56.

Hunt, P., Whiting, J., Nonchev, S., Sham, M. H., Marshall, H., Graham, A., Cook, M., Allemann, R., Rigby, P. W., Gulisano, M. et al. (1991). The branchial Hox code and its implications for gene regulation, patterning of the nervous system and head evolution. *Development* **Suppl 2**, 63-77.

Hutson, M. R. and Kirby, M. L. (2007). Model systems for the study of heart development and disease. Cardiac neural crest and conotruncal malformations. *Semin Cell Dev Biol* **18**, 101-10.

Hutson, M. R., Zhang, P., Stadt, H. A., Sato, A. K., Li, Y. X., Burch, J., Creazzo, T. L. and Kirby, M. L. (2006). Cardiac arterial pole alignment is sensitive to FGF8 signaling in the pharynx. *Dev Biol.*

Huynh, T., Chen, L., Terrell, P. and Baldini, A. (2007). A fate map of Tbx1 expressing cells reveals heterogeneity in the second cardiac field. *Genesis* **45**, 470-5.

Ikeya, M., Lee, S. M., Johnson, J. E., McMahon, A. P. and Takada, S. (1997). Wnt signalling required for expansion of neural crest and CNS progenitors. *Nature* **389**, 966-70.

Ilagan, R., Abu-Issa, R., Brown, D., Yang, Y. P., Jiao, K., Schwartz, R. J., Klingensmith, J. and Meyers, E. N. (2006). Fgf8 is required for anterior heart field development. *Development* **133**, 2435-45.

Ingram, W. J., McCue, K. I., Tran, T. H., Hallahan, A. R. and Wainwright, B. J. (2007). Sonic Hedgehog regulates Hes1 through a novel mechanism that is independent of canonical Notch pathway signalling. *Oncogene.*

Iscove, N. N., Barbara, M., Gu, M., Gibson, M., Modi, C. and Winegarden, N. (2002). Representation is faithfully preserved in global cDNA amplified exponentially from sub-picogram quantities of mRNA. *Nat Biotechnol* **20**, 940-3.

Ishibashi, M., Ang, S. L., Shiota, K., Nakanishi, S., Kageyama, R. and Guillemot, F. (1995). Targeted disruption of mammalian hairy and Enhancer of split homolog-1 (HES-1) leads to up-regulation of neural helix-loop-helix factors, premature neurogenesis, and severe neural tube defects. *Genes Dev* **9**, 3136-48.

Ishibashi, M., Sasai, Y., Nakanishi, S. and Kageyama, R. (1993). Molecular characterization of HES-2, a mammalian helix-loop-helix factor structurally related to Drosophila hairy and Enhancer of split. *Eur J Biochem* **215**, 645-52.

Iso, T., Kedes, L. and Hamamori, Y. (2003). HES and HERP families: multiple effectors of the Notch signaling pathway. *J Cell Physiol* **194**, 237-55.

Iso, T., Sartorelli, V., Chung, G., Shichinohe, T., Kedes, L. and Hamamori, Y. (2001a). HERP, a new primary target of Notch regulated by ligand binding. *Mol Cell Biol* **21**, 6071-9.

Iso, T., Sartorelli, V., Poizat, C., Iezzi, S., Wu, H. Y., Chung, G., Kedes, L. and Hamamori, Y. (2001b). HERP, a novel heterodimer partner of HES/E(spl) in Notch signaling. *Mol Cell Biol* **21**, 6080-9.

Ito, T., Udaka, N., Yazawa, T., Okudela, K., Hayashi, H., Sudo, T., Guillemot, F., Kageyama, R. and Kitamura, H. (2000). Basic helix-loop-helix transcription factors regulate the neuroendocrine differentiation of fetal mouse pulmonary epithelium. *Development* **127**, 3913-21.

Ivins, S., Lammerts van Beuren, K., Roberts, C., James, C., Lindsay, E., Baldini, A., Ataliotis, P. and Scambler, P. J. (2005). Microarray analysis detects differentially expressed genes in the pharyngeal region of mice lacking Tbx1. *Dev Biol* **285**, 554-69.

Jalali, G. R., Vorstman, J. A., Errami, A., Vijzelaar, R., Biegel, J., Shaikh, T. and Emanuel, B. S. (2007). Detailed analysis of 22q11.2 with a high density MLPA probe set. *Hum Mutat.*

Jamieson, R. V., Perveen, R., Kerr, B., Carette, M., Yardley, J., Heon, E., Wirth, M. G., van Heyningen, V., Donnai, D., Munier, F. et al. (2002). Domain disruption and mutation of the bZIP transcription factor, MAF, associated with cataract, ocular anterior segment dysgenesis and coloboma. *Hum Mol Genet* **11**, 33-42.

Jarriault, S., Le Bail, O., Hirsinger, E., Pourquie, O., Logeat, F., Strong, C. F., Brou, C., Seidah, N. G. and Isra l, A. (1998). Delta-1 activation of notch-1 signaling results in HES-1 transactivation. *Mol Cell Biol* **18**, 7423-31.

Jasin, M. and Zalamea, P. (1992). Analysis of Escherichia coli beta-galactosidase expression in transgenic mice by flow cytometry of sperm. *Proc Natl Acad Sci U S A* **89**, 10681-5.

Jensen, J., Pedersen, E. E., Galante, P., Hald, J., Heller, R. S., Ishibashi, M., Kageyama, R., Guillemot, F., Serup, P. and Madsen, O. D. (2000). Control of endodermal endocrine development by Hes-1. *Nat Genet* **24**, 36-44.

Jerome, L. A. and Papaioannou, V. E. (2001). DiGeorge syndrome phenotype in mice mutant for the T-box gene, Tbx1. *Nat Genet* **27**, 286-91.

Jerome-Majewska, L. A., Jenkins, G. P., Ernstoff, E., Zindy, F., Sherr, C. J. and Papaioannou, V. E. (2005). Tbx3, the ulnar-mammary syndrome gene, and Tbx2 interact in mammary gland development through a p19Arf/p53-independent pathway. *Dev Dyn* **234**, 922-33.

Ji, W., Zhou, W., Gregg, K., Lindpaintner, K., Davis, S. and Davis, S. (2004). A method for gene expression analysis by oligonucleotide arrays from minute biological materials. *Anal Biochem* **331**, 329-39.

Jiang, X., Rowitch, D. H., Soriano, P., McMahon, A. P. and Sucov, H. M. (2000). Fate of the mammalian cardiac neural crest. *Development* **127**, 1607-16.

Johnson, D. S., Mortazavi, A., Myers, R. M. and Wold, B. (2007). Genome-wide mapping of in vivo protein-DNA interactions. *Science* **316**, 1497-502.

Jokiaho, I., Salo, A., Niemi, K. M., Blomstedt, G. C. and Pihkala, J. (1989). Deletion 3q27----3qter in an infant with mild dysmorphism, parietal meningocele, and neonatal miliaria rubra-like lesions. *Hum Genet* **83**, 302-4.

Joutel, A., Corpechot, C., Ducros, A., Vahedi, K., Chabriat, H., Mouton, P., Alamowitch, S., Domenga, V., Cecillion, M., Marechal, E. et al. (1996). Notch3 mutations in CADASIL, a hereditary adult-onset condition causing stroke and dementia. *Nature* **383**, 707-10.

Jouve, C., Palmeirim, I., Henrique, D., Beckers, J., Gossler, A., Ish-Horowicz, D. and Pourquie, O. (2000). Notch signalling is required for cyclic expression of the hairy-like gene HES1 in the presomitic mesoderm. *Development* **127**, 1421-9.

Kaartinen, V., Dudas, M., Nagy, A., Sridurongrit, S., Lu, M. M. and Epstein, J. A. (2004). Cardiac outflow tract defects in mice lacking ALK2 in neural crest cells. *Development* **131**, 3481-90.

Kaern, M., Elston, T. C., Blake, W. J. and Collins, J. J. (2005). Stochasticity in gene expression: from theories to phenotypes. *Nat Rev Genet* **6**, 451-64.

Kageyama, R., Ohtsuka, T. and Kobayashi, T. (2007). The Hes gene family: repressors and oscillators that orchestrate embryogenesis. *Development* **134**, 1243-51.

Kalajzic, I., Staal, A., Yang, W. P., Wu, Y., Johnson, S. E., Feyen, J. H., Krueger, W., Maye, P., Yu, F., Zhao, Y. et al. (2005). Expression profile of osteoblast lineage at defined stages of differentiation. *J Biol Chem* **280**, 24618-26.

Kamakura, S., Oishi, K., Yoshimatsu, T., Nakafuku, M., Masuyama, N. and Gotoh, Y. (2004). Hes binding to STAT3 mediates crosstalk between Notch and JAK-STAT signalling. *Nat Cell Biol* **6**, 547-54.

Kamath, S. G., Chen, N., Enkemann, S. A. and Sanchez-Ramos, J. (2005). Transcriptional profile of NeuroD expression in a human fetal astroglial cell line. *Gene Expr* **12**, 123-36.

Kaneta, M., Osawa, M., Sudo, K., Nakauchi, H., Farr, A. G. and Takahama, Y. (2000). A role for pref-1 and HES-1 in thymocyte development. *J Immunol* **164**, 256-64.

Karim, F. D., Guild, G. M. and Thummel, C. S. (1993). The Drosophila Broad-Complex plays a key role in controlling ecdysone-regulated gene expression at the onset of metamorphosis. *Development* **118**, 977-88.

Karmakar, R. and Bose, I. (2006). Stochastic model of transcription factor-regulated gene expression. *Phys Biol* **3**, 200-8.

Kawasaki, T., Kitsukawa, T., Bekku, Y., Matsuda, Y., Sanbo, M., Yagi, T. and Fujisawa, H. (1999). A requirement for neuropilin-1 in embryonic vessel formation. *Development* **126**, 4895-902.

Keith Ho, H. C., McGrath, K. E., Brodbeck, K. C., Palis, J. and Schick, B. P. (2001). Serglycin proteoglycan synthesis in the murine uterine decidua and early embryo. *Biol Reprod* **64**, 1667-76.

Kelly, K. F. and Daniel, J. M. (2006). POZ for effect--POZ-ZF transcription factors in cancer and development. *Trends Cell Biol* **16**, 578-87.

Kelly, R. G., Brown, N. A. and Buckingham, M. E. (2001). The arterial pole of the mouse heart forms from Fgf10-expressing cells in pharyngeal mesoderm. *Dev Cell* **1**, 435-40.

Kelly, R. G., Jerome-Majewska, L. A. and Papaioannou, V. E. (2004). The del22q11.2 candidate gene Tbx1 regulates branchiomeric myogenesis. *Hum Mol Genet* **13**, 2829-40.

Kelly, R. G. and Papaioannou, V. E. (2007). Visualization of outflow tract development in the absence of Tbx1 using an FgF10 enhancer trap transgene. *Dev Dyn* **236**, 821-8.

Kendziorski, C., Irizarry, R. A., Chen, K. S., Haag, J. D. and Gould, M. N. (2005). On the utility of pooling biological samples in microarray experiments. *Proc Natl Acad Sci U S A* **102**, 4252-7.

Kendziorski, C. M., Zhang, Y., Lan, H. and Attie, A. D. (2003). The efficiency of pooling mRNA in microarray experiments. *Biostatistics* **4**, 465-77.

Kim, T. H., Barrera, L. O., Qu, C., Van Calcar, S., Trinklein, N. D., Cooper, S. J., Luna, R. M., Glass, C. K., Rosenfeld, M. G., Myers, R. M. et al. (2005). Direct isolation and identification of promoters in the human genome. *Genome Res* **15**, 830-9.

Kimber, W. L., Hsieh, P., Hirotsune, S., Yuva-Paylor, L., Sutherland, H. F., Chen, A., Ruiz-Lozano, P., Hoogstraten-Miller, S. L., Chien, K. R., Paylor, R. et al.

(1999). Deletion of 150 kb in the minimal DiGeorge/velocardiofacial syndrome critical region in mouse. *Hum Mol Genet* **8**, 2229-37.

Kirby, M. L., Gale, T. F. and Stewart, D. E. (1983). Neural crest cells contribute to normal aorticopulmonary septation. *Science* **220**, 1059-61.

Kirby, M. L. and Waldo, K. L. (1995). Neural crest and cardiovascular patterning. *Circ Res* **77**, 211-5.

Kirk, E. P., Sunde, M., Costa, M. W., Rankin, S. A., Wolstein, O., Castro, M. L., Butler, T. L., Hyun, C., Guo, G., Otway, R. et al. (2007). Mutations in cardiac T-box factor gene TBX20 are associated with diverse cardiac pathologies, including defects of septation and valvulogenesis and cardiomyopathy. *Am J Hum Genet* **81**, 280-91.

Kispert, A. and Herrmann, B. G. (1993). The Brachyury gene encodes a novel DNA binding protein. *Embo J* **12**, 3211-20.

Kita, A., Imayoshi, I., Hojo, M., Kitagawa, M., Kokubu, H., Ohsawa, R., Ohtsuka, T., Kageyama, R. and Hashimoto, N. (2007). Hes1 and Hes5 control the progenitor pool, intermediate lobe specification, and posterior lobe formation in the pituitary development. *Mol Endocrinol* **21**, 1458-66.

Kitamoto, T., Takahashi, K., Takimoto, H., Tomizuka, K., Hayasaka, M., Tabira, T. and Hanaoka, K. (2005). Functional redundancy of the Notch gene family during mouse embryogenesis: analysis of Notch gene expression in Notch3-deficient mice. *Biochem Biophys Res Commun* **331**, 1154-62.

Kitamura, K., Miura, H., Miyagawa-Tomita, S., Yanazawa, M., Katoh-Fukui, Y., Suzuki, R., Ohuchi, H., Suehiro, A., Motegi, Y., Nakahara, Y. et al. (1999). Mouse Pitx2 deficiency leads to anomalies of the ventral body wall, heart, extra- and periocular mesoderm and right pulmonary isomerism. *Development* **126**, 5749-58.

Kleinjan, D. A. and van Heyningen, V. (2005). Long-range control of gene expression: emerging mechanisms and disruption in disease. *Am J Hum Genet* **76**, 8-32.

Klur, S., Toy, K., Williams, M. P. and Certa, U. (2004). Evaluation of procedures for amplification of small-size samples for hybridization on microarrays. *Genomics* **83**, 508-17.

Kochilas, L., Merscher-Gomez, S., Lu, M. M., Potluri, V., Liao, J., Kucherlapati, R., Morrow, B. and Epstein, J. A. (2002). The role of neural crest during cardiac development in a mouse model of DiGeorge syndrome. *Dev Biol* **251**, 157-66.

Kochilas, L. K., Potluri, V., Gitler, A., Balasubramanian, K. and Chin, A. J. (2003). Cloning and characterization of zebrafish tbx1. *Gene Expr Patterns* **3**, 645-51.

Kodama, Y., Hijikata, M., Kageyama, R., Shimotohno, K. and Chiba, T. (2004). The role of notch signaling in the development of intrahepatic bile ducts. *Gastroenterology* **127**, 1775-86.

Koibuchi, N. and Chin, M. T. (2007). CHF1/Hey2 plays a pivotal role in left ventricular maturation through suppression of ectopic atrial gene expression. *Circ Res* **100**, 850-5.

Kokubo, H., Lun, Y. and Johnson, R. L. (1999). Identification and expression of a novel family of bHLH cDNAs related to Drosophila hairy and enhancer of split. *Biochem Biophys Res Commun* **260**, 459-65.

Kokubo, H., Miyagawa-Tomita, S., Nakazawa, M., Saga, Y. and Johnson, R. L. (2005). Mouse hesr1 and hesr2 genes are redundantly required to mediate Notch signaling in the developing cardiovascular system. *Dev Biol* **278**, 301-9.

Kokubo, H., Miyagawa-Tomita, S., Tomimatsu, H., Nakashima, Y., Nakazawa, M., Saga, Y. and Johnson, R. L. (2004). Targeted disruption of hesr2 results in atrioventricular valve anomalies that lead to heart dysfunction. *Circ Res* **95**, 540-7.

Kokubo, H., Tomita-Miyagawa, S., Hamada, Y. and Saga, Y. (2007). Hesr1 and Hesr2 regulate atrioventricular boundary formation in the developing heart through the repression of Tbx2. *Development* **134**, 747-55.

Koop, K. E., MacDonald, L. M. and Lobe, C. G. (1996). Transcripts of Grg4, a murine groucho-related gene, are detected in adjacent tissues to other murine neurogenic gene homologues during embryonic development. *Mech Dev* **59**, 73-87.

Kopinke, D., Sasine, J., Swift, J., Stephens, W. Z. and Piotrowski, T. (2006). Retinoic acid is required for endodermal pouch morphogenesis and not for pharyngeal endoderm specification. *Dev Dyn* **235**, spc1.

Koppel, A. M., Feiner, L., Kobayashi, H. and Raper, J. A. (1997). A 70 amino acid region within the semaphorin domain activates specific cellular response of semaphorin family members. *Neuron* **19**, 531-7.

Koshiba-Takeuchi, K., Takeuchi, J. K., Arruda, E. P., Kathiriya, I. S., Mo, R., Hui, C. C., Srivastava, D. and Bruneau, B. G. (2006). Cooperative and antagonistic interactions between Sall4 and Tbx5 pattern the mouse limb and heart. *Nat Genet* **38**, 175-83.

Kotarsky, H., Tabasum, I., Mannisto, S., Heikinheimo, M., Hansson, S. and Fellman, V. (2007). BCS1L is expressed in critical regions for neural development during ontogenesis in mice. *Gene Expr Patterns* **7**, 266-73.

Koyano-Nakagawa, N., Kim, J., Anderson, D. and Kintner, C. (2000). Hes6 acts in a positive feedback loop with the neurogenins to promote neuronal differentiation. *Development* **127**, 4203-16.

Kraus, F., Haenig, B. and Kispert, A. (2001). Cloning and expression analysis of the mouse T-box gene Tbx18. *Mech Dev* **100**, 83-6.

Krause, A., Zacharias, W., Camarata, T., Linkhart, B., Law, E., Lischke, A., Miljan, E. and Simon, H. G. (2004). Tbx5 and Tbx4 transcription factors interact with a new chicken PDZ-LIM protein in limb and heart development. *Dev Biol* **273**, 106-20.

Krebs, L. T., Shutter, J. R., Tanigaki, K., Honjo, T., Stark, K. L. and Gridley, T. (2004). Haploinsufficient lethality and formation of arteriovenous malformations in Notch pathway mutants. *Genes Dev* **18**, 2469-73.

Krebs, L. T., Xue, Y., Norton, C. R., Sundberg, J. P., Beatus, P., Lendahl, U., Joutel, A. and Gridley, T. (2003). Characterization of Notch3-deficient mice: normal embryonic development and absence of genetic interactions with a Notch1 mutation. *Genesis* **37**, 139-43.

Kume, T., Deng, K. Y., Winfrey, V., Gould, D. B., Walter, M. A. and Hogan, B. L. (1998). The forkhead/winged helix gene Mfl is disrupted in the pleiotropic mouse mutation congenital hydrocephalus. *Cell* **93**, 985-96.

Kume, T., Jiang, H., Topczewska, J. M. and Hogan, B. L. (2001). The murine winged helix transcription factors, Foxc1 and Foxc2, are both required for cardiovascular development and somitogenesis. *Genes Dev* **15**, 2470-82.

Kurahashi, H. and Emanuel, B. S. (2001). Long AT-rich palindromes and the constitutional t(11;22) breakpoint. *Hum Mol Genet* **10**, 2605-17.

Kurahashi, H., Shaikh, T. H., Hu, P., Roe, B. A., Emanuel, B. S. and Budarf, M. L. (2000). Regions of genomic instability on 22q11 and 11q23 as the etiology for the recurrent constitutional t(11;22). *Hum Mol Genet* **9**, 1665-70.

Kuroda, K., Tani, S., Tamura, K., Minoguchi, S., Kurooka, H. and Honjo, T. (1999). Delta-induced Notch signaling mediated by RBP-J inhibits MyoD expression and myogenesis. *J Biol Chem* **274**, 7238-44.

Kutejova, E., Engist, B., Mallo, M., Kanzler, B. and Bobola, N. (2005). Hoxa2 downregulates Six2 in the neural crest-derived mesenchyme. *Development* **132**, 469-78.

Kwang, S. J., Brugger, S. M., Lazik, A., Merrill, A. E., Wu, L. Y., Liu, Y. H., Ishii, M., Sangiorgi, F. O., Rauchman, M., Sucov, H. M. et al. (2002). Msx2 is an immediate downstream effector of Pax3 in the development of the murine cardiac neural crest. *Development* **129**, 527-38.

Kwee, L., Baldwin, H. S., Shen, H. M., Stewart, C. L., Buck, C., Buck, C. A. and Labow, M. A. (1995). Defective development of the embryonic and extraembryonic circulatory systems in vascular cell adhesion molecule (VCAM-1) deficient mice. *Development* **121**, 489-503.

Lai, C. Q., Parnell, L. D. and Ordovas, J. M. (2005). The APOA1/C3/A4/A5 gene cluster, lipid metabolism and cardiovascular disease risk. *Curr Opin Lipidol* **16**, 153-66.

Lambrechts, D. and Carmeliet, P. (2004). Genetics in zebrafish, mice, and humans to dissect congenital heart disease: insights in the role of VEGF. *Curr Top Dev Biol* **62**, 189-224.

Lamolet, B., Pulichino, A. M., Lamonerie, T., Gauthier, Y., Brue, T., Enjalbert, A. and Drouin, J. (2001). A pituitary cell-restricted T box factor, Tpit, activates POMC transcription in cooperation with Pitx homeoproteins. *Cell* **104**, 849-59.

Lampert, J. M., Holzschuh, J., Hessel, S., Driever, W., Vogt, K. and von Lintig, J. (2003). Provitamin A conversion to retinal via the beta,beta-carotene-15,15'-oxygenase (bcox) is essential for pattern formation and differentiation during zebrafish embryogenesis. *Development* **130**, 2173-86.

Lardelli, M., Dahlstrand, J. and Lendahl, U. (1994). The novel Notch homologue mouse Notch 3 lacks specific epidermal growth factor-repeats and is expressed in proliferating neuroepithelium. *Mech Dev* **46**, 123-36.

Laugwitz, K. L., Moretti, A., Lam, J., Gruber, P., Chen, Y., Woodard, S., Lin, L. Z., Cai, C. L., Lu, M. M., Reth, M. et al. (2005). Postnatal isl1+ cardioblasts enter fully differentiated cardiomyocyte lineages. *Nature* **433**, 647-53.

Le Lievre, C. S. and Le Douarin, N. M. (1975). Mesenchymal derivatives of the neural crest: analysis of chimaeric quail and chick embryos. *J Embryol Exp Morphol* **34**, 125-54.

Lee, E. C., Yu, D., Martinez de Velasco, J., Tessarollo, L., Swing, D. A., Court, D. L., Jenkins, N. A. and Copeland, N. G. (2001). A highly efficient Escherichia coli-based chromosome engineering system adapted for recombinogenic targeting and subcloning of BAC DNA. *Genomics* **73**, 56-65.

Lee, H. Y., Wroblewski, E., Philips, G. T., Stair, C. N., Conley, K., Reedy, M., Mastick, G. S. and Brown, N. L. (2005). Multiple requirements for Hes 1 during early eye formation. *Dev Biol* **284**, 464-78.

Lee, T. I., Johnstone, S. E. and Young, R. A. (2006). Chromatin immunoprecipitation and microarray-based analysis of protein location. *Nat Protoc* **1**, 729-48.

Leimeister, C., Dale, K., Fischer, A., Klamt, B., Hrabe de Angelis, M., Radtke, F., McGrew, M. J., Pourquie, O. and Gessler, M. (2000). Oscillating expression of c-Hey2 in the presomitic mesoderm suggests that the segmentation clock may use combinatorial signaling through multiple interacting bHLH factors. *Dev Biol* **227**, 91-103.

Leimeister, C., Externbrink, A., Klamt, B. and Gessler, M. (1999). Hey genes: a novel subfamily of hairy- and Enhancer of split related genes specifically expressed during mouse embryogenesis. *Mech Dev* **85**, 173-7.

Lemmers, C., Michel, D., Lane-Guermonprez, L., Delgrossi, M. H., Medina, E., Arsanto, J. P. and Le Bivic, A. (2004). CRB3 binds directly to Par6 and regulates the morphogenesis of the tight junctions in mammalian epithelial cells. *Mol Biol Cell* **15**, 1324-33.

Lettice, L. A., Heaney, S. J., Purdie, L. A., Li, L., de Beer, P., Oostra, B. A., Goode, D., Elgar, G., Hill, R. E. and de Graaff, E. (2003). A long-range Shh enhancer regulates expression in the developing limb and fin and is associated with preaxial polydactyly. *Hum Mol Genet* **12**, 1725-35.

Lettice, L. A., Horikoshi, T., Heaney, S. J., van Baren, M. J., van der Linde, H. C., Breedveld, G. J., Joosse, M., Akarsu, N., Oostra, B. A., Endo, N. et al. (2002). Disruption of a long-range cis-acting regulator for Shh causes preaxial polydactyly. *Proc Natl Acad Sci U S A* **99**, 7548-53.

Levy, A., Demczuk, S., Aurias, A., Depetris, D., Mattei, M. G. and Philip, N. (1995). Interstitial 22q11 microdeletion excluding the ADU breakpoint in a patient with DiGeorge syndrome. *Hum Mol Genet* **4**, 2417-9.

Lewandoski, M., Meyers, E. N. and Martin, G. R. (1997). Analysis of Fgf8 gene function in vertebrate development. *Cold Spring Harb Symp Quant Biol* **62**, 159-68.

Li, J., Chen, F. and Epstein, J. A. (2000). Neural crest expression of Cre recombinase directed by the proximal Pax3 promoter in transgenic mice. *Genesis* **26**, 162-4.

Li, Q. Y., Newbury-Ecob, R. A., Terrett, J. A., Wilson, D. I., Curtis, A. R., Yi, C. H., Gebuhr, T., Bullen, P. J., Robson, S. C., Strachan, T. et al. (1997). Holt-Oram syndrome is caused by mutations in TBX5, a member of the Brachyury (T) gene family. *Nat Genet* **15**, 21-9.

Liao, J., Kochilas, L., Nowotschin, S., Arnold, J. S., Aggarwal, V. S., Epstein, J. A., Brown, M. C., Adams, J. and Morrow, B. E. (2004). Full spectrum of malformations in velo-cardio-facial syndrome/DiGeorge syndrome mouse models by altering Tbx1 dosage. *Hum Mol Genet* **13**, 1577-85.

Lin, L., Bu, L., Cai, C. L., Zhang, X. and Evans, S. (2006). Isl1 is upstream of sonic hedgehog in a pathway required for cardiac morphogenesis. *Dev Biol* **295**, 756-63.

Lin, Q., Schwarz, J., Bucana, C. and Olson, E. N. (1997). Control of mouse cardiac morphogenesis and myogenesis by transcription factor MEF2C. *Science* **276**, 1404-7.

Lindsay, E. A. (2001). Chromosomal microdeletions: dissecting del22q11 syndrome. *Nat Rev Genet* **2**, 858-68.

Lindsay, E. A. and Baldini, A. (2001). Recovery from arterial growth delay reduces penetrance of cardiovascular defects in mice deleted for the DiGeorge syndrome region. *Hum Mol Genet* **10**, 997-1002.

Lindsay, E. A., Botta, A., Jurecic, V., Carattini-Rivera, S., Cheah, Y. C., Rosenblatt, H. M., Bradley, A. and Baldini, A. (1999). Congenital heart disease in mice deficient for the DiGeorge syndrome region. *Nature* **401**, 379-83.

Lindsay, E. A., Vitelli, F., Su, H., Morishima, M., Huynh, T., Pramparo, T., Jurecic, V., Ogunrinu, G., Sutherland, H. F., Scambler, P. J. et al. (2001). Tbx1 haploinsufficieny in the DiGeorge syndrome region causes aortic arch defects in mice. *Nature* **410**, 97-101.

Lingbeek, M. E., Jacobs, J. J. and van Lohuizen, M. (2002). The T-box repressors TBX2 and TBX3 specifically regulate the tumor suppressor gene p14ARF via a variant T-site in the initiator. *J Biol Chem* **277**, 26120-7.

Litingtung, Y., Lei, L., Westphal, H. and Chiang, C. (1998). Sonic hedgehog is essential to foregut development. *Nat Genet* **20**, 58-61.

Liu, C., Liu, W., Lu, M. F., Brown, N. A. and Martin, J. F. (2001). Regulation of left-right asymmetry by thresholds of Pitx2c activity. *Development* **128**, 2039-48.

Liu, C., Liu, W., Palie, J., Lu, M. F., Brown, N. A. and Martin, J. F. (2002). Pitx2c patterns anterior myocardium and aortic arch vessels and is required for local cell movement into atrioventricular cushions. *Development* **129**, 5081-91.

Liu, K. J., Arron, J. R., Stankunas, K., Crabtree, G. R. and Longaker, M. T. (2007a). Chemical rescue of cleft palate and midline defects in conditional GSK-3beta mice. *Nature* **446**, 79-82.

Liu, X., Chen, Q., Kuang, C., Zhang, M., Ruan, Y., Xu, Z. C., Wang, Z. and Chen, Y. (2007b). A 4.3 kb Smad7 promoter is able to specify gene expression during mouse development. *Biochim Biophys Acta* **1769**, 149-52.

Liu, Y., Helms, A. W. and Johnson, J. E. (2004). Distinct activities of Msx1 and Msx3 in dorsal neural tube development. *Development* **131**, 1017-28.

Loots, G. G., Locksley, R. M., Blankespoor, C. M., Wang, Z. E., Miller, W., Rubin, E. M. and Frazer, K. A. (2000). Identification of a coordinate regulator of interleukins 4, 13, and 5 by cross-species sequence comparisons. *Science* **288**, 136-40.

Loots, G. G. and Ovcharenko, I. (2004). rVISTA 2.0: evolutionary analysis of transcription factor binding sites. *Nucleic Acids Res* **32**, W217-21.

Ludlow, L. B., Schick, B. P., Budarf, M. L., Driscoll, D. A., Zackai, E. H., Cohen, A. and Konkle, B. A. (1996). Identification of a mutation in a GATA binding site of the platelet glycoprotein Ibbeta promoter resulting in the Bernard-Soulier syndrome. *J Biol Chem* **271**, 22076-80.

Lumsden, A., Sprawson, N. and Graham, A. (1991). Segmental origin and migration of neural crest cells in the hindbrain region of the chick embryo. *Development* **113**, 1281-91.

Luukko, K., Ylikorkala, A. and Makela, T. P. (2001). Developmentally regulated expression of Smad3, Smad4, Smad6, and Smad7 involved in TGF-beta signaling. *Mech Dev* **101**, 209-12.

Ma, A. D. and Abrams, C. S. (1999). Pleckstrin induces cytoskeletal reorganization via a Rac-dependent pathway. *J Biol Chem* **274**, 28730-5.

Macatee, T. L., Hammond, B. P., Arenkiel, B. R., Francis, L., Frank, D. U. and Moon, A. M. (2003). Ablation of specific expression domains reveals discrete functions of ectoderm- and endoderm-derived FGF8 during cardiovascular and pharyngeal development. *Development* **130**, 6361-74.

MacLean, G., Abu-Abed, S., Dolle, P., Tahayato, A., Chambon, P. and Petkovich, M. (2001). Cloning of a novel retinoic-acid metabolizing cytochrome P450, Cyp26B1, and comparative expression analysis with Cyp26A1 during early murine development. *Mech Dev* **107**, 195-201.

Maeda, J., Yamagishi, H., McAnally, J., Yamagishi, C. and Srivastava, D. (2006). Tbx1 is regulated by forkhead proteins in the secondary heart field. *Dev Dyn* **235**, 701-10.

Mahadevan, N. R., Horton, A. C. and Gibson-Brown, J. J. (2004). Developmental expression of the amphioxus Tbx1/ 10 gene illuminates the evolution of vertebrate branchial arches and sclerotome. *Dev Genes Evol* **214**, 559-66.

Mahoney, M. G., Simpson, A., Aho, S., Uitto, J. and Pulkkinen, L. (2002). Interspecies conservation and differential expression of mouse desmoglein gene family. *Exp Dermatol* **11**, 115-25.

Manley, N. R. and Capecchi, M. R. (1995). The role of Hoxa-3 in mouse thymus and thyroid development. *Development* **121**, 1989-2003.

Marguerie, A., Bajolle, F., Zaffran, S., Brown, N. A., Dickson, C., Buckingham, M. E. and Kelly, R. G. (2006). Congenital heart defects in Fgfr2-IIIb and Fgf10 mutant mice. *Cardiovasc Res* **71**, 50-60.

Mark, M., Ghyselinck, N. B. and Chambon, P. (2004). Retinoic acid signalling in the development of branchial arches. *Curr Opin Genet Dev* **14**, 591-8.

Markwald, R. R., Fitzharris, T. P. and Manasek, F. J. (1977). Structural development of endocardial cushions. *Am J Anat* **148**, 85-119.

Markwald, R. R., Fitzharris, T. P. and Smith, W. N. (1975). Sturctural analysis of endocardial cytodifferentiation. *Dev Biol* **42**, 160-80.

Masamizu, Y., Ohtsuka, T., Takashima, Y., Nagahara, H., Takenaka, Y., Yoshikawa, K., Okamura, H. and Kageyama, R. (2006). Real-time imaging of the somite segmentation clock: revelation of unstable oscillators in the individual presomitic mesoderm cells. *Proc Natl Acad Sci U S A* **103**, 1313-8.

McQuade, L., Christodoulou, J., Budarf, M., Sachdev, R., Wilson, M., Emanuel, B. and Colley, A. (1999). Patient with a 22q11.2 deletion with no overlap of the minimal DiGeorge syndrome critical region (MDGCR). *Am J Med Genet* **86**, 27-33.

McTaggart, K. E., Budarf, M. L., Driscoll, D. A., Emanuel, B. S., Ferreira, P. and McDermid, H. E. (1998). Cat eye syndrome chromosome breakpoint clustering: identification of two intervals also associated with 22q11 deletion syndrome breakpoints. *Cytogenet Cell Genet* **81**, 222-8.

Mears, A. J., Duncan, A. M., Budarf, M. L., Emanuel, B. S., Sellinger, B., Siegel-Bartelt, J., Greenberg, C. R. and McDermid, H. E. (1994). Molecular characterization of the marker chromosome associated with cat eye syndrome. *Am J Hum Genet* **55**, 134-42.

Mears, A. J., el-Shanti, H., Murray, J. C., McDermid, H. E. and Patil, S. R. (1995). Minute supernumerary ring chromosome 22 associated with cat eye syndrome: further delineation of the critical region. *Am J Hum Genet* **57**, 667-73.

Meilhac, S. M., Esner, M., Kelly, R. G., Nicolas, J. F. and Buckingham, M. E. (2004). The clonal origin of myocardial cells in different regions of the embryonic mouse heart. *Dev Cell* **6**, 685-98.

Merscher, S., Funke, B., Epstein, J. A., Heyer, J., Puech, A., Lu, M. M., Xavier, R. J., Demay, M. B., Russell, R. G., Factor, S. et al. (2001). TBX1 is responsible for cardiovascular defects in velo-cardio-facial/DiGeorge syndrome. *Cell* **104**, 619-29.

Meyers, E. N., Lewandoski, M. and Martin, G. R. (1998). An Fgf8 mutant allelic series generated by Cre- and Flp-mediated recombination. *Nat Genet* **18**, 136-41.

Mjaatvedt, C. H., Nakaoka, T., Moreno-Rodriguez, R., Norris, R. A., Kern, M. J., Eisenberg, C. A., Turner, D. and Markwald, R. R. (2001). The outflow tract of the heart is recruited from a novel heart-forming field. *Dev Biol* **238**, 97-109.

Momma, K. (2007). Cardiovascular anomalies associated with chromosome 22q11.2 deletion. *Int J Cardiol* **114**, 147-9.

Monvoisin, A., Alva, J. A., Hofmann, J. J., Zovein, A. C., Lane, T. F. and Iruela-Arispe, M. L. (2006). VE-cadherin-CreERT2 transgenic mouse: a model for inducible recombination in the endothelium. *Dev Dyn* **235**, 3413-22.

Moon, A. M., Guris, D. L., Seo, J. H., Li, L., Hammond, J., Talbot, A. and Imamoto, A. (2006). Crkl deficiency disrupts Fgf8 signaling in a mouse model of 22q11 deletion syndromes. *Dev Cell* **10**, 71-80.

Moore-Scott, B. A. and Manley, N. R. (2005). Differential expression of Sonic hedgehog along the anterior-posterior axis regulates patterning of pharyngeal pouch endoderm and pharyngeal endoderm-derived organs. *Dev Biol* **278**, 323-35.

Moraes, F., Novoa, A., Jerome-Majewska, L. A., Papaioannou, V. E. and Mallo, M. (2005). Tbx1 is required for proper neural crest migration and to stabilize spatial patterns during middle and inner ear development. *Mech Dev* **122**, 199-212.

Moran, N., Morateck, P. A., Deering, A., Ryan, M., Montgomery, R. R., Fitzgerald, D. J. and Kenny, D. (2000). Surface expression of glycoprotein ib alpha is dependent on glycoprotein ib beta: evidence from a novel mutation causing Bernard-Soulier syndrome. *Blood* **96**, 532-9.

Moretti, A., Caron, L., Nakano, A., Lam, J. T., Bernshausen, A., Chen, Y., Qyang, Y., Bu, L., Sasaki, M., Martin-Puig, S. et al. (2006). Multipotent embryonic isl1+ progenitor cells lead to cardiac, smooth muscle, and endothelial cell diversification. *Cell* **127**, 1151-65.

Mori, A. D., Zhu, Y., Vahora, I., Nieman, B., Koshiba-Takeuchi, K., Davidson, L., Pizard, A., Seidman, J. G., Seidman, C. E., Chen, X. J. et al. (2006). Tbx5-dependent rheostatic control of cardiac gene expression and morphogenesis. *Dev Biol* **297**, 566-86.

Morris, S. M., Tallquist, M. D., Rock, C. O. and Cooper, J. A. (2002). Dual roles for the Dab2 adaptor protein in embryonic development and kidney transport. *Embo J* **21**, 1555-64.

Morrow, B., Goldberg, R., Carlson, C., Das Gupta, R., Sirotkin, H., Collins, J., Dunham, I., O'Donnell, H., Scambler, P., Shprintzen, R. et al. (1995). Molecular definition of the 22q11 deletions in velo-cardio-facial syndrome. *Am J Hum Genet* **56**, 1391-403.

Moses, K. A., DeMayo, F., Braun, R. M., Reecy, J. L. and Schwartz, R. J. (2001). Embryonic expression of an Nkx2-5/Cre gene using ROSA26 reporter mice. *Genesis* **31**, 176-80.

Mukai, J., Liu, H., Burt, R. A., Swor, D. E., Lai, W. S., Karayiorgou, M. and Gogos, J. A. (2004). Evidence that the gene encoding ZDHHC8 contributes to the risk of schizophrenia. *Nat Genet* **36**, 725-31.

Mulder, G. B., Manley, N. and Maggio-Price, L. (1998). Retinoic acid-induced thymic abnormalities in the mouse are associated with altered pharyngeal morphology, thymocyte maturation defects, and altered expression of Hoxa3 and Pax1. *Teratology* **58**, 263-75.

Muller, C. W. and Herrmann, B. G. (1997). Crystallographic structure of the T domain-DNA complex of the Brachyury transcription factor. *Nature* **389**, 884-8.

Muller, P., Kietz, S., Gustafsson, J. A. and Strom, A. (2002). The anti-estrogenic effect of all-trans-retinoic acid on the breast cancer cell line MCF-7 is dependent on HES-1 expression. *J Biol Chem* **277**, 28376-9.

Muller, T. S., Ebensperger, C., Neubuser, A., Koseki, H., Balling, R., Christ, B. and Wilting, J. (1996). Expression of avian Pax1 and Pax9 is intrinsically regulated in the pharyngeal endoderm, but depends on environmental influences in the paraxial mesoderm. *Dev Biol* **178**, 403-17.

Murata, K., Hattori, M., Hirai, N., Shinozuka, Y., Hirata, H., Kageyama, R., Sakai, T. and Minato, N. (2005). Hes1 directly controls cell proliferation through the transcriptional repression of p27Kip1. *Mol Cell Biol* **25**, 4262-71.

Muyrers, J. P., Zhang, Y. and Stewart, A. F. (2001). Techniques: Recombinogenic engineering--new options for cloning and manipulating DNA. *Trends Biochem Sci* **26**, 325-31.

Nagasawa, T., Hirota, S., Tachibana, K., Takakura, N., Nishikawa, S., Kitamura, Y., Yoshida, N., Kikutani, H. and Kishimoto, T. (1996). Defects of B-cell

lymphopoiesis and bone-marrow myelopoiesis in mice lacking the CXC chemokine PBSF/SDF-1. *Nature* **382**, 635-8.

Naiche, L. A., Harrelson, Z., Kelly, R. G. and Papaioannou, V. E. (2005). T-box genes in vertebrate development. *Annu Rev Genet* **39**, 219-39.

Nakagawa, O., Nakagawa, M., Richardson, J. A., Olson, E. N. and Srivastava, D. (1999). HRT1, HRT2, and HRT3: a new subclass of bHLH transcription factors marking specific cardiac, somitic, and pharyngeal arch segments. *Dev Biol* **216**, 72-84.

Nakajima, Y., Yamagishi, T., Hokari, S. and Nakamura, H. (2000). Mechanisms involved in valvuloseptal endocardial cushion formation in early cardiogenesis: roles of transforming growth factor (TGF)-beta and bone morphogenetic protein (BMP). *Anat Rec* **258**, 119-27.

Nakamura, Y., Sakakibara, S., Miyata, T., Ogawa, M., Shimazaki, T., Weiss, S., Kageyama, R. and Okano, H. (2000). The bHLH gene hes1 as a repressor of the neuronal commitment of CNS stem cells. *J Neurosci* **20**, 283-93.

Nakaya, M. A., Habas, R., Biris, K., Dunty, W. C., Jr., Kato, Y., He, X. and Yamaguchi, T. P. (2004). Identification and comparative expression analyses of Daam genes in mouse and Xenopus. *Gene Expr Patterns* **5**, 97-105.

Neubuser, A., Koseki, H. and Balling, R. (1995). Characterization and developmental expression of Pax9, a paired-box-containing gene related to Pax1. *Dev Biol* **170**, 701-16.

Nguyen Ba-Charvet, K. T., Brose, K., Marillat, V., Kidd, T., Goodman, C. S., Tessier-Lavigne, M., Sotelo, C. and Chedotal, A. (1999). Slit2-Mediated chemorepulsion and collapse of developing forebrain axons. *Neuron* **22**, 463-73.

Niederreither, K., Vermot, J., Le Roux, L, Schuhbaur, B., Chambon, P. and Dolle, P. (2003). The regional pattern of retinoic acid synthesis by RALDH2 is essential for the development of posterior pharyngeal arches and the enteric nervous system. *Development* **130**, 2525-34.

Niederreither, K., Vermot, J., Messaddeq, N., Schuhbaur, B., Chambon, P. and Dolle, P. (2001). Embryonic retinoic acid synthesis is essential for heart morphogenesis in the mouse. *Development* **128**, 1019-31.

Nikolova, M., Chen, X. and Lufkin, T. (1997). Nkx2.6 expression is transiently and specifically restricted to the branchial region of pharyngeal-stage mouse embryos. *Mech Dev* **69**, 215-8.

Nishibatake, M., Kirby, M. L. and Van Mierop, L. H. (1987). Pathogenesis of persistent truncus arteriosus and dextroposed aorta in the chick embryo after neural crest ablation. *Circulation* **75**, 255-64.

Nissen, R. M., Yan, J., Amsterdam, A., Hopkins, N. and Burgess, S. M. (2003). Zebrafish foxi one modulates cellular responses to Fgf signaling required for the integrity of ear and jaw patterning. *Development* **130**, 2543-54.

Niswander, L. and Martin, G. R. (1992). Fgf-4 expression during gastrulation, myogenesis, limb and tooth development in the mouse. *Development* **114**, 755-68.

Noden, D. M. (1983). The role of the neural crest in patterning of avian cranial skeletal, connective, and muscle tissues. *Dev Biol* **96**, 144-65.

Nowotschin, S., Liao, J., Gage, P. J., Epstein, J. A., Campione, M. and Morrow, B. E. (2006). Tbx1 affects asymmetric cardiac morphogenesis by regulating Pitx2 in the secondary heart field. *Development* **133**, 1565-73.

Nuthall, H. N., Husain, J., McLarren, K. W. and Stifani, S. (2002). Role for Hes1-induced phosphorylation in Groucho-mediated transcriptional repression. *Mol Cell Biol* **22**, 389-99.

O'Donnell, H., McKeown, C., Gould, C., Morrow, B. and Scambler, P. (1997). Detection of an atypical 22q11 deletion that has no overlap with the DiGeorge syndrome critical region. *Am J Hum Genet* **60**, 1544-8.

Ohsako, S., Hyer, J., Panganiban, G., Oliver, I. and Caudy, M. (1994). Hairy function as a DNA-binding helix-loop-helix repressor of Drosophila sensory organ formation. *Genes Dev* **8**, 2743-55.

Ohtsuka, T., Ishibashi, M., Gradwohl, G., Nakanishi, S., Guillemot, F. and Kageyama, R. (1999). Hes1 and Hes5 as notch effectors in mammalian neuronal differentiation. *Embo J* **18**, 2196-207.

Ohtsuka, T., Sakamoto, M., Guillemot, F. and Kageyama, R. (2001). Roles of the basic helix-loop-helix genes Hes1 and Hes5 in expansion of neural stem cells of the developing brain. *J Biol Chem* **276**, 30467-74.

Oliver, G., Wehr, R., Jenkins, N. A., Copeland, N. G., Cheyette, B. N., Hartenstein, V., Zipursky, S. L. and Gruss, P. (1995). Homeobox genes and connective tissue patterning. *Development* **121**, 693-705.

Ounap, K., Ilus, T. and Bartsch, O. (2005). A girl with inverted triplication of chromosome 3q25.3 --> q29 and multiple congenital anomalies consistent with 3q duplication syndrome. *Am J Med Genet A* **134**, 434-8.

Ovcharenko, I., Loots, G. G., Giardine, B. M., Hou, M., Ma, J., Hardison, R. C., Stubbs, L. and Miller, W. (2005). Mulan: multiple-sequence local alignment and visualization for studying function and evolution. *Genome Res* **15**, 184-94.

Papaioannou, V. E. (2001). T-box genes in development: from hydra to humans. *Int Rev Cytol* **207**, 1-70.

Papapetrou, C., Edwards, Y. H. and Sowden, J. C. (1997). The T transcription factor functions as a dimer and exhibits a common human polymorphism Gly-177-Asp in the conserved DNA-binding domain. *FEBS Lett* **409**, 201-6.

Park, E. J., Ogden, L. A., Talbot, A., Evans, S., Cai, C. L., Black, B. L., Frank, D. U. and Moon, A. M. (2006). Required, tissue-specific roles for Fgf8 in outflow tract formation and remodeling. *Development* **133**, 2419-33.

Park, J. I., Kim, S. W., Lyons, J. P., Ji, H., Nguyen, T. T., Cho, K., Barton, M. C., Deroo, T., Vleminckx, K., Moon, R. T. et al. (2005). Kaiso/p120-catenin and TCF/beta-catenin complexes coordinately regulate canonical Wnt gene targets. *Dev Cell* **8**, 843-54.

Paroush, Z., Finley, R. L., Jr., Kidd, T., Wainwright, S. M., Ingham, P. W., Brent, R. and Ish-Horowicz, D. (1994). Groucho is required for Drosophila neurogenesis, segmentation, and sex determination and interacts directly with hairy-related bHLH proteins. *Cell* **79**, 805-15.

Pasini, A., Jiang, Y. J. and Wilkinson, D. G. (2004). Two zebrafish Notch-dependent hairy/Enhancer-of-split-related genes, her6 and her4, are required to maintain the coordination of cyclic gene expression in the presomitic mesoderm. *Development* **131**, 1529-41.

Pasqualetti, M., Ori, M., Nardi, I. and Rijli, F. M. (2000). Ectopic Hoxa2 induction after neural crest migration results in homeosis of jaw elements in Xenopus. *Development* **127**, 5367-78.

Paxton, C., Zhao, H., Chin, Y., Langner, K. and Reecy, J. (2002). Murine Tbx2 contains domains that activate and repress gene transcription. *Gene* **283**, 117-24.

Paylor, R., Glaser, B., Mupo, A., Ataliotis, P., Spencer, C., Sobotka, A., Sparks, C., Choi, C. H., Oghalai, J., Curran, S. et al. (2006). Tbx1 haploinsufficiency is linked to

behavioral disorders in mice and humans: implications for 22q11 deletion syndrome. *Proc Natl Acad Sci U S A* **103**, 7729-34.

Paylor, R., Hirotsune, S., Gambello, M. J., Yuva-Paylor, L., Crawley, J. N. and Wynshaw-Boris, A. (1999). Impaired learning and motor behavior in heterozygous Pafah1b1 (Lis1) mutant mice. *Learn Mem* **6**, 521-37.

Paylor, R. and Lindsay, E. (2006). Mouse Models of 22q11 Deletion Syndrome. *Biol Psychiatry*.

Paylor, R., McIlwain, K. L., McAninch, R., Nellis, A., Yuva-Paylor, L. A., Baldini, A. and Lindsay, E. A. (2001). Mice deleted for the DiGeorge/velocardiofacial syndrome region show abnormal sensorimotor gating and learning and memory impairments. *Hum Mol Genet* **10**, 2645-50.

Peirson, S. N., Butler, J. N. and Foster, R. G. (2003). Experimental validation of novel and conventional approaches to quantitative real-time PCR data analysis. *Nucleic Acids Res* **31**, e73.

Peng, S., Sommerfelt, M. A., Berta, G., Berry, A. K., Kirk, K. L., Hunter, E. and Sorscher, E. J. (1993). Rapid purification of recombinant baculovirus using fluorescence-activated cell sorting. *Biotechniques* **14**, 274-7.

Peng, X., Wood, C. L., Blalock, E. M., Chen, K. C., Landfield, P. W. and Stromberg, A. J. (2003). Statistical implications of pooling RNA samples for microarray experiments. *BMC Bioinformatics* **4**, 26.

Pennacchio, L. A. and Rubin, E. M. (2001). Genomic strategies to identify mammalian regulatory sequences. *Nat Rev Genet* **2**, 100-9.

Pennisi, D. J., Wilkinson, L., Kolle, G., Sohaskey, M. L., Gillinder, K., Piper, M. J., McAvoy, J. W., Lovicu, F. J. and Little, M. H. (2007). Crim1KST264/KST264 mice display a disruption of the Crim1 gene resulting in perinatal lethality with defects in multiple organ systems. *Dev Dyn* **236**, 502-11.

Pfeifer, D., Kist, R., Dewar, K., Devon, K., Lander, E. S., Birren, B., Korniszewski, L., Back, E. and Scherer, G. (1999). Campomelic dysplasia translocation breakpoints are scattered over 1 Mb proximal to SOX9: evidence for an extended control region. *Am J Hum Genet* **65**, 111-24.

Phillips, H. M., Murdoch, J. N., Chaudhry, B., Copp, A. J. and Henderson, D. J. (2005). Vangl2 acts via RhoA signaling to regulate polarized cell movements during development of the proximal outflow tract. *Circ Res* **96**, 292-9.

Phillips, H. M., Rhee, H. J., Murdoch, J. N., Hildreth, V., Peat, J. D., Anderson, R. H., Copp, A. J., Chaudhry, B. and Henderson, D. J. (2007). Disruption of planar cell polarity signaling results in congenital heart defects and cardiomyopathy attributable to early cardiomyocyte disorganization. *Circ Res* **101**, 137-45.

Phillips, M. T., Kirby, M. L. and Forbes, G. (1987). Analysis of cranial neural crest distribution in the developing heart using quail-chick chimeras. *Circ Res* **60**, 27-30.

Pilichou, K., Nava, A., Basso, C., Beffagna, G., Bauce, B., Lorenzon, A., Frigo, G., Vettori, A., Valente, M., Towbin, J. et al. (2006). Mutations in desmoglein-2 gene are associated with arrhythmogenic right ventricular cardiomyopathy. *Circulation* **113**, 1171-9.

Pilz, D. T., Kuc, J., Matsumoto, N., Bodurtha, J., Bernadi, B., Tassinari, C. A., Dobyns, W. B. and Ledbetter, D. H. (1999). Subcortical band heterotopia in rare affected males can be caused by missense mutations in DCX (XLIS) or LIS1. *Hum Mol Genet* **8**, 1757-60.

Pinte, S., Stankovic-Valentin, N., Deltour, S., Rood, B. R., Guerardel, C. and Leprince, D. (2004). The tumor suppressor gene HIC1 (hypermethylated in cancer 1) is

a sequence-specific transcriptional repressor: definition of its consensus binding sequence and analysis of its DNA binding and repressive properties. *J Biol Chem* **279**, 38313-24.

Piotrowski, T., Ahn, D. G., Schilling, T. F., Nair, S., Ruvinsky, I., Geisler, R., Rauch, G. J., Haffter, P., Zon, L. I., Zhou, Y. et al. (2003). The zebrafish van gogh mutation disrupts tbx1, which is involved in the DiGeorge deletion syndrome in humans. *Development* **130**, 5043-52.

Piotrowski, T. and Nusslein-Volhard, C. (2000). The endoderm plays an important role in patterning the segmented pharyngeal region in zebrafish (Danio rerio). *Dev Biol* **225**, 339-56.

Piscione, T. D., Wu, M. Y. and Quaggin, S. E. (2004). Expression of Hairy/Enhancer of Split genes, Hes1 and Hes5, during murine nephron morphogenesis. *Gene Expr Patterns* **4**, 707-11.

Pissarra, L., Henrique, D. and Duarte, A. (2000). Expression of hes6, a new member of the Hairy/Enhancer-of-split family, in mouse development. *Mech Dev* **95**, 275-8.

Plageman, T. F., Jr. and Yutzey, K. E. (2004). Differential expression and function of Tbx5 and Tbx20 in cardiac development. *J Biol Chem* **279**, 19026-34.

Plageman, T. F., Jr. and Yutzey, K. E. (2005). T-box genes and heart development: putting the "T" in heart. *Dev Dyn* **232**, 11-20.

Plageman, T. F., Jr. and Yutzey, K. E. (2006). Microarray analysis of Tbx5-induced genes expressed in the developing heart. *Dev Dyn* **235**, 2868-80.

Plump, A. S., Erskine, L., Sabatier, C., Brose, K., Epstein, C. J., Goodman, C. S., Mason, C. A. and Tessier-Lavigne, M. (2002). Slit1 and Slit2 cooperate to prevent premature midline crossing of retinal axons in the mouse visual system. *Neuron* **33**, 219-32.

Poot, M. and Arttamangkul, S. (1997). Verapamil inhibition of enzymatic product efflux leads to improved detection of beta-galactosidase activity in lacZ-transfected cells. *Cytometry* **28**, 36-41.

Prall, O. W., Menon, M. K., Solloway, M. J., Watanabe, Y., Zaffran, S., Bajolle, F., Biben, C., McBride, J. J., Robertson, B. R., Chaulet, H. et al. (2007). An Nkx2-5/Bmp2/Smad1 negative feedback loop controls heart progenitor specification and proliferation. *Cell* **128**, 947-59.

Prescott, K., Ivins, S., Hubank, M., Lindsay, E., Baldini, A. and Scambler, P. (2005). Microarray analysis of the Df1 mouse model of the 22q11 deletion syndrome. *Hum Genet* **116**, 486-96.

Puech, A., Saint-Jore, B., Funke, B., Gilbert, D. J., Sirotkin, H., Copeland, N. G., Jenkins, N. A., Kucherlapati, R., Morrow, B. and Skoultchi, A. I. (1997). Comparative mapping of the human 22q11 chromosomal region and the orthologous region in mice reveals complex changes in gene organization. *Proc Natl Acad Sci U S A* **94**, 14608-13.

Puech, A., Saint-Jore, B., Merscher, S., Russell, R. G., Cherif, D., Sirotkin, H., Xu, H., Factor, S., Kucherlapati, R. and Skoultchi, A. I. (2000). Normal cardiovascular development in mice deficient for 16 genes in 550 kb of the velocardiofacial/DiGeorge syndrome region. *Proc Natl Acad Sci U S A* **97**, 10090-5.

Qian, L., Liu, J. and Bodmer, R. (2005). Slit and Robo control cardiac cell polarity and morphogenesis. *Curr Biol* **15**, 2271-8.

Quinlan, R., Martin, P. and Graham, A. (2004). The role of actin cables in directing the morphogenesis of the pharyngeal pouches. *Development* **131**, 593-9.

Raetzman, L. T., Cai, J. X. and Camper, S. A. (2007). Hes1 is required for pituitary growth and melanotrope specification. *Dev Biol* **304**, 455-66.

Raft, S., Nowotschin, S., Liao, J. and Morrow, B. E. (2004). Suppression of neural fate and control of inner ear morphogenesis by Tbx1. *Development* **131**, 1801-12.

Rana, M. S., Horsten, N. C., Tesink-Taekema, S., Lamers, W. H., Moorman, A. F. and van den Hoff, M. J. (2007). Trabeculated right ventricular free wall in the chicken heart forms by ventricularization of the myocardium initially forming the outflow tract. *Circ Res* **100**, 1000-7.

Rauch, A., Pfeiffer, R. A., Leipold, G., Singer, H., Tigges, M. and Hofbeck, M. (1999). A novel 22q11.2 microdeletion in DiGeorge syndrome. *Am J Hum Genet* **64**, 659-66.

Rauch, A., Zink, S., Zweier, C., Thiel, C. T., Koch, A., Rauch, R., Lascorz, J., Huffmeier, U., Weyand, M., Singer, H. et al. (2005). Systematic assessment of atypical deletions reveals genotype-phenotype correlation in 22q11.2. *J Med Genet.*

Restifo, L. L. and White, K. (1991). Mutations in a steroid hormone-regulated gene disrupt the metamorphosis of the central nervous system in Drosophila. *Dev Biol* **148**, 174-94.

Reyes, M. R., LeBlanc, E. M. and Bassila, M. K. (1999). Hearing loss and otitis media in velo-cardio-facial syndrome. *Int J Pediatr Otorhinolaryngol* **47**, 227-33.

Riethmacher, D., Brinkmann, V. and Birchmeier, C. (1995). A targeted mutation in the mouse E-cadherin gene results in defective preimplantation development. *Proc Natl Acad Sci U S A* **92**, 855-9.

Rizzu, P., Haddad, B. R., Vallcorba, I., Alonso, A., Ferro, M. T., Garcia-Sagredo, J. M. and Baldini, A. (1997). Delineation of a duplication map of chromosome 3q: a new case confirms the exclusion of 3q25-q26.2 from the duplication 3q syndrome critical region. *Am J Med Genet* **68**, 428-32.

Roberts, C., Ivins, S., Cook, A. C., Baldini, A. and Scambler, P. J. (2006). Cyp26 genes a1, b1 and c1 are down-regulated in Tbx1 null mice and inhibition of Cyp26 enzyme function produces a phenocopy of DiGeorge Syndrome in the chick. *Hum Mol Genet* **15**, 3394-410.

Roberts, C., Ivins, S. M., James, C. T. and Scambler, P. J. (2005). Retinoic acid down-regulates Tbx1 expression in vivo and in vitro. *Dev Dyn* **232**, 928-38.

Robertson, G., Hirst, M., Bainbridge, M., Bilenky, M., Zhao, Y., Zeng, T., Euskirchen, G., Bernier, B., Varhol, R., Delaney, A. et al. (2007). Genome-wide profiles of STAT1 DNA association using chromatin immunoprecipitation and massively parallel sequencing. *Nat Methods* **4**, 651-7.

Robin, N. H. and Shprintzen, R. J. (2005). Defining the clinical spectrum of deletion 22q11.2. *J Pediatr* **147**, 90-6.

Ruchoux, M. M., Domenga, V., Brulin, P., Maciazek, J., Limol, S., Tournier-Lasserve, E. and Joutel, A. (2003). Transgenic mice expressing mutant Notch3 develop vascular alterations characteristic of cerebral autosomal dominant arteriopathy with subcortical infarcts and leukoencephalopathy. *Am J Pathol* **162**, 329-42.

Ruhin, B., Creuzet, S., Vincent, C., Benouaiche, L., Le Douarin, N. M. and Couly, G. (2003). Patterning of the hyoid cartilage depends upon signals arising from the ventral foregut endoderm. *Dev Dyn* **228**, 239-46.

Rutenberg, J. B., Fischer, A., Jia, H., Gessler, M., Zhong, T. P. and Mercola, M. (2006). Developmental patterning of the cardiac atrioventricular canal by Notch and Hairy-related transcription factors. *Development* **133**, 4381-90.

Saga, Y., Miyagawa-Tomita, S., Takagi, A., Kitajima, S., Miyazaki, J. and Inoue, T. (1999). MesP1 is expressed in the heart precursor cells and required for the formation of a single heart tube. *Development* **126**, 3437-47.

Sahut-Barnola, I., Godt, D., Laski, F. A. and Couderc, J. L. (1995). Drosophila ovary morphogenesis: analysis of terminal filament formation and identification of a gene required for this process. *Dev Biol* **170**, 127-35.

Saint-Jeannet, J. P., He, X., Varmus, H. E. and Dawid, I. B. (1997). Regulation of dorsal fate in the neuraxis by Wnt-1 and Wnt-3a. *Proc Natl Acad Sci U S A* **94**, 13713-8.

Saitta, S. C., Harris, S. E., Gaeth, A. P., Driscoll, D. A., McDonald-McGinn, D. M., Maisenbacher, M. K., Yersak, J. M., Chakraborty, P. K., Hacker, A. M., Zackai, E. H. et al. (2004). Aberrant interchromosomal exchanges are the predominant cause of the 22q11.2 deletion. *Hum Mol Genet* **13**, 417-28.

Saitta, S. C., McGrath, J. M., Mensch, H., Shaikh, T. H., Zackai, E. H. and Emanuel, B. S. (1999). A 22q11.2 deletion that excludes UFD1L and CDC45L in a patient with conotruncal and craniofacial defects. *Am J Hum Genet* **65**, 562-6.

Sakata, Y., Kamei, C. N., Nakagami, H., Bronson, R., Liao, J. K. and Chin, M. T. (2002). Ventricular septal defect and cardiomyopathy in mice lacking the transcription factor CHF1/Hey2. *Proc Natl Acad Sci U S A* **99**, 16197-202.

Sakata, Y., Koibuchi, N., Xiang, F., Youngblood, J. M., Kamei, C. N. and Chin, M. T. (2006). The spectrum of cardiovascular anomalies in CHF1/Hey2 deficient mice reveals roles in endocardial cushion, myocardial and vascular maturation. *J Mol Cell Cardiol* **40**, 267-73.

Sargent, C., Burn, J., Baraitser, M. and Pembrey, M. E. (1985). Trigonocephaly and the Opitz C syndrome. *J Med Genet* **22**, 39-45.

Sasai, Y., Kageyama, R., Tagawa, Y., Shigemoto, R. and Nakanishi, S. (1992). Two mammalian helix-loop-helix factors structurally related to Drosophila hairy and Enhancer of split. *Genes Dev* **6**, 2620-34.

Scambler, P. J. (2000). The 22q11 deletion syndromes. *Hum Mol Genet* **9**, 2421-6.

Schilling, T. F. (1997). Genetic analysis of craniofacial development in the vertebrate embryo. *Bioessays* **19**, 459-68.

Schilling, T. F. and Kimmel, C. B. (1994). Segment and cell type lineage restrictions during pharyngeal arch development in the zebrafish embryo. *Development* **120**, 483-94.

Schinzel, A., Schmid, W., Fraccaro, M., Tiepolo, L., Zuffardi, O., Opitz, J. M., Lindsten, J., Zetterqvist, P., Enell, H., Baccichetti, C. et al. (1981). The "cat eye syndrome": dicentric small marker chromosome probably derived from a no.22 (tetrasomy 22pter to q11) associated with a characteristic phenotype. Report of 11 patients and delineation of the clinical picture. *Hum Genet* **57**, 148-58.

Schleiffarth, J. R., Person, A. D., Martinsen, B. J., Sukovich, D. J., Neumann, A., Baker, C. V., Lohr, J. L., Cornfield, D. N., Ekker, S. C. and Petryk, A. (2007). Wnt5a is required for cardiac outflow tract septation in mice. *Pediatr Res* **61**, 386-91.

Schneider, J. E., Bose, J., Bamforth, S. D., Gruber, A. D., Broadbent, C., Clarke, K., Neubauer, S., Lengeling, A. and Bhattacharya, S. (2004). Identification of cardiac malformations in mice lacking Ptdsr using a novel high-throughput magnetic resonance imaging technique. *BMC Dev Biol* **4**, 16.

Schweickert, A., Campione, M., Steinbeisser, H. and Blum, M. (2000). Pitx2 isoforms: involvement of Pitx2c but not Pitx2a or Pitx2b in vertebrate left-right asymmetry. *Mech Dev* **90**, 41-51.

Self, M., Lagutin, O. V., Bowling, B., Hendrix, J., Cai, Y., Dressler, G. R. and Oliver, G. (2006). Six2 is required for suppression of nephrogenesis and progenitor renewal in the developing kidney. *Embo J* **25**, 5214-28.

Seo, S. and Kume, T. (2006). Forkhead transcription factors, Foxc1 and Foxc2, are required for the morphogenesis of the cardiac outflow tract. *Dev Biol* **296**, 421-36.

Shaikh, T. H., Kurahashi, H. and Emanuel, B. S. (2001). Evolutionarily conserved low copy repeats (LCRs) in 22q11 mediate deletions, duplications, translocations, and genomic instability: an update and literature review. *Genet Med* **3**, 6-13.

Shaikh, T. H., Kurahashi, H., Saitta, S. C., O'Hare, A. M., Hu, P., Roe, B. A., Driscoll, D. A., McDonald-McGinn, D. M., Zackai, E. H., Budarf, M. L. et al. (2000). Chromosome 22-specific low copy repeats and the 22q11.2 deletion syndrome: genomic organization and deletion endpoint analysis. *Hum Mol Genet* **9**, 489-501.

Shaikh, T. H., O'Connor, R. J., Pierpont, M. E., McGrath, J., Hacker, A. M., Nimmakayalu, M., Geiger, E., Emanuel, B. S. and Saitta, S. C. (2007). Low copy repeats mediate distal chromosome 22q11.2 deletions: sequence analysis predicts breakpoint mechanisms. *Genome Res* **17**, 482-91.

Shih, H. P., Gross, M. K. and Kioussi, C. (2007). Cranial muscle defects of Pitx2 mutants result from specification defects in the first branchial arch. *Proc Natl Acad Sci U S A* **104**, 5907-12.

Shimizu, K., Chiba, S., Saito, T., Kumano, K., Hamada, Y. and Hirai, H. (2002). Functional diversity among Notch1, Notch2, and Notch3 receptors. *Biochem Biophys Res Commun* **291**, 775-9.

Sinha, S., Abraham, S., Gronostajski, R. M. and Campbell, C. E. (2000). Differential DNA binding and transcription modulation by three T-box proteins, T, TBX1 and TBX2. *Gene* **258**, 15-29.

Sobin, C., Kiley-Brabeck, K. and Karayiorgou, M. (2005). Lower prepulse inhibition in children with the 22q11 deletion syndrome. *Am J Psychiatry* **162**, 1090-9.

Spiteri, E., Babcock, M., Kashork, C. D., Wakui, K., Gogineni, S., Lewis, D. A., Williams, K. M., Minoshima, S., Sasaki, T., Shimizu, N. et al. (2003). Frequent translocations occur between low copy repeats on chromosome 22q11.2 (LCR22s) and telomeric bands of partner chromosomes. *Hum Mol Genet* **12**, 1823-37.

Srivastava, D., Thomas, T., Lin, Q., Kirby, M. L., Brown, D. and Olson, E. N. (1997). Regulation of cardiac mesodermal and neural crest development by the bHLH transcription factor, dHAND. *Nat Genet* **16**, 154-60.

Stalmans, I., Lambrechts, D., De Smet, F., Jansen, S., Wang, J., Maity, S., Kneer, P., von der Ohe, M., Swillen, A., Maes, C. et al. (2003). VEGF: a modifier of the del22q11 (DiGeorge) syndrome? *Nat Med* **9**, 173-82.

Stalsberg, H. and DeHaan, R. L. (1969). The precardiac areas and formation of the tubular heart in the chick embryo. *Dev Biol* **19**, 128-59.

Stanford, W. L., Cohn, J. B. and Cordes, S. P. (2001). Gene-trap mutagenesis: past, present and beyond. *Nat Rev Genet* **2**, 756-68.

Steidl, C., Leimeister, C., Klamt, B., Maier, M., Nanda, I., Dixon, M., Clarke, R., Schmid, M. and Gessler, M. (2000). Characterization of the human and mouse HEY1, HEY2, and HEYL genes: cloning, mapping, and mutation screening of a new bHLH gene family. *Genomics* **66**, 195-203.

Steinbach, P., Adkins, W. N., Jr., Caspar, H., Dumars, K. W., Gebauer, J., Gilbert, E. F., Grimm, T., Habedank, M., Hansmann, I., Herrmann, J. et al. (1981). The dup(3q) syndrome: report of eight cases and review of the literature. *Am J Med Genet* **10**, 159-77.

Stennard, F. A., Costa, M. W., Elliott, D. A., Rankin, S., Haast, S. J., Lai, D., McDonald, L. P., Niederreither, K., Dolle, P., Bruneau, B. G. et al. (2003). Cardiac T-box factor Tbx20 directly interacts with Nkx2-5, GATA4, and GATA5 in regulation of gene expression in the developing heart. *Dev Biol* **262**, 206-24.

Stennard, F. A., Costa, M. W., Lai, D., Biben, C., Furtado, M. B., Solloway, M. J., McCulley, D. J., Leimena, C., Preis, J. I., Dunwoodie, S. L. et al. (2005). Murine T-box transcription factor Tbx20 acts as a repressor during heart development, and is essential for adult heart integrity, function and adaptation. *Development*.

Stennard, F. A. and Harvey, R. P. (2005). T-box transcription factors and their roles in regulatory hierarchies in the developing heart. *Development* **132**, 4897-910.

Stockhausen, M. T., Sjolund, J. and Axelson, H. (2005). Regulation of the Notch target gene Hes-1 by TGFalpha induced Ras/MAPK signaling in human neuroblastoma cells. *Exp Cell Res* **310**, 218-28.

Stoller, J. Z. and Epstein, J. A. (2005). Identification of a novel nuclear localization signal in Tbx1 that is deleted in DiGeorge syndrome patients harboring the 1223delC mutation. *Hum Mol Genet* **14**, 885-92.

Stottmann, R. W., Choi, M., Mishina, Y., Meyers, E. N. and Klingensmith, J. (2004). BMP receptor IA is required in mammalian neural crest cells for development of the cardiac outflow tract and ventricular myocardium. *Development* **131**, 2205-18.

Strom, A., Arai, N., Leers, J. and Gustafsson, J. A. (2000). The Hairy and Enhancer of Split homologue-1 (HES-1) mediates the proliferative effect of 17beta-estradiol on breast cancer cell lines. *Oncogene* **19**, 5951-3.

Struyf, S., Burdick, M. D., Peeters, E., Van den Broeck, K., Dillen, C., Proost, P., Van Damme, J. and Strieter, R. M. (2007). Platelet factor-4 variant chemokine CXCL4L1 inhibits melanoma and lung carcinoma growth and metastasis by preventing angiogenesis. *Cancer Res* **67**, 5940-8.

Su, D., Ellis, S., Napier, A., Lee, K. and Manley, N. R. (2001). Hoxa3 and pax1 regulate epithelial cell death and proliferation during thymus and parathyroid organogenesis. *Dev Biol* **236**, 316-29.

Sullivan, K. E. (2004). The clinical, immunological, and molecular spectrum of chromosome 22q11.2 deletion syndrome and DiGeorge syndrome. *Curr Opin Allergy Clin Immunol* **4**, 505-12.

Sun, J., Kamei, C. N., Layne, M. D., Jain, M. K., Liao, J. K., Lee, M. E. and Chin, M. T. (2001). Regulation of myogenic terminal differentiation by the hairy-related transcription factor CHF2. *J Biol Chem* **276**, 18591-6.

Sutherland, H. F., Kim, U. J. and Scambler, P. J. (1998). Cloning and comparative mapping of the DiGeorge syndrome critical region in the mouse. *Genomics* **52**, 37-43.

Suzuki, K., Fukui, H., Kayahara, T., Sawada, M., Seno, H., Hiai, H., Kageyama, R., Okano, H. and Chiba, T. (2005). Hes1-deficient mice show precocious differentiation of Paneth cells in the small intestine. *Biochem Biophys Res Commun* **328**, 348-52.

Szaniszlo, P., Wang, N., Sinha, M., Reece, L. M., Van Hook, J. W., Luxon, B. A. and Leary, J. F. (2004). Getting the right cells to the array: Gene expression microarray analysis of cell mixtures and sorted cells. *Cytometry A* **59**, 191-202.

Taddei, I., Morishima, M., Huynh, T. and Lindsay, E. A. (2001). Genetic factors are major determinants of phenotypic variability in a mouse model of the DiGeorge/del22q11 syndromes. *Proc Natl Acad Sci U S A* **98**, 11428-31.

Taelman, V., Van Wayenbergh, R., Solter, M., Pichon, B., Pieler, T., Christophe, D. and Bellefroid, E. J. (2004). Sequences downstream of the bHLH domain of the

Xenopus hairy-related transcription factor-1 act as an extended dimerization domain that contributes to the selection of the partners. *Dev Biol* **276**, 47-63.

Tahayato, A., Dolle, P. and Petkovich, M. (2003). Cyp26C1 encodes a novel retinoic acid-metabolizing enzyme expressed in the hindbrain, inner ear, first branchial arch and tooth buds during murine development. *Gene Expr Patterns* **3**, 449-54.

Takasato, M., Osafune, K., Matsumoto, Y., Kataoka, Y., Yoshida, N., Meguro, H., Aburatani, H., Asashima, M. and Nishinakamura, R. (2004). Identification of kidney mesenchymal genes by a combination of microarray analysis and Sall1-GFP knockin mice. *Mech Dev* **121**, 547-57.

Takeuchi, J. K., Mileikovskaia, M., Koshiba-Takeuchi, K., Heidt, A. B., Mori, A. D., Arruda, E. P., Gertsenstein, M., Georges, R., Davidson, L., Mo, R. et al. (2005). Tbx20 dose-dependently regulates transcription factor networks required for mouse heart and motoneuron development. *Development*.

Takeuchi, J. K., Ohgi, M., Koshiba-Takeuchi, K., Shiratori, H., Sakaki, I., Ogura, K., Saijoh, Y. and Ogura, T. (2003). Tbx5 specifies the left/right ventricles and ventricular septum position during cardiogenesis. *Development* **130**, 5953-64.

Tallquist, M. D. and Soriano, P. (2000). Epiblast-restricted Cre expression in MORE mice: a tool to distinguish embryonic vs. extra-embryonic gene function. *Genesis* **26**, 113-5.

Tam, P. P., Parameswaran, M., Kinder, S. J. and Weinberger, R. P. (1997). The allocation of epiblast cells to the embryonic heart and other mesodermal lineages: the role of ingression and tissue movement during gastrulation. *Development* **124**, 1631-42.

Tam, P. P. and Rossant, J. (2003). Mouse embryonic chimeras: tools for studying mammalian development. *Development* **130**, 6155-63.

Tanaka, M., Schinke, M., Liao, H. S., Yamasaki, N. and Izumo, S. (2001). Nkx2.5 and Nkx2.6, homologs of Drosophila tinman, are required for development of the pharynx. *Mol Cell Biol* **21**, 4391-8.

Tanaka, M., Yamasaki, N. and Izumo, S. (2000). Phenotypic characterization of the murine Nkx2.6 homeobox gene by gene targeting. *Mol Cell Biol* **20**, 2874-9.

Tomita, K., Hattori, M., Nakamura, E., Nakanishi, S., Minato, N. and Kageyama, R. (1999). The bHLH gene Hes1 is essential for expansion of early T cell precursors. *Genes Dev* **13**, 1203-10.

Tomita, K., Ishibashi, M., Nakahara, K., Ang, S. L., Nakanishi, S., Guillemot, F. and Kageyama, R. (1996). Mammalian hairy and Enhancer of split homolog 1 regulates differentiation of retinal neurons and is essential for eye morphogenesis. *Neuron* **16**, 723-34.

Trainor, P. A., Tan, S. S. and Tam, P. P. (1994). Cranial paraxial mesoderm: regionalisation of cell fate and impact on craniofacial development in mouse embryos. *Development* **120**, 2397-408.

Trembath, D. G., Semina, E. V., Jones, D. H., Patil, S. R., Qian, Q., Amendt, B. A., Russo, A. F. and Murray, J. C. (2004). Analysis of two translocation breakpoints and identification of a negative regulatory element in patients with Rieger's syndrome. *Birth Defects Res A Clin Mol Teratol* **70**, 82-91.

Trumpp, A., Depew, M. J., Rubenstein, J. L., Bishop, J. M. and Martin, G. R. (1999). Cre-mediated gene inactivation demonstrates that FGF8 is required for cell survival and patterning of the first branchial arch. *Genes Dev* **13**, 3136-48.

Tucker, A. S. and Lumsden, A. (2004). Neural crest cells provide species-specific patterning information in the developing branchial skeleton. *Evol Dev* **6**, 32-40.

Uehara, M., Yashiro, K., Mamiya, S., Nishino, J., Chambon, P., Dolle, P. and Sakai, Y. (2007). CYP26A1 and CYP26C1 cooperatively regulate anterior-posterior patterning of the developing brain and the production of migratory cranial neural crest cells in the mouse. *Dev Biol* **302**, 399-411.

Urban, A. E., Korbel, J. O., Selzer, R., Richmond, T., Hacker, A., Popescu, G. V., Cubells, J. F., Green, R., Emanuel, B. S., Gerstein, M. B. et al. (2006). High-resolution mapping of DNA copy alterations in human chromosome 22 using high-density tiling oligonucleotide arrays. *Proc Natl Acad Sci U S A* **103**, 4534-9.

Valenta, T., Lukas, J., Doubravska, L., Fafilek, B. and Korinek, V. (2006). HIC1 attenuates Wnt signaling by recruitment of TCF-4 and beta-catenin to the nuclear bodies. *Embo J* **25**, 2326-37.

Van Wayenbergh, R., Taelman, V., Pichon, B., Fischer, A., Kricha, S., Gessler, M., Christophe, D. and Bellefroid, E. J. (2003). Identification of BOIP, a novel cDNA highly expressed during spermatogenesis that encodes a protein interacting with the orange domain of the hairy-related transcription factor HRT1/Hey1 in Xenopus and mouse. *Dev Dyn* **228**, 716-25.

Veitch, E., Begbie, J., Schilling, T. F., Smith, M. M. and Graham, A. (1999). Pharyngeal arch patterning in the absence of neural crest. *Curr Biol* **9**, 1481-4.

Vermot, J., Niederreither, K., Garnier, J. M., Chambon, P. and Dolle, P. (2003). Decreased embryonic retinoic acid synthesis results in a DiGeorge syndrome phenotype in newborn mice. *Proc Natl Acad Sci U S A* **100**, 1763-8.

Verzi, M. P., McCulley, D. J., De Val, S., Dodou, E. and Black, B. L. (2005). The right ventricle, outflow tract, and ventricular septum comprise a restricted expression domain within the secondary/anterior heart field. *Dev Biol* **287**, 134-45.

Vincentz, J. W., McWhirter, J. R., Murre, C., Baldini, A. and Furuta, Y. (2005). Fgf15 is required for proper morphogenesis of the mouse cardiac outflow tract. *Genesis* **41**, 192-201.

Viragh, S. and Challice, C. E. (1973). Origin and differentiation of cardiac muscle cells in the mouse. *J Ultrastruct Res* **42**, 1-24.

Vitelli, F., Morishima, M., Taddei, I., Lindsay, E. A. and Baldini, A. (2002a). Tbx1 mutation causes multiple cardiovascular defects and disrupts neural crest and cranial nerve migratory pathways. *Hum Mol Genet* **11**, 915-22.

Vitelli, F., Taddei, I., Morishima, M., Meyers, E. N., Lindsay, E. A. and Baldini, A. (2002b). A genetic link between Tbx1 and fibroblast growth factor signaling. *Development* **129**, 4605-11.

Vitelli, F., Viola, A., Morishima, M., Pramparo, T., Baldini, A. and Lindsay, E. (2003). TBX1 is required for inner ear morphogenesis. *Hum Mol Genet* **12**, 2041-8.

Vitelli, F., Zhang, Z., Huynh, T., Sobotka, A., Mupo, A. and Baldini, A. (2006). Fgf8 expression in the Tbx1 domain causes skeletal abnormalities and modifies the aortic arch but not the outflow tract phenotype of Tbx1 mutants. *Dev Biol* **295**, 559-70.

von Both, I., Silvestri, C., Erdemir, T., Lickert, H., Walls, J. R., Henkelman, R. M., Rossant, J., Harvey, R. P., Attisano, L. and Wrana, J. L. (2004). Foxh1 is essential for development of the anterior heart field. *Dev Cell* **7**, 331-45.

Von Stetina, S. E., Watson, J. D., Fox, R. M., Olszewski, K. L., Spencer, W. C., Roy, P. J. and Miller, D. M., 3rd. (2007). Cell-specific microarray profiling experiments reveal a comprehensive picture of gene expression in the C. elegans nervous system. *Genome Biol* **8**, R135.

Wakabayashi, N., Kageyama, R., Habu, T., Doi, T., Morita, T., Nozaki, M., Yamamoto, M. and Nishimune, Y. (2000). A novel cis-acting element regulates HES-

1 gene expression in P19 embryonal carcinoma cells treated with retinoic acid. *J Biochem (Tokyo)* **128**, 1087-95.

Waldo, K., Miyagawa-Tomita, S., Kumiski, D. and Kirby, M. L. (1998). Cardiac neural crest cells provide new insight into septation of the cardiac outflow tract: aortic sac to ventricular septal closure. *Dev Biol* **196**, 129-44.

Waldo, K. L., Hutson, M. R., Stadt, H. A., Zdanowicz, M., Zdanowicz, J. and Kirby, M. L. (2005a). Cardiac neural crest is necessary for normal addition of the myocardium to the arterial pole from the secondary heart field. *Dev Biol* **281**, 66-77.

Waldo, K. L., Hutson, M. R., Ward, C. C., Zdanowicz, M., Stadt, H. A., Kumiski, D., Abu-Issa, R. and Kirby, M. L. (2005b). Secondary heart field contributes myocardium and smooth muscle to the arterial pole of the developing heart. *Dev Biol* **281**, 78-90.

Waldo, K. L., Kumiski, D. and Kirby, M. L. (1996). Cardiac neural crest is essential for the persistence rather than the formation of an arch artery. *Dev Dyn* **205**, 281-92.

Waldo, K. L., Kumiski, D. H., Wallis, K. T., Stadt, H. A., Hutson, M. R., Platt, D. H. and Kirby, M. L. (2001). Conotruncal myocardium arises from a secondary heart field. *Development* **128**, 3179-88.

Wales, M. M., Biel, M. A., el Deiry, W., Nelkin, B. D., Issa, J. P., Cavenee, W. K., Kuerbitz, S. J. and Baylin, S. B. (1995). p53 activates expression of HIC-1, a new candidate tumour suppressor gene on 17p13.3. *Nat Med* **1**, 570-7.

Wall, N. A. and Hogan, B. L. (1995). Expression of bone morphogenetic protein-4 (BMP-4), bone morphogenetic protein-7 (BMP-7), fibroblast growth factor-8 (FGF-8) and sonic hedgehog (SHH) during branchial arch development in the chick. *Mech Dev* **53**, 383-92.

Wallin, J., Eibel, H., Neubuser, A., Wilting, J., Koseki, H. and Balling, R. (1996). Pax1 is expressed during development of the thymus epithelium and is required for normal T-cell maturation. *Development* **122**, 23-30.

Walshe, J. and Mason, I. (2003). Fgf signalling is required for formation of cartilage in the head. *Dev Biol* **264**, 522-36.

Warming, S., Costantino, N., Court, D. L., Jenkins, N. A. and Copeland, N. G. (2005). Simple and highly efficient BAC recombineering using galK selection. *Nucleic Acids Res* **33**, e36.

Washington Smoak, I., Byrd, N. A., Abu-Issa, R., Goddeeris, M. M., Anderson, R., Morris, J., Yamamura, K., Klingensmith, J. and Meyers, E. N. (2005). Sonic hedgehog is required for cardiac outflow tract and neural crest cell development. *Dev Biol* **283**, 357-72.

Wassarman, K. M., Lewandoski, M., Campbell, K., Joyner, A. L., Rubenstein, J. L., Martinez, S. and Martin, G. R. (1997). Specification of the anterior hindbrain and establishment of a normal mid/hindbrain organizer is dependent on Gbx2 gene function. *Development* **124**, 2923-34.

Waters, S. T. and Lewandoski, M. (2006). A threshold requirement for Gbx2 levels in hindbrain development. *Development* **133**, 1991-2000.

Wei, C. L., Wu, Q., Vega, V. B., Chiu, K. P., Ng, P., Zhang, T., Shahab, A., Yong, H. C., Fu, Y., Weng, Z. et al. (2006). A global map of p53 transcription-factor binding sites in the human genome. *Cell* **124**, 207-19.

Weksberg, R., Stachon, A. C., Squire, J. A., Moldovan, L., Bayani, J., Meyn, S., Chow, E. and Bassett, A. S. (2006). Molecular characterization of deletion breakpoints in adults with 22q11 deletion syndrome. *Hum Genet.*

Wendling, O., Dennefeld, C., Chambon, P. and Mark, M. (2000). Retinoid signaling is essential for patterning the endoderm of the third and fourth pharyngeal arches. *Development* **127**, 1553-62.

Wenzel, P. L. and Leone, G. (2007). Expression of Cre recombinase in early diploid trophoblast cells of the mouse placenta. *Genesis* **45**, 129-34.

White, J. A., Guo, Y. D., Baetz, K., Beckett-Jones, B., Bonasoro, J., Hsu, K. E., Dilworth, F. J., Jones, G. and Petkovich, M. (1996). Identification of the retinoic acid-inducible all-trans-retinoic acid 4-hydroxylase. *J Biol Chem* **271**, 29922-7.

White, J. A., Ramshaw, H., Taimi, M., Stangle, W., Zhang, A., Everingham, S., Creighton, S., Tam, S. P., Jones, G. and Petkovich, M. (2000). Identification of the human cytochrome P450, P450RAI-2, which is predominantly expressed in the adult cerebellum and is responsible for all-trans-retinoic acid metabolism. *Proc Natl Acad Sci U S A* **97**, 6403-8.

Wieser, R., Fritz, B., Ullmann, R., Muller, I., Galhuber, M., Storlazzi, C. T., Ramaswamy, A., Christiansen, H., Shimizu, N. and Rehder, H. (2005). Novel rearrangement of chromosome band 22q11.2 causing 22q11 microdeletion syndrome-like phenotype and rhabdoid tumor of the kidney. *Hum Mutat* **26**, 78-83.

Winkler, C., Elmasri, H., Klamt, B., Volff, J. N. and Gessler, M. (2003). Characterization of hey bHLH genes in teleost fish. *Dev Genes Evol* **213**, 541-53.

Winnier, G. E., Kume, T., Deng, K., Rogers, R., Bundy, J., Raines, C., Walter, M. A., Hogan, B. L. and Conway, S. J. (1999). Roles for the winged helix transcription factors MF1 and MFH1 in cardiovascular development revealed by nonallelic noncomplementation of null alleles. *Dev Biol* **213**, 418-31.

Wright, T. J., Hatch, E. P., Karabagli, H., Karabagli, P., Schoenwolf, G. C. and Mansour, S. L. (2003). Expression of mouse fibroblast growth factor and fibroblast growth factor receptor genes during early inner ear development. *Dev Dyn* **228**, 267-72.

Wu, J. Y., Feng, L., Park, H. T., Havlioglu, N., Wen, L., Tang, H., Bacon, K. B., Jiang, Z., Zhang, X. and Rao, Y. (2001). The neuronal repellent Slit inhibits leukocyte chemotaxis induced by chemotactic factors. *Nature* **410**, 948-52.

Xin, M., Small, E. M., van Rooij, E., Qi, X., Richardson, J. A., Srivastava, D., Nakagawa, O. and Olson, E. N. (2007). Essential roles of the bHLH transcription factor Hrt2 in repression of atrial gene expression and maintenance of postnatal cardiac function. *Proc Natl Acad Sci U S A* **104**, 7975-80.

Xiong, W. C. and Montell, C. (1993). tramtrack is a transcriptional repressor required for cell fate determination in the Drosophila eye. *Genes Dev* **7**, 1085-96.

Xu, H. and Baldini, A. (2007). Genetic pathways to mammalian heart development: Recent progress from manipulation of the mouse genome. *Semin Cell Dev Biol* **18**, 77-83.

Xu, H., Cerrato, F. and Baldini, A. (2005). Timed mutation and cell-fate mapping reveal reiterated roles of Tbx1 during embryogenesis, and a crucial function during segmentation of the pharyngeal system via regulation of endoderm expansion. *Development* **132**, 4387-95.

Xu, H., Chen, L. and Baldini, A. (2007a). In vivo genetic ablation of the periotic mesoderm affects cell proliferation survival and differentiation in the cochlea. *Dev Biol* **310**, 329-40.

Xu, H., Morishima, M., Wylie, J. N., Schwartz, R. J., Bruneau, B. G., Lindsay, E. A. and Baldini, A. (2004). Tbx1 has a dual role in the morphogenesis of the cardiac outflow tract. *Development* **131**, 3217-27.

Xu, H., Viola, A., Zhang, Z., Gerken, C. P., Lindsay-Illingworth, E. A. and Baldini, A. (2007b). Tbx1 regulates population, proliferation and cell fate determination of otic epithelial cells. *Dev Biol* **302**, 670-82.

Yagi, H., Furutani, Y., Hamada, H., Sasaki, T., Asakawa, S., Minoshima, S., Ichida, F., Joo, K., Kimura, M., Imamura, S. et al. (2003). Role of TBX1 in human del22q11.2 syndrome. *Lancet* **362**, 1366-73.

Yajima, I., Belloir, E., Bourgeois, Y., Kumasaka, M., Delmas, V. and Larue, L. (2006). Spatiotemporal gene control by the Cre-ERT2 system in melanocytes. *Genesis* **44**, 34-43.

Yamagishi, C., Hierck, B. P., Gittenberger-De Groot, A. C., Yamagishi, H. and Srivastava, D. (2003a). Functional attenuation of UFD1l, a 22q11.2 deletion syndrome candidate gene, leads to cardiac outflow septation defects in chicken embryos. *Pediatr Res* **53**, 546-53.

Yamagishi, H., Maeda, J., Hu, T., McAnally, J., Conway, S. J., Kume, T., Meyers, E. N., Yamagishi, C. and Srivastava, D. (2003b). Tbx1 is regulated by tissue-specific forkhead proteins through a common Sonic hedgehog-responsive enhancer. *Genes Dev* **17**, 269-81.

Yamagishi, H. and Srivastava, D. (2003). Unraveling the genetic and developmental mysteries of 22q11 deletion syndrome. *Trends Mol Med* **9**, 383-9.

Yamazaki, H., Sakata, E., Yamane, T., Yanagisawa, A., Abe, K., Yamamura, K., Hayashi, S. and Kunisada, T. (2005). Presence and distribution of neural crest-derived cells in the murine developing thymus and their potential for differentiation. *Int Immunol* **17**, 549-58.

Yang, D., Zhang, J., Chen, C., Xie, M., Sperling, S., Fang, F., Chen, B., Li, X. and Zhang, H. (2007). BMPR IA Downstream Genes Related to VSD. *Pediatr Res* **Publish Ahead of Print**.

Yang, D. H., Smith, E. R., Roland, I. H., Sheng, Z., He, J., Martin, W. D., Hamilton, T. C., Lambeth, J. D. and Xu, X. X. (2002). Disabled-2 is essential for endodermal cell positioning and structure formation during mouse embryogenesis. *Dev Biol* **251**, 27-44.

Yang, L., Cai, C. L., Lin, L., Qyang, Y., Chung, C., Monteiro, R. M., Mummery, C. L., Fishman, G. I., Cogen, A. and Evans, S. (2006). Isl1Cre reveals a common Bmp pathway in heart and limb development. *Development* **133**, 1575-85.

Yashiro, K., Zhao, X., Uehara, M., Yamashita, K., Nishijima, M., Nishino, J., Saijoh, Y., Sakai, Y. and Hamada, H. (2004). Regulation of retinoic acid distribution is required for proximodistal patterning and outgrowth of the developing mouse limb. *Dev Cell* **6**, 411-22.

Yelbuz, T. M., Waldo, K. L., Kumiski, D. H., Stadt, H. A., Wolfe, R. R., Leatherbury, L. and Kirby, M. L. (2002). Shortened outflow tract leads to altered cardiac looping after neural crest ablation. *Circulation* **106**, 504-10.

Yoshiura, S., Ohtsuka, T., Takenaka, Y., Nagahara, H., Yoshikawa, K. and Kageyama, R. (2007). Ultradian oscillations of Stat, Smad, and Hes1 expression in response to serum. *Proc Natl Acad Sci U S A* **104**, 11292-7.

Yu, D., Ellis, H. M., Lee, E. C., Jenkins, N. A., Copeland, N. G. and Court, D. L. (2000). An efficient recombination system for chromosome engineering in Escherichia coli. *Proc Natl Acad Sci U S A* **97**, 5978-83.

Yuan, W., Zhou, L., Chen, J. H., Wu, J. Y., Rao, Y. and Ornitz, D. M. (1999). The mouse SLIT family: secreted ligands for ROBO expressed in patterns that suggest a role in morphogenesis and axon guidance. *Dev Biol* **212**, 290-306.

Zackai, E. H. and Emanuel, B. S. (1980). Site-specific reciprocal translocation, t(11;22) (q23;q11), in several unrelated families with 3:1 meiotic disjunction. *Am J Med Genet* **7**, 507-21.

Zaffran, S., Kelly, R. G., Meilhac, S. M., Buckingham, M. E. and Brown, N. A. (2004). Right ventricular myocardium derives from the anterior heart field. *Circ Res* **95**, 261-8.

Zaragoza, M. V., Lewis, L. E., Sun, G., Wang, E., Li, L., Said-Salman, I., Feucht, L. and Huang, T. (2004). Identification of the TBX5 transactivating domain and the nuclear localization signal. *Gene* **330**, 9-18.

Zhang, Q., Wang, S. Y., Fleuriel, C., Leprince, D., Rocheleau, J. V., Piston, D. W. and Goodman, R. H. (2007). Metabolic regulation of SIRT1 transcription via a HIC1:CtBP corepressor complex. *Proc Natl Acad Sci U S A* **104**, 829-33.

Zhang, Z. and Baldini, A. (2008). In vivo response to high-resolution variation of Tbx1 mRNA dosage. *Hum Mol Genet* **17**, 150-7.

Zhang, Z., Cerrato, F., Xu, H., Vitelli, F., Morishima, M., Vincentz, J., Furuta, Y., Ma, L., Martin, J. F., Baldini, A. et al. (2005). Tbx1 expression in pharyngeal epithelia is necessary for pharyngeal arch artery development. *Development* **132**, 5307-15.

Zhang, Z., Huynh, T. and Baldini, A. (2006). Mesodermal expression of Tbx1 is necessary and sufficient for pharyngeal arch and cardiac outflow tract development. *Development* **133**, 3587-95.

Zheng, J. L., Shou, J., Guillemot, F., Kageyama, R. and Gao, W. Q. (2000). Hes1 is a negative regulator of inner ear hair cell differentiation. *Development* **127**, 4551-60.

Zhong, T. P., Childs, S., Leu, J. P. and Fishman, M. C. (2001). Gridlock signalling pathway fashions the first embryonic artery. *Nature* **414**, 216-20.

Zhong, T. P., Rosenberg, M., Mohideen, M. A., Weinstein, B. and Fishman, M. C. (2000). gridlock, an HLH gene required for assembly of the aorta in zebrafish. *Science* **287**, 1820-4.

Zhu, X., Zhang, J., Tollkuhn, J., Ohsawa, R., Bresnick, E. H., Guillemot, F., Kageyama, R. and Rosenfeld, M. G. (2006). Sustained Notch signaling in progenitors is required for sequential emergence of distinct cell lineages during organogenesis. *Genes Dev* **20**, 2739-53.

Zine, A., Aubert, A., Qiu, J., Therianos, S., Guillemot, F., Kageyama, R. and de Ribaupierre, F. (2001). Hes1 and Hes5 activities are required for the normal development of the hair cells in the mammalian inner ear. *J Neurosci* **21**, 4712-20.

Zoupa, M., Seppala, M., Mitsiadis, T. and Cobourne, M. T. (2006). Tbx1 is expressed at multiple sites of epithelial-mesenchymal interaction during early development of the facial complex. *Int J Dev Biol* **50**, 504-10.

Zweier, C., Sticht, H., Aydin-Yaylagul, I., Campbell, C. E. and Rauch, A. (2007). Human TBX1 missense mutations cause gain of function resulting in the same phenotype as 22q11.2 deletions. *Am J Hum Genet* **80**, 510-7.

Zwijsen, A., van Rooijen, M. A., Goumans, M. J., Dewulf, N., Bosman, E. A., ten Dijke, P., Mummery, C. L. and Huylebroeck, D. (2000). Expression of the inhibitory Smad7 in early mouse development and upregulation during embryonic vasculogenesis. *Dev Dyn* **218**, 663-70.

APPENDIX A: DYSREGULATED GENES

CD attached on the back cover includes the full list of 1553 downregulated genes identified in the microarray which werer downregulated to 0.83 in 5 out of 6 *Df1/Tbx1*^{lacZ} arrays compared to *Tbx1*$^{+/lacZ}$ arrays. A list of the 171 upregulated genes which were upregulated to 1.17 in 5 out of 6 *Df1/Tbx1*^{lacZ} chips compared to *Tbx1*$^{+/lacZ}$ chips, are also included.